SVENSKA GEOFYSISKA FÖRENINGEN

VOLUME 10, NUMBER 1 **Tellus** FEBRUARY 1958

A QUARTERLY JOURNAL OF GEOPHYSICS

Vertical Circulation and Release of Kinetic Energy during the Development of Hurricane Hazel into an Extratropical Storm

By E. PALMÉN, Academy of Finland

(Manuscript received June 5, 1957)

Abstract

The thermal structure of the atmosphere over the eastern and central parts of the U. S. on October 15, 1954, when the tropical hurricane "Hazel" entered the American continent and rapidly was transformed into an extratropical cyclone of great intensity, is analyzed by the aid of upper air charts and vertical cross sections. The field of divergence and vertical velocity is determined from the horizontal wind field at different levels for the synoptic time October 15, 1500 GCT, and the results are used for computing the precipitation in the region of strongest ascent of the warm and moist air of the tropical disturbance and for a determination of the release of kinetic energy in the whole region due to vertical solenoidal circulations associated with the general sinking of the cold polar air masses and the simultaneous ascent of the warm tropical air masses. The production of kinetic energy is also computed directly from the work done by the horizontal pressure forces in the same area. Both methods give a production of kinetic energy of about 19×10^{10} kilojoules or 19×10^{20} ergs per second over an area 366×10^4 km^2 large. Only a small part of the energy released is again dissipated due to friction in the same area, whereas the essential part is exported outwards from the source region, thus furnishing the surrounding atmosphere with large amounts of kinetic energy.

In the last section some general conclusions are made concerning the budget of kinetic energy in the whole Northern Hemisphere, considering the net effect of the disturbances in the westerlies, the mean meridional circulations, the mean meridional flux of kinetic energy and the frictional dissipation.

1. Introduction

The unusual behavior of the tropical cyclone "Hazel" (October 1954) over the North American continent has been discussed by KRUEGER (1954), MOOK (1955), DAVIS (1954), KNOX (1955) and by HUGHES, BAER, BIRCHFIELD and KAYLOR (1955). In these papers the unusual path of the cyclone over the U.S. mainland, the acceleration of the movement and the rapid change of the storm, from a typical tropical cyclone into an extratropical disturbance of great intensity, were attributed to the simultaneous wave pattern of the upper air flow in the extratropical westerlies. Due to a rare coincidence a strong extratropical development occurred over the eastern parts of the U.S., and the tropical cyclone became rapidly absorbed into this new development, with the result that the decay that normally occurs when tropical cyclones move inland did not happen in this case.

As was pointed out by Knox the rapid change of "Hazel" from a tropical into an extratropical storm occurred between October 15, 1500 GCT and October 16, 0300 GCT. In the present study only this stage of the development will be subjected to a detailed analysis. The synoptic situation and the development of the extratropical cyclone "Hazel" during this time of transition are in many respects of general interest, since the case offers an opportunity for the comparison of tropical and extratropical storms with respect to their sources of energy. On account

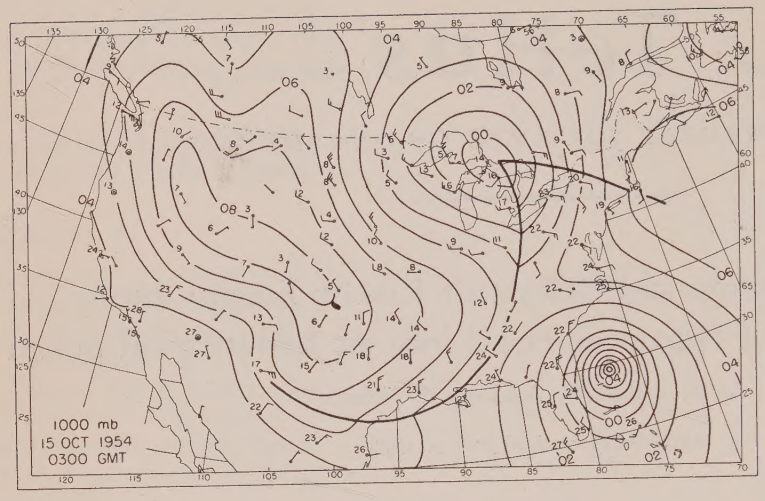

Fig. 1.

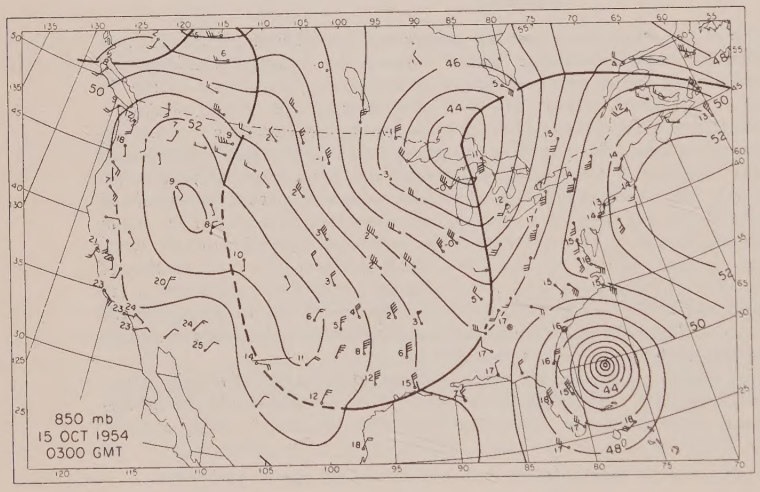

Fig. 2.

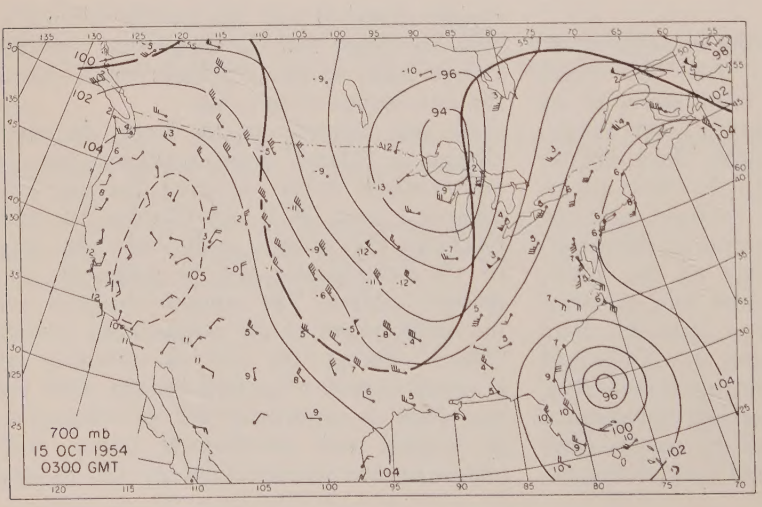

Fig. 3.

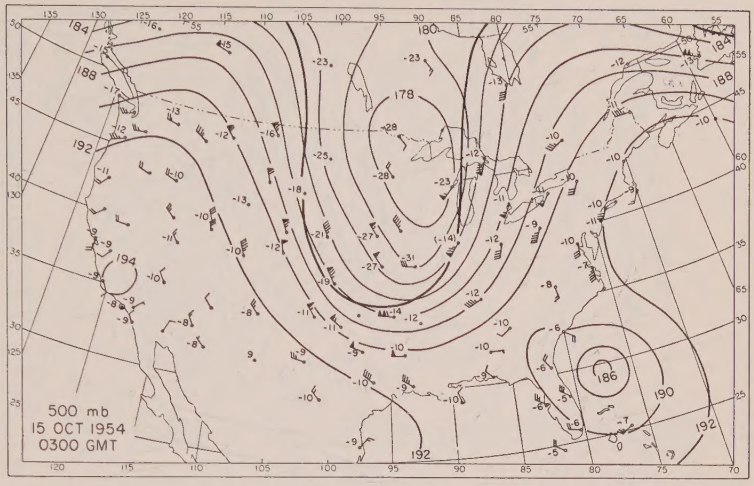

Fig. 4.

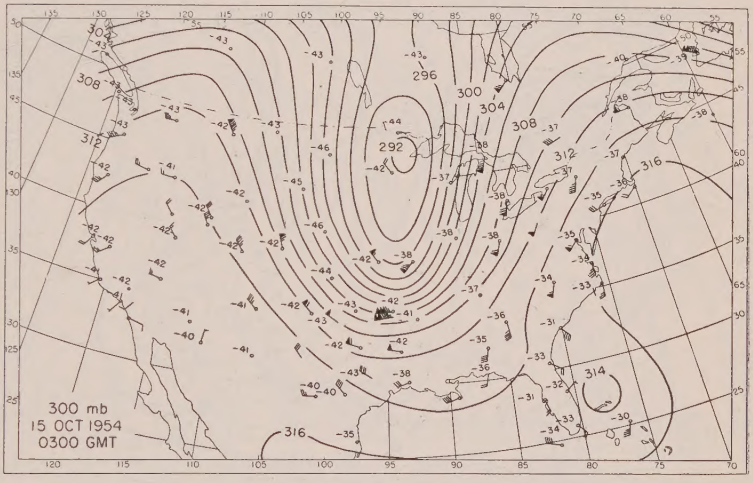

Fig. 5.

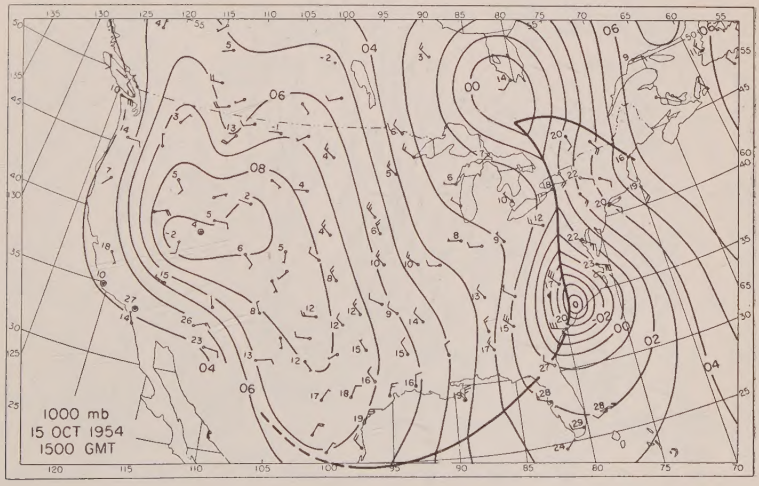

Fig. 6.

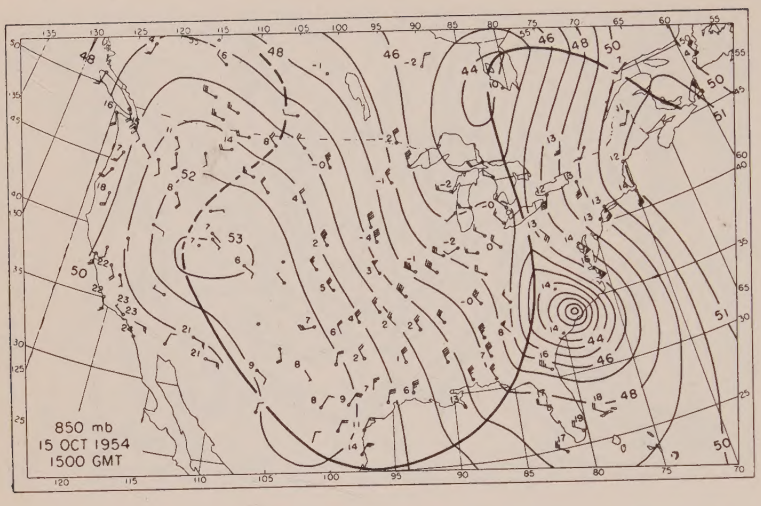

Fig. 7.

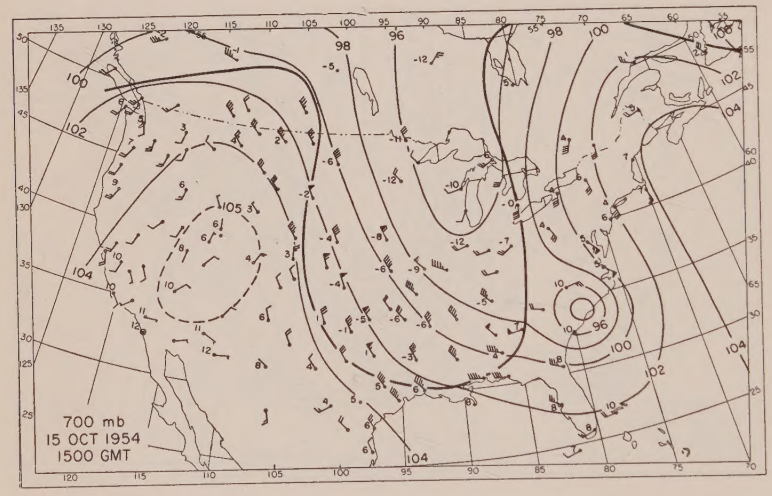

Fig. 8.

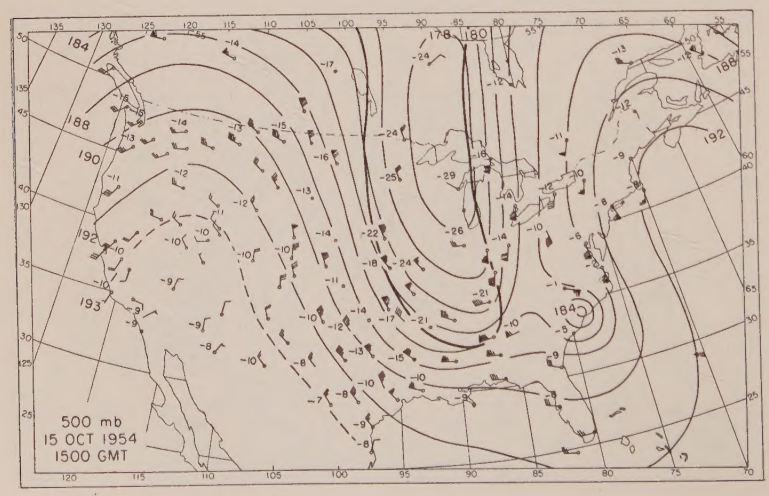

Fig. 9.

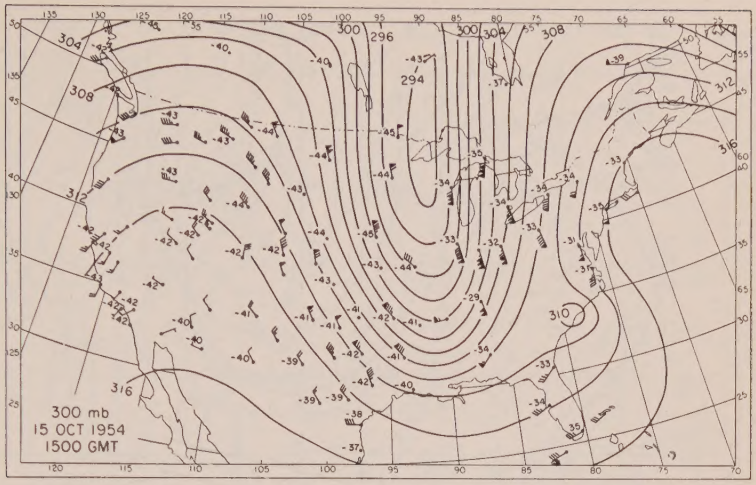

Fig. 10.

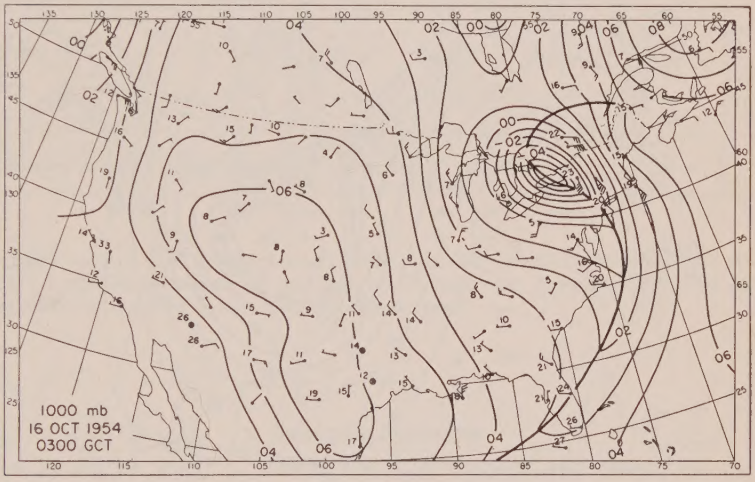

Fig. 11.

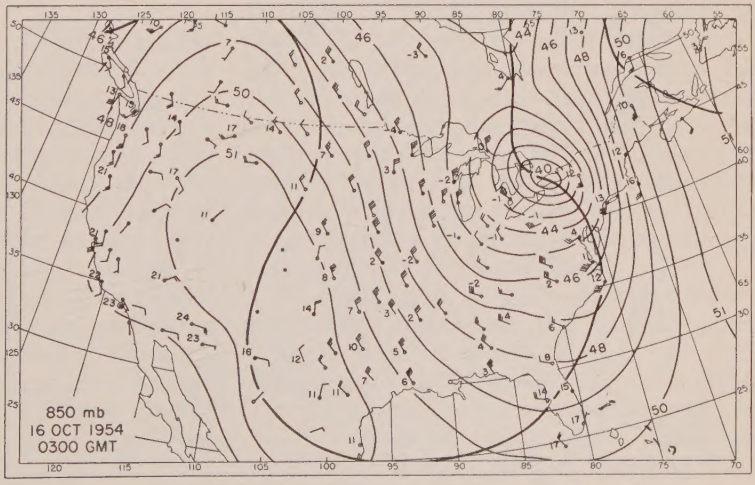

Fig. 12.

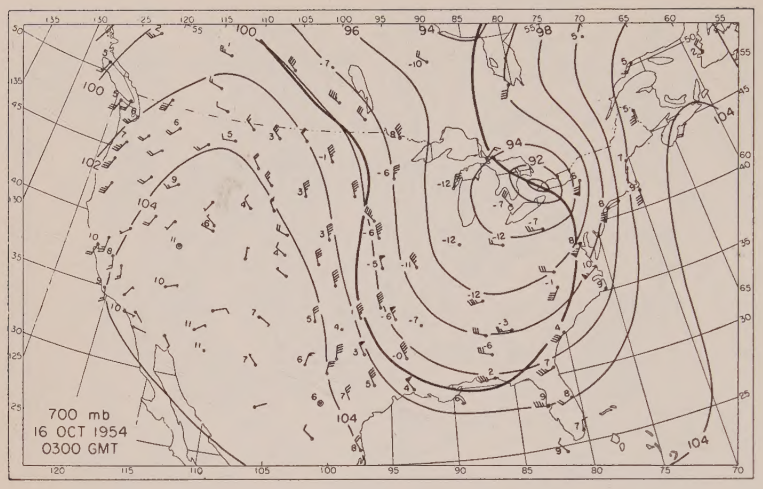

Fig. 13.

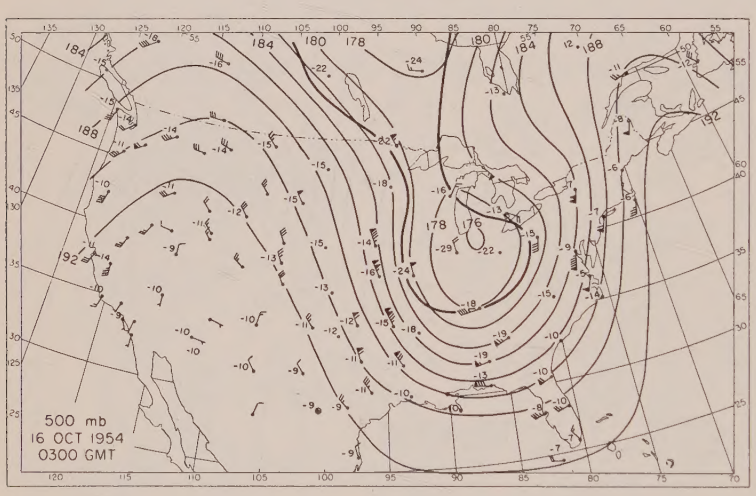

Fig. 14.

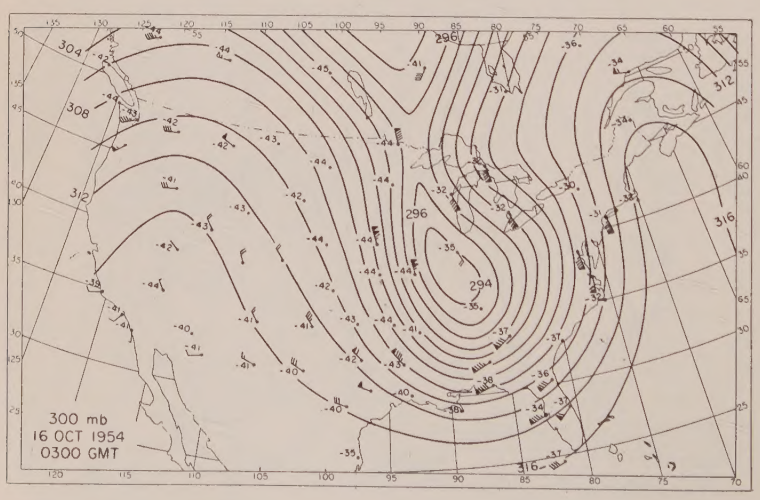

Fig. 15.

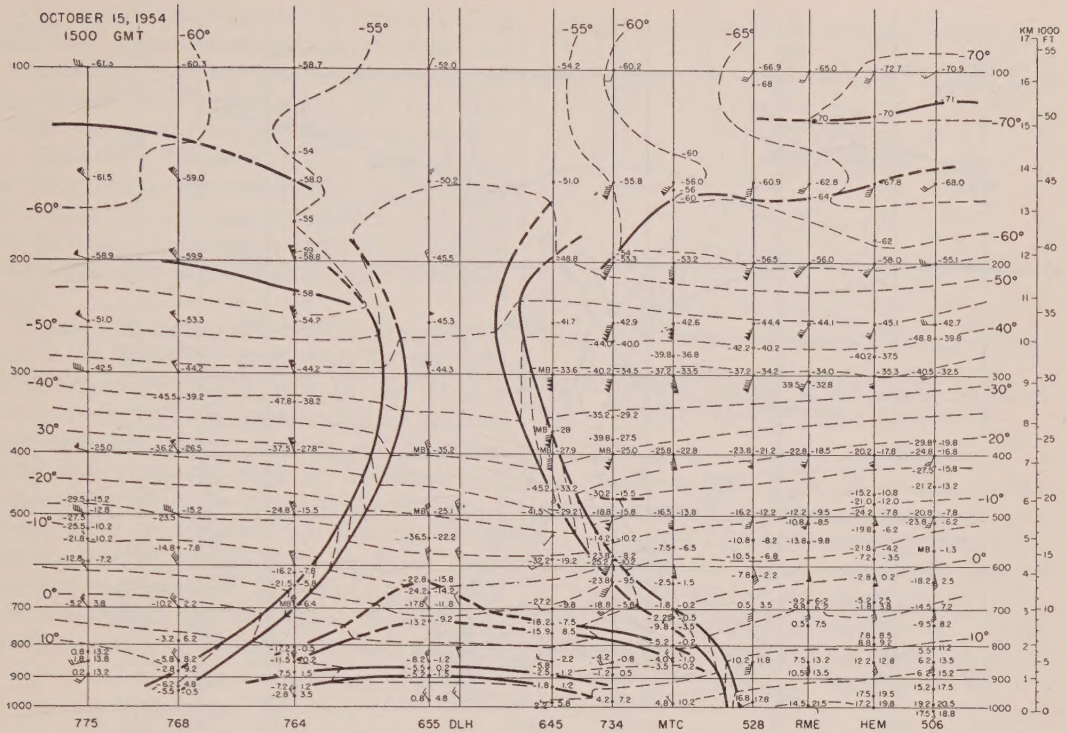

Fig. 16. Vertical cross-section, October 15, 1500 GCT, approximately along parallel 45° N. Thin dashed lines are isotherms, and heavy lines frontal boundaries, inversions or tropopauses. Temperature, dewpoint and wind are indicated at standard levels and significant points.

of the unusual path of the storm, a large number of upper air stations could be used, both for the synoptic analyses and for different kinds of computations.

The principal aim of the investigation was to determine directly from the observed winds and pressures the field of divergence, the vertical velocity, and the release of kinetic energy due to vertical solenoidal circulations. The synoptic time, October 15, 1500 GCT, was selected for the experiment because the principal development at that time occurred in a region with a relatively dense network of upper air stations. An extension of the experimental investigation to other synoptic times would have been very desirable; however, due to the sparseness of aerological stations over the Atlantic Ocean and over eastern Canada, the results would hardly have been satisfactory.

2. Synoptic Situation

In Figs. 1—15 the synoptic charts for the 1,000, 850, 700, 500 and 300 mb surfaces for October 15, 0300, 1500 and October 16, 0300 GCT are reproduced. The charts contain only temperatures, winds, contour lines and the principal fronts. By principal fronts is here meant a boundary separating the warm air from a frontal zone of finite thickness in regions where the front was sufficiently distinct. Concerning details of the surface maps the readers are referred to aforementioned investigations of cyclone "Hazel".

As can be seen from the charts an intense cold front approached the tropical storm "Hazel" when it moved in over the U.S. mainland around October 15, 1500 GCT. The cold air mass to the west and the northwest was of great depth and reached to the tropopause level along a tongue extending from

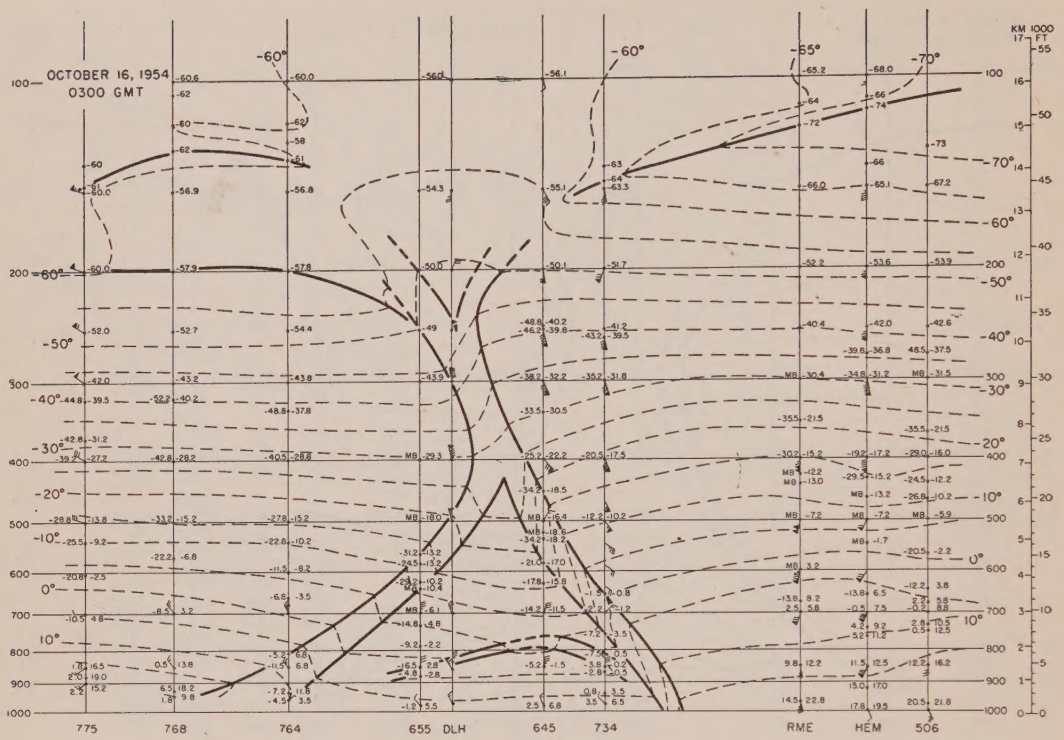

Fig. 17. Vertical cross section, October 16, 0300 GCT, approximately along parallel 45° N. Symbols as in Fig. 16.

northern Canada southward to about 38° N. At the 500 mb level, temperatures in the range from -27 to -31° C were found on October 15, 0300 GCT, as far south as 38° N, which is unusually cold for this time of the year. The temperature contrasts between the two principal air masses were extremely large; at the 500 mb level differences as large as 15° C were found in the vicinity of the cold front, with an over-all contrast of 25—28° C between the cold trough and the tropical air over the cyclone.

The thermal structure of the atmosphere is shown in greater detail in two vertical cross sections approximately along latitude 45° N for October 15, 1500 GCT and 16, 0300 GCT (Figs. 16 and 17). The cold air of polar origin is well distinguished from the surrounding warmer air masses. Especially the eastern boundary is extremely well marked. Here the frontal boundary can be followed up to levels where the temperature difference between the principal air masses normally vanishes. In the present case the front at these upper levels is still marked by very strong horizontal wind shear.

Twelve hours later the western warm air in the same zonal cross section has reached the eastern warm air above the 430-mb level, thus forming a pronounced zone of strong horizontal wind shear with the characteristics of an occluded front in the upper troposhere and in the tropopause region. In this respect the development was similar to the occlusion process associated with the strong cyclogenesis in November, 1950 (PALMÉN, 1953).[1] At lower levels the cold air was still well distinguished from the surrounding warm air, as can be seen from Fig. 17.

[1] The essential difference between the synoptic situation on October 15, 1954 and on November 25, 1950 was that in the latter case no tropical storm existed prior to the development. In spite of this the general development showed great similarities.

The frontal contours at the 500-mb level for four consecutive synoptic times are presented in Fig. 18. The figure shows the movement and deformation of the cold tongue during the period October 14, 1500—16, 0300 GCT. In spite of a net flow of cold air southwards across latitude circles (e.g., 50° or 45° N) the area occupied by the cold air decreased, indicating a general subsidence inside the cold mass (PALMÉN and NEWTON, 1951).

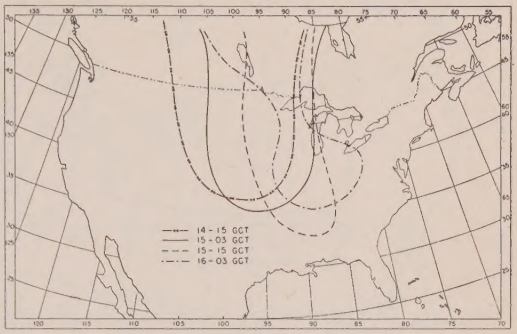

Fig. 18. Frontal contours at the 500-mb surface on October 14, 1500 to October 16, 0300 GCT.

A more detailed picture of the temperature and wind fields on both sides of the cold front over the eastern part of the U.S. is given in Fig. 19. In this zonal cross section, approximately along latitude 40° N, three radiosonde stations and, in addition, one wind station show the characteristic change of temperature and wind in the soundings penetrating the frontal layer. Both the temperature contrast and the wind shear reach maximal values in the upper troposphere, between 500 and 300 mb. Around 400 mb the wind changes from W 30 kts to SSE 140 kts through a vertical distance of about 1.6 km across the front, corresponding to an increase of the wind component normal to the cross section of about 72 m sec^{-1}. The temperature field inside the frontal layer gives a corresponding value of 65 m

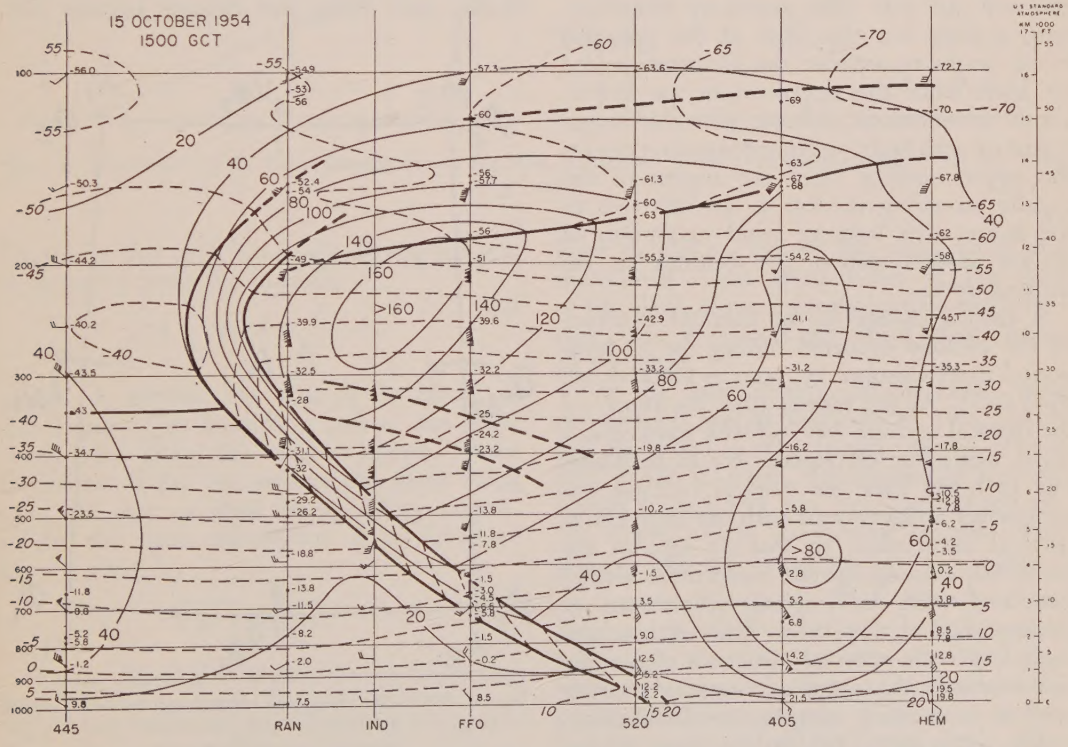

Fig. 19. Vertical cross-section, October 15, 1500 GCT, approximately along parallel 40° N. Thin dashed lines are isotherms, and heavy lines mark frontal boundaries or tropopauses. The thin solid lines mark isotachs at intervals of 20 kt of observed wind, without regard to direction.

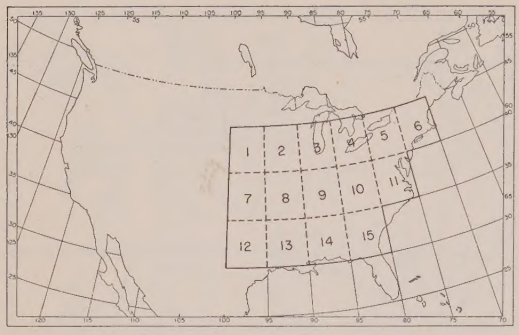

Fig. 20. The 15 different blocks used in the computations.

sec^{-1} as the increase of the geostrophic component normal to the cross section.

The cross section shows a wind maximum of more than 160 kts around 250 mb, almost vertically above the intersection between the frontal layer and the 500-mb surface. A second layer with pronounced vertical stability and a secondary maximum in the vertical wind shear is indicated by dashed lines between 400 and 300 mb. This ascendary boundary, with a slope less than that of the principal front, seems to separate the almost saturated air aloft from the dryer warm air below. Cloud observations indicate that this upper warm air with high moisture content represents the upper outflow from the region of the rapidly ascending motion in the rain area of the storm. The separate wind maximum of 80 kts around station 405 belongs to the tropical storm.

A radical change in the thermal structure of the cyclone occurred during the 12-hour period from October 15, 1500 to October 16, 0300 GCT. At the former time the center of the tropical cyclone was still well marked as a warm depression throughout the troposphere, but 12 hours later the tropical cyclone was completely amalgamated with the large extratropical disturbance, so that no sign of the previously existing separate center of circulation associated with the tropical cyclone can be distinguished at any level. Both at low and high levels the thermal structure shows the characteristics of a typical extratropical cyclone with its asymmetric temperature distribution.

The temperature field in the upper troposphere shows some interesting features during the period from October 15 to 16. During this period of the development an unusually warm mass of air with high dewpoint temperatures, indicating saturation or supersaturation in respect of ice, spread out at the 300 and 200 mb levels over the region of the Great Lakes and southeastern Canada.[2] The potential wet-bulb temperature of this upper air equalled that of the surface layer over the ocean to the southeast of the American continent, whereas the air at the same levels to the west of the upper trough was considerably colder. The analysis shows that this warm and moist air could not have been brought around the upper trough, but was oceanic tropical air which had been lifted from the surface layers in the central parts of the tropical cyclone.

3. Computation of Divergence and Vertical Velocity

For the computation of the divergence field and vertical velocity on October 15, 1500 GCT, the area indicated in Fig. 20 was used. The total area was divided into 15 different blocks, each being five degrees latitude and

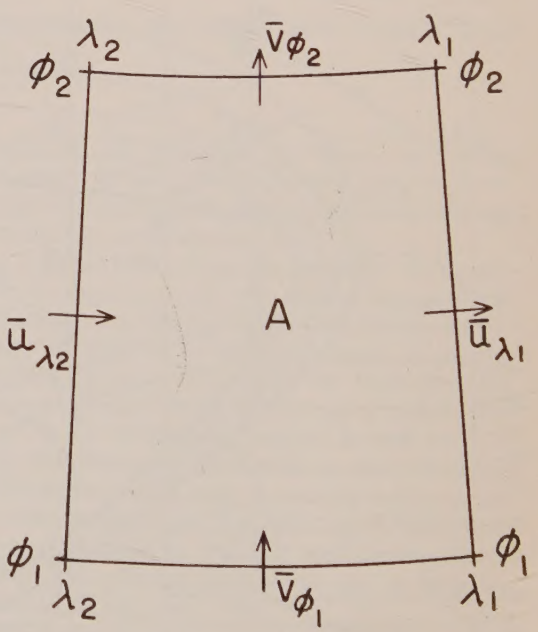

Fig. 21. Schematic picture of a block and the mean values of zonal and meridional wind components used for the computations of divergence.

[2] The dewpoint temperatures have not been plotted in the charts and cross-sections.

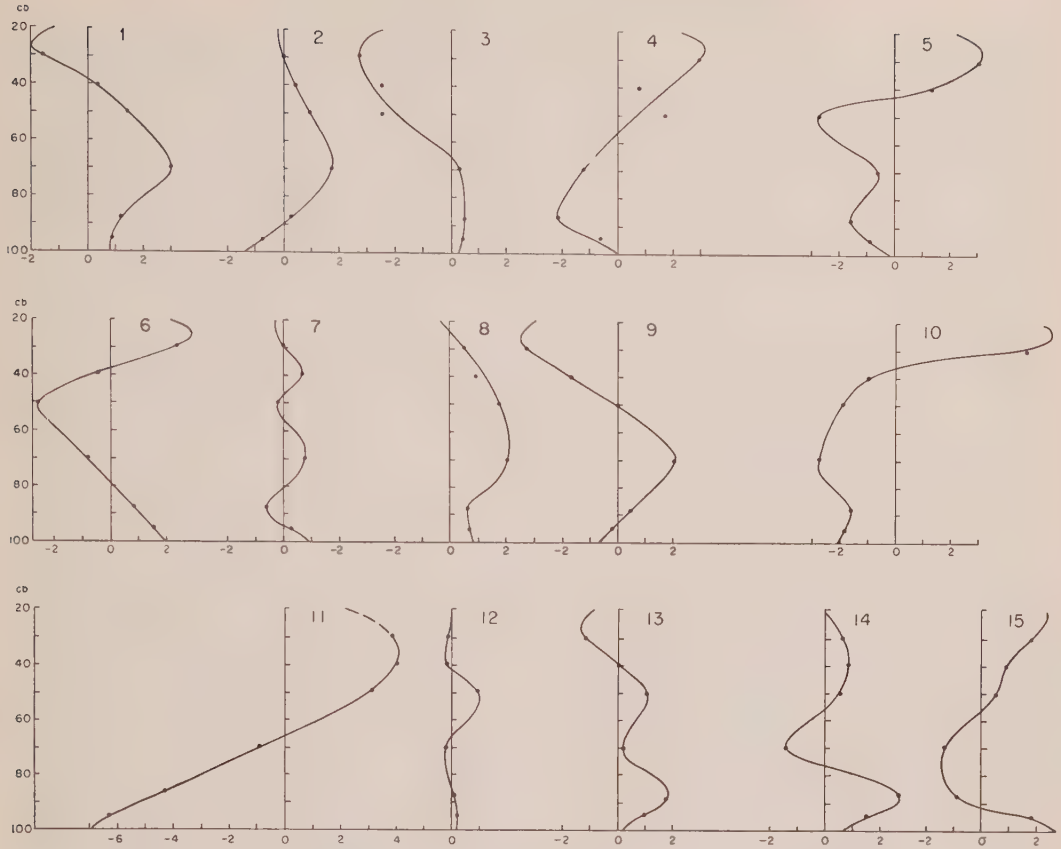

Fig. 22. Distribution of the mean divergence as a function of pressure in the 15 different blocks of Fig. 20. Unit: 10^{-5} sec^{-1}.

longitude. For each block the divergence was determined from the formula.

$$\int_{A_i} \nabla_H \cdot \mathbf{v}\, \delta A = \int_{L_i} v_n\, \delta L \qquad (1)$$

where A_i denotes the area of the block, L_i the length of its boundary, and v_n the wind component along the exterior normal of the boundary. If the bar denotes the mean value over the area, or over the boundary, respectively, the mean divergence at an arbitrary level is given by

$$\overline{\nabla_H \cdot \mathbf{v}} = \frac{L_i}{A_i}\overline{v_n} \qquad (2)$$

For the practical computation the following formula was used (see Fig. 21)

$$L_i \overline{v_n} = a(\varphi_2 - \varphi_1)(\overline{u}_{\lambda_1} - \overline{u}_{\lambda_2}) + a(\lambda_2 - \lambda_1)(\overline{v}_{\varphi_2} \cos \varphi_2 - \overline{v}_{\varphi_1} \cos \varphi_1) \qquad (3)$$

Here $\overline{u}_\lambda$ and $\overline{v}_\varphi$ denote the mean zonal and meridional wind components at the sides of the block, φ and λ signify latitude and longitude, and a denotes the radius of the figure of the earth.

For the determination of the mean wind components special wind charts were plotted for the 2,000, 4,000, 10,000, 18,000, 23,000 and 30,000 ft. levels, corresponding approximately to 940, 870, 700, 500, 400 and 300 mb. On these charts component isotachs were drawn, and the values for $\overline{u}_{\lambda_1}$, $\overline{u}_{\lambda_2}$, and $\overline{v}_{\varphi_1}$, $\overline{v}_{\varphi_2}$, were computed. The analysis of the original wind field was extended to a somewhat larger area than that indicated in Fig. 20.

The accuracy of these determinations depends essentially upon the number of stations and the quality of the observed winds. Most meteorologists who have tried to compute the divergence field from actual wind observa-

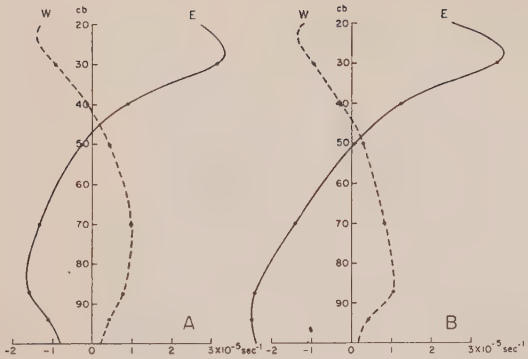

Fig. 23.
A: Mean divergence in 9 western blocks and in 6 eastern blocks.
B: Mean divergence in 6 western blocks and 4 eastern blocks.

tions have found the method rather unsatisfactory due to numerous errors and local deviations in the observed winds. In the case discussed here the divergence was expected to be relatively large since strong development was involved. It is reasonable, therefore, to assume that the errors would not substantially distort the large-scale divergence patterns.

The result of the computations for each of the 15 blocks in Fig. 20 is presented in Fig. 22 which gives the divergence as a function of pressure. At a first glance at the different curves the results do not appear very satisfactory because of numerous irregularities of a type obviously caused by errors in the original wind data or in the isotachs analyses. One exception can be seen in block 11 where the distribution of the divergence is very regular, with large negative values in the lowest layers and large positive values above about 600 mb. This block covers most of the region of heavy precipitation in the most active part of the tropical cyclone, where the divergence necessarily must reach extreme values.

A considerably more satisfactory picture results, however, if mean values of the divergence are determined for larger areas. If the total area in Fig. 20 is divided into two parts, a western and an eastern area separated by the meridian 85 W, the western part is essentially covered by cold polar air masses, at least up to the middle of the troposphere, while the eastern part, from the layer 1,000—700 mb and upwards, is occupied by warm air masses. Fig. 23 A gives the distribution of the mean divergence in the two different regions, with 9 of the blocks in Fig. 20 in the western region and 6 of the blocks in the eastern region. In the western region (i.e., the region of cold air) the mean divergence is positive in the lower layers up to around 415 mb with convergence above that level, while in the eastern part the lower layers up to 465 mb is characterized by convergence and the layers above 465 mb by divergence. The mean level of non-divergence is around 440 mb. The upper divergence in the eastern part is large, reaching values of about 3.2×10^{-5} sec^{-1} at the 300-mb level.

Both the horizontal and vertical distribution of the divergence correspond closely to the picture presented by PETTERSSEN and BRADBURY (1954) for another case of strong development (November 23—27, 1952). In their case, however, the divergence field was computed from the geostrophic vorticity field.

The characteristic difference between the behavior of the cold and warm air is still clearer if some of the blocks in Fig. 20 are excluded. In Fig. 23 B, the mean divergence for the 6 western blocks (Nos. 2, 3, 8, 9, 13, 14) and the 4 eastern blocks (Nos. 4, 5, 10, 11) is presented. The eastern group now contains essentially the region of precipitation or the area covered by the upper cloud sheet which extended from the active part of the cyclone, while the western part is occupied by cold air up to high altitudes. The mean level of non-divergence is now around 470 mb, with pronounced convergence (2.5×10^{-5} sec^{-1}) in the surface layers of the rain and cloud area and a very strong upper divergence (with maximum values of 4×10^{-5} sec^{-1}) around or just below the tropopause level.

From the equation of continuity one obtains

$$\left[\varrho w\right]_{H_1}^{H_2} = -\frac{1}{g}\int_{p_2}^{p_1} \nabla_H \cdot \mathbf{v}\, \delta p - \int_{H_1}^{H_2} \left(\frac{\partial \varrho}{\partial t} + \mathbf{v} \cdot \nabla_H \varrho\right) \delta z \qquad (4)$$

where ϱ is the density, w the vertical wind component, g the acceleration of gravity,

Table 1. Mean vertical velocity (cm sec^{-1}) in the different blocks

Block	Isobaric surfaces, mb						
	900	800	700	600	500	400	300
1	−0.7	−2.4	−5.2	−9.8	−14.4	−19.0	−22.1
2	0.6	0.1	−1.2	−3.4	−5.8	−8.0	−10.6
3	−0.4	−0.8	−1.1	0.3	2.4	7.1	16.5
4	0.8	3.0	5.4	7.2	6.7	6.2	2.4
5	0.7	2.4	3.5	5.6	10.2	14.4	12.8
6	−1.3	−2.3	−2.0	−0.5	2.8	6.0	5.9
7	−0.2	0.1	−0.2	−1.2	−1.3	−2.0	−3.5
8	−0.6	−1.4	−3.6	−6.6	−10.4	−15.1	−21.6
9	0.2	−0.6	−2.4	−5.0	− 6.6	−6.6	−3.0
10	1.5	3.6	7.2	11.6	16.8	23.0	27.6
11	5.9	10.3	13.1	14.7	13.7	9.4	2.6
12	−0.2	−0.1	−0.4	0.1	−1.0	−1.8	−1.8
13	−0.8	−2.2	−3.4	−4.3	−6.8	−9.2	−10.6
14	−1.4	−3.6	−4.2	−3.2	−4.0	−6.4	−9.8
15	−1.2	−0.1	1.2	2.7	2.6	2.1	−0.1
Mean	0.2	0.4	0.5	0.5	0.3	0.0	−1.0

and $\nabla_H \cdot \mathbf{v}$ and $\nabla_H \varrho$ are the horizontal divergence and density ascendant, respectively. The equation gives the difference in ϱw between two arbitrary levels H_1 and H_2 with the corresponding pressures p_1 and p_2. The last term in Eq. (4) can be considered to be small as compared with the divergence term. If it is neglected and if w is assumed to be zero at the ground, or approximately at p = 1,000 mb, one obtains the values of the vertical velocity shown in Table 1.

The mean values over all of the 15 blocks indicate a slight mean convergence in the lowest atmospheric layers and divergence above 700 mb. Whether this mean divergence field is real or the result of an accumulation of different errors is difficult to decide.

If the vertical velocities are combined in the manner shown in Fig. 23, into a western and eastern group separated by the meridian 85° W, one obtains the mean values given in Table 2.

Since the western groups essentially represent the cold air to the west of the front at the level 700—600 mb and the eastern groups represent the warm air to the east of the front, Table 2 shows that, on the average, the warm air is ascending and the cold air descending, resulting in an energy producing vertical circulation. This mean vertical circulation was essentially in a zonal direction.

4. Precipiation and Divergence Field

The precipitation pattern during the period from October 15 to 16 shows clearly the rapid amalgamation of the tropical cyclone "Hazel" with the large extratropical disturbance which developed over the eastern part of the American continent. At the beginning of the period two separate rain areas could be distinguished, but already on October 15, 1500 GCT both areas were combined into an elongated rain band essentially along the front, with maximum intensity just west of the surface front.

Table 2. Mean vertical velocity (cm sec^{-1}) in the 9 or 6 western blocks and in the 6 or 4 eastern blocks.

Group	Isobaric surfaces, mb						
	900	800	700	600	500	400	300
9 W	−0.5	−1.2	−2.4	−3.6	−5.6	−6.8	−7.4
6 E	1.1	2.8	4.7	6.9	8.8	10.2	8.5
6 W	−0.4	−1.4	−2.7	−3.7	−5.2	−6.4	−6.5
4 E	2.2	4.8	7.3	9.8	11.9	13.2	11.3

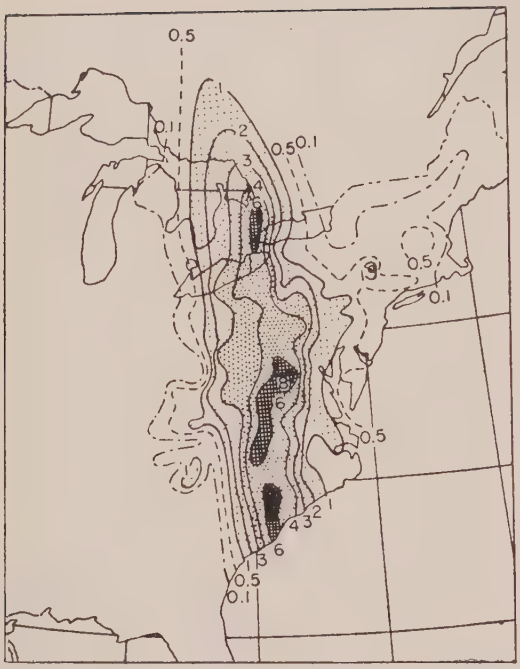

Fig. 24. Precipitation, in inches, during the 24 hour period October 15, 0600 to October 16, 0600 GCT.

In Fig. 24 the amounts of precipitation during the 24 hour period from October 15, 0600 to October 16, 0600 GCT are presented. The amounts are very large. One station reported 10.6 inches, and a band 100—200 km wide and about 1,500 km long, with values between 4 and 8 inches, extended along the front in Fig. 6. The total amount of precipitation in the whole area bounded to the north by latitude 45° N, to the west by the meridian 85° W and to the southeast by the Atlantic Coast can be estimated to about 53×10^{12} kg of water during the 24 hour period. The corresponding release of latent heat of condensation amounts to about 32×10^{18} calories, or 134×10^{15} kilojoules, or 134×10^{25} ergs, corresponding to 155×10^{10} kj sec^{-1}. This, according to HUGHES (1952) and RIEHL (1954) is 2.7 times the average release of latent heat in a tropical hurricane. The additional release of heat of fusion cannot readily be estimated.

In tropical hurricanes the essential source of energy is the latent heat of condensation. Only 2 to 3 per cent of the latent heat is, however, transformed into kinetic energy (PALMÉN and JORDAN, 1955). In extratropical storms the kinetic energy is mainly derived from the "available" potential energy due to juxtaposition of air masses of different temperature. However, considering the large amount of latent heat released in the precipitation area of cyclone "Hazel", it seems probable that the role of the condensation of water vapor is far from unimportant for the development. We shall return to this question later.

In the previous discussion of the vertical component of the air motion it was pointed out that the blocks 4, 5, 10 and 11 in Fig. 20 are characterized by ascending warm air. Especially in block 11 the ascending component is very pronounced at the levels of the principal cloud formation, reaching values of 15 cm sec^{-1} around the 600-mb level (Table 1). It is therefore of interest to compare in greater detail the fields of divergence, vertical velocity and precipitation in that particular block.

The total amount of water vapor transported inwards into a given block is expressed by

$$-\int_0^{\infty}\int_0^{L_i} q\varrho v_n \delta L \delta z \qquad (5)$$

where q denotes the specific humidity. The integral can be transformed into

$$-\frac{L_i}{g}\int_0^{p_0}\left(\bar{q}\,\bar{v}_n + \overline{q' v_n'}\right)\delta p$$

where the bar again denotes the mean value of the quantity in question along the boundary at a given level (isobaric surface) and primed letters denote the local deviation from the mean values. The second term in expression (6) depends upon the correlation between the v_n' and q' at the lateral boundary. Assuming that there is no local change with time of the amount of water vapor inside the block the precipitation must equal the total influx of moisture across the boundary of the block + the evaporation from the ground. If the precipitation and evaporation per unit time inside the block are denoted by P and E respectively, we have

$$P = E - \frac{L_i}{g}\int_0^{p_0}\left(\bar{q}\bar{v}_n + \overline{q' v_n'}\right)\delta p \qquad (7)$$

Formula (7) has recently and with satisfactory results been used by BRADBURY (1956) for the computation of the precipitation in selected storms.

If the block is not very large the variation of specific humidity at the boundary can be neglected and $\bar{q}$ can be replaced by the mean value of specific humidity inside the block. For the case investigated here the evaporation is negligible over most of the block due to the prevailing weather. Considering Eq. (2) we therefore obtain

$$P \approx -\frac{A_i}{g}\int_0^{p0} \overline{\bar{q}\,\overline{\nabla_H \cdot \mathbf{v}}}\,\delta p \qquad (8)$$

where A_i again denotes the horizontal area of the block.

The distribution of mean divergence as a function of pressure in block 11 is shown in Fig. 22, and $\bar{q}$ can be computed from the synoptic charts on October 15, 1500 GCT. If the area is expressed in m^2, the gravity constant in $m\ sec^{-2}$, and the pressure is given in cb, the value of the total amount of water P precipitated over the area will be given in tons per second. Since the precipitated water measured in kg per m^2 closely corresponds to the amount of rain in mm, the precipitation intensity can easily be computed by graphical integration. The values of $\bar{q}$, and $\overline{\nabla_H \cdot \mathbf{v}}$ and the product $\overline{\bar{q}\nabla_H \cdot \mathbf{v}}$ are given in Table 3. The graphical evaluation of the integral in Eq. (8) was made from Fig. 25 representing the distribution of $\overline{\bar{q}\nabla_H \cdot \mathbf{v}}$ between 100 and 20 cb. The values above the 20 cb level were considered to be negligible, as can be inferred by extrapolation of the values given in Table 3 and Fig. 25. The graphical evaluation gave a precipitation intensity of 1.42×10^{-6} tons per m^2 and second, corresponding to 5.1 mm per hour or 30.6 mm during a 6 hour period.

TABLE 3.

Mean divergence, mean specific humidity and their product in Block 11 for October 15, 1500 GCT

Isobaric layer, cb	$\bar{q}$	$\overline{\nabla_H \cdot \mathbf{v}}$	$\overline{\bar{q}\,\nabla_H \cdot \mathbf{v}}$
100—90	16.0×10^{-3}	-6.2×10^{-5}	-99.2×10^{-8}
90—80	13.8	−3.8	−52.4
80—70	11.5	−1.9	−21.9
70—60	9.0	0.1	0.9
60—50	6.2	2.4	14.9
50—40	3.8	3.7	14.1
40—30	1.7	4.0	6.8
30—20	0.4	3.2	1.3

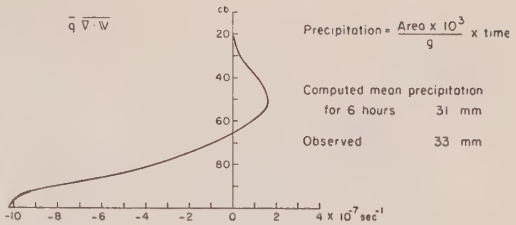

Fig. 25. Distribution of the product of specific humidity (q) and divergence, ($\nabla_H \cdot \mathbf{V}$) in block 11 on October 15, 1500 GCT.

Fig. 26 gives the precipitation (in inches) during the 6 hour period from October 15, 1200 to 1800 GCT centered at the synoptic time used for the above computation. For Block 11 the mean observed precipitation was evaluated to be 1.3 inches, or 33.0 mm. The agreement with the theoretically computed precipitation intensity (30.6 mm) is very good, showing that the distribution of divergence in Block 11, as shown in Fig. 22, cannot be too far from the correct one.

From the agreement between the computed and observed precipitation one can conclude that it is possible to use wind observations for computing the simultaneous precipitation if the computation is made over an area sufficiently large to eliminate the effects of different errors. Eq. (8) would have real prognistic value if the divergence field could be predicted. Very promising results have recently been achieved in that respect by ESTOQUE (1956).

5. Budget of Kinetic Energy

The vertical circulation with sinking cold air and ascending warm air results in transformation of potential energy into kinetic energy. Theoretically, it should be possible to compute the increase of kinetic energy from the decrease of potential + internal energy of the whole system. However, this method is not practicable. The difficulty can best be understood if one considers the order of magnitude of the total kinetic energy

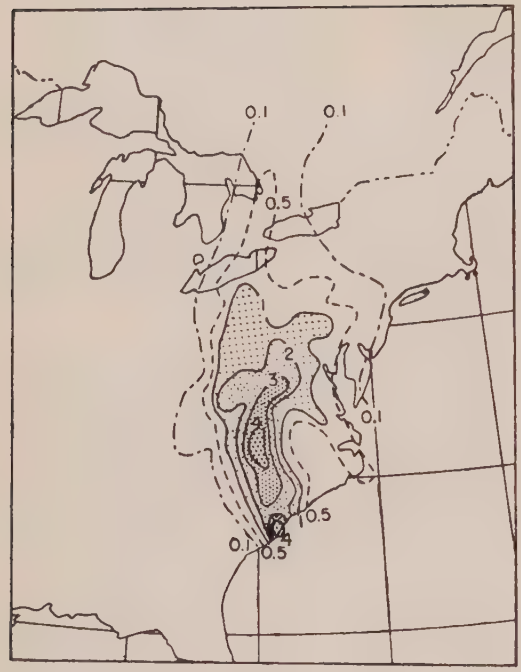

Fig. 26. Precipitation, in inches, during the 6 hours period October 15, 1200—1800 GCT.

K in a given volume compared with the sum of the potential energy P and the internal energy I. As Lorenz (1955) has pot. energy out the average ratio of K to $P+I$ in the atmosphere is of the order of magnitude 1/2,000. Considering only the available pot. energy A as defined by Lorenz, the ratio K/A is of the order of magnitude 1/10. Hence a moderate change in A would result in a large change in K compared with the existing value of K. The difficulty arises especially because no limited portion of the atmosphere can be considered as closed and no process as purely adiabatic. Consequently a moderate advection, or the existence of heat sources and sinks, makes it almost impossible to compute $\partial K/\partial t$ from $\partial P/\partial t$, as Spar (1950) has shown in some selected synoptic cases.

In the previous section the release of latent heat in the rain area of cyclone "Hazel" was estimated to be 134×10^{15} kilojoules during the 24 hour period from October 15, 0600, to October 16, 0600 GCT. Since this release essentially occurred in the warm air its effect was a considerable increase of the available potential energy counteracting the decrease of this form of energy due to the vertical circulation. Also, the net flux of potential energy across the boundaries was very large compared with the flux of kinetic energy, so that small errors in the former could strongly influence any budget of the total energy.

The only practical method for establishing an energy budget is, therefore, to confine the computation to the release and flux of kinetic energy only. In computing the kinetic energy flux of deep air masses it is permissible to neglect the contribution of the vertical flux across the horizontal boundaries here 1000 and 200 mb.

If the kinetic energy of the horizontal movement per unit volume is denoted by K, the change of horizontal kinetic energy in a given volume can be expressed by

$$\frac{\partial}{\partial t}\int_V K\delta V = -\int_V \left(\frac{\partial p}{\partial x}u + \frac{\partial p}{\partial x}v\right)\delta V \qquad (9)$$

$$-\int_S \tfrac{1}{2}\varrho\,(u^2+v^2)\,v_n\delta S + \int_V \left(\frac{\partial \tau_{xz}}{\partial z}u + \frac{\partial \tau_{yz}}{\partial z}v\right)\delta V$$

Here u, v are the zonal and meridional wind components, $-\partial p/\partial x$, $-\partial p/\partial y$, the corresponding horizontal components of the pressure gradient, v_n is the horizontal wind component normal to the bounding vertical surface S of the volume, τ_{xz}, τ_{yz} denote the zonal and meridional components of the shearing stress at a given level z. In Eq. (9) the first term to the right represents the work done by the horizontal pressure forces, the second term represents the net outflux of kinetic energy across the boundary, and the third term gives the frictional dissipation of kinetic energy inside the volume.

If A_i again denotes the horizontal area of an arbitrary block in Fig. 20 the first term in Eq. (9) can be written

$$\int_V \left(\frac{\partial p}{\partial x}u + \frac{\partial p}{\partial y}v\right)\delta V = A_i\int_{p_2}^{p_1}\left(u\overline{\frac{\partial Z}{\partial x}} + v\overline{\frac{\partial Z}{\partial y}}\right)\delta p \qquad (10)$$

where Z denotes the height of an arbitrary isobaric surface. If we again introduce the mean values over the area A_i, and the corre-

sponding deviations from the mean values, the right hand side of Eq. (10) may be written

$$A_i \int_{p_2}^{p_1} \left[-\overline{u}\frac{\partial \overline{Z}}{\partial x} + \overline{v}\frac{\partial \overline{Z}}{\partial y} \right] \delta p$$

$$+ A_i \int_{p_2}^{p_1} \left[\overline{u'\left(\frac{\partial Z}{\partial x}\right)'} + \overline{v'\left(\frac{\partial Z}{\partial y}\right)'} \right] \delta p \qquad (11)$$

The first term gives the negative rate of change of kinetic energy in the layer between the isobaric surfaces p_1, and p_2, computed from the mean values of the wind and the slope of the isobaric surface, while the second term represents the influence of the variations of the quantities in the block. With the data available the values of the second terms in the 15 different blocks can hardly be computed. If the blocks are not too large it is permissible, as a first approximation, to consider $\overline{u}$, $\overline{v}$, $\frac{\partial \overline{Z}}{\partial x}$, and $\frac{\partial \overline{Z}}{\partial y}$, as point values valid for the whole area A_i, and to disregard the second term.

The mean slope of the isobaric surfaces 850, 700, 500, 400 and 300 mb were computed for the 15 different blocks in Fig. 20, and the zonal and meridional components of the slope were multiplied by the corresponding mean values of the wind components determined by interpolation from the values of u and v in the 2,000, 4,000, 10,000, 18,000, 23,000 and 30,000-ft charts. In this manner it was possible to obtain values of the products in expression (11) from independent analyses of the wind and pressure fields, thus avoiding the use of the geostrophic approximation. The resulting work done by the horizontal pressure forces (or the production of kinetic energy if friction be neglected) per layer of 1 cb thickness and unit time is presented in Table 4, for October 15, 1500 GCT.

TABLE 4.

Work done by the pressure forces, unit: 10^8 kj/cb/sec.

Block	Isobaric surfaces, mb				
	850	700	500	400	300
1	0.32	1.75	0.85	3.00	−4.87
2	0.70	2.58	1.14	−0.58	−3.66
3	−0.83	0.04	2.43	1.00	37.61
4	−0.24	1.29	4.50	18.36	16.81
5	0.81	1.69	2.94	4.56	7.30
6	−0.21	0.19	2.29	0.71	−0.45
7	0.34	−1.48	−0.44	−4.73	−9.90
8	0.56	1.88	−0.23	6.94	−3.78
9	0.92	−1.50	−0.11	8.35	20.39
10	2.97	−1.17	2.96	5.65	17.92
11	1.98	2.17	−1.90	−0.12	−1.87
12	−0.51	1.34	−1.68	−5.58	−3.09
13	−0.62	−1.54	−6.26	−8.09	−5.86
14	0.52	−0.15	−4.20	−3.56	3.95
15	0.79	4.51	4.58	4.78	7.61
Total	7.50	11.60	6.87	30.69	78.11

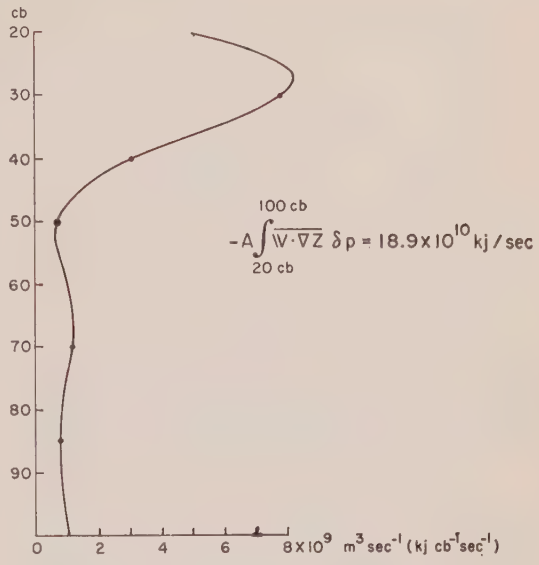

Fig. 27. Work done by the horizontal pressure forces per layer of 1 cb in all 15 blocks. Unit: 10^9 m^3 sec^{-1} (kj cb^{-1} sec^{-1}).

The table naturally shows many irregularities due, at least in part, to unsatisfactory wind data and errors in the mean values of the heights of the isobaric surfaces. However, in the values for the total rate of increase of kinetic energy at the different isobaric levels a large part of these errors is probably eliminated.

In Fig. 27 the work term in Eq. (9) for the 15 blocks is presented graphically as a function of pressure, using the values given in Table 4. The curve was extrapolated to the 200-mb level assuming a maximum value (about 85×10^8 kj/cb/sec) at the level of strongest wind around 260 mb. By graphical integration the total release of kinetic energy in the

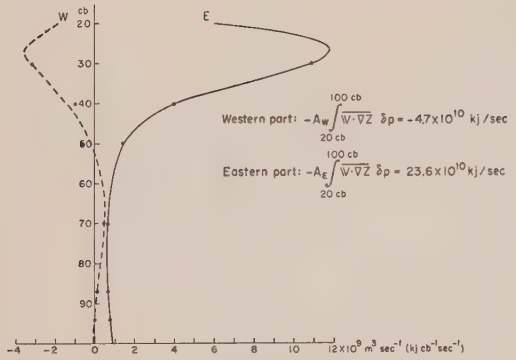
W
E
cb
20
30
40
50
60
70
80
90
Western part: $-A_W \int_{20\,cb}^{100\,cb} \overline{w \cdot \nabla Z}\, \delta p = -4.7 \times 10^{10}$ kj/sec
Eastern part: $-A_E \int_{20\,cb}^{100\,cb} \overline{w \cdot \nabla Z}\, \delta p = 23.6 \times 10^{10}$ kj/sec
-4 -2 0 2 4 6 8 10 12 $\times 10^9$ m³ sec⁻¹ (kj cb⁻¹ sec⁻¹)

Fig. 28. Work done by the horizontal pressure forces per layer of 1 cb, the western part (dashed curve) and in the eastern part (solid curve) of the total area A. Unit as in Fig. 27.

atmospheric layer between 1,000 and 200 mb was determined to be 18.9×10^{10} kj/sec. No attempt was made to extend the computation to the uppermost atmospheric layer, but the indications are that the net contribution of this uppermost part of the atmosphere cannot be very large.

The total work computed from Fig. 27 is very large if compared with the average generation of kinetic energy in tropical hurricanes; this latter has been estimated by PALMÉN and JORDAN (1955) to be 12.9×10^{24} ergs/day or 1.5×10^{10} kj/sec. The energy production in cyclone "Hazel" was accordingly about 12.6 times larger. However, the area of the "mean tropical hurricane" in the computation by PALMÉN and JORDAN corresponded to a circular area with a radius of 6° latitude, or to about 139×10^4 km², whereas the total area of the 15 blocks used in the present computation is 366×10^4 km². Per unit area the generation of kinetic energy in the case of "Hazel" is, therefore, about 4.8 times larger than in a mean tropical cyclone. This seems surprising at the first glance. However, in tropical cyclones the area of strongest wind (30—60 m sec^{-1}) is confined to a relatively narrow ring around the center in the lowest part of the atmosphere, whereas in cyclone "Hazel", at the time when it had acquired the essential characteristics of a large extratropical storm, velocities of about 50 to 80 m sec^{-1} appeared over much larger areas between 500 and 150 mb. In real tropical cyclones, also, the relase of kinetic energy essentially occurs in the lowest layers of the atmosphere, between the ground and 700 mb, whereas the release of kinetic energy in the case of "Hazel", according to Fig. 27, was relatively moderate in the lowest layers.

The major release of kinetic energy according to Fig. 27 occurred in the upper troposphere and in the tropopause region. Here the flow was strongly accelerated as can be seen e.g., from the 300 mb chart for the synoptic time in question (Fig. 10). The wind arrows to the east of the upper trough show here large deviations from the geostrophic wind, the angle of inflow across the contour lines reaching values of 20—35° with velocities of 100—160 knots. At this level the velocity of the jet stream is rapidly accelerated from about 100 knots to the west of the trough to 160 knots to the east of the trough.

It is of interest to compute the release of kinetic energy separately for the regions west and east of the upper trough line. At the 300-mb level the trough approximately coincided with the 90° W meridian. For the 6 western and the 9 eastern blocks the work term in Eq. (9) is represented graphically in Fig. 28. The graphical integration up to 200 mb gives for the western part a negative value of -4.7×10^{10} kj sec^{-1}, while for the eastern part a positive value of 23.6×10^{10} kj sec^{-1} is found, the sum being 18.9×10^{10} kj sec^{-1} for the whole area. Thus the region to the west of the trough is a region of consumption of kinetic energy, whereas the area to the east

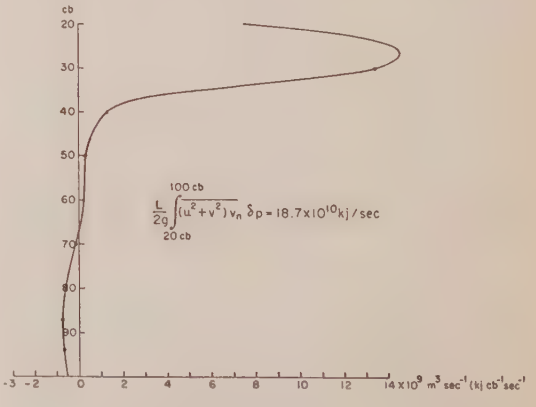

Fig. 29. Net export of kinetic energy per 1 cb layer from the whole area A.

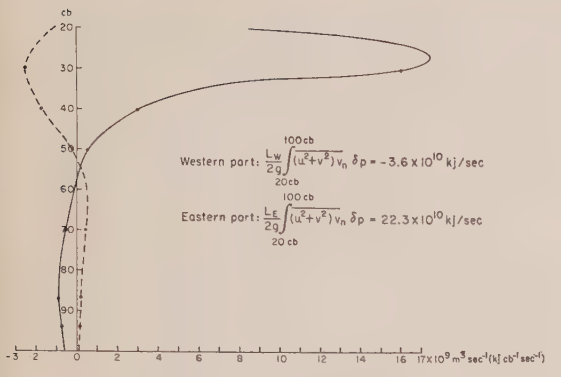
cb
Western part: $\frac{L_W}{2g}\int_{20cb}^{100cb}(\overline{u^2+v^2})v_n\,\delta p = -3.6\times10^{10}$ kj/sec
Eastern part: $\frac{L_E}{2g}\int_{20cb}^{100cb}(\overline{u^2+v^2})v_n\,\delta p = 22.3\times10^{10}$ kj/sec
17×10^9 m^3 sec^{-1}(kj cb^{-1} sec^{-1})

Fig. 30. Net export of kinetic energy per 1 cb layer from the western part of the area A (dashed curves) and from the eastern part (solid curve).

of the trough is a region of very strong generation.

The second term on the right of Eq. (9) can be written:

$$\int_S \tfrac{1}{2}\varrho(u^2+v^2)v_n\,\delta S = \frac{L}{2g}\int_{p_2}^{p_1}\overline{(u^2+v^2)v_n}\,\delta p \qquad (12)$$

where L denotes the total length of the boundary of the area considered in Fig. 20. The values of the integral for layers of one cb thickness are presented graphically in Fig. 29. Integrated from 100 to 20 cb the curve gives a net outflux of kinetic energy across the boundary amounting to 18.7×10^{10} kj sec^{-1}. This net export is very nearly the same as the generation inside the region. It follows then that, at this particular time, practically no change of kinetic energy would occur if the frictional dissipation were neglected.

If, as before, we divide the total region into two parts, a western and an eastern part, the export across the corresponding boundaries will be as shown in Fig. 30. Into the western part there is now a net import of kinetic energy of 3.6×10^{10} kj sec^{-1}, whereas there is a net export of 22.3×10^{10} kj sec^{-1} from the eastern part. The region of consumption of kinetic energy is also a region of import of kinetic energy, while the region of generation shows a net export of about the same amount as that generated. This, again, indicates that the local changes are relatively small compared with the generation and the export.

The total kinetic energy in the 15 blocks in the layer between 1,000 and 200 mb was determined from

$$\frac{A}{2g}\int_{20\text{ cb}}^{100\text{ cb}}(\overline{u^2}+\overline{v^2})\,\delta p \qquad (13)$$

where A denotes the total area of the 15 blocks. For the graphical determination of the total kinetic energy Fig. 31 was used, showing the distribution in terms of kilojouls per cb. The total kinetic energy on October 15, 1500 GCT was computed to be 89.2×10^{14} kj. The difference between generation and net export if extended over a 12 hour period would, according to previous determination, amount to only 0.9×10^{14} kj, a value that is negligible compared with the kinetic energy existing in the whole region.

The frictional dissipation is difficult to compute, but an attempt will here be made to estimate it. The third term to the right in Eq. (9) can be transformed in the following manner:

$$\int_V\left(u\frac{\partial\tau_{xz}}{\partial z}+v\frac{\partial\tau_{yz}}{\partial z}\right)\delta V =$$

$$A\int_0^\infty\frac{\partial}{\partial z}(\overline{u\tau_{xz}}+\overline{v\tau_{yz}})\,\delta z - A\int_0^\infty\left(\overline{\tau_{xz}\frac{\partial u}{\partial z}}+\right.$$

$$\left.+\overline{\tau_{yz}\frac{\partial v}{\partial z}}\right)\delta z \qquad (14)$$

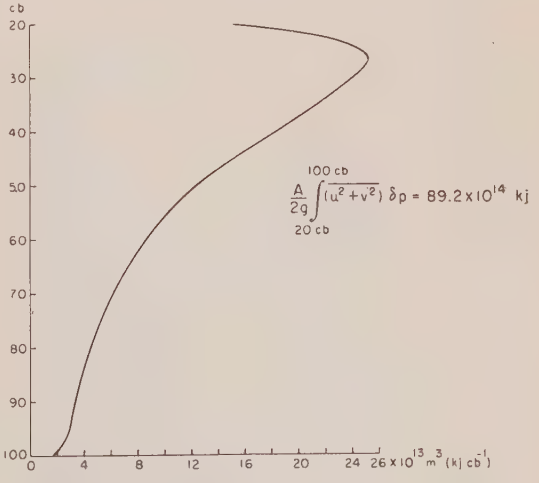

Fig. 31. Total kinetic energy per 1 cb layer over the whole area A. Unit: 10^{13} m^3 (kj cb^{-1}).

Since the frictional stress vanishes at the top of the atmosphere and the components of the shearing stress can be expressed by

$$\tau_{xz} = \mu \frac{\partial u}{\partial z} \quad \tau_{yz} = \mu \frac{\partial v}{\partial z} \tag{15}$$

where μ denotes the coefficient of eddy viscosity, the frictional dissipation can be written in the form

$$-A\left(\overline{u_0\tau_{x0}} + \overline{v_0\tau_{y0}}\right) - A\int_0^\infty \mu\left[\overline{\left(\frac{\partial u}{\partial z}\right)^2} + \overline{\left(\frac{\partial v}{\partial z}\right)^2}\right]\delta z \tag{16}$$

if μ is considered constant in the horizontal. The first term represents the dissipation due to the surface friction and the second term the internal dissipation in the atmosphere.

We shall here make a rough estimate of the first term in expression (16). If the surface stress τ_0 is expressed by the well known formula

$$\tau_0 = k\varrho_0 V_0^2 \tag{17}$$

where k is the drag coefficient, ϱ_0 the density of the air at the surface, and V_0 the total wind velocity at "anemometer level" the first term in expression (16) can be written

$$-A\overline{k\varrho_0 V_0^3} \tag{18}$$

For ϱ_0 the mean values at the ground, or about 1.2×10^{-3} ton m^{-3}, can be used. The drag coefficient k is not constant, but varies strongly depending on the roughness of the ground and possibly also with the wind velocity. For the estimate of the frictional dissipation a mean value of 0.004 for k was used which is about twice the normal value over a water surface. The mean value of V_0^3 was det ermined from the surface map for the synoptic time October 15, 1500 GCT by simply computing its arithmetic mean for all wind observations in the 15 blocks. The computation gave a frictional dissipation of 0.94×10^{10} kj sec^{-1}.

If we assume, with BRUNT (1939), that the internal frictional dissipation of kinetic energy in the atmosphere is about the same as the dissipation computed from the first term in (16), the total frictional dissipation in the 15 blocks would amount to about 2×10^{10} kj sec^{-1}, a value that is only about 10 per cent of the total generation of kinetic energy in the same region. Since the generation of kinetic energy in the region was practically equal to the net export from the region the local decrease would amount to the frictional dissipation or to 2×10^{10} kj sec^{-1}, corresponding to about 17×10^{14} kj a day, which is less than 20 per cent of the total kinetic energy between 1,000 and 200 mb in the region. The kinetic energy produced by the sinking cold air and ascending warm air in the extratropical cyclone "Hazel" was to a very large extent available for export out of the source region. This export occurred, according to Fig. 29, essentially between 400 and 200 mb in the form of an upper jet stream leaving the active disturbance.

The budget of kinetic energy outlined here gives some clues to the problem of the formation and maintenance of the upper jet stream in the belt of westerlies. The jet stream is developed or accelerated inside an active disturbance of the type discussed here as a result of transformation of available potential energy into kinetic energy, which then is rapidly exported as a relatively narrow upper jet out from the system of vertical circulation.

6. Solenoidal Circulation and Release of Kinetec Energy

Returning to Eq. (9), the generation term can be written in the following form:

$$-\int_{p_2}^{p_1}\int_A \boldsymbol{V}\cdot\nabla_H Z\delta A\delta p = \int_{p_2}^{p_1}\int_A Z\nabla_H\cdot\boldsymbol{V}\delta A\delta p - \int_{p_2}^{p_1}\int_L Zv_n\delta L\delta p \tag{19}$$

where δA is an element of the horizontal area and δL an element of length of the boundary separating the area A of the 15 blocks in Fig. 20 from the outside atmosphere. The second term to the right denotes the work done by the atmosphere inside the volume V on the outside atmosphere. In the case of a

closed system v_n is zero and the second term vanishes. The system considered here is, however, not closed, but since we are interested in the vertical circulation inside the volume considered here we shall not make any attempt at determining this term directly.

The first term on the right of Eq. (19) can be transformed in the following manner:

$$\int_{p_2}^{p_1}\int_{A} Z\nabla_H \cdot V\delta A\delta p = -\int_{p_2}^{p_1}\int_{A} Z\frac{\partial\omega}{\partial p}\delta A\delta p$$

$$= -\int_{p_2}^{p_1}\int_{A}\frac{\partial(Z\omega)}{\partial p}\delta A\delta p + \int_{p_2}^{p_1}\int_{A}\omega\frac{\partial Z}{\partial p}\delta A\delta p \quad (20)$$

where $\omega \equiv \frac{dp}{dt}$

If the first term on the right is integrated with respect to pressure, and the hydrostatic equation $\frac{\partial Z}{\partial p} = -\frac{\alpha}{g}$ is used, we obtain

$$\int_{p_2}^{p_1}\int_{A} Z\nabla_H \cdot V\delta A\delta p = -\int_{A}[Z\omega]_{p_2}^{p_1}\delta A -$$

$$-\frac{I}{g}\int_{p_2}^{p_1}\int_{A}\alpha\omega\delta A\delta p \quad (21)$$

The divergence was previously computed from the ground (100 cb) to the 20-cb level (Fig. 22). If we use the same upper level and introduce instead of α the absolute temperature T at a constant isobaric surface Eq. (21) may be written

$$\int_{20}^{100\text{ cb}}\int_{A} Z\nabla_H \cdot V\delta A\delta p = A[\bar{Z}\bar{\omega}]_{20\text{ cb}} -$$

$$-\frac{AR}{g}\int_{20}^{100\text{ cb}}\frac{\bar{T}\bar{\omega}}{p}\delta p + A[\overline{Z'\omega'}]_{20\text{ cb}} -$$

$$-\frac{AR}{g}\int_{20}^{100\text{ cb}}\frac{\overline{T'\omega'}}{p}\delta p \quad (22)$$

where R is the gas constant.

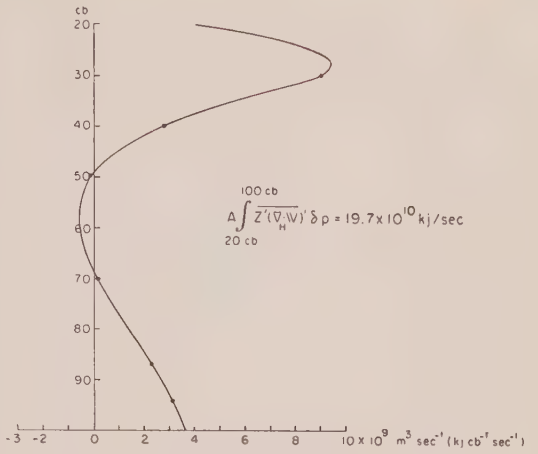

Fig. 32. Mean product of Z' and $(\nabla_H \cdot \mathbf{V})'$ per 1 cb layer in the whole area A. Unit as in Fig. 27.

We see immediately that

$$A\int_{20}^{100\text{ cb}} \bar{Z}\overline{\nabla_H \cdot V}\delta p = A[\bar{Z}\bar{\omega}]_{20\text{ cb}} - \frac{AR}{g}\int_{20}^{100\text{ cb}}\frac{\bar{T}\bar{\omega}}{p}\delta p$$

$$A\int_{20}^{100\text{ cb}} \overline{Z'(\nabla_H \cdot V)'}\,\delta p = A[\overline{Z'\omega'}]_{20\text{ cb}} -$$

$$-\frac{AR}{g}\int_{20}^{100\text{ cb}}\frac{\overline{T'\omega'}}{p}\delta p \quad (23)$$

The first equation represents the change of the potential energy due to a mean vertical displacement in the whole air mass and will not be considered here.

The left hand term in the second Eq. (23) is represented in Fig. 32, and the graphical integration gives 19.7×10^{10} kj sec^{-1}. The first term on the right was computed to $-6.7\times$ $\times 10^{10}$ kj sec^{-1}. The last integral again is represented in Fig. 33, and the graphical integration, considering the negative sign, gives $26.4\times$ $\times 10^{10}$ kj sec^{-1}. The sum of these last two terms equals 19.7×10^{10} kj sec^{-1}.

Previously the rate of increase of kinetic energy in the layer between 100 and 20 cb was determined to be 18.9×10^{10} kj sec^{-1}. This was obtained from the left-hand term of Eq. (19) by replacing $\mathbf{V}$ and ∇Z in the different 15 blocks by $\bar{\mathbf{V}}$ and $\bar{\nabla}\bar{Z}$ computed for each block. In using Eq. (23) the mean

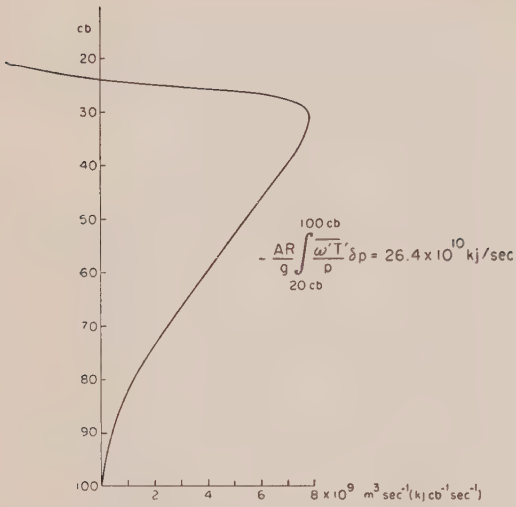

Fig. 33. Negative value of the change of available potential energy due to vertical circulations per 1 cb layer over the whole area A. Unit as in Fig. 27.

value of Z, ω, and T were first determined for each block at a given isobaric surface, then the mean values $\overline{Z}$, $\overline{\omega}$ and $\overline{T}$ for the whole area were obtained and, finally, the deviations Z', ω' and T' from those mean values in each block were determined. The small difference of 0.8×10^{10} kj sec^{-1} could depend upon different kinds of errors in the computation of the mean values of the quantities in the individual blocks, but it could also, at least in part, derive from the neglect of the last term in Eq. (19). In any case this last term must be small, indicating that the rate of change of kinetic energy in the region could be computed with good approximation as if the region were a closed system.

7. General Conclusions

The rate of increase of kinetic energy of the air mass occupying region A in Fig. 20 on October 15, 1 500 GCT has been computed by two different methods to be either 18.9×10^{10} or 19.7×10^{10} kj sec^{-1} in the layer from 1,000 to 200 mb. Within the same region the frictional dissipation was estimated to about 2×10^{10} kj sec^{-1}. The simultaneous net export from the region was found to be 18.7×10^{10} kj sec^{-1}, or approximately the same as the production of kinetic energy. From these values, and using Eq. (9), the local change of kinetic energy could be estimated to -2×10^{10} kj sec^{-1}. Since the total kinetic energy in the fixed region at the same time was about 89×10^{14} kj, the local decrease would have been 19 per cent of the amount, had it persisted over a 24 hour period. On account of the rapid change of the whole synoptic situation it was not possible to compare the computed instantaneous values with the observed local changes.

The computations show that the region considered here was a source region of kinetic energy, and that a large surplus of kinetic energy was exported from the region of the cyclonic disturbance. The kinetic energy was derived from solenoidal circulations, essentially in zonal planes, with cold air sinking in the west and warm moist air ascending in the east. This type of transformation of available potential energy into kinetic energy does not necessarily mean that the potential energy actually decreased, because at the same time the amount of released latent heat (155×10^{10} kj sec^{-1}) was much larger than the released kinetic energy. Consequently it is not permissible to compute the local change of kinetic energy on a synoptic scale from the simultaneous observed change in potential energy.

It is of interest to compare the production of kinetic energy in cyclone "Hazel" with the total budget of kinetic energy in the westerlies of the Northern Hemisphere. The total area A used in the energy computation was 366×10^{10} m^2, whereas the total area of the Northern Hemisphere north of latitude 30° N is 127×10^{12} m^2 or almost 35 times larger. The frictional dissipation of kinetic energy in the region of "Hazel" was estimated to 2×10^{10} kj sec^{-1} or 5.5×10^{-3} kj sec^{-1} per m^2. This dissipation was certainly larger than the mean dissipation in the whole westerlies, which for the winter season has been estimated by PISHAROTY (1955) to be about 2×10^{-3} kj sec^{-1} per m^2.[1] If we use Pisharoty's value the total frictional dissipation of kinetic energy north of latitude 30° N would amount to 37×10^{10} kj sec^{-1}, whereas the above value of 5.5×10^{-3} kj sec^{-1} per m^2 would give a total dissipation of 70×10^{10} kj sec^{-1}. The former value is about 2 times and the latter value 3.5 times the generation of kinetic energy in the area of cyclone "Hazel".

[1] Brunt (1939) has estimated the mean frictional dissipation in the atmosphere to 5×10^{-3} kj sec^{-1} per m^2, but this value is generally considered too large.

Consequently only 2 to 3,5 disturbances of the intensity of "Hazel" would suffice to furnish the whole hemisphere north of latitude 30° N with the kinetic energy necessary for the maintenance of the circulation against the frictional dissipation.

MINTZ (1955) and PISHAROTY (1955) have shown that there is a net import of kinetic energy from the south across latitude 30° N. For January and February their values for the net import amount to an average value of about $17—20 \times 10^{10}$ kj sec^{-1}, and so is about the same as the generation of kinetic energy in "Hazel". This import further reduces the number of active disturbances needed for the maintenance of the kinetic energy of the westerlies.

Since it would be absurd to assume that the source regions of kinetic energy would be limited to only two intense cyclones occupying a very small part of the west-wind belt it it necessary to assume that source and sink regions of kinetic energy alternate and that the kinetic energy generated in a source region is largely transformed into potential energy due to energy consuming circulations in the surroundings. These sources and sinks of kinetic energy are connected with moving disturbances; the total frictional dissipation of kinetic energy north of latitude 30° N must then equal the total net effect of all source and sink regions augmented with the net import from the south.

A schematic description of this process has recently been given by STARR (1954). According to him the available potential energy in the atmosphere due to the mean meridional temperature gradient cannot directly be transformed into kinetic energy as a result of mean meridional circulations with sinking cold air in the north and ascending warm air in the south. The available mean potential energy must first be transformed into available "eddy potential energy", this energy form can then be transferred into "eddy kinetic energy" as a result of vertical circulations essentially in zonal planes. Starr's viewpoints have further been developed by LORENZ (1955). The theory of Starr and Lorenz is primarily valid for the westerlies, whereas for the trade wind belt a "Hadley type" of mean meridional circulation seems to be the dominating mechanism for generation of kinetic energy, at least in winter. The energy release in cyclone "Hazel" is characteristic of the transformation of "eddy potential energy" into "eddy kinetic energy".

Acknowledgements

The writer wishes to express his gratitude to Dr. Sverre Petterssen, Director of the Weather Forecasting Research Center, University of Chicago, for his generous interest, encouragement and advice throughout the work. Thanks are due also to W. L. Schallert, who performed a large part of the computation; to Dorothy Bradbury, who was most helpful in preparing the manuscript; and to Dr. G. W. Platzman for several useful suggestions concerning the energy computations. Thanks are due also to Mrs. Della Friedlander, who performed or supervised the drafting of the figures, and to Mr. A. FINKLIN, who prepared the original charts and cross sections.

REFERENCES

BRADBURY, D., 1956: Tech. Rep. No. 8, Contr. No. AF 19(604)—1293 University of Chicago, Dept. of Meteorology.

BRUNT, D., 1939: Physical and Dynamical Meteorology, Cambridge, p. 285.

DAVIS, W. R., 1954: Monthly Weather Review, Vol. 82, p. 370.

ESTOQUE, M. A., 1956: Tech. Rep. No. 7, Contr. No. AF 19(604)—1293 University of Chicago, Dept. of Metcorology.

HUGHES, L. A., 1952: J. Met., Vol. 9, p. 422.

HUGHES, L. A., BAER, F., BIRCHFIELD, G. E., and KAYLOR, R. E., 1955: Bull. Amer. Met. Soc., Vol. 36, p. 528.

KNOX, J. L., 1955: Bull. Amer. Met. Soc., Vol. 36, p. 239.

KRUEGER, A. F., 1954: Monthly Weather Review, Vol. 82, p. 296.

LORENZ, E. N., 1955: Tellus, Vol. 7, p. 157.

MINTZ, Y., 1955: General Circulation Project, Univ. of Calif., Final Report, XIII.

MOOK, C. P., 1955: Weatherwise, **8**, p. 92.

PALMÉN, E., 1953: General Circulation Project, Univ. of Chicago, Final Report.

PALMÉN, E., and JORDAN, C. L., 1955: Tellus, **7**, p. 186.

PALMÉN, E., and NEWTON, C. W., 1951: J. Met., Vol. 8, p. 25.

PETTERSSEN, S., and BRADBURY, D., 1954: Tech. Rep. Contr. No. AF 19(604)—390 University of Chicago.

PISHAROTY, P., 1955: General Circulation Project, Univ. of Calif., Final Report, XIV.

RIEHL, H., 1954: Tropical Meteorology, McGraw-Hill, New York, p. 322.

SPAR, J., 1950: J. Met., Vol. 7, p. 48.

STARR, V. P., 1954: Tellus, Vol. 6, p. 268.

A Case Study of an Easterly Jet Stream in the Tropics

By M. A. ALAKA,* The University of Chicago

(Manuscript received February 28, 1957)

Abstract

An easterly current at 200 mb over the Southern Bahamas and Florida is identified as a jet stream which had originated in middle latitudes and had travelled along the eastern periphery of the dynamic anticyclone situated over the South Eastern United States. The properties of this current are studied and compared with those associated with middle latitudes jet streams. It is found that although this current is comparatively weak (core velocity about 70 kts), horizontal and vertical wind shears near its axis are comparable with those observed near the usually much stronger middle latitudes jet streams.

The mechanism responsible for the concentration of the kinetic energy in this narrow current is shown to be independent of any temperature contrast between two air masses in the lower and middle troposphere. The jet is further shown to be maintained by pressure heads and the continuous production and destruction of kinetic energy involved in its maintenance and motion occur as a result of accelerations in more or less laminar flow rather than by lateral or frictional stresses. Finally, the observed weather distribution is found to be influenced by the resonance and interference of the upper jet stream with waves in the lower easterlies.

1. Introduction

The concentration of kinetic energy in the atmosphere into narrow jets has increasingly engaged the interest of meteorologists in recent years in view of the frequency and wide geographical range of their occurrence, and the important role they play in determining weather conditions. But in spite of the impressive list of studies and some ingenious attempts[1] to account for them, the last word has not been said concerning the nature of the concentrating mechanism. In fact, "the development of an adequate theory for the concentration of momentum into narrow streaks looms as a problem of major importance, perhaps the most important unsolved problem in planetary hydrodynamics" (ROSSBY, 1953).

In order to design a proper framework within which to fit such a theory, the essential features of these currents must be separated from the extraneous or incidental. A good way of weeding out the latter is afforded by comparing different conditions under which wind concentrations occur. The numerous studies of jet streams in various localities and seasons in the middle and high latitudes provide one means for such a comparison. They show, for instance, that while some jet streams seem to be tied with the surface temperature gradient, others, particularly in summer, are limited to the high troposphere. On the other hand, all jets studied to date show near-zero values of absolute vorticity to the right of the jet axis, looking downstream.

The recent introduction of "synoptic" methods of observation in oceanography (FUGLISTER, 1951) which has brought out with clarity the remarkable similarities in the patterns of current concentration in atmosphere and ocean also helps in narrowing down the search for the concentrating mechanism within the right

[1] For a survey of these attempts, the reader is referred to RIEHL, ALAKA, JORDAN and RENARD (1952), Chap. VII.

* Present affiliation: Secretariat, World Meteorological Organization, Geneva, Switzerland.

framework by relegating to secondary importance the compressibility of the atmosphere and the mode of energy infusion (RIEHL, ALAKA, JORDAN and RENARD, 1954).

Still another method for sifting the essential from the extraneous is provided by controlled experiments in the laboratory. For instance, the importance of dynamic stability generated by the earth's rotation is brought out by the fact that jets injected in a non-rotating fluid sheet tend to mix rapidly with the environment, forming widening wake streams, whereas in rotating fluids, narrow jets appear capable of retaining their concentration for appreciable periods of time (FULTZ, 1951).

The above studies represent different links in the chain of research on jet streams. Another link would be provided by descriptions and analyses of jet streams in low latitudes, especially easterly jet streams, and by comparing their structure and life cycle with that of the extratropical currents. In contrast with middle and high latitudes, however, where the observational network in some areas permits not only locating jet streams with some precision, but also studying in detail their structural properties, life cycle, geographical distribution, and movement, our knowledge of jet streams in tropical regions is fragmentary. Upper air observations are so thinly distributed over large areas that a reliable analysis of the wind field in the upper troposphere is in general all but impossible. Consequently, our information concerning the very existence and geographical incidence of jet streams in the tropics is based in large measure on isolated observations or mean time sections which are individually inconclusive.

In the last few years, however, the amount of raob and rawin observations in the region south of the United States has been increased sufficiently so that this region now contains what may be termed the nearest approximation to a *network* of high-tropospheric reports in lower latitudes. Therefore, in the course of an experiment in tropical analysis and forecasting conducted in Miami during the summer of 1953[1], close watch was kept for indications of easterly jet occurrence south of latitude 30°. Evidence was soon forthcoming; the present paper deals with the best-documented case encountered.

2. Previous observations of low latitude jet streams

In spite of scarce data, several types of jet streams in low latitudes have received brief mention in the literature:

a. *Westerly jets originating at high latitudes and migrating deep into tropical regions, usually in accompaniment with the polar front:* These are chiefly winter phenomena and may be illustrated by the case studied by CRESSMAN (1950) when a westerly jet centered at latitude 40° N on March 20, 1948, drifted southward to latitude 20° N by March 25.

b. *Westerly jets originating in the tropics:* An example of these is the case noted by RIEHL (1954) when a jet stream with a maximum speed over 100 knots passed near Johnston Island (lat. 17° N) on July 24, 1951 and over Hawaii the following day. There was definite indication that it could not have originated in extratropical regions and must have developed in the tropics. As another example, we may cite the case studied by COLÓN (1954), of the high winds over Puerto Rico during the period March 29 – April 2, 1953.

c. *The subtropical westerly jet* (PALMÉN, 1951) which occurs in general during the winter months and which helps account for the fact that the average northern hemispheric westerlies during winter show a maximum around latitude 25° – 30° N (PETTERSSEN, 1950).

d. *Easterly jets originating in the tropics:* There is an abundance of reports of high-tropospheric easterly winds in excess of 50 knots in different localities in the tropics and a tendency by some meteorologists to call these winds jet streams without simultaneous reference to winds in neighboring localities.[2] Clearly, while jet streams are characterized by relatively strong winds, it is fallacy to consider all strong winds as forming part of a jet. Therefore, isolated observations of high winds do not necessarily indicate the existence of jets. And whereas it is undoubtedly our experience in the higher

[1] The work was undertaken under contract with the Office of Naval Research and was conducted under the leadership of Professor H. Riehl.

[2] For a list of articles on this subject the reader is referred to "Meteorological Abstracts and Bibliography": American Meteor. Soc., July. 1953.

Fig. 1. Map showing some of the stations mentioned in the present study.

latitudes that very strong winds do not usually prevail over very wide belts, thus strengthening the probability that the observed high winds form part of a pattern characterized by a lateral concentration of kinetic energy, this still remains to be shown.

e. *Easterly jets originating in middle latitudes:* Occasionally, during southward motion, a jet stream of the temperate zone splits and one branch travels along the periphery of a dynamic anticyclone as a northerly or northeasterly current. NEWTON and CARSON (1953) have investigated such a case in summer in connexion with the formation of shear lines. Under favorable conditions, such a splinter current may be expected to appear at the equatorward periphery of the subtropical high as an easterly jet.

3. Scope of study

The case to be presented deals with a situation of the last class described. First intimation of its occurrence came when High Rock, Grand Bahama Island (Fig. 1) reported a 200 mb wind speed of 53 knots from due East on July 31, 1953 at 1500 GCT. Twelve hours later, a wind of 52 knots from the same direction appeared at Miami. By August 2, the wind speed had reached 62 knots at Coffin Hills, Eleuthera Island, and increased to 60 knots at Miami, and to 62 knots at High Rock. Wind directions were bracketed between 80° – 110°. Neither Havana nor Patrick AFB partook in the wind variations to any marked degree. A time section of the wind speeds at nearby stations, projected on the 82° W meridian (Fig. 2), suggested that the above sequence of events was concomitant with the westward advance of a *narrow current similar to jet streams* in lateral concentration of kinetic energy, albeit with less intense maximum velocities than is ordinarily observed in jet stream cores.

Due to lack of detailed and reliable data, none of the jet streams mentioned in the literature could be studied in a manner even remotely comparable to that possible in the middle latitudes. The present paper is a first attempt to make such a study. The network of upper air observations allows a reasonably adequate three-dimensional analysis. Our first objective will be to describe and examine the

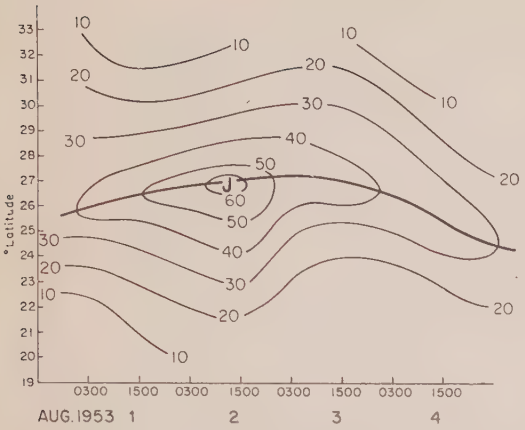

Fig. 2. A time section of the wind speed in knots, at 200 mb along the 82 W meridian, during the period August 1—4, 1953.

thermal and wind structure of the current. Next, an attempt will be made to determine, as far as possible, the mechanism by which the energy of the current is created and destroyed. Finally, the role of the vorticity changes in bringing about the observed weather will be discussed.

4. Analysis

In order to obtain as complete a picture as possible, the following charts and diagrams were prepared for the period July 31 – August 4, 1957:

a) *Time sections* at the stations shown in figure 1. Figures 3 a – c represent a selection of these sections.

b) *Contour maps* at 500 and 200 mb (24-hr continuity); these are not reproduced here.

c) 500 – 200 mb thickness maps (24-hour continuity).

d) *Streamlines and isotachs* at 200 mb (12-hour continuity). The 0300 GCT maps are shown in Figures 4 a – d. Streamlines were drawn from isogons.

e) *Space cross sections* of temperature and height deviations from Schacht's mean tropical atmosphere and of the easterly component of the observed wind at 82° W (24-hour continuity, Figures 5 a – h).

f) *Charts showing distribution of weather and cloudiness* (Figure 6).

g. *Relative vorticity:* We denote the vertical component of the absolute vorticity[1] by ζ_a and write

$$\zeta_a = f + \zeta = f + \frac{V}{r_s} + \frac{\partial V}{\partial n} \qquad (1)$$

where ζ is the vertical component of the relative vorticity,[2] r_s the radius or curvature of the streamlines taken positive for cyclonic circulation and $\partial V/\partial n$ the wind shear normal to the current considered positive when cyclonic.

In most representations of the horizontal wind distribution across jet maxima, whether drawn from observations (cf. Fig. 10) or from theoretical considerations, the cyclonic and anticyclonic limbs of the profile meet in a cusp at the jet axis. This, if correct, implies that the shear term $\partial V/\partial n$ in equation (1) is discontinuous at the jet axis. The 200 mb relative vorticity fields presented in Figures 7 a – d were computed on this assumption. In all cases, the jet axis marks a discontinuity in the relative vorticity.

5. Synoptic Situation

a. *The broadscale setting:* Throughout the period to be discussed, one long wave trough in the westerlies persists in the East Pacific Ocean as shown by 700-mb 5-day mean charts of the Extended Forecast Section, U.S. Weather Bureau; another trough lies near 60° W and the intermediate ridge occupies the Eastern United States. Over the continent the strongest 700-mb westerlies are situated above 40° N everywhere. They pass over the top of the mean ridge between 45° and 50° N. Since, in addition, the limit of the mid-tropospheric easterlies lies north of 30° N, the region on which our interest centers is as well shielded from the influence and interference of extratropical weather systems as ever happens. This permits the fullest development of disturbances and patterns of weather evolution that are typical of the tropics in midsummer.

In the lower troposphere a train of waves travels westwards in the easterlies south of 25° – 30° N during the period. Events in the high troposphere are partly connected with the lower waves, and partly independent of them. Thus the jet stream to be demonstrated for the

[1] Hereafter simply called the absolute vorticity.
[2] Hereafter simply called the relative vorticity.

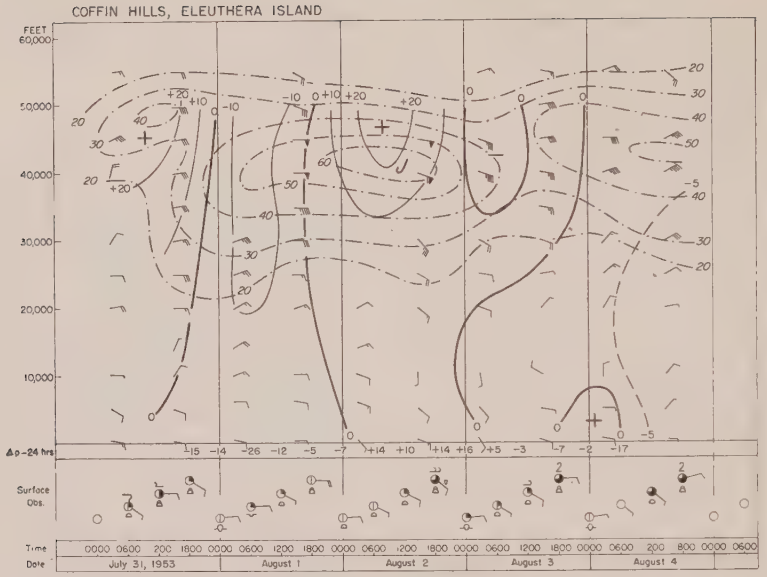

Fig. 3 a. Time section at Coffin Hills, Eleuthera Island during the period July 31—August 4, 1953. Full and dashed lines are isolines of 24-hour height changes in tens of feet; dash-dotted lines are isolines in knots. Twentyhour surface pressure tendencies in tenths of millibars are given in the row labelled △p-24 hrs.

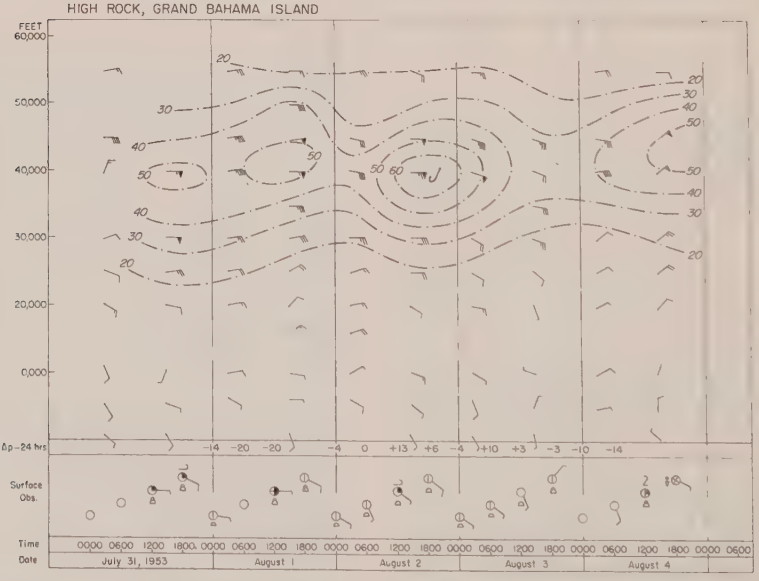

Fig. 3 b. Time section for High Rock, Grand Bahama Island. Lines are isotachs in knots.

high levels has no counterpart in the lower easterlies. On the other hand, we find a westward progression of cyclonic vortices which are closely linked to the wave troughs below.

b. *The 200-mb wind field (Fig. 4 a–d):* The analysis for August 1 (Fig. 4 a) shows a narrow easterly current advancing over the Bahamas. At 0300 GCT the leading edge of the inner-

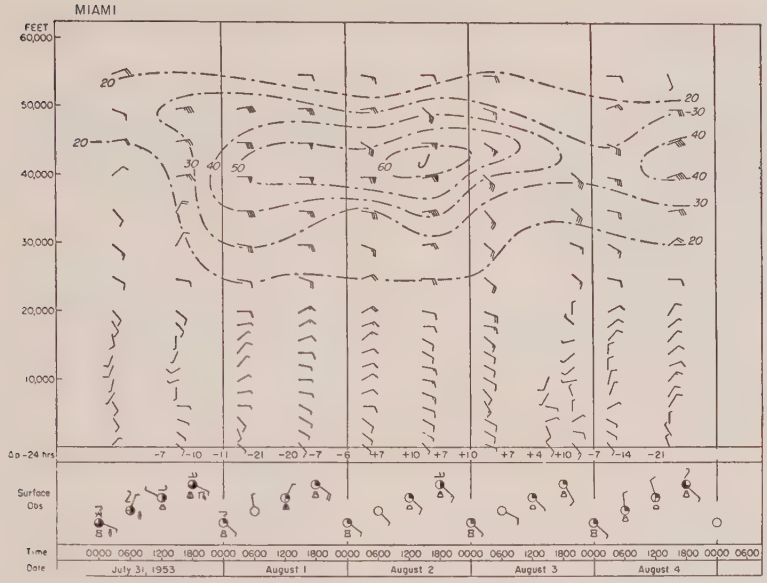

Fig. 3 c. Same as Fig. 3 b, for Miami, Florida.

most isotach, with a value of 50 knots, is just west of Miami which reports a 53 knot wind. A wind maximum is indicated northeast from there on the assumption (discussed below) of the continuity of the current with the winds reported by Ship H and Bermuda, together with the time sections for Coffin Hills (Fig. 3 a), High Rock (Fig. 3 b), and Miami (Fig. 3 c). Each of these stations shows a wind maximum subsequent to this time. If the isotach field is divided into four quadrants by the axis of the current, denoted by the thick line, and a line perpendicular to it drawn through the point of maximum wind speed (not entered on diagram), the cyclonic vortex noted in the 200-mb contour field can be located in the left forward quadrant.

The downstream propagation of the wind maximum can be seen from the successive positions of the leading edge of the 50-knot isotach, shown in Figure 8. The positions are fixed on the basis of a 43-knot wind at Burwood on August 3, 0300 GCT and an 48-knot wind at Shreveport on August 4, 1500 GCT and the assumption of a nearly constant rate of propagation between these observations. On this basis the leading edge of the 50-knot isotach shows a movement of about 3° latitude during the next 24 hours. This is about the same as the distance travelled by the cyclonic vortex, which thus retains unchanged its spatial correspondence with the wind maximum. This correspondence seems to persist throughout the period.

The maximum winds remain about the same or increase slightly up to August 2, 1500 GCT but show an unmistakable tendency to diminish thereafter as is evidenced by the progressively smaller area which can be enclosed within the 50 knot isotach after this date.

On August 3, 0300 GCT (Fig. 4 c), the fact

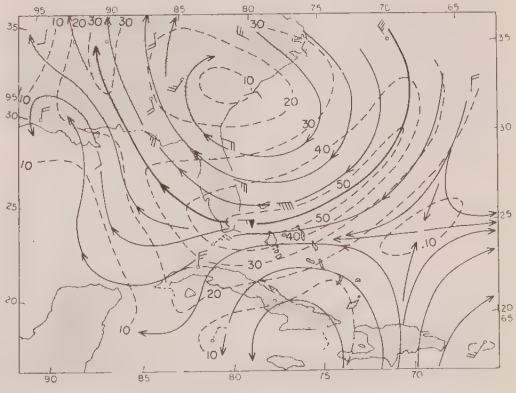

Fig. 4 a. 200-mb streamlines (full lines) and isotachs in knots (dashed lines) at 0300 GCT, August 1, 1953. Thick line denotes axis of current.

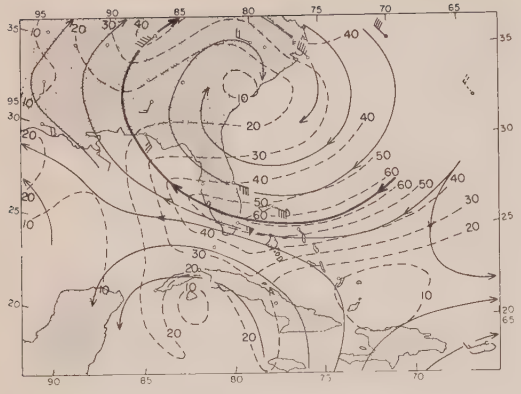

Fig. 4 b. 200-mb streamlines and isotachs, August 2, 0300 GCT.

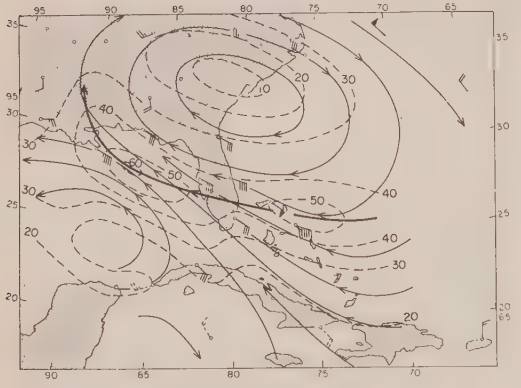

Fig. 4 c. 200-mb streamlines and isotachs, August 3, 0300 GCT.

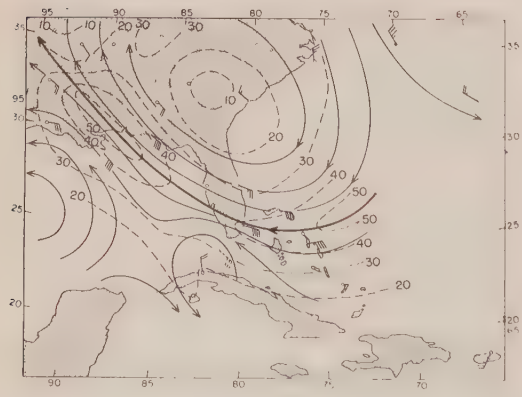

Fig. 4 d. 200-mb streamlines and isotachs, August 4, 0300 GCT.

that the winds at Miami and Tampa are weaker than that reported by either High Rock to the east or Burwood to the west, suggested a split of the current into two maxima. The new cyclonic vortex at 200 mb, drawn near Havana 24 hours later, is also located in the left front quadrant with respect to the rear maximum.

6. The Origin of the Current

The wind analysis in Figure 4 a is based on the inference that the easterly current which appeared over the Bahamas, originated in the middle latitudes as a branch of a split westerly jet which curved around the eastern periphery of the sub-tropical high cell centered over the eastern United States. The following evidence supports this inference:

a. On July 29, a jet stream with core velocities exceeding 130 knots was situated over the United States at about latitude 45° N. In the southerly fringe of the jet, the 200 mb wind directions changed from W—WNW over the continent to NW—N near the east coast, suggesting southward turning. Figure 9 shows the 200 mb winds at Bermuda and Ship H (latitude 36.8° N, longitude 69.6° W) during the period July 29 – 31. At Bermuda the wind direction fluctuated between N and NE. These observations together with the 45-knot northerly wind recorded at Ship H on July 30, suggest that a southern limb of the middle latitude jet stream was being injected into the tropics between the east coast and Bermuda.

b. On August 1, 0300 GCT, the 200 mb wind was northeasterly at Bermuda and easterly over the Bahamas and Miami. The 200 mb contours (not reproduced here) drawn for these winds and the reported heights show a channel extending from latitude 35° N to the Bahamas. By contrast, the contour field to the east of the Bahamas drawn to fit the southwesterly wind at San Juan and the southeasterly wind at Guantanamo, make it improbable that the current over the Bahamas was derived from the eastern or central tropical Atlantic.

Thus, unless the strong winds developed very close to the Bahamas, the inference is inevitable that the current appearing east of Florida must have been propagated from the middle latitudes. This statement, however, should not

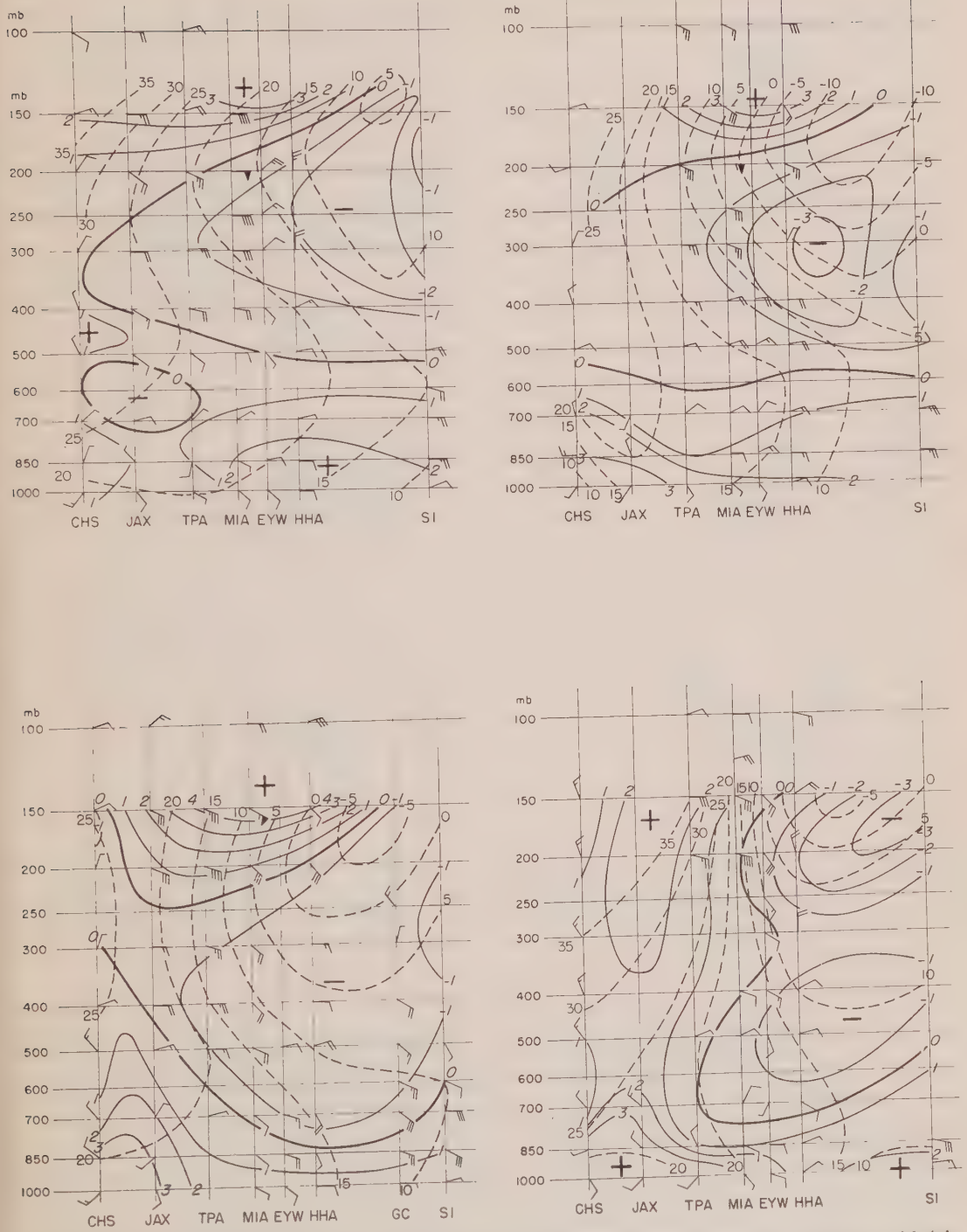

Fig. 5 a—d. Meridional cross sections showing temperature anomalies in degrees centigrade (full lines), and height anomalies in tens of feet from Schacht's mean tropical atmosphere at 0300 GCT on: (a) August 1, (b) August 2, (c) August 3, (d) August 4, 1953.

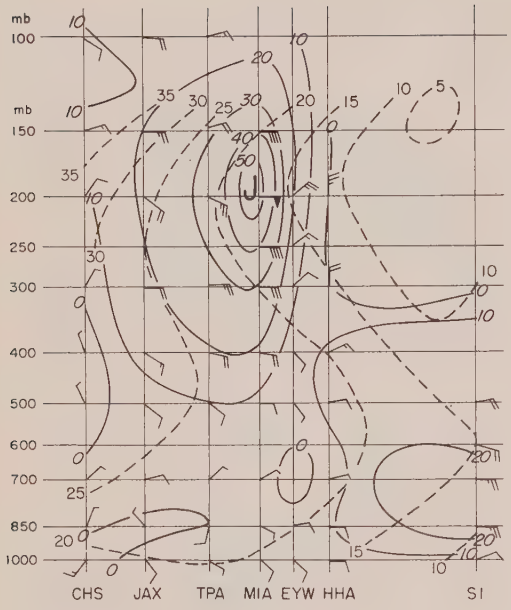

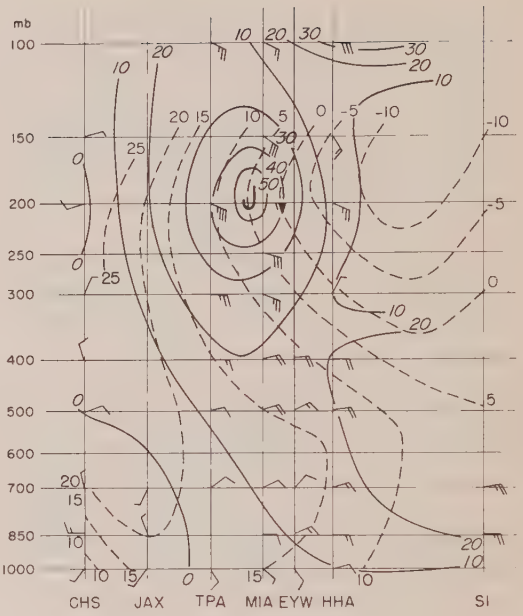

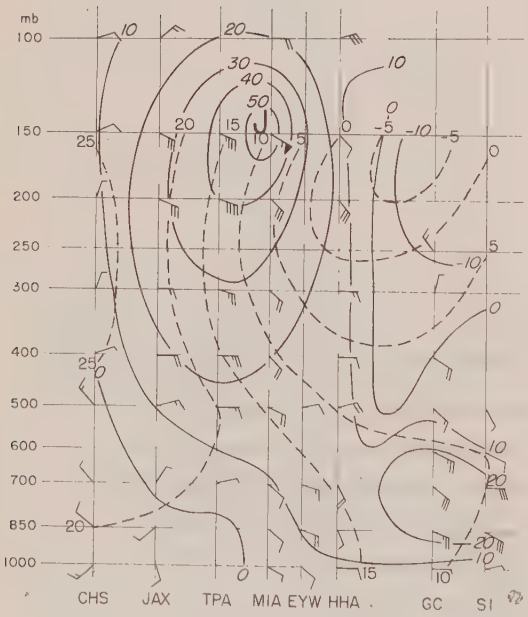

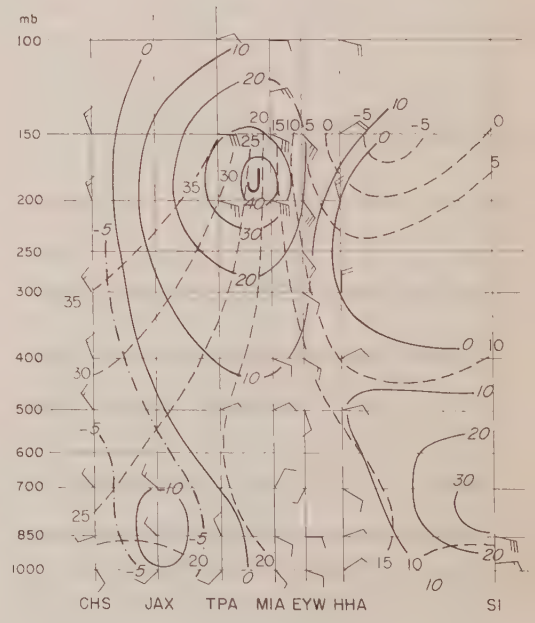

Fig. 5 e—h. Height anomalies in tens of feet from Schacht's mean tropical atmosphere (dashed lines) and isotachs of the observed zonal wind component in knots (full lines, easterly wind positive) at 0300 GCT on (e) August 1, (f) August 2, (g) August 3, (h) August 4, 1953.

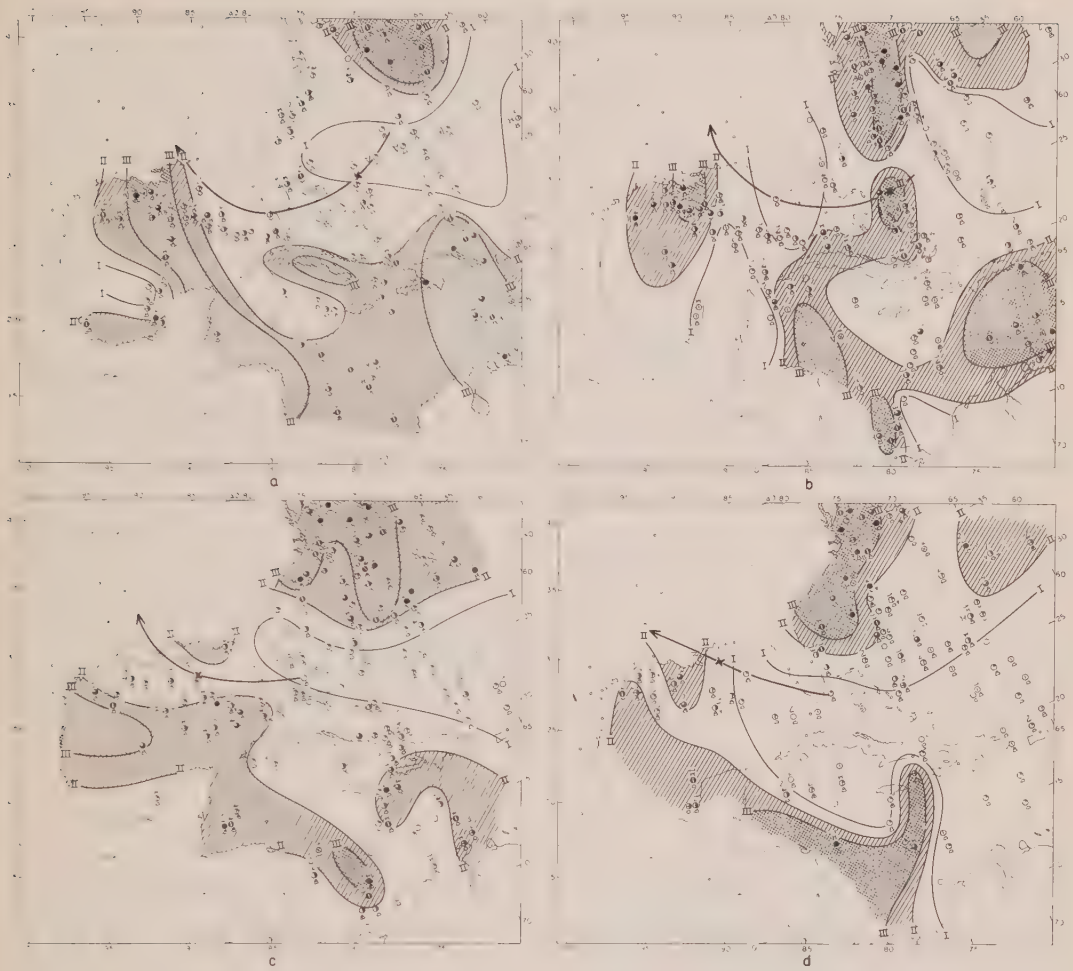

Fig. 6. Maps showing distribution of cloud cover on (a) August 1, (b) August 2, (c) August 3, (d) August 4, 1953. Lines marked III separate areas (cross hatched), where low cloud cover exceeds 5/10, from areas (hatched) where total cloud cover exceeds 5/10. Lines marked II separate latter from areas with total cloud cover less than 5/10 and more than 3/10. Lines marked I enclose areas where total cloud cover is less than 3/10. Maps are constructed from 6-hourly ship reports during 24-hour periods beginning 1830 GCT (see text).

be taken to imply that merely an injection of high kinetic energy from the north is taking place. As shown by Figure 8, the 50 knot isotach moves at only 7.5 knots, about an order of magnitude less than the wind speed itself. This involves a continuous production of kinetic energy in the entrance zone as the air particles overtake the speed pattern, and a corresponding dissipation in the exit zone ahead of the speed maximum while the jet travels through the tropics.

7. Kinetic and Thermal Structure: a Comparison with other Jet Streams

a. *Is this current a jet stream?:* In order to answer this question, we have to define the term "jet stream". When first introduced into meteorology this term referred to a narrow current with high westerly winds embedded in a relatively quiescent ambient atmosphere and meandering eastward around the hemisphere. Since that time, studies have revealed a marked "streakiness" in the kinetic texture of

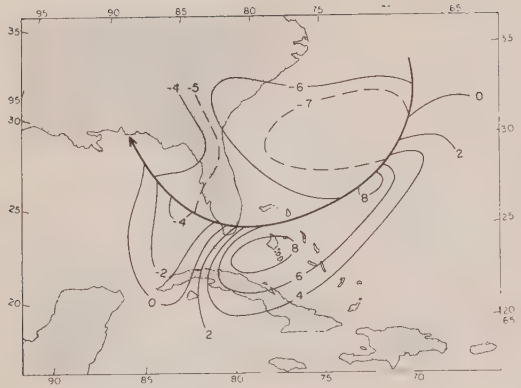

Fig. 7 a. Relative vorticity (10^{-5} sec^{-1}) at 200 mb on August 1, 1953 at 0300 GCT.

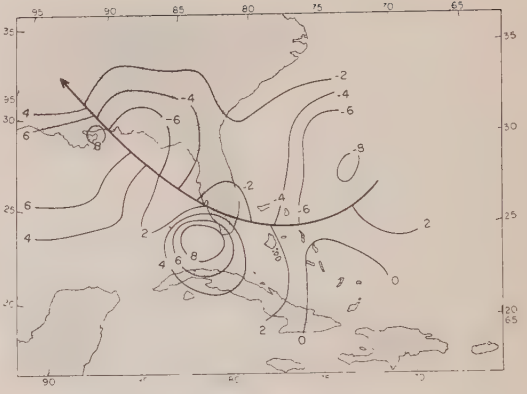

Fig. 7 d. Same as Fig. 9 c, for August 4.

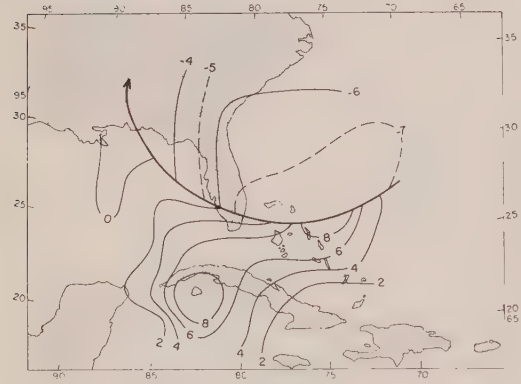

Fig. 7 b. Same as Fig. 9 a, for August 2.

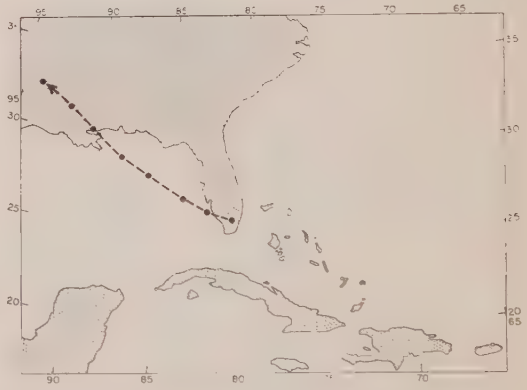

Fig. 8. Successive 12-hourly positions of the leading edge of the 50-knot isotach starting on August 1, 1953, 0300 GCT.

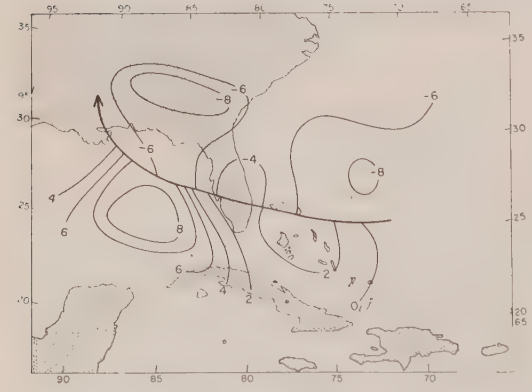

Fig. 7 c. Same as Fig. 9 b, for August 3.

JULY 1953	29		30		31	
	03 hr.	15 hr.	03 hr.	15 hr.	03 hr.	15 hr.
BERMUDA						
SHIP H						

Fig. 9. 200-mb wind at Bermuda and Ship H (lat. 36.8° N; long. 69.6° W).

this general current. The energy concentration occurs along multiple axes of limited geographical extent along which wind maxima alternate with regions of lower wind speed. The maxima are characterized by a vertical as well as a lateral concentration of momentum. They retain their identity for short periods of time but undergo constant modification as they propagate downstream with a speed considerably less than that of the wind of which their cores are composed. Following recent usage, we shall call a jet stream each individual axis along which the wind speed is concentrated laterally and vertically and which features one or more velocity maxima with the characteristics of life cycle and motion described above.

In the present case, the lateral and vertical concentration of the current is clearly revealed by Figures 4 a – d and 5 e – h. The wind distribution pattern can be traced over a period of four or more days as the leading edge of the current moves slowly from the Bahamas westward through the Gulf of Mexico, then northwestward to the United States. The successive 12-hourly positions of the leading edge of the 50-knot isotach (Fig. 8) show an average rate of motion of about 10 knots or about $^1/_5$ of its denomination.

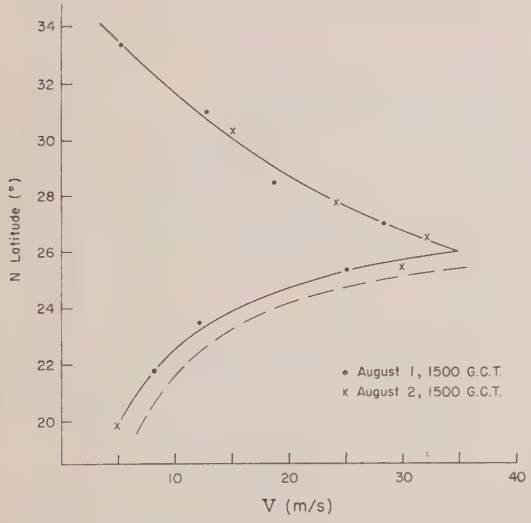

Fig. 10. A composite wind profile (solid line) along the 82° W meridian drawn from wind observations on August 1 and 2, at 1500 GCT by projecting the observed winds at nearby stations on the meridian. Points are plotted according to their distance from the wind maximum on each day. The dashed curve shows the distribution of wind velocity, drawn for the appropriate latitude belt, when the ratio of the absolute vorticity to the wind velocity is a constant with a value of $(150\ \text{km})^{-1}$.

Thus, in accordance with the definition stated above, the easterly current is a jet stream. An interesting feature of the present jet stream is its comparatively weak core velocities. Jet streams – or at least those of middle latitudes – have always been associated with high wind speeds. We note here the tendency of the currents in the upper troposphere to concentrate into narrow bands irrespective of the amount of maximum speed.

In spite of the weak core velocities, the present easterly jet reveals some structural features which appear to be determined by the same properties characteristic of the more intense westerly jet streams of the middle latitudes. Of these we cite the following:

b. *Cyclonic wind shear:* In a recent study, RIEHL and MAYNARD (1954) have noted that on the low pressure side of some jet streams the ratio of the absolute vorticity to the wind velocity is a constant (k) with a value of $(150\ \text{kms})^{-1}$. By integrating the differential equation describing this relation for straight currents they found that

$$V = \frac{f}{k} + \left(V_0 - \frac{f}{k}\right) e^{-kn} \qquad (2)$$

where V is the wind speed expressed in meters per second and is equal to V_0 at the reference point, and n is the distance normal to the current from the reference to the computed point.

Figure 10 represents a composite wind profile drawn from wind observations on August 1 and 2 at 1500 GCT projected on the 82° W meridian. The points are plotted according to their distance from the maximum wind on each day. The lower branch represents the wind profile on the low pressure side of the current. The dashed curve shows the meridional distribution of the wind velocity according to equation (2), drawn for the appropriate latitude belt. The fit between the latter and the observed wind profile is remarkable.

c. *Anticyclonic wind shear:* Computations based on both observed (RIEHL and MAYNARD, 1954) and geostrophic winds (PALMÉN and NEWTON, 1948) have revealed that on the high-pressure side of jet streams, the anticyclonic shears are such that the absolute vorticity has small positive values, with a small core of zero

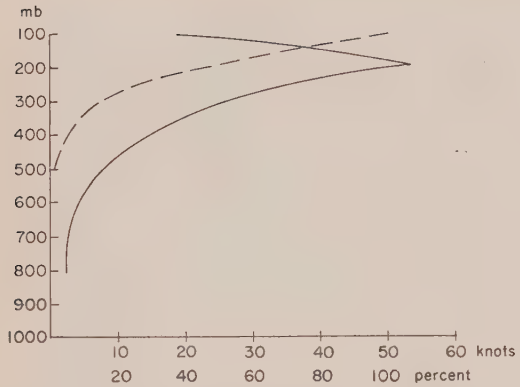

Fig. 11. Vertical profile (solid line) of easterly wind component through jet axis at 82° W meridian on August 1, 1953, 0300 GCT. Dashed line represents curve of cumulative percentage of kinetic energy from 1,000—100 mb.

or negative absolute vorticity within 150 kms from the axis. Our vorticity computations presented in Figure 7 bear out this fact. The negative relative vorticities to the right of the jet axis are everywhere numerically slightly less than, or equal to, the Coriolis parameter, except in narrow regions where they are numerically slightly higher than the Coriolis parameter, indicating negative absolute vorticity.

d. *Vertical concentration:* A majority of jets, especially those occurring at lower latitudes and in summer are restricted to a shallow layer in the upper troposphere. Often conditions at 500 mb give no indication of those higher up. The present case is no exception in this respect, as is readily revealed by an inspection of figures 3 a – c and 5 e – h. The vertical concentration of the kinetic energy is graphically portrayed by Figure 11 in which the full line represents the vertical profile of the easterly wind component[1] on August 1, 0300 GCT at the latitude of strongest easterly wind along the 82° W meridian (see Fig. 5 e). The average shear between 300 and 200 mb is about 4×10^{-3} sec^{-1}. The dashed curve shows the cumulative percentage of the kinetic energy from 1,000 to 100 mb, corresponding to the wind profile. Only a negligible percentage of the kinetic energy is found below 400 mb and fifty-four percent of the total is concentrated in the shallow layer 100 – 200 mb.

The vertical shear of 4×10^{-3} sec^{-1} is of the same order of magnitude as that observed in the much more intense middle latitude westerly jets in winter. But a distinguishing feature of the latter is the co-existence of a frontal layer beneath the jet core which contributes an appreciable percentage of the total vertical wind shear. For example, the mean cross-section drawn by PALMÉN and NEWTON (1948) from 12 cases in December, 1946, shows that fully one-third of the total increase in the troposphere occurs in the shallow frontal layer. No such layer exists in the present case.

e. *The thermal structure:* The thermal field shown by the full lines of figure 5 a – d reflects the independence of the concentrating mechanism of any temperature contrast between two air masses in the lower and middle troposphere. In fact, on August 1 and 2 (Fig. 7 a, b) the layers below 500 mb show a "reversed" temperature gradient, indicating a decrease of wind with height at the latitude of the jet core. On August 3 and 4 (Fig. 5 c, d) the northward temperature gradient underneath the jet core extends nearer to the surface but it is quite certain that no air mass contrast is involved.

8. The Balance of Forces

The continuous production and destruction of kinetic energy in jet stream regions is associated with a distinctive pattern of particle acceleration and deceleration. The manner in which this pattern is related to the structure and motion of jets is best studied by considering the laws of motion valid for particles near jet stream axes.

Aside from the vertical pressure force which is balanced by the force of virtual gravity, the balance of forces on a particle in relative horizontal motion is conveniently described by two equations: A tangential equation,

$$\frac{dV}{dt} = -g\frac{\partial h}{\partial s} + F_s \qquad (3)$$

and a normal equation,

$$\frac{V^2}{R} + fV = -g\frac{\partial h}{\partial n} + F_n \qquad (4)$$

In the above equations V is the horizontal wind speed, h the geodynamic height, s and n

[1] This profile closely approximates that of the total wind in view of the small deviation of the latter from the easterly direction.

unit distances respectively along and to the left of the direction of motion, f the Coriolis parameter, R the radius of curvature of the trajectory, and F_s and F_n the respective frictional forces in the s and n directions.

The frictional forces in the free atmosphere are in general assumed negligible in comparison with the other terms in equations (3) and (4). The validity of this assumption is not *a priori* evident in jet stream regions where strong lateral and vertical wind shears occur. We shall, therefore, attempt to determine to what extent such an assumption is justified in the present case. We thus write

$$\frac{dV}{dt} = -g\frac{\partial h}{\partial s} \tag{5}$$

or

$$V_2 - V_1 = -g\int_{t_1}^{t_2}\frac{\partial h}{\partial s}dt \tag{6}$$

and find out whether this equation is balanced.

The integration of equation (6) is performed along a trajectory traversed during the time interval $t_1 - t_2$. The subscripts 1 and 2 respectively refer to quantities at the initial and terminal points of the trajectory.

The computation of the right-hand side of equation (6) in its present form involves measurement, along the trajectory, of the angles between contours and wind. In view of the smallness of these angles the error in their measurement may be percentually large. In order to circumvent this difficulty, we write,

$$\frac{dh}{dt} = \frac{\partial h}{\partial t} + V\frac{\partial h}{\partial s} + w\frac{\partial h}{\partial z}$$

and if we neglect vertical motion, equation (5) becomes

$$V\frac{dV}{dt} = -g\left(\frac{dh}{dt} - \frac{\partial h}{\partial t}\right)$$

Multiplying both sides by dt, integrating over the period $t_1 - t_2$, and denoting the heights at t_1 and t_2 repectively by h and h' we have

$$\frac{V_2^2 - V_1^2}{2} = -g\left[(h_2' - h_1) - \int_{t_1}^{t_2}\frac{\partial h}{\partial t}dt\right]$$

The integral on the right-hand side of the above equation expresses the local height change occurring over the trajectory during the time $t_2 - t_1$. We assume a linear distribution of this quantity; this assumption is justified if no extreme values of local height changes occur between the initial and terminal points of the trajectories. The integral then becomes

$$\int_{t_1}^{t_2}\frac{\partial h}{\partial t}dt = \frac{h'_1 - h_1}{2} + \frac{h'_2 - h_2}{2} \tag{7}$$

Substituting the above value and defining $\overline{V} = \frac{V_1 + V_2}{2}$, equation (6) reduces to

$$V_2 - V_1 = -g/\overline{V}\left[\frac{(h'_2 + h_2)}{2} - \frac{(h_1 + h'_1)}{2}\right] \tag{8}$$

Putting $\frac{h_2 + h_2'}{2} = \bar{h}_2$, the mean height at the terminal point of the trajectory during the time interval $t_1 - t_2$, and $\frac{h_1 + h_1'}{2} = \bar{h}_1$, the mean height at the initial point of the trajectory during the same time interval we have,

$$V_2 - V_1 = -g/\overline{V}(\bar{h}_2 - \bar{h}_1) \tag{9}$$

The terms of equation (9) are readily computable from contour and wind maps. Table 1 shows the result of six such computations performed during the period August 1 – 3. The computations were made along 12-hour trajectories starting at Miami and High Rock at 0300 GCT. These stations were selected because of their positions near the axis of the jet, and also because the ends of the 12-hour trajectories were located over or near the southern United States where height and wind observations at nearby stations made the computations easier to perform and subject to less error. Furthermore, the passage of the wind maximum across these stations makes the computations representative of conditions both ahead and behind the jet.

The above method, aside from the fact that it does not depend on the measurement of the small cross-contour angles of the wind, has the added advantage that the acceleration of a particle along a trajectory is measured even though the acceleration is zero at the initial

and terminal points of the trajectory. Consider, for instance, the trajectory of the particle between two maps, and assume that on both these maps, the streamlines and the contours coincide. Nevertheless, the particle is accelerated during the time interval between the two maps and this acceleration can be computed by evaluating the right-hand side of equation (9).

The computations are, of course, subject to error. The uncertainty in drawing the trajectories and the assumption of linear variation of height changes in time and space constitute the main sources of error. However, because of the low wind speeds and the comparatively short distances involved, the error in locating the terminal points of the trajectory is smaller than would be the case in fast-moving westerlies.

A simple test of the accuracy of the trajectories and also of the consistency of the analysis of the wind and pressure fields can be made with the help of equation (4). Again neglecting friction, we solve for the radius of curvature of the trajectory:

$$R = -\frac{V^2}{fV + g\dfrac{\partial h}{\partial n}} \qquad (10)$$

Table 2 compares the radius of curvature thus computed with that measured from the trajectories at Miami and High Rock on August 2 – 4. The correspondence between the two quantities is very close.

Tables 1 and 2 indicate that the jet is maintained by pressure heads and that the continuous production and destruction of kinetic energy occurs as a result of accelerations in more or less laminar flow rather than by lateral or vertical frictional stresses.

The unbalance between wind and pressure is further illustrated in Figure 12 in which the easterly components of winds observed at 0300 GCT during the period August 1 – 4 are plotted against the corresponding geostrophic winds. Both the observed and computed winds were averaged along the 82° W meridian over a belt 4° of latitude in width, centered at the latitude of maximum winds. The shift from super- to sub-geostrophic winds attending the passage of the wind maximum across the 82° W meridian between August 1 and 4 is clearly discernible. The fact that on August 3 after the passage of the maximum, the winds are still supergeostrophic is associated with the rapidly weakening core winds after August 2.

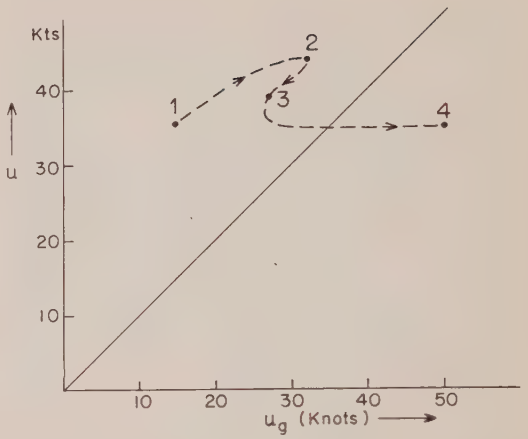

Fig. 12. 200-mb geostrophic vs. observed easterly component averaged over 4° L zone centered at latitude of maximum wind, at 0300 GCT during the period August 1—4, 1953.

Table 1. A comparison of the left hand side (column A) and the right hand side (column B) of equation 8 made from measurements along 12-hour trajectories at 200 mb starting at Miami and High Rock at 0300 GCY (see text).

Station	Date	A (mps)	B (mps)
Miami	August 1	12.0	10.6
High Rock	August 1	7.5	7.4
Miami	August 2	15.0	10.7
High Rock	August 2	1.5	.7
Miami	August 3	—3.0	14.1
High Rock	August 3	3.0	1.9

Tabel 2. A comparison between the measured and computed radii of trajectory curvatures at 200 mb on August 1—3, 1953, 0300 GCT at Miami and High Rock. All curvatures are anticyclonic.

Station	Date	Measured (°latitude)	Computed (°latitude)
Miami	August 1	9.0	7.5
High Rock.....	August 1	9.0	7.5
Miami	August 2	15.0	12.5
High Rock	August 2	8.5	7.5
Miami	August 3	35.0	35.0
High Rock	August 3	20.0	15,0

9. Divergence and Vorticity; Distribution of Weather Activity

The distribution of upper tropospheric divergence can also be determined by considering the distribution of vorticity which, in the present case, depends mainly on the wind shear normal to the jet axis.

a. *The distribution of vorticity:* Figure 7 shows that with the exception of August 1, 0300 GCT, the relative vorticity is positive to the left and negative to the right of the axis indicating the preponderance of the shear over the curvature term in equation (1).

The distribution of the positive relative vorticity to the left of the axis is such that a vorticity maximum is associated with every speed maximum and the cyclonic vortex which accompanies it. The movement of these vorticity maxima in response to the movement of the jet center is easy to follow by comparing Figures 4 a–d and 7 a–d. The relative vorticity in general increases downstream behind the wind maxima and decreases ahead of them. The maximum relative vorticities computed do not exceed twice the Coriolis parameter – a value much less than that observed on the low pressure side of some vigorous middle latitude jet streams in winter.

To the right of the axis the relative vorticity decreases downstream behind the wind maxima and increases ahead of them. Here, the negative relative vorticity is numerically less than or equal to the earth's vorticity except in a small region some distance away from the velocity maxima where its value numerically exceeds the Coriolis parameter, indicating small negative values of the absolute vorticity. Such small values are within the limit of computational error but should not *ipso facto* be discounted as spurious. A discussion of the vorticity equation will help elucidate this point. Stripped of the small frictional and solenoidal terms and also of the terms relating to the curvature of the earth's surface, the vorticity equation is as follows:

$$\frac{d\zeta_a}{dt} = -\zeta_a \operatorname{div}_2 \mathbf{v} + \frac{\partial V}{\partial z}\frac{\partial w}{\partial n} \qquad (11)$$

The first term shows that divergence reduces and convergence increases the vorticity of a particle and the last term describes the influence of vertical motion in changing vorticity about the vertical. In general, the latter term is considered insignificant compared to the divergence term and the vorticity equation is often written

$$\frac{d\zeta_a}{dt} = -\zeta_a \operatorname{div}_2 \mathbf{v} \qquad (12)$$

There is little doubt that equation (12) is accurate enough in most cases, especially in regions of strong cyclonic vorticity as, for instance, to the left of jet stream axes. In such cases particle vorticity changes are very sensitive to horizontal divergence, or convergence. Air subject to sustained convergence will increase its cyclonic vorticity without any theoretical limit. On the other hand, when ζ_a approaches zero the vorticity changes become insensitive to horizontal divergence. Indeed, equation (12) does not allow for the decrease of the absolute vorticity below zero. Accordingly, if this equation always represented the true condition of the atmosphere negative absolute vorticities would be dynamically inadmissible.

But, as pointed out by BJERKNES (1951), as ζ_a approaches zero, the divergence term becomes less important than the last term of equation (11) and the vorticity equation becomes

$$\frac{d\zeta_a}{dt} = \frac{\partial V}{\partial z}\frac{\partial w}{\partial n} \qquad (13)$$

This equation does not place any restriction against the occurrence of negative absolute vorticities and lends credence to the existence of such values in limited regions to the right of jet stream axes, as indicated by figures 7 a – d, and as has also been found by previous investigators (RIEHL and MAYNARD, 1954; PALMÉN and NEWTON, 1948).

b. *The distribution of divergence:* The distribution of divergence can be discussed by applying equations (12) and (13), respectively, to the left- and right-hand portions of jet streams. Considering the left side of a steady jet stream with its axis oriented east—west, moving down stream with constant speed c, we may write from equation (12),

$$(V - c)\frac{\partial \zeta}{\partial s} = -\zeta_a \operatorname{div}_2 \mathbf{v} \qquad (14)$$

neglecting the vertical vorticity transport. Upstream from the wind maximum $\partial\zeta/\partial s$ is positive indicating convergence. In the downstream quadrant $\partial\zeta/\partial s$ is negative; here divergence prevails. If the 200-mb chart is located above a level or surface of non-divergence located somewhere in the middle troposphere, it follows from mass continuity reasoning that the air must ascend upstream and descend downstream from the wind maximum.

Proceeding to the right of the jet stream axis and applying equation (13)

$$(V-c)\frac{\partial\zeta}{\partial s}=\frac{\partial V}{\partial z}\frac{\partial w}{\partial n}, \quad \text{or}$$

$$\frac{\partial w}{\partial n}=\frac{(V-c)\,\partial\zeta/\partial s}{\partial V/\partial z}$$

In the right rear quadrant the vorticity decreases downstream and therefore the term $\frac{\partial V}{\partial z}\frac{\partial w}{\partial n}$ is negative. At 200 mb, $\partial V/\partial z$ is positive as can be seen from Figures 3 and 5. Therefore $\partial w/\partial n$ must be negative, i.e., w increases to the right. The order of magnitude of this rate of increase can be estimated. Since

$$\frac{\partial V}{\partial z}\sim 10^{-3}$$

$$\frac{\partial w}{\partial n}\sim\frac{10^{3}\cdot 10^{-12}}{10^{-3}}\sim 10^{6}$$

or 1 cm sec^{-1}/10 km.

The horizontal shear of the vertical motion normal to the current is thus very sharp near the jet axis. In view of the small vertical velocities in the atmosphere, the subsidence prevailing to the left of the axis must soon give way to rising motion, active weather conditions, and upper air divergence to the right of the axis. But this rapid increase in vertical motion will not persist a long distance from the axis since the advective term $(V-c)\,\partial\zeta/\partial s$ decreases rapidly away from the jet stream axis.

A similar argument can be applied along the leading edge of jet streams to show that active weather conditions with upper air divergence in the left front quadrant rapidly give way to settled conditions and upper air convergence across the jet axis.

The above discussion deals with the simple case of a jet with its axis oriented east—west. When the latter has a north—south component, the above model is modified in the following manner: where the flow is directed toward lower latitudes, conditions of organized convection are accentuated and vice-versa.

In summary, we may state that the distribution of vorticity visualizes, under model conditions, upper divergence, and therefore upward motion and active weather conditions in the front left and rear right quadrants; and upper convergence and therefore descending motion and inactive weather conditions in the front right and rear left quadrants.

c. *A discussion of the weather situation:* An instance when the weather distribution closely follows model conditions, is that occurring to the right of the jet axis during the period studied. The area or organized convection situated west of Bermuda on August 1, and whose leading edge reaches the north-west coast of Florida by August 4, follows the movement of the jet maximum and is all the time located in the rear right quadrant of the jet stream. The prevalence of suppressed convection over Florida on August 2 is similarly attributable to the downstream increase of vorticity in the right front quadrant of the jet stream.

Often conditions are more complicated when the weather is determined by a combination of two or more weather producing systems, each with its own typical weather distribution. Certain weather features are then intensified while others are damped, depending on the phases in which the different systems meet. The weather distribution to the left of the jet axis during the period August 1–4 provides an interesting illustration of this fact. Three different weather producing systems, each ordinarily capable of occurring indepedently of the other two, and each characterized by a distinctive weather pattern co-exist:

1. Waves in the lower easterlies. The weather distribution, associated with these systems differs from case to case depending on the slope of the trough and ridge lines with height and the vertical variation of the basic current (Riehl, 1954). More often than not, however, there is a tendency for organized convection to occur to the east of the surface trough line and suppressed convection to the west of it.

2. Zones of wind shear in the upper troposphere. Such zones frequently occur over the

Caribbean in summer. Typically, they have a west—east orientation with easterly winds to the north and westerly winds to the south. They slope northward with height with unsettled weather often occurring beneath this slope (RIEHL, 1954).

3. A jet stream with a model weather distribution as described at the beginning of this section.

The actual weather distribution can be discussed from the viewpoint of net particle vorticity changes resulting from the resonance or interference of the above systems.

These changes are brought about in a different manner near and away from jet streams. Near jet stream axes, vorticity is determined mainly by the horizontal wind shear. Vertical motion is determined chiefly by the horizontal variation of this quantity near the level of strongest winds, while the vertical transport plays only a secondary role. Away from jet streams, on the other hand, vorticity is determined mainly by the curvature of the streamlines, and the variation of this property with height may be as important as the horizontal transport of vorticity.

The above fact is illustrated by the area of organized convection situated west of Puerto Rico, and that occurring over Cuba on August 1 (Fig. 6). Over the former area, the 15 knot wind at San Juan is greater than the rate of westward propagation of the trough line. Air particles in this region are therefore approaching the trough and gaining cyclonic curvature. This indicates that convergence predominates at least up to this level. Particles rising through this level lose cyclonic curvature as they arrive into the anticyclonically curved flow at 200 mb where divergence, therefore, prevails.

Over Cuba, on the other hand, the curvature is more cyclonic at 200 mb than at 500 mb; nor does the cyclonic curvature decrease downstream at the former surface. The organized convection is due to the downstream decrease of vorticity occurring at 200 mb due to the strong horizontal wind shear associated with the jet stream.

The above case also illustrates the interference between the easterly wave trough and the jet stream. The area of disturbed weather occurs to the west of the surface position of the trough line[1] which is ordinarily characterized by suppressed convection. Air particles are moving away from the trough line at 500 mb, thereby losing cyclonic curvature. At 200 mb, particles flowing into the region are, if anything, gaining cyclonic curvature. This situation would be conducive to upper air convergence and descending motion except for the presence of the jet stream which is so situated that the downstream decrease of vorticity at 200 mb associated with it (Fig. 7 a) produces a net upper air divergence.

The area of organized convection over the western part of the Gulf of Mexico on August 3 is one in which the jet stream and the easterly wave trough meet in the same phase. The downstream decrease of vorticity at 200 mb (Fig. 7 c) due to the advance of the jet stream north of this region occurs east of the surface position of the surface wave trough as determined from the time section of Brownsville. Both are favorable for organized convection.

10. Acknowledgements

The writer wishes to thank Professor Herbert Riehl for his help and for much advice and criticism during this study. Thanks are also due to Mrs. Della Friedlander who drafted the figures, and Mr. John Bryant who photographed them.

[1] As deduced from time-sections.

REFERENCES

RIEHL, H., ALAKA, M. A., JORDAN, C. L., and RENARD, R., 1954: The Jet Stream. *Meteorological Monographs.* Amer. Meteor. Soc., **2.** No. 7, 100 pp.

BJERKNES, J., 1951: Extratropical Cyclones. *Compendium of Meteorology*, pp. 577—598.

COLÓN, J., 1954: A Case Study of the High Tropospheric Wind Field Over the Caribbean Region in Spring. Mimeo. report, Dept. of Meteor., Univ. of Chicago, prepared under Contract N° N6ori-02036, Project NR 085003, Office of Naval Research.

CRESSMAN, G. P., 1950: Variations in the Structure of the Upper Westerlies. *J. Meteor.*, **7**, 39—47.

FULTZ, D., 1951: Experimental Analogies to Atmospheric Motion. *Compendium of Meteorology*, pp. 1235—1248.

FUGLISTER, F. C., 1951: Multiple Currents in the Gulf Stream System. *Tellus*, **3**, 230—233.

NEWTON, C. W., and CARSON, J. E., 1953: Structure of Wind Field and Vorticity in Summer. *Tellus*, **5**, 321—339.

Palmén, E., 1951: The Role of Atmospheric Disturbances in the General Circulation. *Q. J. Met. Soc.*, **77**, 337—354.

—, and Newton, C. W., 1948: A Study of the Mean Wind and Temperature Distribution in the Vicinity of the Polar Front in Winter. *J. Meteor.*, **5**, 220—226.

Petterssen, S., 1950: General Circulation. *Cent. Proc. Roy. Met. Soc.*, 120—155.

Riehl, H., 1948: Studies of Upper Air Conditions in Low Latitudes, I. *Misc. Report N° 24*, Dept. of Meteor., Univ. of Chicago.

—, 1954: *Tropical Meteorology*. New York: McGraw-Hill Book Co., 392 pp.

Riehl, H., and Maynard, H., 1954: Exploration of the Jet Stream by Aircraft During the Winter of 1953. Mimeo. Final Report prepared under Contract N° 189s-88360 between Project AROWA of the Bureau of Aeronautics, Department of the Navy and Dept. of Meteor., Univ. of Chicago.

Rossby, C.-G., 1953: A Comparison of Current Patterns in the Atmosphere and in the Ocean Basins. *Proc. U.G.G.I., 9th Gen. Assembly, Brussels, Autumn 1951* (publ. 1953).

Schacht, E. J., 1946: A Mean Hurricane Sounding for the Caribbean Area. *Bull. Am. Meteor. Soc.*, **27**, 324.

The Easterly Jet Stream in the Tropics*

By P. KOTESWARAM, Meteorological Office, Calcutta Airport

(Manuscript received February 2, 1957)

Abstract

It is shown that in summer an easterly jet stream overlies southern Asia in the high troposphere with core near 15° N. This current is quasi-geostrophic. Below the level of strongest winds temperatures decrease from right to left across the current looking downstream; above the level of strongest wind (150-100 mb) the reverse is true. Distribution of cloudiness and precipitation in the lower monsoon correspond to that noted in association with westerly jet streams in the temperate zone: precipitation downstream from the region with the highest winds to left of the axis, upstream to the right.

The foregoing holds on individual days and climatically during the monsoon season as a whole. Since an easterly jet stream is observed only over southern Asia (and Africa), but not over the Pacific and Atlantic oceans, it is suggested that the current originates in connection with the large-scale arrangement of land masses and oceans, and with the elevated heat source of the Tibetan plateau.

Introduction

Numerous writers have studied high tropospheric jet streams as an important part of the general circulation. During the last decade jet streams have been located and described in various parts of the world. Progress has been most satisfactory in middle and high latitudes, while in the tropics the high location of jet streams and scarcity of data has retarded research. Several attempts have been made to locate and study westerly jet streams in the tropics. CHAUDHURY (1951) constructed a cross-section along 75° E based on data from the winter of 1946. YEH (1950) has analyzed the jet over China. The author (1953) has studied location and characteristics of the jet stream over India and Burma during the cool season; he also computed mean vertical motions (1954). RIEHL (1954) has pointed out the intermittent existence of a westerly jet stream in the central tropical Pacific during summer.

Easterly winds in the high troposphere have presented many puzzling features. Mean upper wind charts prepared by VENKITESHWARAN (1950) for India and surroundings show a wide belt of easterlies in the high troposphere and stratosphere over India during summer. Strong winds from the east have been noted over southern India in summer during periods of weak monsoon when pilot balloons could be followed to great heights. With the aid of these winds KRISHNA RAO (1952) inferred the existence of an easterly jet stream and constructed a vertical cross-section. KRISHNA RAO and GANESAN (1953) pointed out that these winds may reach 110 mph during July and August in the tropopause layer. FROST (1952) noted that at Aden the easterlies reach an average maximum of 70 knots between 150 and 100 mbs in summer. DAVIS and SAMSON (1952) noted winds of similar strength over Nairobi which they attributed to an easterly jet stream near the equator. They found that

* This research was performed under contracts between the Office of Naval Research and The University of Chicago, while the writer was on leave of absence at The University of Chicago.

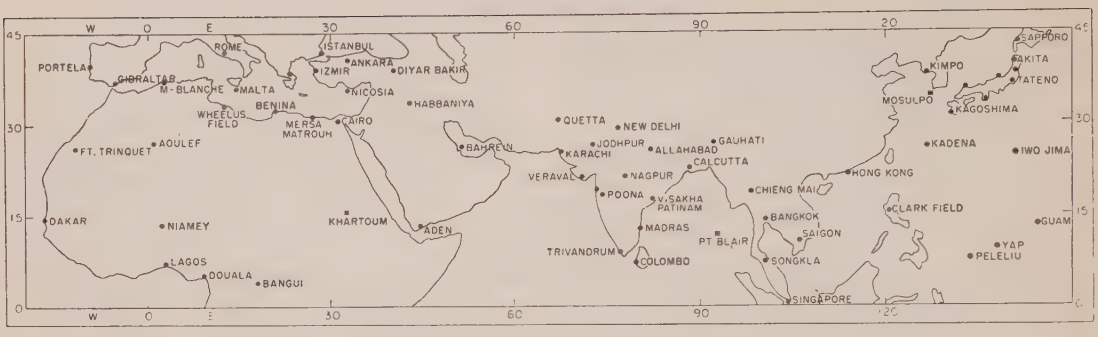

Fig. 1. Radiosonde and Rawin stations used in analysis.

the easterlies reach highest speeds during December—February and July—September, both dry seasons at Nairobi. Austin (1953) further analyzed the rawin observations at Aden, and Hay (1953) those at Singapore and Hongkong. The latter found that high-level easterlies prevail throughout the year at Singapore and in summer at Hongkong. They attain speeds of 90 knots at Singapore and 80 knots at Hongkong but the thickness of the layer of strongest winds is confined to a few thousand feet. Clarkson (1956) made a statistical analysis of Singapore winds; he finds them remarkably constant in direction; speeds occasionally reach to 100 knots in August and September. He also observed that the high-level meridional flow is strongest from north at the peak of the summer monsoon season; the reverse occurs during the winter monsoon.

While all these observations confirm the existence of strong easterlies in the high troposphere in some parts of the tropics, they do not necessarily indicate the existence of jet streams, since this requires strong lateral as well as vertical shear. The first welldocumented case study of an easterly jet stream (Alaka 1955) was made in the Caribbean where such currents are rare but where a good network of rawinsonde stations exists. Alaka found an easterly current with central speed of 75 knots. The current was confined to the region of the southern Bahamas and Florida; the strongest winds were situated near 200—150 mb. Alaka thought that this current had originated in middle latitudes and appeared at the southern periphery of a subtropical high after curving around this cell. A similar case has been discussed by Newton and Carson (1953) in connection with the formation of summer shearlines over the United States.

Since strong easterlies are frequent over southern Asia and eastern Africa, but rare over the Pacific and Atlantic Ocean areas, it was considered appropriate to study the high-tropospheric flow of the tropics over Asia and Africa with a view to jet stream analysis and an understanding of the upper wind circulation in these regions and their interaction with the large-scale circulation feature of the lower troposphere—the summer monsoon. The main features of the analysis are presented in this paper. Fuller details are available in a research report of the Department of Meteorology, University of Chicago (1956).

Data Utilized and Methods of Analysis

A survey as just indicated requires good rawin coverage. Unfortunately, daily analysis with radiosonde data alone is unreliable in the tropics since instrumental errors often have the same magnitude as synoptic differences. Radiosonde data averaged for the whole summer of 1955, however, give a fairly representative picture of the high-tropospheric flow pattern. Establishment of rawin stations at Madras, India, and in Thailand has been very useful, though one would wish for a still closer network. Collection of data from many sources is always difficult; in this respect the daily northern hemisphere data published by the U.S. Weather Bureau since July 1955 have proved very helpful. Data for India have been obtained from the Indian Daily Weather Report.

The area studied covers the tropics from the equator to 40° N, and from 20° W to 150° E.

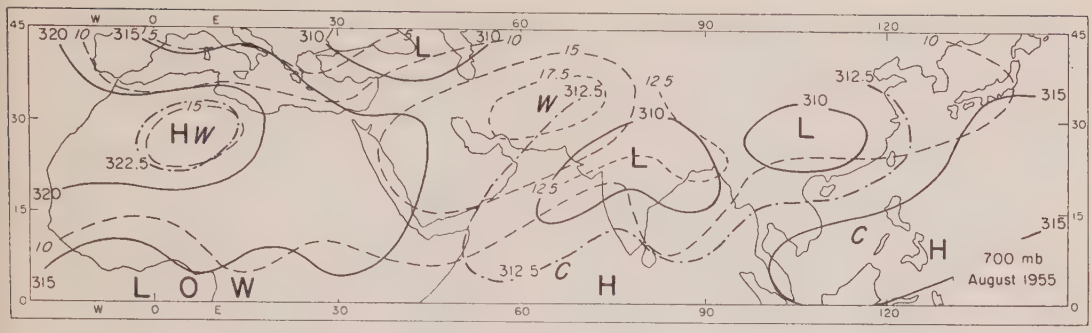

Fig. 2 a.

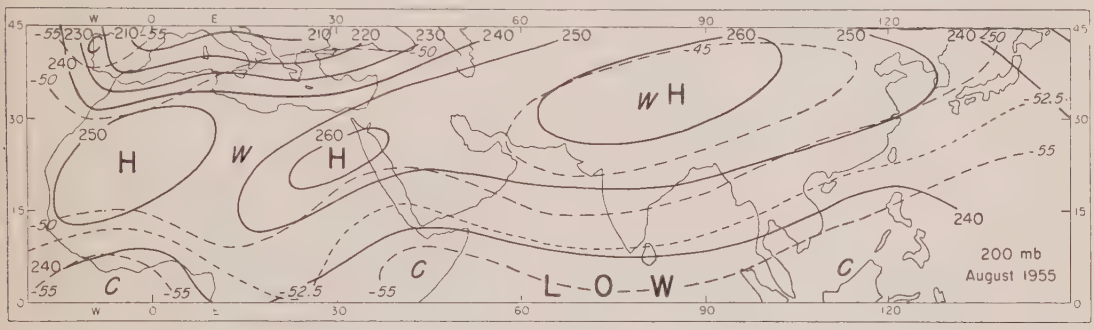

Fig. 2 b.

Fig. 2 a and 2 b. Mean isotherms (°C, dashed) and contours (10's m, first digit omitted at 200 mb) for August 1955 at 700 mb and 200 mb.

Fig. 1 shows the rawin and radiosonde stations in this area. The following types of analysis were performed.

Vertical time section
Horizontal space-time sections
Stream lines on isobaric surfaces
Isotachs on isobaric surfaces
Vertical cross-sections

Techniques used in preparation of these analyses are well known and need not be repeated. Time sections were made for as many stations as possible; the sections extended over the whole summer of 1955. They are as valuable for analysis of jet stream maxima as for features such as passages of wave troughs and closed circulations. A horizontal space-time section was constructed for the Indian area at 40,000 feet projecting each rawin station at its appropriate parallel; the purpose of the section was to observe the relations between the southwest monsoon and the high-tropospheric flow patterns.

For reasons already indicated, streamline analysis was preferred to constant pressure analysis. With an adequate number of stations streamlines give a reliable picture of the broad flow patterns. No attempt was made to draw streamlines with the isogon technique; for this the network of stations was not sufficiently dense. Isotach analysis was carried out at 300 200 and 100 mb.

Structure of the Tropical Troposphere in Summer

Climatology of upper winds: Most prominent in the lower troposphere is the equatorial trough which migrates as far as latitudes 20—25° N over the Asian-African continent during the northern summer; it is accompanied by the spectacular summer monsoon of southern Asia. A broad westerly current overlies the Arabian Sea, Bay of Bengal and the Gulf of Siam. Occasionally it reaches across the South China Sea to the western Pacific. This current—called southwest monsoon in

India and Indian westerlies farther east—extends to 10,000—20,000 feet, occasionally 30,000 feet. It is a persistent feature of the general circulation over southern Asia from June to October.

PALMER (1951, 1953) concluded after a study of the Marshall Island region that the equatorial westerlies in the low levels merely represent a statistical mean of individual westerly currents connected with westward moving cyclones and that they do not form a branch of the general circulation. RIEHL (1954), on the other hand, pointed out the great steadiness of the westerly component of the Indian monsoon. It should be mentioned here that the low latitude westerlies are confined to southern Asia and parts of equatorial Africa; they do not appear as a persistent current anywhere else. Thus any model of the general circulation must account for this special location.

In the high troposphere, a train of cyclonic and anticyclonic vortices tends to progress westward at least over the western Pacific (RIEHL, 1948) and over the Atlantic. Over the Asian monsoon region such vortices occur only rarely; high-level winds are generally easterly south of the Himalayas and westerly to their north. Similar cells also exist over the deserts of Africa and Arabia.

Mean Flow during summer: As an illustration of the mean flow pattern during summer Fig. 2 gives mean contours and isotherms at 700 and 200 mb for August 1955 over tropical Asia and Africa. These two levels generally represent the flow patterns in the lower and upper tropospheres respectively. Noteworthy is the existence of a Low over India and farther east at 700 mb, while to the west no such Low can be found. The surface heat lows which generally extend from northwest Africa to northwest India are shallow and restricted to the layer below 700 mb. Aloft a high is located over these regions; this high extends to the tropopause. Over the Asian monsoon region the subtropical anticyclone builds only above 500 mb. This anticyclone overlies the Tibetan plateau and probably extends to southwestern China.

Most striking at 200 mb is the concentrated contour gradient north of the African cell indicating a westerly jet over the Mediterranean. We note a similar though weaker gradient south of the Asian subtropical high, which *suggests an easterly jet stream over southern Asia.* The easterly gradient reaches its highest value between 150 and 100 mb; here the strongest easterlies will be located.

Mean temperature field and "intertropical front": In the low troposphere isotherms are concentrated off the Arabian coast, because of juxtaposition of desert air (T_c) and monsoon air or equatorial westerlies (E_m). The discontinuity between these airmasses has been given various names, such as intertropical front, equatorial convergence, etc. RAMANATHAN and BANERJI (1931) and SAWYER (1947) have studied this discontinuity. The former postulated a nose-like structure of the "front" since the steep lapse rate in the desert air would result in lower temperatures aloft than in the monsoon air. SAWYER utilized this structure to explain thunderstorms over northwest India. However, since the anticyclone over Arabia and Iran is associated with low-tropospheric divergence and descent, small temperature lapse rates are often observed in the desert air well above the surface layer with the result that temperatures remain higher in desert than in monsoon air. Above 300 mb the isotherms in Fig. 2 extend east-west with lower temperatures toward the equator. Thus the "nose" structure of the "ITF" is quite doubtful. In the low troposphere there is frequently a stable inversion where T_c overlies E_m; weather along the "front" then consists in stcu above the monsoon layer as often experienced at Karachi.

Over India the equatorial trough, locally called "monsoon trough", extends from western Pakistan to the head of the Bay of Bengal. The monsoon curves around this trough from the Bay of Bengal into northern India and the Himalayan foothills, resulting in the well-known monsoon circulation. No thermal contrast is observed in the trough, though there is a slight decrease of temperature from north to south.

Since the monsoon trough produces most summer precipitation over India, many Indian meteorologists have pictured it as a warm front type discontinuity, relying upon the slightly higher temperatures of the easterlies north of the trough. The easterlies are called "turned monsoon air" (*EmT*) (ROY 1946) or tropical maritime air from the far east (MALURKAR 1950, DESAI 1951 a). Many attempts

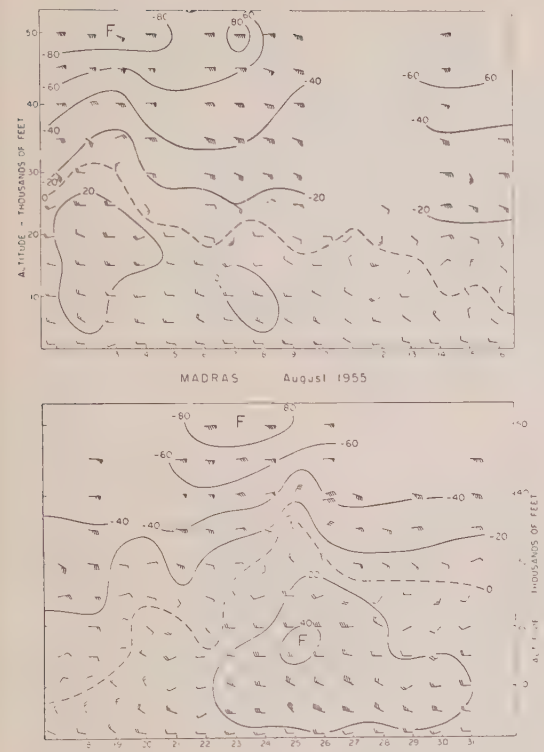

Fig. 3. Vertical time section of upper winds at Madras for August 1955, Easterly speeds negative. Short barb 5 knots, long barb 10 knots, pennant 50 knots.

to explain Indian weather with "fronts" have resulted from this assumption. The ITF which BJERKNES (1933) had terminated at the Himalayas was extended through the monsoon trough by DESAI (1951 b). Without repeating the well-known arguments about non-existence of fronts in tropical regions, it would suffice to speak of a convergence zone.

High Tropospheric Jet Stream

The mean flow pattern just described has indicated strong easterlies at high levels along the southern margin of Asia. In order to determine whether these winds are concentrated in jet streams, daily analysis up to 100 mb was undertaken for July and August 1955. As mentioned earlier, low latitude data are still scarce and high level ascents are missing on many days. Nevertheless, sufficient evidence remains to demonstrate the existence of a core of easterlies near 15° N. This current forms off the east coast of China and extends through India and Arabia at least as far as the Sudan. A second current appears to start near 10° N along the African west coast; it must dissipate over the eastern Atlantic since it is not observed in the Caribbean or along the Guiana coast of South America.

Time sections: Time sections of the following rawin stations have been examined, for the following stations: New Delhi (28° 35′ N, 77° 12′ E), Calcutta (22° 39′ N 88° 27′ E), Bombay (19° 05′ N, 72° 53′ E) and Madras (13° N, 80° 11′ E). Similar data do not exist at lower latitudes over India,[1] but the time section for Singapore (1° 22′ N, 103° 59′ E) has been looked into for comparison. Fig. 3 gives the time section for Madras for August 1955. Zero speed is marked with a dashed line, easterlies with negative sign and westerlies with positive sign. Observations are mostly for 0300 Z, supplemented by 1 500 Z data when the former were missing.

The following features have been noted:

1) Winds are mostly easterly at New Delhi up to 50,000 feet, but speeds rarely exceed 30 knots even at the top of the troposphere.

2) At Calcutta, monsoon westerlies predominate in the lower levels during the better part of the month. These westerlies frequently reach 20,000 feet, occasionally 30,000 feet. The high-tropospheric current is easterly and fairly steady with occasional ondulations. Easterly winds increase between 30,000 and 50,000 feet, where speeds of 30—50 knots are regularly attained.

3) Lower westerlies and upper easterlies are more steady at Bombay than farther north. The surface of separation lies generally near 20,000 feet, though with ondulations. As at Calcutta, the easterlies build between 30,000 and 50,000 feet, where speeds reach 60—70 knots.

4) Madras is the southernmost station in this series. Here also, the monsoon westerlies generally have a depth of 20,000 feet and occasionally they extend to 30,000 feet. The speed of the westerlies is greater than farther north; speeds as high as 40 knots are attained. In the upper easterlies 60—80 knots are reported at 50,000 feet. The flow in the high troposphere is quite steady, more so than near the ground; there are, however, some interruptions of the rapid easterly flow, as from August 7 to 9.

[1] A rawin station has been started at Trivandrum in September 1956.

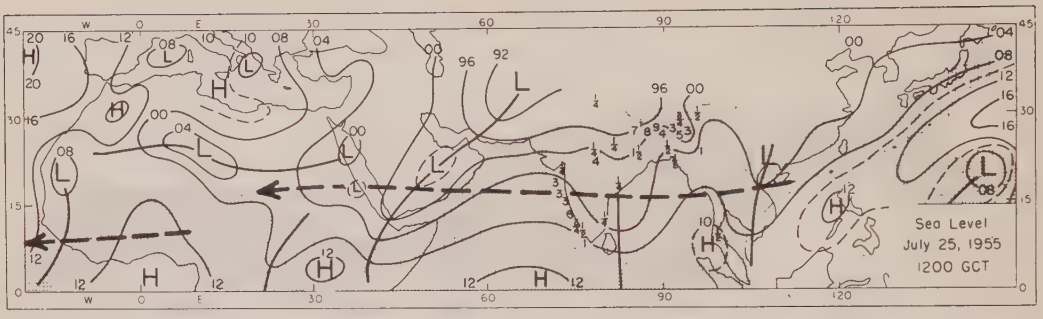

Fig. 4 a. Sea leval isobars (mb. first two digits omitted) July 25, 1955. Clouded area shaded. Figures over India and neighbourhood indicate 24 hours rainfall in inches.

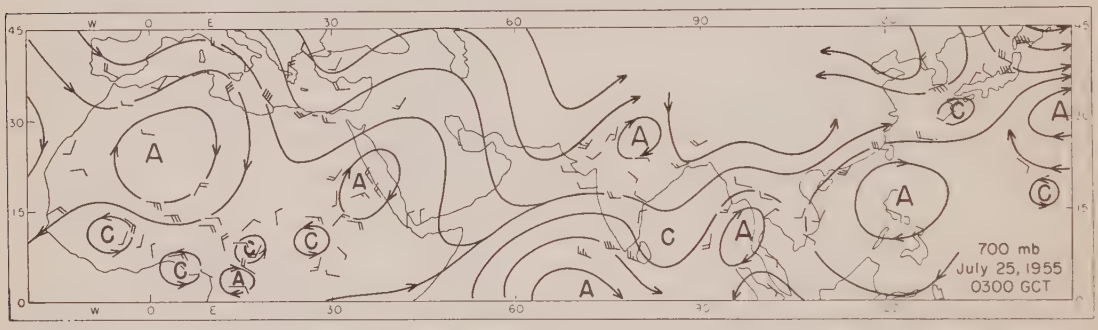

Fig. 4 b. Streamlines at 700 mbs, July 25, 1955.

The time sections indicate that the speed of the easterlies increases with decreasing latitude at the highest tropospheric levels. Singapore lies far off the longitude considered but its time section affords an interesting comparison with those of India. Here also, there are lower westerlies. These are generally confined below 15,000 feet; during part of the period they are not present. As over India steady easterlies blow in the upper troposphere and speeds as high as 80—90 knots occur. Speeds however are variable, ranging from 20 to 80 knots at 50,000 feet.

The situation of July 25, 1955: On this day the observations were reasonably complete and the upper wind structure was quite definite, with easterly speeds above 100 knots. The flow pattern as standard isobaric levels upto 100 mbs have been examined. Fig. 4 shows surface isobars, also streamlines at 700 and 200 mb. Isotachs have been drawn at 200 mb.

a) Wind structure: At the surface (Fig. 4 a) we observe a series of "heat lows", situated roughly along latitude 20° N; the easternmost of the lows lies over western Pakistan near 30° N. A monsoon trough is not present over India. The situation is one which is locally described by the statement that the monsoon trough lies close to the Himalayas. The flow over India and farther east is mainly westerly. A southwesterly current extends off the Asiatic coast to Japan and then merges with the temperate westerlies. The equatorial westerlies are strong in the Arabian Sea.

At 700 mb (Fig. 4 b) the situation over Africa and Arabia looks quite different. The surface heat lows have given way to subtropical anticyclones. In contrast, the westerly flow persists over Asia, and a pattern of well marked troughs and ridges in the westerlies is discernible.

The low latitude westerlies are replaced everywhere by easterlies at 500 mb. The African and Arabian cells persist and new ones appear over Iran, India and the Phillippines. The configuration of the easterlies is wavy, with an apparent "wave length" of 25° longitude over the North Indian Ocean and the western Pacific.

The subtropical anticyclones arrange them-

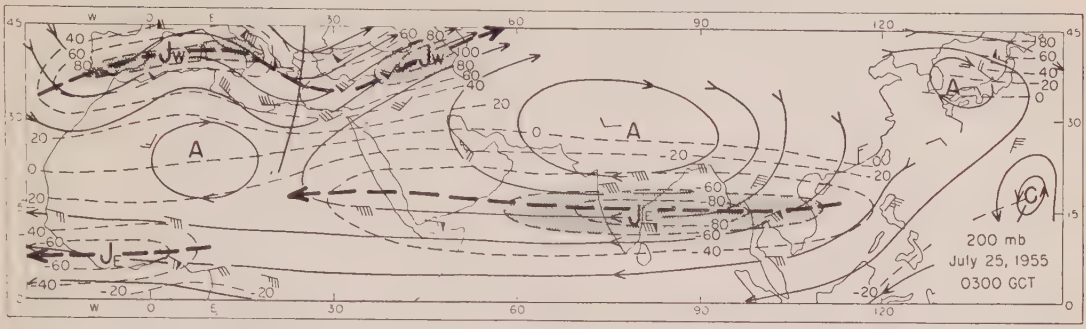

Fig. 4 c. Streamlines and isotachs 200 mbs, July 25, 1955. Jet axis marked heavy and wind maxima shaded.

selves roughly along 25° N at 300 mb over the Asian and African continents as the easterly flow in the lower latitudes increases in speed and becomes less wavy. North of the anticyclones, a well marked westerly current overlies the Mediterranean and Iraq, with characteristics of a jet stream. Such a current is also observed over northern Japan.

The 200-mb chart (fig. 4 c) indicates intensification of both easterly and westerly currents with two well marked anticyclones over northern Africa and the Himalayan plateau. Wind speeds exceed 100 knots in the westerlies and 80 knots in the easterlies. Concentration of the easterlies into a narrow current is clearly seen from 300 mb upward. At Bangkok (13° N) the speed is 69 knots compared to 47 knots at Chiengmai (18.5° N) and 32 knots at Songkla (7° N). One also notes equatorward flow in the "entrance" region (Hongkong 360°, 15 knots) and poleward flow in the "exit" region (Bahrein 140°, 27 knots).

The 100-mb pattern is similar to that at 200 mb except that the westerly current weakens between these two surfaces, while the easterly current strengthens, at least to about 150 mb. At Bangkok 102 knots is reported. At Aden the highest speed occurs at 48,000 feet (81 knots); then there is a rapid upward decrease to 38 knots at 53,000 feet. The center of the easterly current lies roughly along 15° N. It starts building over the South China Sea. The greatest strength is attained over southern India, while over Africa the current is weakening. The core of the easterlies appears to lie at a somewhat higher altitude in the eastern portions (Bangkok 55,000 feet) than in the western part (Aden 48,000 ft).[2]

b) Thermal Structure: The thermal pattern, as that of the winds, resembles the mean charts described earlier. At 700 mb the warmest air is located over Arabia, Iran and western Pakistan; the strongest temperature gradient is found over the Arabian Sea. At 500 mb the warmest air is situated in the subtropical ridge near 25° N. The 300-mb pattern resembles that at 500 mb except that temperature gradients on both sides of the subtropical ridge are stronger. At 200 mb, the temperature gradient over southern Asia is still well marked. In contrast, the gradient has reversed over northern Africa and Japan indicating that the 200-mb surface lies above the strongest westerlies.

The thermal pattern at 100 mb is spectacular. The temperature field has reversed in the easterlies in accord with the wind observations. A belt of very cold air extends from the Palau Island across Thailand and central India to Arabia and upper Egypt. Another cold pool starts near the coast of equatorial Africa and reaches into the Atlantic. Analysis of the 100-mb temperature field over the Atlantic and Pacific Oceans and over Central America indicates that this pool of coldest air is confined to the equatorial zone over the rest of the globe. It is only over the Asian-African continents that it appears at

[4] Songkla (7° N) reports 100 knots at 50,000 feet. This speed is considered doubtful because speeds are only 40 to 50 knots at 45,000 and 55,000 feet. The report has been omitted from the analysis.

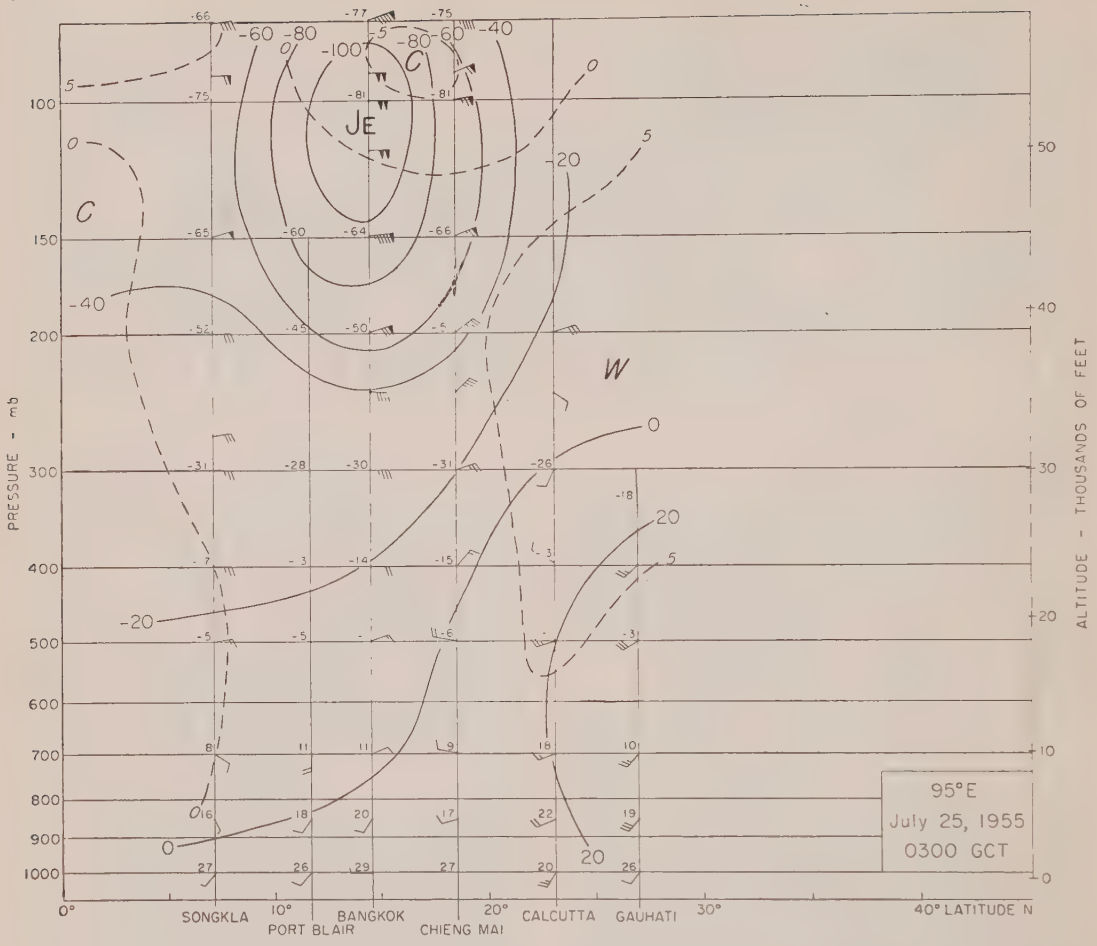

Fig. 5 a. Vertical cross-section of wind and of temperature anomaly (°C) from the mean tropical atmosphere along 95° E July 25, 1955. Isotachs solid, east components marked negative. Isolines of temperature anomaly dashed. Double dashed line is tropopause.

higher latitudes in association with the concentrated easterly current.

c) Vertical cross-sections: Vertical cross-sections have been constructed along six meridians over Asia and Africa. Isotachs and isanomals of temperature from the mean tropical atmosphere (SCHACHT 1946) have been drawn. Fig. 5 presents the vertical section along longitudes 95° E and 45° E. The following features are observed:

At 145° E only one jet stream is present—north of 45° N in the westerlies. An easterly maximum is noticed near 30° N at 100 mb and is probably part of the stratospheric easterly circulation which is known to reach at least 50 knots, often more, in the lower stratosphere (RIEHL 1948).

The stratospheric easterlies near 30° N are also found at 125° E. In addition another easterly maximum appears over the Philippines, probably the beginnings of the current which extends across the whole of southern Asia. Concentration of easterly kinetic energy takes place only above 250 mb in a layer about 10,000 feet thick.

At 95° E—Fig. 5 (a)—we observe the core with easterly speeds above 100 knots, described earlier. Again the current is hardly in evidence below 200 mb. Temperatures decrease from right to left across the current, looking downstream, below the core if the Port Blair report which evidently does not fit is omitted. Above the core the temperature field reverses.

The picture at 75° E is similar to that at

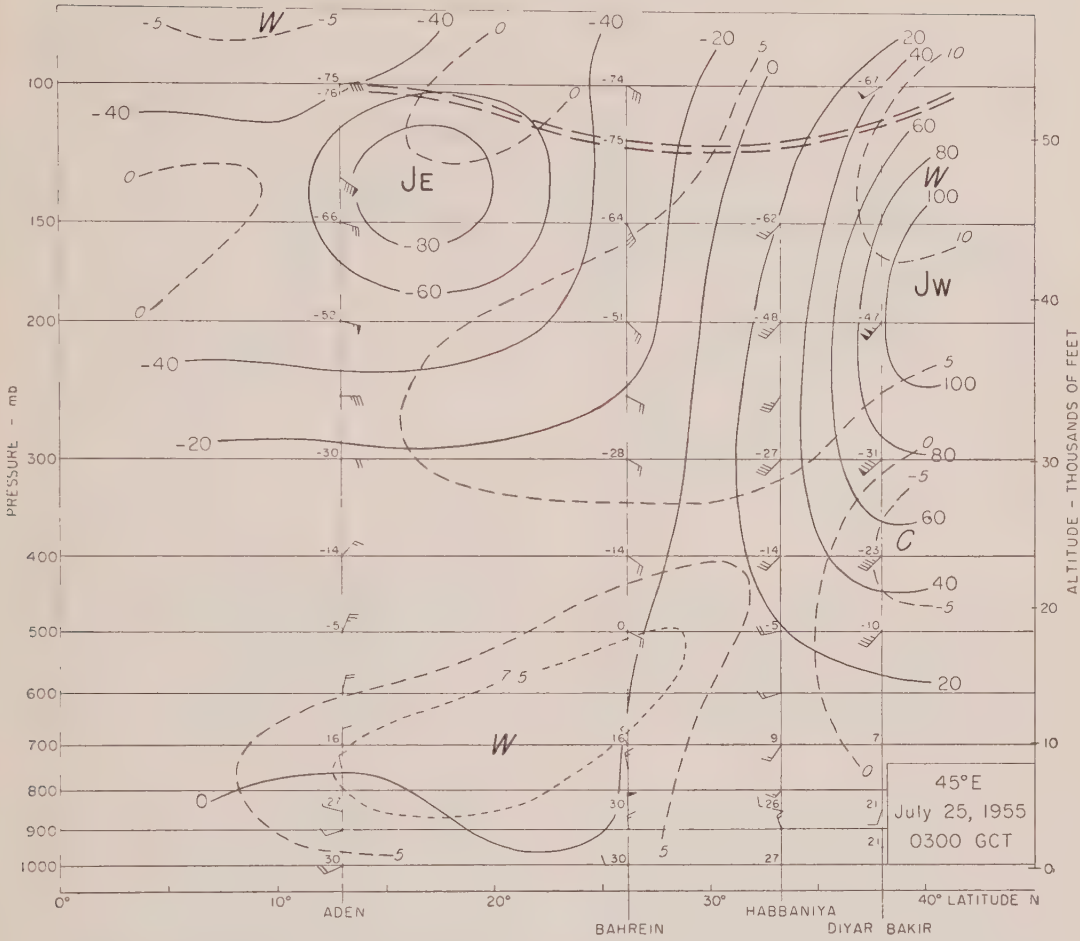

Fig. 5 b. Vertical cross-section of wind and of temperature anomaly along 45° E, July 25, 1955.

95° E both as regards wind and temperature structure. A 100 knot center could be inferred though direct evidence is lacking as the Madras ascent broke off at 200 mb. On the previous day a maximum of 89 knots had been reported at 100 mb.

We enter the decaying portion of the easterly current near 45° E—Fig. 5 (b). The core speed still exceeds 80 knots, however; the latitude of the core is the same as farther east but its altitude is about 7,000 feet lower. We observe the equatorward portion of a westerly current near 40° N. Large temperature gradients are encountered. In the lower and middle troposphere temperatures decrease poleward north of 25° N; above a transition layer with indifferent temperature field near 300 mb we find the warmest temperatures in the north with a gradual decrease southward—the pattern conducive to decrease of the westerly and increase of the easterly current with height. Above 100 mb we see still another reversal in the region of the easterly current. Thus the temperature fields associated with both easterly and westerly jet streams are particularly well brought out by this section.

At 30° E the easterly current has diminished further in intensity. The core speed is only slightly above 60 knots, and highest speeds occur between 200 and 100 mb. The temperature field resembles that at 45° E; the double jet stream regime is still in evidence.

At the Greenwich meridian, a wind maximum of 40 knots persists at 15° N which may

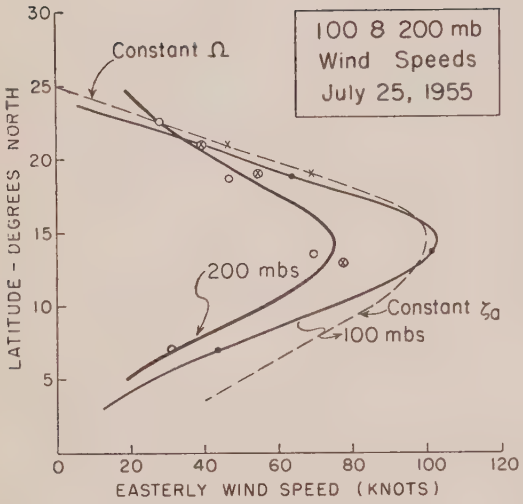

Fig. 6 a. Meridional profile of the east component at 100 mb and 200 mb using combined data from India and Thailand for July 25, 1955.

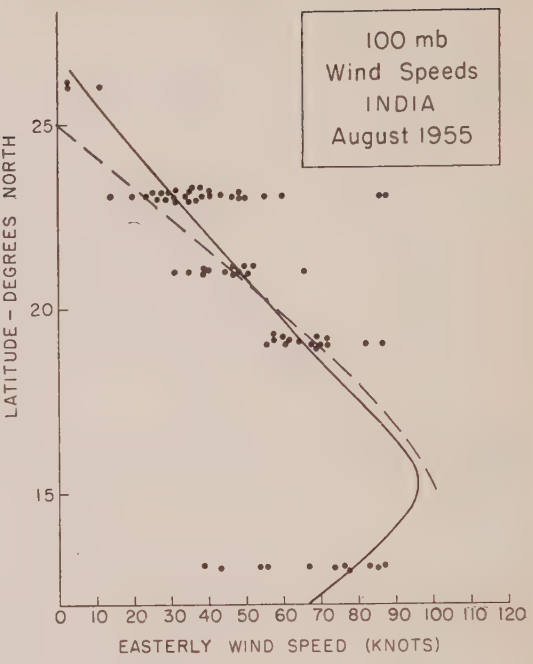

Fig. 6 b. Meridional profile of the east component at 100 mb for India using all observations for August 1955.

be a remnant of the Asian easterly current. A new core appears near 10° N with center at 200 mb. This current is also of limited thickness (about 15,000 feet), but the associated temperature field is complex and cannot be analyzed further in the present context.

d) Distribution of momentum and vorticity: Fig. 6 (a) shows meridional profiles of easterly wind speed at 200 and 100 mb using combined data from India and Thailand. The dashed line represents constant absolute angular momentum on the anticyclonic side assuming zero relative zonal velocity at 25° N, the latitude of equatorial trough and high tropospheric ridge line. On the cyclonic side, the dashed line represents constant absolute vorticity using the earth's vorticity at 15° N, the latitude of the core of the current, for the constant. The fit of the values at 100 mb, the level of strongest wind on the anticyclonic side, is quite good. In order to see to what extent constant angular momentum was observed over longer periods, a meridional wind profile was drawn at 100 mb using all rawin observations over India during August 1955 (Fig. 6 b). Dots represent individual observations, the full line is the mean speed profile and the dashed line is the same as in Fig. 6 a. The average anticyclonic shear amounts to nearly 4×10^{-5} sec^{-1}, while the mean value of the Coriolis parameter in the area considered is 5×10^{-5} sec^{-1}. Thus the mean wind distribution indicates nearly constant absolute angular momentum, or zero vorticity, on the anticyclonic side of the easterly core, quite similar to what is found on the anticyclonic side of mid-latitude westerly jet streams.

Lack of sufficient data prevents discussion of the wind distribution on the cyclonic side.

e) Vertical shear: We have seen during the analysis of the vertical cross-sections that concentration of easterly kinetic energy occurs only in a thin layer in the high troposphere. Fig. 7 shows vertical wind profiles for a number of stations situated close to the easterly core from longitude 120° E to 0°. In all of these profiles the easterlies increase, or the westerlies decrease, from the ground upward. The profiles are curved so that the strongest shear occurs just under the maximum speeds; the

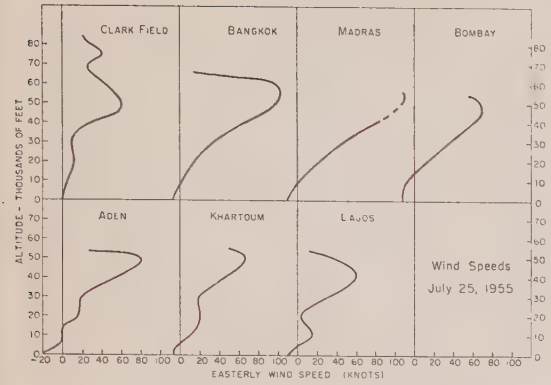

Fig. 7. Vertical profile of the east component at seven stations, July 25, 1955.

value of the strongest shear is $4—5\times 10^{-3}$ sec^{-1}. Above the level of strongest wind the profiles cannot be drawn with much accuracy due to lack of data. At some stations notably Bangkok and Aden, the upper shear greatly exceeds the lower one with values as high as 20×10^{-3} sec^{-1} at Bangkok. In contrast, the upper shear at Clark Field is very weak.

f) Rainfall and Cloudiness: Fig. 4 (a) shows the distribution of cloudiness over southern Asia and Africa at 1 200 Z, July 25, 1955, and rainfall in inches for the 24 hours ending at 0 300 Z, July 26, over India, Pakistan, Burma and Ceylon. The heavy dashed line marks the position of the easterly core. Concentration of cloudiness north of the core east of 75° E and south of the core farther west indicates the vertical currents associated with the core, i.e. ascent east of 75° E and descent west of this longitude north of the core and the reverse on the south side. Since, as noted earlier, the current is accelerating east of 75° E and decelerating farther west, a "direct" crosstream circulation is implied for the "entrance" zone of the current and an "indirect" circulation at the exit. Such a distribution of vertical circulation has previously been noted by the author and PARTHASARATHY (1954) in the mean westerly jet stream over India in the pre- and postmonsoon seasons. Since all of these results are in substantial agreement with findings in temperate zone jet streams, it follows that the type of vertical circulation pattern observed is independent of latitude or orientation of a jet stream. It also follows that there should be a close connection between fluctuations in the upper easterly current and fluctuations in the low-level monsoon. Before considering this subject we shall try to establish, using climatic data, to what extent the results of July 25, 1955, can be generalized for the summer monsoon season.

The easterly current related to rainfall over Asia and Africa in summer

Analysis of daily charts during the summer of 1955 has shown that easterly jet streams regularly exist over southern Asia and Africa during the summer monsoon season near 15° N. Assuming then, that the easterly jet is an average feature over this area during summer and that large scale ascent takes place north of the entrance and south of the exit region, we may examine the mean rainfall distribution over Asia and Africa with reference to the jet stream. Fig. 8 shows the average July rainfall and the average jet stream position. Rainfall data have been taken from HAURWITZ and AUSTIN (1944); for the Indian area charts published by the INDIA METEOROLOGICAL DEPARTMENT (1949) have been used. Over Asia, the rainy belt lies mostly north of the axis of the current, with

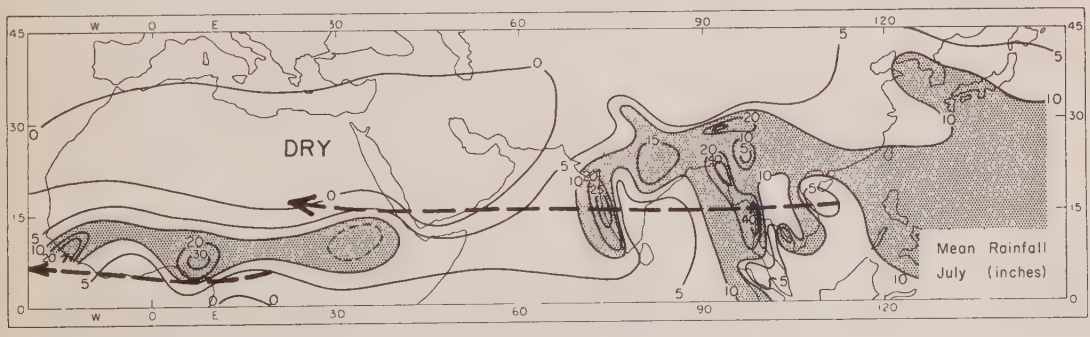

Fig. 8. Average July rainfall (inches) and easterly Jet stream position during August 1955.

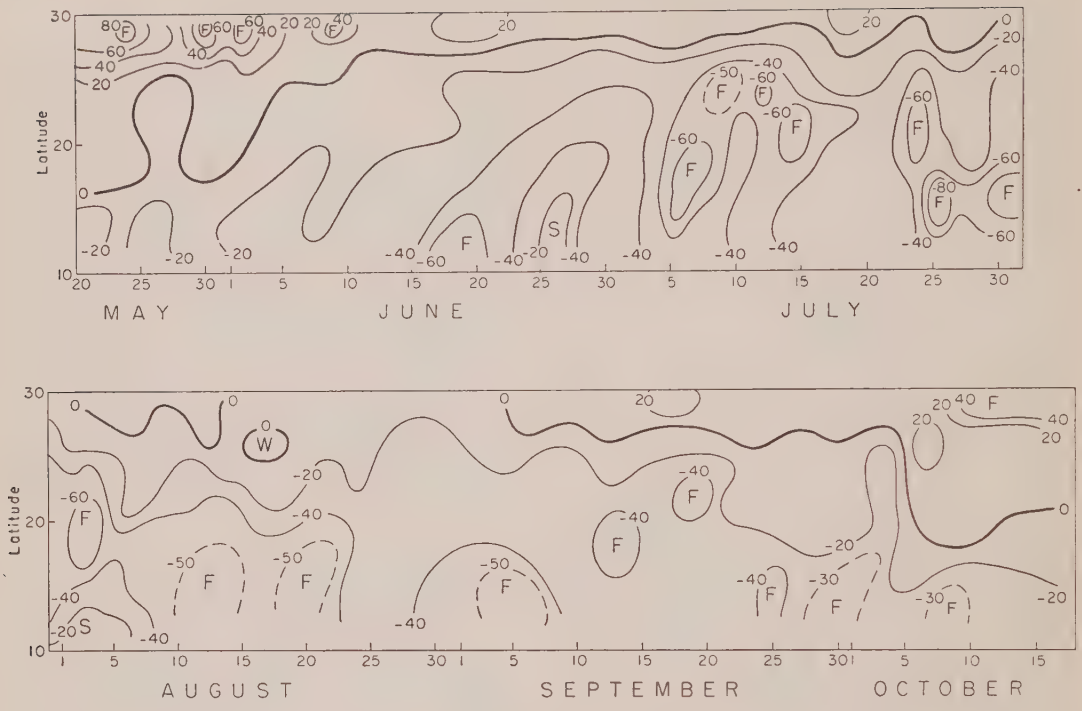

Fig. 9. Space-time section of 200 mb wind speed over India for the summer of 1955 (east components negative).

the exception of the mountainous west coast of India and the Tennaserim coast of Burma. But even along those coasts rainfall generally diminishes southward, as is well known. While interpreting the map, one should remember that the easterly current is not always in the accelerating stage over the Bay of Bengal; during periods when it decelerates in this region, there may be copious precipitation in the southern areas. The climatological distribution can be expected only to bring out the preponderant features. Since on most days the current accelerates east of the Indian Peninsula, the extensive rain areas over northeastern India, Burma and farther east are in accord with the large-scale ascent to be expected over these areas from the jet stream consideration.

West of the Indian peninsula the pattern is reversed. Here the current decelerates in the mean and large scale descent over the well-known deserts is the result. In fact, the deserts themselves may be attributed to this sinking in the higher levels in spite of intense surface heating. South of the axis of the current rainfall is confined to the region south of 10° N over Africa. Here, as noted in a previous paragraph, the principal upper-air feature probably is a new current forming at very low latitudes over Africa.

It thus appears that the easterly jet stream plays an important role in shaping the summer rainfall distribution over Asia and Africa, that it forms a part of the general monsoon system and that the monsoon in the low troposphere must be related to the high-tropospheric easterly current.

Fluctuations in the Monsoon Season

Burst of the monsoon: Yin (1949) has suggested that the monsoon bursts when the wintertime westerly jet stream, known to circle the southern periphery of the Himalayas, moves far enough north so that the major portion of the mass flow in this current is detoured to the north of the high mountain ranges. He noted that the monsoon advances first over Burma and later over India, and attributed this to a

westward shift of the through in the westerlies located over the Bay of Bengal during the cool season. This shift occurs together with the northward displacement of the westerlies aloft. The author and PARTHASARATHY (1954) have also observed a progressive northward shift of the mean westerly wind maximum during the pre-monsoon season.

Fig. 9 shows a time-space section of 200-mb wind speeds for the whole monsoon period from May to October 1955. The northward shift of the westerlies at the time of the burst of the monsoon on the west coast of the Indian peninsula is spectacular. However, strong westerly winds are still reported intermittently by stations north of 30° N even after the onset of the monsoon. Peshawar (34°), for instance, reported a westerly wind of 64 knots and Lahore (31.5° N) 42 knots on June 6, 1954, when the monsoon had advanced halfway up the peninsula. One June 12 Lahore reported 280°, 67 knots, at 30,000 feet and Peshawar 270°, 55 knots. By that time the monsoon had extended to 20° N. It thus appears that the westerlies make incursions into western Pakistan even after the onset of the monsoon and that not untill the subtropical anticyclone is established over the Himalayas will westerly winds disappear completely from the region south of the mountains.

It is of interest to investigate the location of the easterly jet stream at the time of onset of the monsoon. Fig. 10 shows the upper winds at Madras for the period May 23—30, 1955. Unfortunately most balloons stopped at or below 200 mb. One can see however that the easterlies are still light on May 25 but reach values over 60 knots on May 27. A trough formed off the Malabar coast on the 26th and the monsoon advanced into Malabar by the 28th, when Trivandrum had 4 inches of rain. On may 29th the India daily weather report announced that the monsoon had revived over Malabar.[3] At that time upper winds at Aden were still weak; 27 knots from 100° was observed at 100 mb on May 27. Easterlies exceeding 50 knots set in at Aden after June 6. Thus it is probable that the easterly current which had advanced to southern India on May 27 was in the decelerating stage and that the core was so placed that the ascending

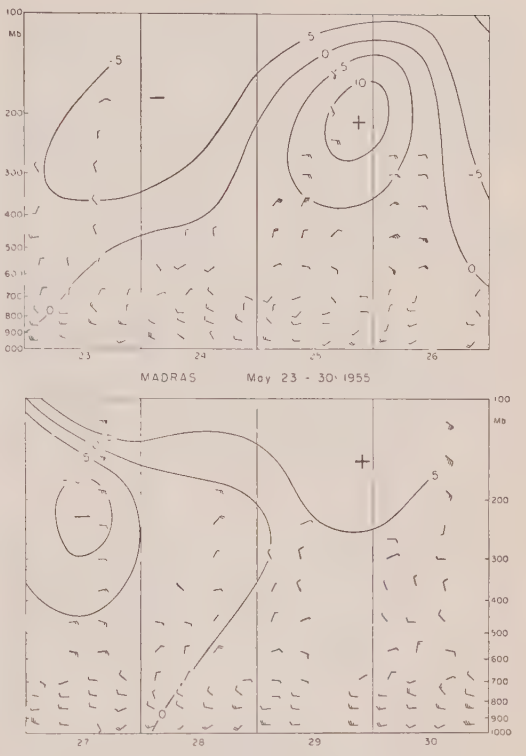

Fig. 10. Vertical time section of upper winds at Madras May 23—30, 1955.

motion occurred to the left of the axis looking downstream.

The coincident arrival of monsoon and upper easterlies is probably not fortuitous but indicates a general pattern. As is well known, the monsoon at first develops at more easterly longitudes in the middles of May and successively advances over the Bay of Bengal and the Arabian Sea. The upper easterly current likewise appears to form initially east of India and then extend itself downstream across India to Arabia.

Surges and breaks of monsoon: The northward shift of the monsoon rain belt along the western coast of India and the periodic pulsations of the intensity of the monsoon are connected with similar shifts and pulsations in the upper easterlies.

During "breaks" in the monsoon, the monsoon trough shifts to the Himalayas and westerlies dominate the whole of southern Asia below 500 mb. In the upper troposphere however easterlies continue to prevail. The

[3] There was a temporary advance of the monsoon on May 20 in association with a Bay of Bengal depression.

high-level easterly jet is well marked and occupies a more northerly position than average. When the current reverts to lower latitudes and begins to decelerate over the Arabian Sea, a revival of the monsoon takes place along the Indian west coast, as happened on July 25, 1955.

Fig. 10 illustrates the shift in the position of the easterly core in 1955; it also gives a general picture of its latitudinal oscillations. A gradual northward advance, followed by sudden retreat to low latitudes, are the main features during July. At the beginning of August, the current again moves northward to about 18° N, then gradually drops off toward south until the current becomes unimportant coincident with the time of withdrawal of the southwest monsoon.

Conclusion

This paper has shown that an easterly jet stream overlies tropical Asia and Africa in the summer monsoon season and that this current forms an important part of the general circulation in those regions. Over the Atlantic and Pacific oceans no such jet stream exists; instead the high tropospheric circulation consists of a train of vortices (RIEHL 1948). We must conclude from this marked difference that the land-sea distribution plays a major part of shaping the flow pattern of the southern periphery of Asia. The equatorial region is covered entirely by ocean, the region north of 20° N by land. This arrangement prescribes maximum surface heating far to the north of the equator in the northern summer. In addition, the surface on which the insolation is absorbed and reradiated is greatly elevated in the region of the vast Tibetan plateau which extends to 700 mb over a wide area and to 500 mb and above in the high ranges. The large extent and high elevation serve to heat directly the middle troposphere and to produce a strong solenoid field in the upper troposphere for driving a clockwise circulation.

Thus the high-level anticyclone over northern India and Tibet appears to be thermally driven whereas the cells overlying Arabia and Africa are "dynamic" highs associated with descent and production of deserts. Along the northern margin of India the high-level circulation does not act to suppress, rather to assist large-scale ascent in the equatorial trough. The outflow from the trough is maintained by the combined solenoid field resulting from the high surface heat source plus condensation heating. At least the equatorward branch of the outflow moves at nearly constant absolute angular momentum where the constant is the earth's momentum at latitude 25° N, close to the region of high heat source and strong condensation heating as shown earlier (Figs. 6 a, b). In this way the upper jet stream is produced and it is not without interest to observe that this current in the mean reaches its greatest intensity approximately south of the western margin of the high plateau.

Acknowledgements

The author wishes to express his grateful thanks to Prof. Herbert Riehl for his kind interest in this work and for his stimulating discussions and helpful suggestions and to Mrs Della Friedlander for the drawings.

REFERENCES:

ALAKA, M. A., 1955: A case study of an easterly Jet Stream in the Tropics. *Dept. of Meteorology, Univ. Chicago*, multigraphed March 1955.

AUSTIN, E. R., 1953: Upper winds of Aden. *Quart. J. Roy. Meteor. Soc.*, **79**, p. 528.

BJERKNES, V. ET AL, 1953: *Physicalische Hydrodynamik*, Berlin: Julius Springer.

CHADHURY, A. M., 1950: On the vertical distribution of wind and temperature over Indo-Pakistan along the meridian 76° E in Winter. *Tellus*, **2**, p. 56.

CLARKSON, L. S., 1956: Analysis of winds at 40,000 ft. and 50,000 ft. over Singapore. *Meteor. Mag.*, **85**, p. 1.

DAVIS, D. A., and SAMSON, H. W., 1952: Easterly Jets over East Africa. *Weather*, **7**, p. 343.

DESAI, B. N., 1951: Some aspects of tropical meteorology with special reference to the Indian Weather—An examination of Malurkars's concepts regarding them. *Ind. J. Meteor. Geophys.*, **2**, p. 113.

FROST, R., 1952: Upper air circulation in low latitudes in relation to certain climatological discontinuities. *Professional Notes No.* **107**, U. K. Met. Office (Air Ministry).

HAY, R. F. M., 1953: High-level strong Easterlies over Singapore and Hong Kong. *Weather*, **8**, p. 206.

HAURWITZ, B., and AUSTIN, J. M., 1944: *Climatology*. New York: McGraw-Hill Book Co.

India Meteorological Department, 1943: *Climatological Atlas for Airmen*.

KOTESWARAM, P., 1953: An analysis of the high tropospheric wind circulation over India in winter. *Ind. J. Meteor. Geophys.*, **4**, p. 13.

KOTESWARAM, P., ET AL, 1953: Characteristics of the upper troposphere, tropopause and the lower stratosphere over Trivandrum. *Ind. J. Meteor. Geophys.*, **4**, p. 111.

KOTESWARAM, P., and PARTHASARATHY, S., 1954: The mean Jet Stream over India in the pre-monsoon and post monsoon seasons and vertical motions associated with sub-tropical Jet Streams. *Ind. J. Meteor.Geophys.*, **5**, p. 138.

KOTESWARAM, P., 1956: The easterly Jet Streams over the Tropics. *Research Report*, Dept. of Meteor., Univ. Chicago, multigraphed.

KRISHNA RAO, P. R., 1952: Probable regions of Jet Streams in the upper air over India. *Current Science*, **21**, March 1952, Current Science Association, Bangalore.

KRISHNA RAO, and GANESAN, V., 1953: The mean Jet Stream over India and Burma in winter. *Ind. J. Meteor. Geophys.*, **4**, p. 193.

MALURKAR, S. L., 1950: Notes on analysis of weather of India and neighbourhood. *Memoirs of India Met. Dept.*, **28**, pt. 5.

NEWTON, C. W., and CARSON, J. E., 1953: Structure of wind field and variations of vorticity in a summer situation. *Tellus*, **5**, p. 321.

PALMÉN, E., 1951: The rôle of atmospheric disturbances in the general circulation. *Quart. J. Roy. Meteor. Soc.*, **77**, p. 337.

PALMER, C. E., 1951: *Compendium of Meteorology*. Boston: American Meteorological Society, 1951.

PALMER, C. E., 1952: Tropical meteorology. *Quart. J. Roy Meteor. Soc.*, **78**, p. 126.

RAMANATHAN, K. R., and BANERJI, H. C., 1931: A study of two pre-monsoon storms in the Bay of Bengal and a comparison of their structure with that of the Bay storms in the winter months. *Scientific Notes*, India Met. Dept., **4**, p. 34.

RIEHL, H., 1948: On the formation of typhoons. *J. Meteor.*, **5**, p. 247.

RIEHL, H., 1954: *Tropical Meteorology*. New York: McGraw-Hill Book Co.

ROY, A. K., 1946: Air Masses in India. *Technical Notes*, India Met. Dept. No. **16**.

SAWYER, J. S., 1947: The structure of the Inter-tropical Front over North India during the South-west monsoon. *Quart. J. Roy. Met. Soc.*, **73**, p. 346.

SCHACHT, E. J., 1946: A mean hurricane sounding for the Caribbean area. *Bull. Amer. Meteor. Soc.*, **27**, p. 324.

VENKITESHWARAN, S. P., 1950: Winds at 10 kms and above over India and its neighbourhood. *Memoirs of the India Met. Dept.*, **28**, p. 55.

YEH, T. C., 1950: The circulation of the high troposphere over China in the winter of 1945—46. *Tellus*, **2**, p. 173.

YIN, M. T., 1949: A synoptic-aerologic study of the onset of the Summer Monsoon over India and Burma. *J. Meteor.*, **6**, p. 393.

On the General Circulation over Eastern Asia (II)[1]

Staff Members of the Section of Synoptic and Dynamic Meteorology, Institute of Geophysics and Meteorology, Academia Sinica

(Manuscript received June 5, 1957)

Abstract

The principal weather system over Eastern Asia are considered in the different seasons. Section 3a contains a discussion of the winter and the transitional seasons, while sections 3b considers the summer situation. The influence of the Tibetan Plateau on the circulation over the Far East and the weather over China is discussed in the last section.

3. A brief survey of principal weather systems over Eastern Asia

We have seen that the basic currents over Eastern Asia have distinct seasonal differences. So also are the principal weather systems. Therefore in the following we shall discuss the principal weather systems over Asia according to season.

a) Winter and transitional season.

In winter and transitional seasons westerlies prevail over much of the continent. The synoptic systems encountered are mainly disturbances in the westerlies. Among these cold waves and extratropical cyclones are by far the most important. As over other parts of the northern hemisphere cold waves break out during the period of large scale changes of the general circulation in middle latitudes. In winter and transitional seasons there is a major trough off the Asiatic coast. But this quasi-stationary trough is subject to a great variation. This long wave system over the Asiatic coast starts after a period of "anchoring" at its normal position to move eastward with a rapid decrease in intensity. At the same time there is a strong development of an upper trough over the continent. This developed trough moves out of the continent and reforms a new quasi-stationary major trough at the normal position. With this development there will be an outbreak of a cold wave. Figs. 15a—c illustrate this process.

According to the origin of the cold air and the synoptic development we divide the cold waves into four categories. In the first category the Arctic Sea to west of Nova Zembla is the site for the cold air from which the arctic air through the North Scandinavia, the White Sea and the Barents Sea goes to the north European part of Soviet Union and then from West Siberia and Mongolia invades China. With this cold air is a developing upper short-wave trough which reaches its highest development east of 130° E and then becomes a major trough off the coast. In the second category the site of cold air is the part of the Arctic Sea north of the Asiatic continent. This cold air moves southward to West Siberia. Below 60° N it turns SE-ward and invades Mongolia and China. During its southward

[1] Continued from Vol. 9, No. 4.

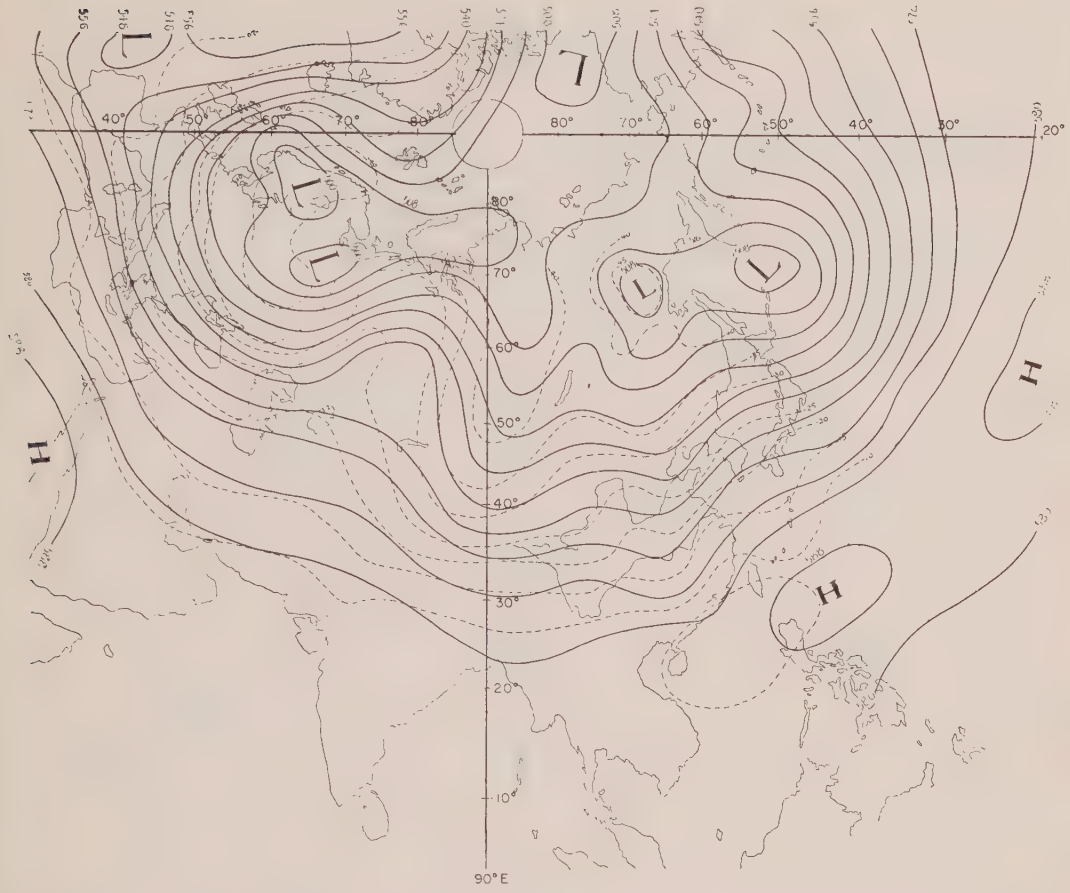

Fig. 15 a. 500-mb chart for February 16, 1955, 1500 Z. The long-wave trough off the Asiatic coast began to move eastward, while a short-wave trough has moved into western Siberia from Europe.

invasion a pressure ridge develops over Urals aloft. At the same time a short wave trough moves southeastward to the east of Urals. As it moves eastward it shows a marked deepening and replaces the original major trough as it crosses the coast. In the third category the source of cold air is originated in West Siberia. During winter a large anticyclone may be stagnant over Western Siberia and Mongolia for many days. The maintenance of this stationary high pressure is related to the blocking over Urals. The air in this high cools through radiation. Gradually it becomes very cold and the surface pressure increases gradually up to a very high value. At last with the collapse of the Ural blocking this intensive cold high breaks out southward and leads to a severe cold weather in China. The fourth category is usually ill-defined. In the beginning there usually appears a wedge of high pressure behind a weak cold front over Ukraine. This wedge moves with the cold front into Asia and gradually develops into an anticyclone. Then the anticyclone turns southeastward across Mongolia and invades China. This type of cold wave generally takes place in connection with strong cyclogenesis over Mongolia.

Extratropical cyclones are also important winter weather systems over Asia. However, because of the confluence of upper currents (see § 1 b), over the continent, except Mongolia and Northeast China, cyclone very seldom develops. We have not seen over this part of the world any developed cyclone which can

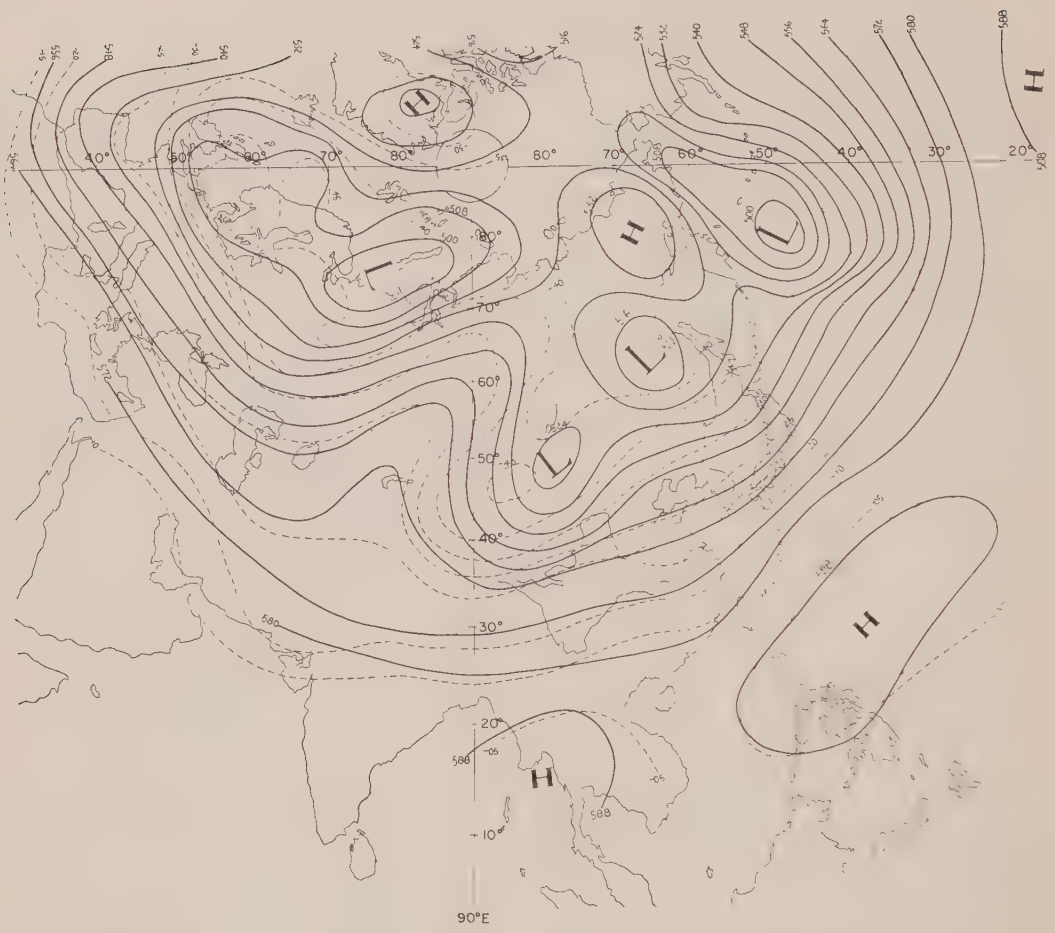

Fig. 15 b. 500-mb chart for February 17, 1955, 1500 Z. On the continent the short-wave trough continued to move eastward and deepened rapidly. The original longwave trough has approached Aleutian Islands.

be compared with those intense cyclones usually observed over North America. The process of cyclone development over the northern part is different from that over the southern part of Eastern Asia. In Mongolia and Northeast China it is a process of development of secondary cyclones. The cyclones over West Siberia from the west are usually old occluded systems and their intensity decreases as moving eastward (fig. 16 a). But when they reach Lake Baikal a secondary cyclone may form near the occlusion point or in retarding part of the cold front. Fig. 16 b will serve as an example of the cyclone development at this stage. This newly formed cyclone usually deepens rapidly as it move eastward. At the same time the mother cyclone to the north very quickly fills. The cyclone reaches its top development when arriving at Northeast China (fig. 16 c). As it moves further eastward it gradually fills and feeds in the Aleutian center of action. The frequency of this type of cyclone is maximum and the intensity also highest in spring. In autumn there is a secondary maximum.

There are two types of cyclogenesis over the Lower Yangtze Valley and the adjacent seas. The first type occurs on cold fronts. When the cold front associated with a cold wave arrives at the Yellow Sea or the East China Sea, it decelerates rapidly. On the decelerated part of the cold front disturbances usually develop. This type of cyclogenesis is similar to the A type of cyclogenesis along the American east

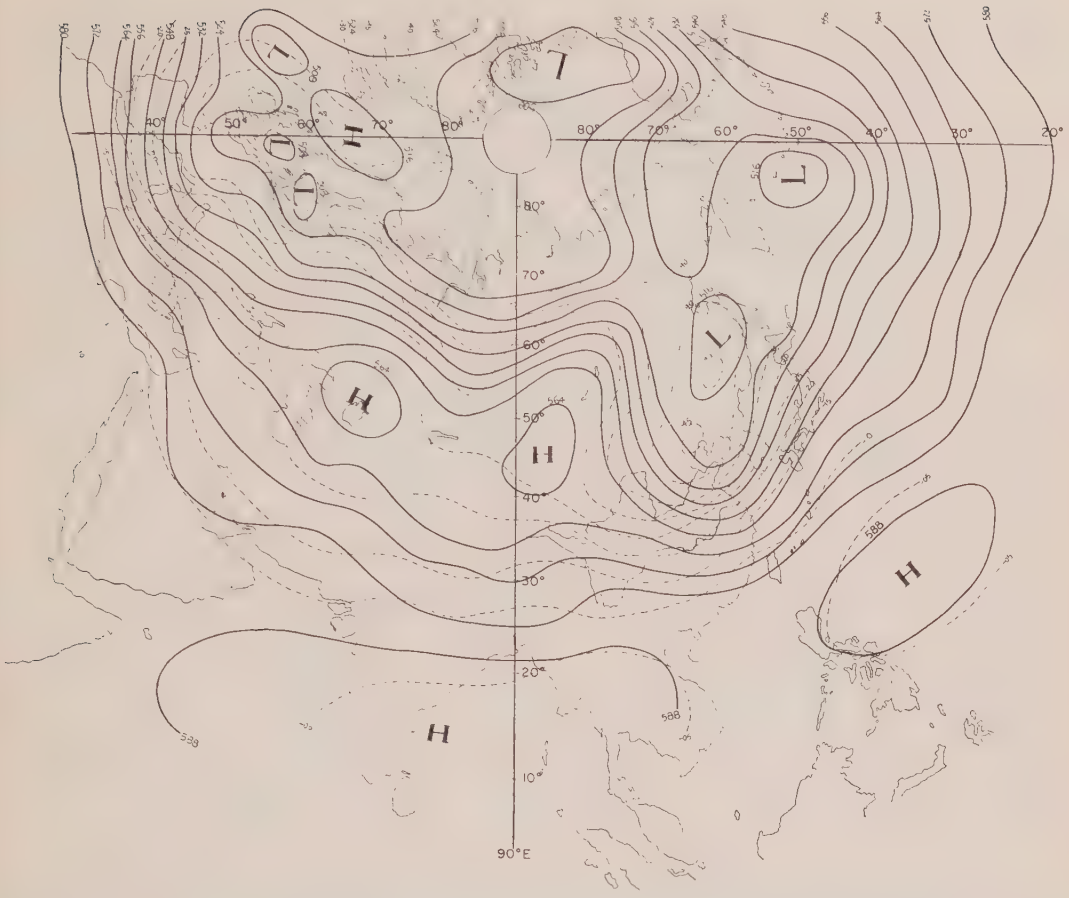

Fig. 15 c. 500-mb chart for February 19, 1955, 1500 Z. The short-wave trough developed to a major trough along the coast, while the original long-wave trough turned into a minor system in the region of Aleutian Islands.

coast described by MILLER (1946). The other type of cyclogenesis is associated with the upper trough coming from the Tibetan Plateau. This upper trough generally fills as it moves eastward. But if there appears strong warm advection in the lower troposphere as the upper trough arrives at the coast, then appears cyclogenesis. On the continent this type of cyclone is in its initial stage, it may only develop over the sea. Figs. 17 a—b illustrate the formation and development of this type of cyclone.

Long wave troughs very seldom come from the west to Eastern Asia. All the major troughs over this continent are developed from minor troughs. There are several kinds of minor troughs moving over East Asia from the west. The first invades East Asia from NW to the rear of the trough where continuous supply of cold air facilitates its development. In winter and the transitional seasons almost all the severe cold air outbreaks and the cyclogenesis over Mongolia are associated with this kind of upper troughs. The second kind of upper minor troughs move to China from the west through the Plateau. The third is the upper disturbance in the jet stream south of the Tibetan Plateau. It may cross Indo-Pakistan to arrive at China. All upper troughs of the second and third types show filling as they move eastward. They are generally very weak when they arrive at China. Thus, they are very indistinct on the surface chart, but they have definite weather with them. Besides, during the period of fairly zonal

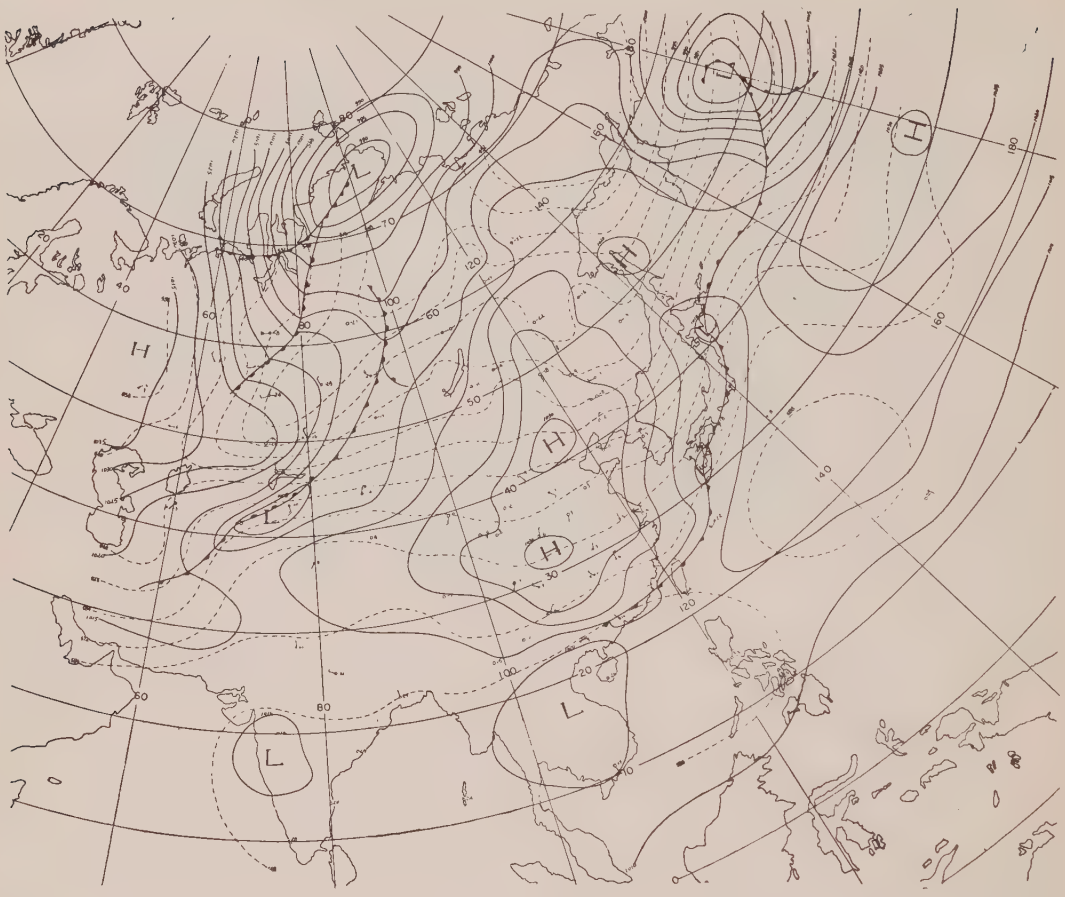

Fig. 16 a. Surface chart for March 18, 1957, 1800 Z, with 500-mb contours (dashed lines) at 1500 Z superimposed. Note that an old occluded front has moved into Western Siberia from Europe.

circulation minor troughs usually form over Sinkiang and move eastward.

Over the SW mountainous region (just to east of the Tibetan Plateau) there usually form small vortices in the lower troposphere (below 700 mb). The vortex in fig. 18 is an example. These small vortices have definite contributions to the bad weather in SW China. Sometimes the bad weather associated with these small vortices may extend to central China. These vortices are different from the cut-off lows in North America. They are much smaller in size.

b) Summer situation

In summer the westerlies retreat to the north of the Yellow River. Over south China the SW monsoon prevails while along the east coast the SE monsoon appears. According to the form and position of the boundary between the westerlies and the SE or SW monsoons, a great variety of flow patterns may appear over this continent. But there are still well-defined and important weather systems, though many are feeble and complicated. The first is the west Pacific subtropical ridge which frequently extends to the continent (fig. 19). Its dominance leads to severe hot and dry weather. The retreat from and advance to the continent of the subtropical ridge is closely related to the middle latitude westerly circulation. During a high circulation index period the west Pacific subtropical ridge is strong and its position does not vary much. In this period the small dis-

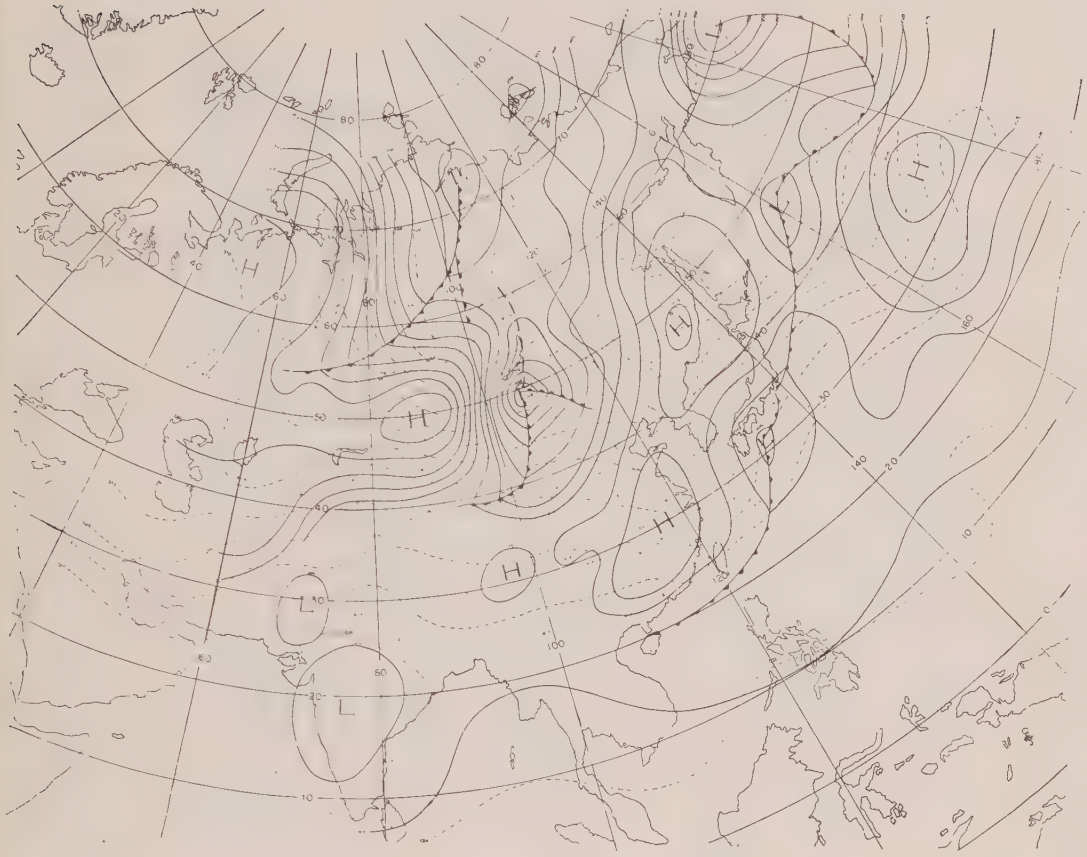

Fig. 16 b. Surface chart for March 20, 1957, 1800 Z, with 500-mb contours (dashed lines) at 1500 Z supermiposed. Note that to the south-east of Lake Baikal a depression has formed, while the old occlusion has filled up rapidly.

turbances in the westerlies move eastward, these small disturbances lead to small oscillations of the position of the subtropical ridge. During a low circulation index period its inland intrusion is the least.

The typhoon is one of the main important weather systems in summer. The number of occurrence and intensity of typhoon has a close connection with the upper subtropical easterlies over the west Pacific and East Asia (see figs. 8 a—e). When the easterlies over this part of the world establish earlier and the intensity is stronger than "normal" then typhoons will also occur earlier and the frequency is higher than "normal". The summer of 1953 was an example of early onset of the upper easterlies. In this year the number of typhoons invading the continent was higher than in other years and the first invasion occurred in the beginning of July 1954 was an example of a late onset of the upper easterlies. In this year the first occurrence of a typhoon was about one month later and the number of typhoons invading the continent was less. It may also be mentioned that the frequency of occurrence of strong[1] typhoons shows a more or less periodic variation. Fig. 20 shows the yearly number of typhoons over the NW Pacific in the period 1920—56. From this curve we see a periodic variation with a period of about 5 years. From the curve we

[1] "Strong" is defined by (1) the innermost close isobar is at least 993 mb and (2) the maximum wind is at least stronger than 8 Beaufort.

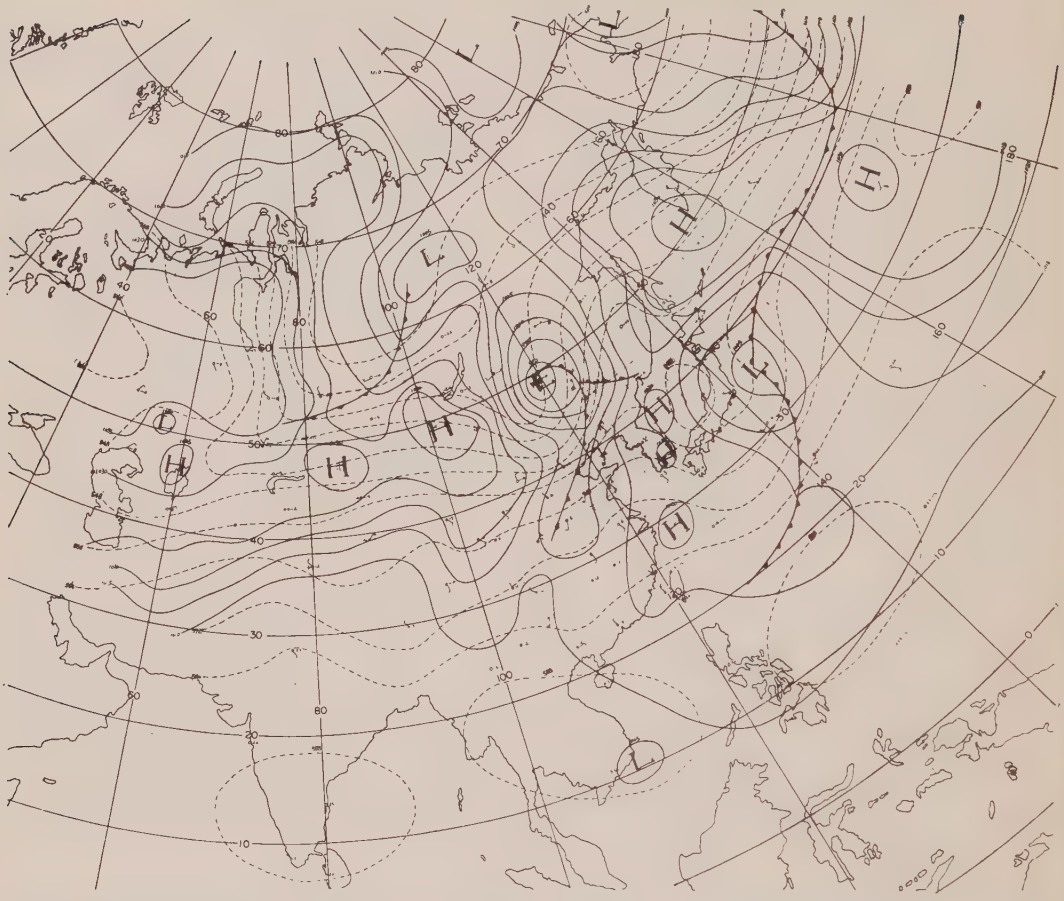

Fig. 16 c. Surface chart for March 21, 1957, 1800 Z, with 500-mb contours (dashed lines) at 1500 Z superimposed. Note that the depression has moved eastward into North-East China.

can also see that there is a strong decrease in the total yearly number of strong typhoons. The average yearly number in the period 1920—1956 is about 20. Before 1935 the yearly number was in general higher than 20 and after 1935 in general lower than 20.

Since the typhoon is an important dangerous weather system to China it is subject to wide studies, statistically and synoptically. It is found that the track and recurvature of a typhoon is closely connected to the circulation over a wide area. Unlike the hurricane, the typhoon usually has two recurvatures. In the first recurvature the track changes from SE-NW to N and in the second recurvature it turns to NE. Thus the track is different from an ideal parabola. The first recurvature usually occurs when the trough over Bering Sea deepens. Fig. 21 is an example of this type of track. The movement of typhoons was also studied theoretically by HSIEH and CHEN (1956).

The third weather system in summer we shall mention is the cold front which comes from NW. Under favorable conditions it may reach as far as south of Yangtze River and lead to a rather cold weather in summer. In NW China its occurrence is rather frequent. Most of the thunderstorm and hail damage in China is in summer associated with this front.

To conclude this section we may add a few words about the intertropical convergence zone. Over the continent is in summer a huge heat low which occupies almost whole India and China. If, during this period, the west

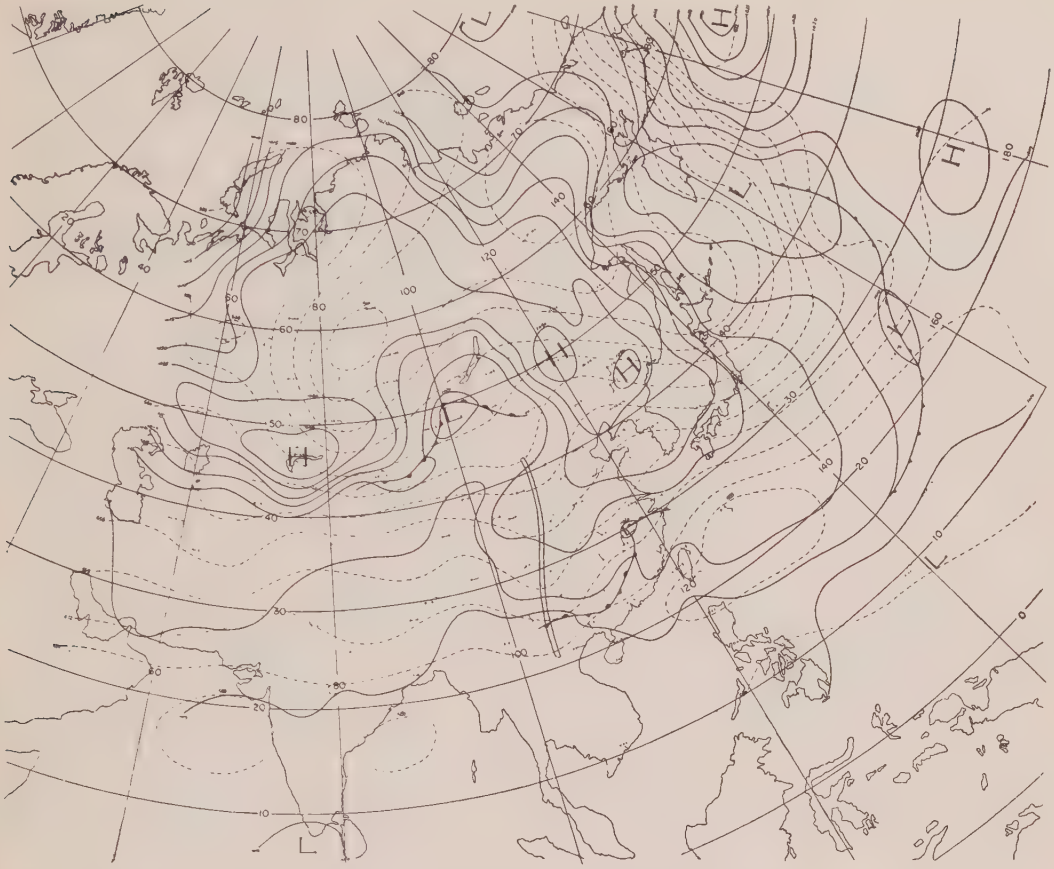

Fig. 17 a. Surface chart for February 1, 1957, 1800 Z, with 500-mb contours (dashed lines) at 1500 Z superimposed. Double heavy lines represent the current trough position on 500-mb level, while double dashed lines trough position 24 hour before. Note that there is cyclogenesis in the Lower Yangtze.

Pacific subtropical anticyclone reaches Japan and the Yellow Sea (35° N), then there will be convergence between the subtropical easterlies and the SW monsoon. Fig. 22 is an example of this convergence line (see also fig. 4). It is warmer north of the convergence zone and cooler to the south of it. Thus the baroclinity is reversed to the normal. The structure of this convergence zone over China is quite similar to that over India (HSIEH, 1951, SAWYER, 1947).

4. The influence of the Tibetan Plateau on the circulation over the Far East and the Weather over China

The Tibetan Plateau has roughly the shape of an ellipsoid. Its major axis is over 3,000 km long and its minor axis over 1,400 km. Connected with the adjacent Plateau, the Sinkiang-Mongolian Plateau, their width can be compared with that of the westerlies and their extension can be compared with the wave length of long wave. Its average height is over 4 km, occupying more than $^1/_3$ of the troposphere. Such a huge intrusion in the westerlies will no doubt have a profound dynamic influence on the general circulation. Considering it as a radiating body well high in the atmosphere it will also have a thermal influence on the circulation. In the following are some concrete dynamic influences of the Tibetan Plateau on the circulation over the Far East and the weather over China.

a) The dynamic effect of the Tibetan Plateau

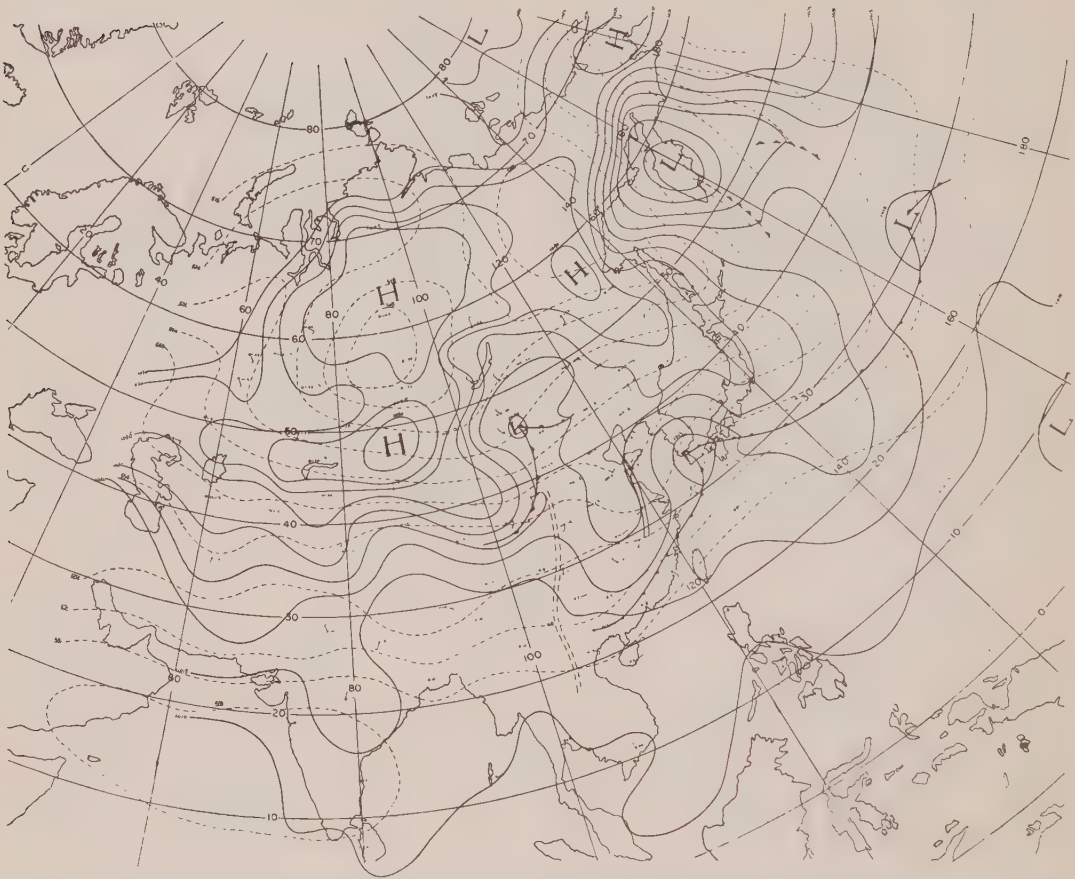

Fig. 17 b. Surface chart for February 2, 1957, 1800 Z, with 500-mb contours (dashed lines) superimposed. The depression formed in the Lower Yangtze has deepened and moved into Yellow Sea.

(i) Splitting and confluencing of the westerlies

The Tibetan Plateau is roughly of ellipsoidal shape with a major axis oriented in W—E direction. This will split the westerlies and force them to flow around it. The splitting of the westerlies is very pronounced on daily 500 mb chart. Due to the fact that in a rotating fluid the motion has a strong tendency to be quasi-two-dimensional (provided that the poleward temperature gradient is not large enough, which is usually the case in the atmosphere) the splitting is also observed well high above the Plateau. Fig. 23 is a typical example of a 500 mb map. On this map there are two branches of the westerlies, one flow to the north and the other to the south of the Plateau. As the two branches encircle around the Plateau a trough is dynamically formed in the southern branch and a ridge dynamically formed in northern branch. Both of them are clearly shown in fig. 23. The warm advection in front of this trough is very important for the weather over the eastern part of the Plateau.

In each branch of the westerlies there is a jet stream as discussed in previous sections.

The southern jet is very steady, not only in its daily position, but also in the average yearly position. The steadiness of this jet has a pronounced influence on the rainfall distribution over China. This is easily explained, since disturbances carrying rain are steered by the upper current.

From the facts that the axis of the southern

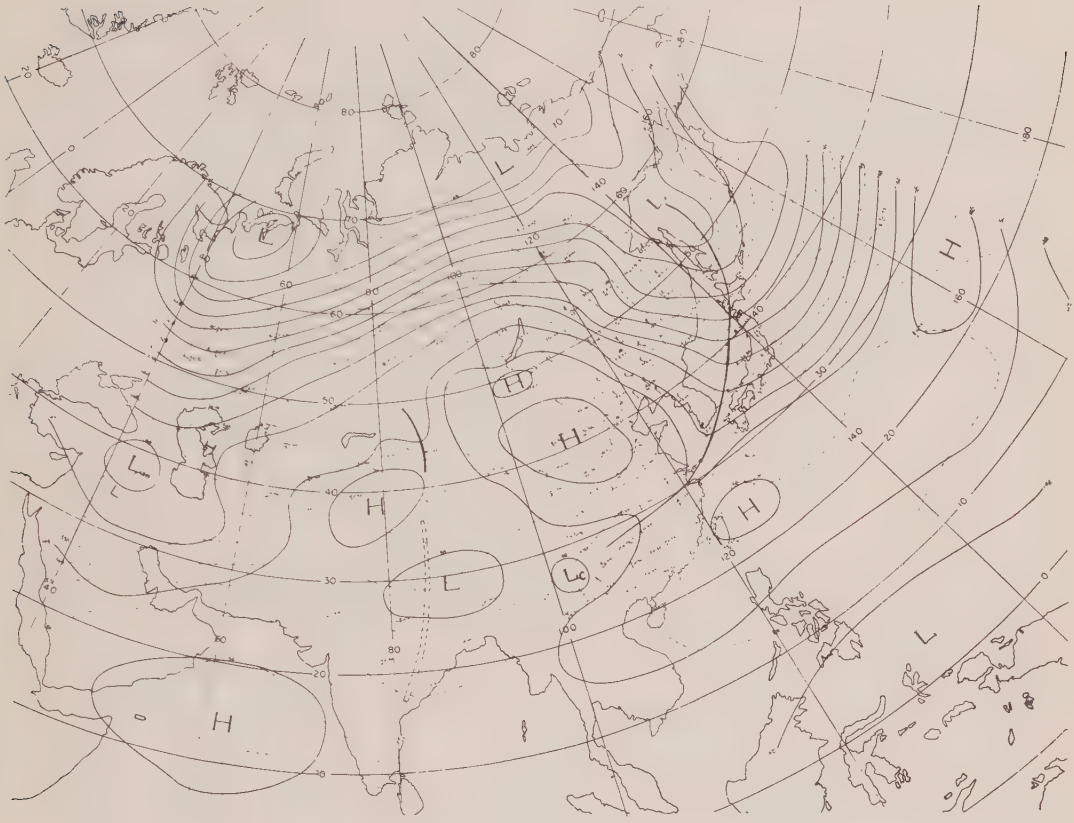

Fig. 18. 850-mb chart for January 11, 1957, 1500 Z, with 500-mb contours (dashed lines) superimposed. Notice that in South-West China there exists a small cyclonic circulation (SW-vortex) marked by Lc.

jet is just along the southern periphery of the Tibetan Plateau and once formed, it is very steady in position, we may conclude that this jet is at least anchored by the Tibetan Plateau. It is also very possible that its very formation is a dynamical result of the Plateau.

In fig. 3 we see a shear line (see I § 1a). The formation of this line may be attributed to the Tibetan Plateau. On this shear line small vortices are very frequently formed (fig. 18). These vortices are called "SW vortices". They are not immovable. But once they move downstream, they usually dissipate. Only under special circumstances they may develop.

The convergence in the lee of the Plateau has a profound influence on the weather development over China. It hinders the development of cyclones over most part of Eastern China. This explains that once the above mentioned vortices move downstream they dissipate. Only over NE China which is out of the convergence zone cyclones may have pronounced development.

(ii) The damping effect on the large eastward moving troughs

The Tibetan Plateau has the effect to cut the large eastward moving troughs into two sections. The southern part is left to the west of the Plateau. It gradually dissipates there or it may sometimes cross Pamir to reach the Indo-subcontinent and then move downstream in the southern branch of the westerlies. The northern part of the mother trough keeps on shifting eastward but with decreasing intensity. It has a chance to redevelop only after reaching Lake Baikal. To illustrate this process we have prepared figs. 24 a—b. In fig. 24 a we see that a large trough (marked AA) to the east of the

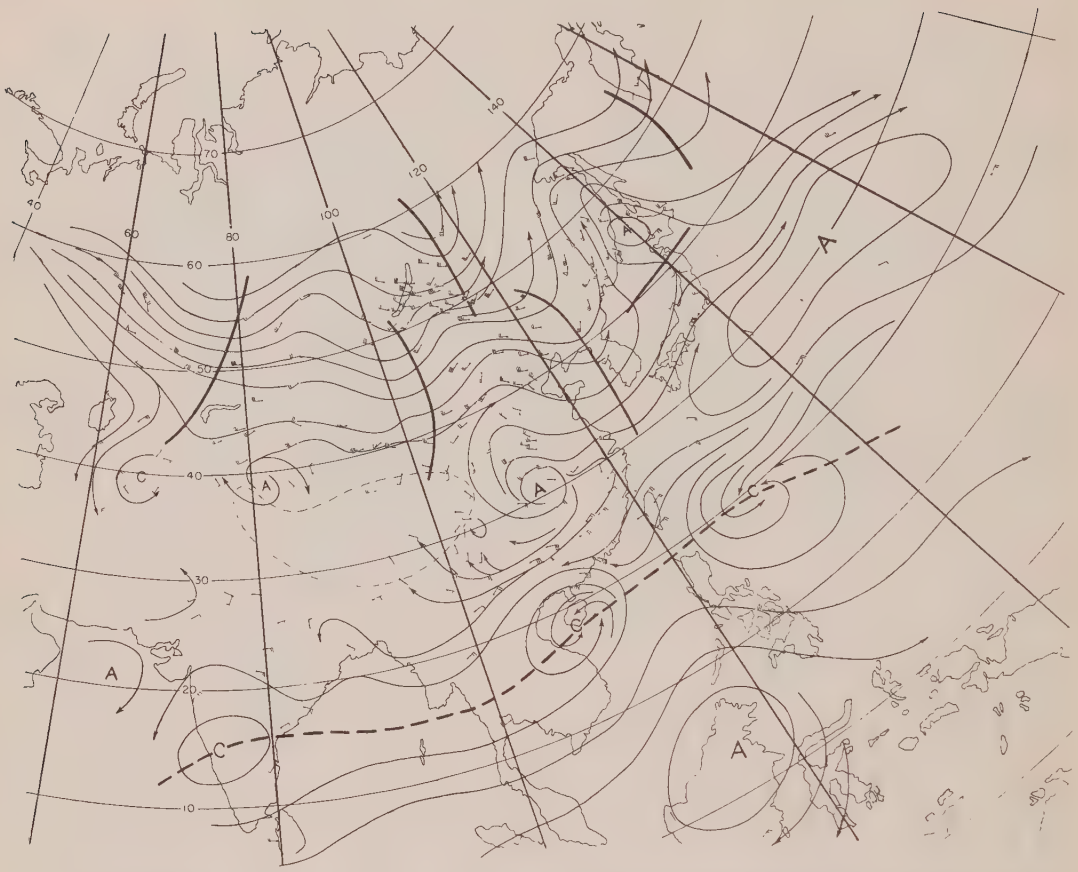

Fig. 19. Streamlines at 3 km for August 31, 1956, 0300 Z, typical flow pattern when subtropical ridge extends to the continent.

Plateau is in the process of breaking. Two days later (fig. 24 b) the northern section moves eastward with decreased intensity while the southern part is left on the original place. It is also frequently observed that as a large trough approaches the Plateau they weaken very rapidly. The southern part of the trough dissipates and only the northern part can be traced eastward.

It must be pointed out, however, that during a period with a zonal current disturbances of small amplitudes may cross over the Plateau.

(iii) The shelter effect

Due to the shelter effect of the Plateau there is a region, the so-called "dead water", in which the wind is weak in the lower layer and major disturbances are almost absent. There are only "SW-vortices" and sometimes minor

Fig. 20. Number of typhoons per year over NW Pacific.

waves. In winter there is very often a thin layer of cold air in this region. This layer of cold air has a definite influence on the weather in SW China. Fig. 25 is an example of a mean sounding for a winter month over Hsinching which illustrates the thermal structure of the atmosphere in the "dead water" region. In this mean sounding an inversion is very pronounced. Its mean intensity reaches 8° C.

To illustrate further the shelter effect we have further computed the distribution of the average west wind speed on the 3 km level in the winter months. Over the region of "dead water" the speed is smallest, even east wind appears. It is interesting to note that there is a symmetrical region of "dead water" to the west of the Plateau.

b) The seasonal variation of the influence on the circulation

All the phenomena discussed above belong to winter situations. In summer the Tibetan Plateau is no longer in the main part of the

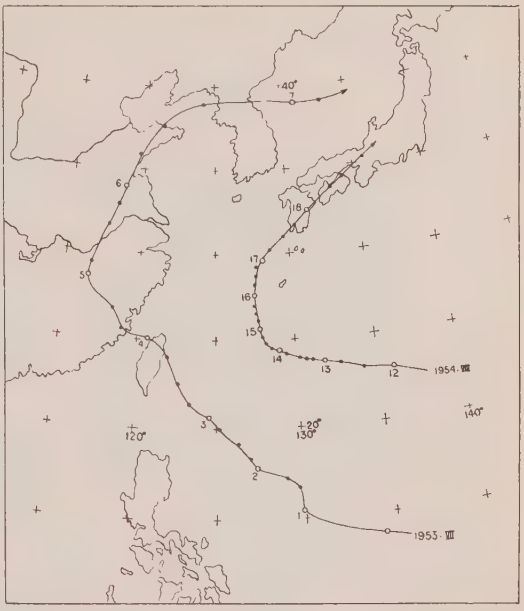

Fig. 21. Examples of the square-headed track of typhoon.

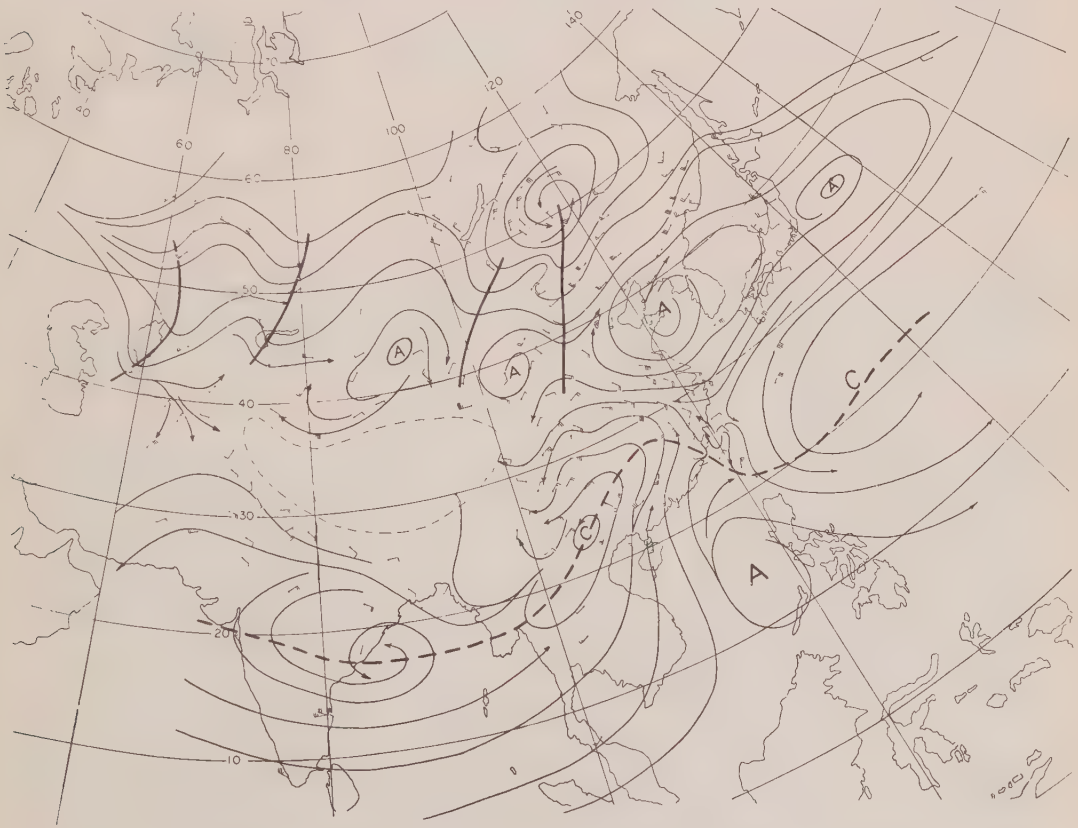

Fig. 22. Streamlines at 3 km for July 29, 1956, 1500 Z, illustrating a monsoon convergence over China.

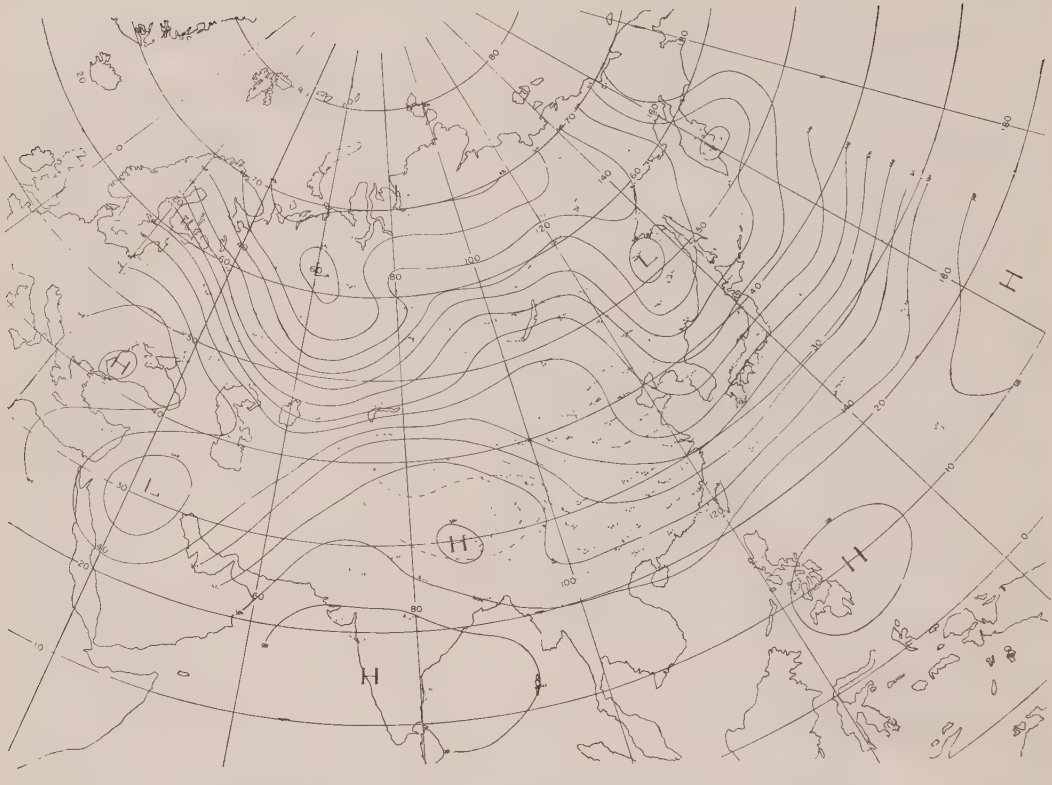

Fig. 23. 500-mb chart for January 22, 1957, 1500 Z. Note that over Tibet the westerlies split into two branches.

westerlies and the situation is entirely different from that of the winter. One striking phenomenon in the summer cases is that in the main (fig. 5) the wind blows cyclonically around the Plateau on the 3 km level, while on 6 km (fig. 2 b), there is a huge anticyclone with its center over the SE corner of the Plateau. On 9 km (figure not reproduced) the center is shifted westward. This indicates that the temperature over the Plateau is higher than the surrounding free air.

From the mean monthly upper air charts one may reach the conclusion that the above anticyclone is nothing but a subtropical high. However, from the distribution of mean vertical motion on 6 km (fig. 2 b) we find that almost over the entire anticyclone there is upward motion with an average speed about 1.00 cm/sec. This upward motion may be estimated to reach as high as 9 km. This is just opposite to the dynamic requirement of a dynamic anticyclone. This indicates that the thermal influence of the Plateau (which will be discussed in a later section) on the formation of this anticyclone is important; at least it helps to form a closed center in the subtropical ridge belt.

In figs. 4—5 we see a low over Indo-Pakistan. This is formed in the following way. As the SW monsoon advances NE-ward, it is forced to turn around by the Arakan Mountain and the Tibetan Plateau resulting an easterly current just south of Himalaya. Thus, the so-called Indian heat low is at least not of purely thermal origin.

From above we may notice that the dynamic influence of the Plateau on the circulation has a very large seasonal variation. This is in contrast to the viewpoint that topographical influence on the circulation does not vary seasonally since topography is a fixed feature in space. The dynamic effect of a mountain

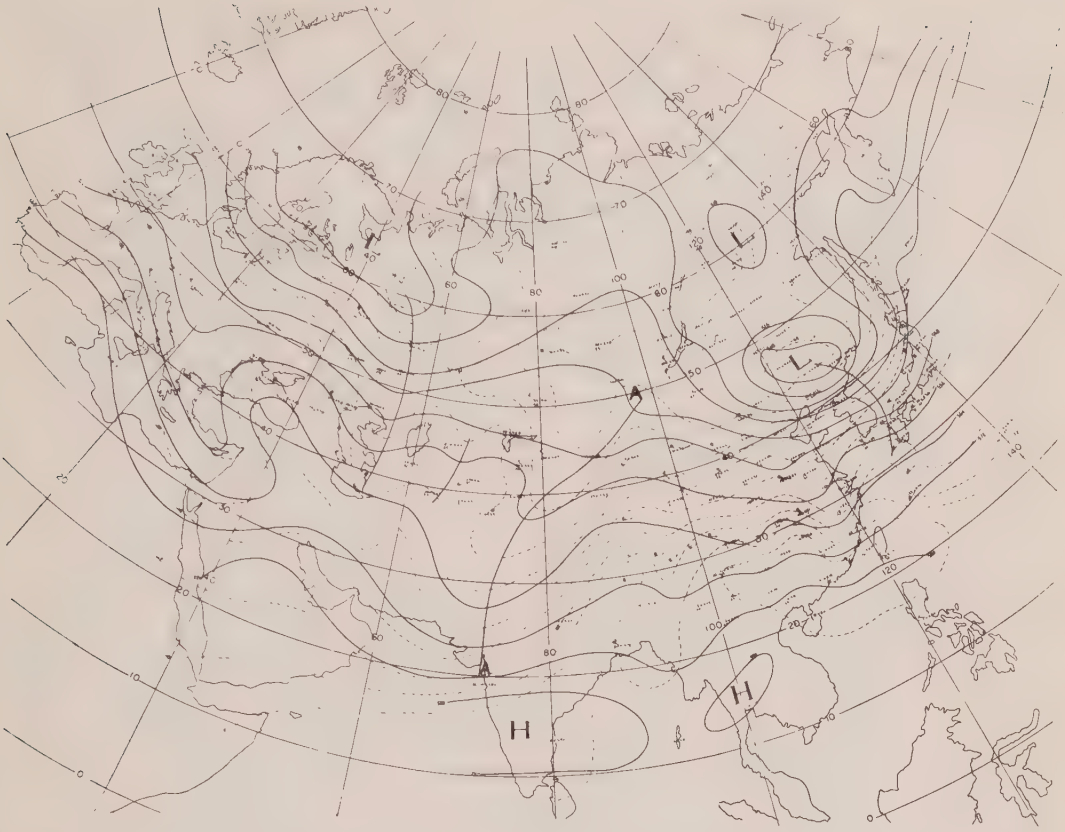

Fig. 24 a. 500-mb chart for February 9, 1957, 1500 Z. Note the long-wave trough AA in the early stage of cut-off.

is closely associated with the current which flows over or around it. Since the current which strikes the Plateau varies seasonally the dynamic effect of the plateau will vary accordingly.

c) The Tibetan Plateau, a warm source or a cold source?

Some meteorologists determine a mountain as a warm or a cold source by comparing the temperature over mountain with the surrounding free air of the same height and latitude. However, temperature is not a proper indicator for this purpose. A region with high (of low) air temperature does not necessarily mean a warm (or a cold) source, because high or low temperature may be produced in several ways, for example by advection, vertical motion, radiation, etc. A warm source must constantly supply heat to the air while a cold source must constantly withdraw heat from the air. In order to keep a quasi-steady state over a warm (or a cold) source the air must be cooled (or warmed) by some other means as by upward (or downward) motion or cold (or warm) advection. Under this definition we have examined whether the Tibetan Plateau is a warm or a cold source.

First we have calculated the short-wave absorption and long-wave cooling between 700 and 500 mb over China. From the calculations over the limited number of upper air stations over the Plateau we may give the following estimate: The average long-wave cooling is about — 1.6° C/day in summer as well as in winter. The short-wave absorption is about 0.6° C/day in summer and 0.2° C/day in winter. Thus, the net radiation cooling is about —1.4° C/day in winter and —1.0° C/day in summer.

Secondly, from the monthly precipitation we have computed the condensation heating. Because the cloud thickness is on the average

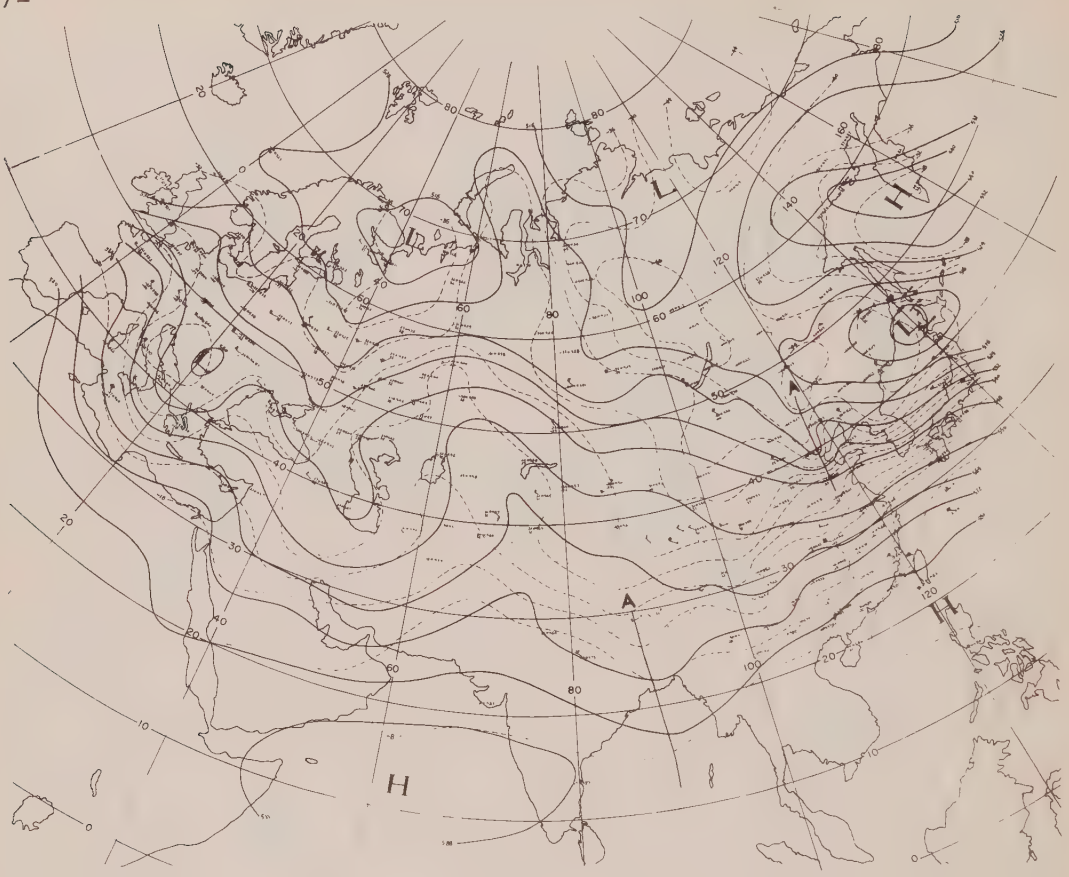

Fig. 24 b. 500-mb chart for February 11, 1957, 1500 Z. The cut-off is complete; the northern part of the trough AA has moved to North China, the southern part has moved eastward along the southern periphery of Tibet.

below 1,500 m and the condensation level is below 1,000 m above the ground over Tibet we may assume that the heat of condensation is totally absorbed by the air with 200 mb thickness above the Plateau. The average monthly precipitation in summer on the Plateau is estimated to be about 60 mm. Thus, the condensation heating is about 2° C/day. In winter the precipitation is very small over the Plateau, the condensation heating may thus be neglected.

From the above the balance between radiational cooling and condensation heating is seen to be + 1.0° C/day in summer and — 1.4° C/day in winter.

We shall first discuss the heat balance over the Plateau in summer. We have seen that over the Plateau the average upward motion is about 1.0 cm/sec, giving an adiabatic cooling about —3.0—3.5° C/day and that the cold advection has been estimated to about —0.2° C/day. The sum of the two terms gives a total cooling about — 3.5° C/day. Together with the above calculated heating the air within the 200 mb thickness over the Plateau suffers a cooling about —2.5° C/day. This cooling must be balanced by some heat supply. From the distribution of the difference between soil and air temperature (chart not shown) it is seen that over the Plateau the soil temperature is on the average more than 5° C higher than that of the air (at 2 meters above ground). This gives a temperature lapse rate of 2.5×10^{-2}° C/cm. Thus, the air may obtain a large amount of heat from the ground through turbulence. Suppose that the heat obtained in this way is entirely absorbed by the air within the investigated 200 mb thickness and just

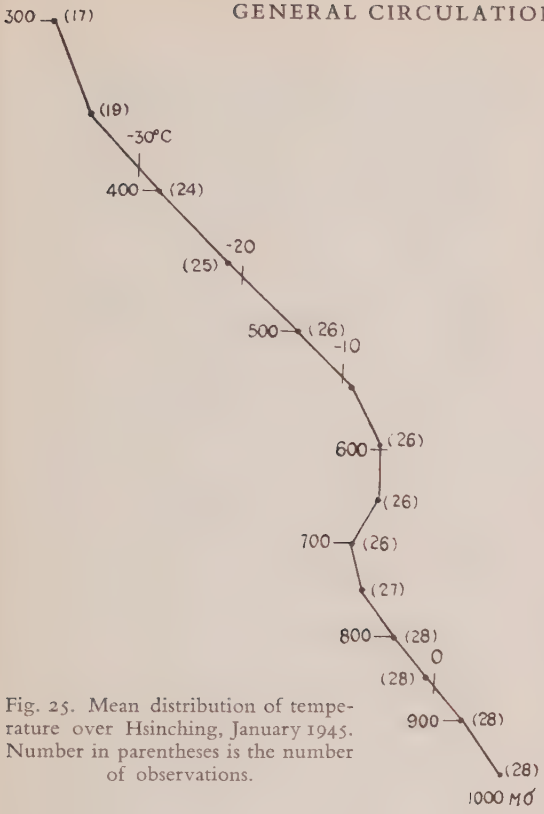

Fig. 25. Mean distribution of temperature over Hsinching, January 1945. Number in parentheses is the number of observations.

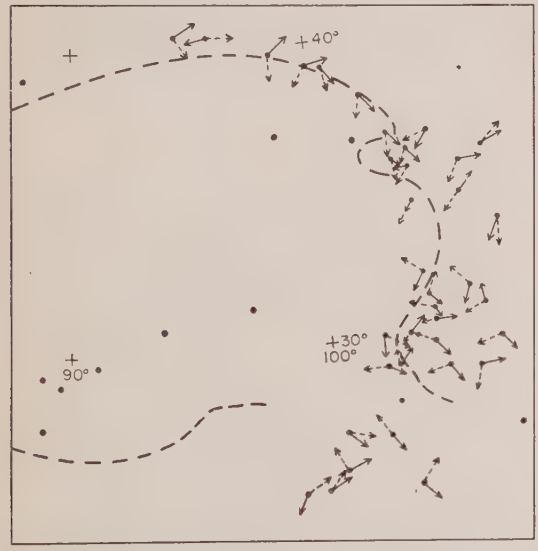

DIURNAL WIND VARIATION ALONG THE CIRCUMFERENCE OF TIBETAN PLATEAU

SOLID ARROW — 6 O'CLOCK
DASHED ARROW — 14 O'CLOCK

Fig. 26. Mean April diurnal wind variation along the circumference of Tibetan Plateau. Solid arrow: wind at 6 o'clock (L.T.), dashed arrow: wind at 14 o'clock (L.T.).

Fig. 27 a. Distribution of the mean amplitude of diurnal variation of pressure over China (April, 1952—53).

balances the cooling, then the average turbulent austausch coefficient near the ground would be about 250 cm² sec. This seems a little too small. This is because that in our computation the heat used for evaporation is left out. When this is considered the coefficient would be raised.

The situation for winter is complicated. It is different for different regions. For the SE Plateau, the net radiation is about —1.4° C/day and the warm advection gives a warming about +1.2° C/day. These two terms are about in balance. In this region we have upward motion of about 1.0 cm/sec in winter. This gives a cooling of about —3.5° C/day. The heat of condensation is negligible here in winter. The cooling must be balanced from the heat obtained from the ground through turbulence. This requires that the soil temperature is higher than the air temperature. This is just what the observations show. On an average the soil temperature is about 1—2° C higher than that of the air in this region.

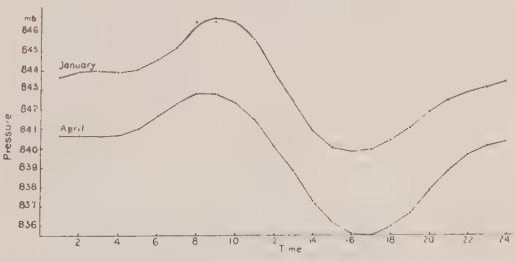

Fig. 27 b. Mean hourly pressure at Si-chang (January and April, 1952—53).

The situation for the rest of the region is difficult to estimate due to the lack of data. However, from the discussions about the vertical motion over the Plateau it seems that there exists a downward motion of about 0.5 cm/sec. Accepting this value, then the adiabatic heating due to this downward motion would over-balance the radiational cooling. Neglecting advection which is not known over this part of the world the Plateau would receive heat from the air, or at least the air would not obtain heat from the Plateau.

From the discussion above it may be concluded that the Plateau is a warm source in summer and its SE part also plays the role of a warm source in winter while the rest is most probably a cold source in winter.

Another thermal influence of the Tibetan Plateau is reflected in the daily wind variation. In the day time the Plateau is heated up much more rapidly than the surrounding free air. At night the Plateau cools much more rapidly than the surrounding free air. In accordance with this thermal variation we may expect that the wind will have a component toward the Plateau in day time and a component out from the Plateau at night. This effect even exists in winter. Fig. 26, the mean for April, is given as an illustration. In this figure the solid arrow is the resultant direction of the surface wind at 6 o'clock in the morning and the dashed arrow is that at 14 o'clock in the afternoon. This figure clearly shows the mentioned effect. A similar situation also exists clearly over Indo-Pakistan. Thus relative to the Plateau there is a convergence of wind in the afternoon and a divergence in the early morning. The order of convergence reaches 10^{-6}/sec which is quite a high value.

It is found that on the east slope of the Plateau the diurnal variation of pressure (fig. 27a) is very great, especially in spring when the diurnal variation of air temperature is largest. For example, the mean diurnal range of pressure variation over Sichang (27.9° N, 102.3° E, fig. 27b) is as large as 7 mb with an average maximum 3-hour tendency of 5 mb at 14^h (120° E.C.T.). This diurnal variation of pressure has only one maximum and one minimum and is just out of phase with the temperature wave. This character suggests a thermal origin of its formation, i.e. this very large diurnal variation of pressure may be related to the diurnal variation of the divergence field mentioned above.

To summarize, we may conclude that the Tibetan Plateau plays a very significant role in the circulation over Asia and the weather development over China. In the past when the influence of the earth's surface on the circulation was mentioned, it usually meant the thermal effect of land-and-sea distribution. This is only one part of the story. From the above discussion we see that the Plateau not only has a mechanical but also a thermal effect on the general circulation.

To be continued in a following issue of this journal.

THIS REPORT IS A SUMMARY OF THE FOLLOWING PAPERS:

Chao Jih-ping, 1956: A preliminary study of the rhythm of the ultrapolar process over Eastern Asia, *Acta Meteor. Sinica*, **27**, 113—126 (in Chinese).

Dao Shih-yen, 1952: An analysis of the weather process during the period of cold air outbreak in China. *Synoptic Monthly*, **2**, 35—51 (in Chinese).

— 1952: An analysis of a major cold wave in November 1951. *Synoptic Monthly*, **2**, 37—46 (in Chinese).

— 1952: The influence of the trough from Indo-Burma on the weather of Southern China in winter. *Acta Meteor. Sinica*, **23**, 172—192 (in Chinese).

— 1954: Some experiences in forecasting cold-waves in China. *Synoptic Monthly*, **4**, 19—21 (in Chinese).

— 1955: An empirical study of the process of cold air outbreaks in Far East in winter-half year. 66 pp. Mimeograph (in Chinese).

— 1956: A statistical study of extratropical cyclones in Far East. Unpublished (in Chinese).

— 1956: The upper air cold trough over China during high index circulation over Far East. *Acta Meteor. Sinica*, **27**, 345—360 (in Chinese).

— 1957: A synoptic and aerological study on a cold wave in the Far East during the period on the breakdown of the blocking situation over Eurasia and Atlantic. *Acta Meteor. Sinica*, **28**, 63—74 (in Chinese).

— Chen Long-shun, 1957: The structure of general circulation over the continent of Asia in summer. To be published (in Chinese).

Jü Chang, 1956: An investigation of the phases of the ultrapolar process which leads to a sudden drop in temperature in China. *Acta Meteor. Sinica*, **27**, 101—112 (in Chinese).

Kao Yü-shih, 1953: The forecast of typhoon movement from the change of circulation pattern. Memoir, No. 1. Institute of Geophysics and Meteorology, 20—82 (in Chinese).

— 1952: The Mai-yü of 1946 over Yangtze Valley. *Acta Meteor. Sinica*, **23**, 61—84 (in Chinese).

Koo Chen-chao, 1951: The upper wind structure over Western China in winter. *Science Record*, **4**, 149—156.

— 1951: On the importance of the dynamical influence

of Tibetan Plateau on the circulation over Eastern Asia. *Scientia Sinica*, **2**, 283—303 (in Chinese).
— 1951: The north west trough and its influence on the weather of China. *Synoptic Monthly*, **8**, 1—17 (in Chinese).
— 1952: The particularity of the circulation over China in spring as revealed by the interdiurnal variation of pressure. *Acta Meteor. Sinica*, **23**, 123—129 (in Chinese).
— 1952: The summer cold wave over NW China. *Synoptic Monthly*, **2**, 3—14 (in Chinese).
— 1953: On the seasonal variation and the formation of the mean circulation pattern. *Acta Meteor. Sinica*, **24**, 69—99 (in Chinese).
— 1953: Some viewpoints in the forecasting of typhoon trajectories over Western Pacific. Memoir, No. 1, Institute of Geophysics and Meteorology, 1—19 (in Chinese).
Kog Chen-chao and Yeh Tu-cheng, 1955: Further examination of the influence of large-scale topography on the weather process over China. *Acta Meteor. Sinica*, **26**, 167—182 (in Chinese).
Liu Kwang-nan, 1953: The "SW-vortices". Mimeograph. 58 pp. (in Chinese).
— Wu Hung-shun, 1956: A preliminary study on the determination of natural synoptic summer season over Asiatic natural synoptic region and the prevailing weather process in this season. *Acta Meteor. Sinica*, **27**, 219—242 (in Chinese).
Pan Jün-fang, 1954: An investigation of the movement of Pacific high pressure in summer. *Acta Meteor. Sinica*, **25**, 101—122 (in Chinese).
Wu Hung-shun and Chen Long-shun, 1956: The structure of general circulation over continent Asia during January—March, 1956. *Acta Meteor. Sinica*, **27**, 361—381 (in Chinese).
Yang Chien-chu, 1953: Utilization of regularities in the historic change of meteorological elements applied to the long-range forecasting for intervals longer than one year. *Acta Meteor. Sinica*, **24**, 100—117 (in Chinese).
— 1954: Composite chart for the variation of upper westerlies and its usage. *Acta Meteor. Sinica*, **25**, 65—90 (in Chinese).
— 1956: The mean monthly changes of air mass of the northern hemisphere. *Acta Meteor. Sinica*, **27**, 37—60 (in Chinese).
— Yao Gih-yen, 1955: On the diurnal variation of atmospheric pressure in China. *Acta Meteor. Sinica*, **26**, 109—124 (in Chinese).
Yeh Tu cheng, 1951: On the orographical and thermal influence of the land-and-sea-distribution on the general circulation of the atmosphere. *J. Chinese Geophys. Soc.*, **2**, 231—254.
— 1952: The seasonal variation of the influence of Tibetan Plateau on the atmospheric circulation. *Science Record*, **5**, 125—137.
— Chu Pao-chen, 1955: The onset of the transitional season in the Far East from the viewpoint of the general circulation. *Acta Meteor. Sinica*, **26**, 71—86 (in Chinese).
— Kao Yü-hsih and Liu Kwang-nan, 1951: A study on the onset and retreat of jet stream over Southern Asia and South-west United States of America in 1945—46. *J. Chinese Geophys. Soc.*, **2**, 255—278.
— Kao Yü-hsih, Pan Jün-fang and Hsü Shu-ying, 1954: A synoptic-statistical study of the cold air activities in China. *Acta Meteor. Sinica*, **25**, 1—22 (in Chinese).
— Lo Szu-wie and Chu Pao-chen, 1957: The wind stucture and heat balance in lower troposphere over Tibetan Plateau and its surroundings. *Acta Meteor. Sinica*, **28**, 108—121 (in Chinese).

REFERENCES

Chaudhury, A. M., 1950: On the vertical distribution of wind and temperature over Indo-Pakistan along meridian 67° E in winter. *Tellus*, **2**, 56—62.
Chen, H. Y., 1952: On the weather types of Mai-yü, *Synoptic Monthly*, **14**, 9—13 (in Chinese).
Chyou, Y. Y., 1956: Temperature and wind fields in cross section along 140° E in winter. *Acta Scientiarum Naturalium Universitatis Pekinesis*, **3**, 63—68 (in Chinese).
Hess, S. L., 1948: Some new mean meridional cross sections through the atmosphere. *J. Meteor*, **5**, 293—300.
Hsieh Yi-fi and Chen Yü-chau, 1951: On the wind and temperature fields over Pacific and Eastern Asia in winter. *J. Chinese Geophys. Soc.*, **2**, 279—288.
— Chen Chu-shih, 1956: The equations of motion of vortices in baroclinic atmosphere and their application in the weather forecasting. *Acta Meteor. Sinica*, **27**, 283—306 (in Chinese).
Koteswaram, P., Raman, C. R. V., and Parthasarathy, S., 1953: The mean jet over India and Burma in winter. *Indian J. Meteor. and Geophys.*, **4**, 111—122.
Miller, J. E., and Mauntis, H. T., 1947: Extratropical cyclogenesis in the Pacific coastal region of Asia. *J. Meteor.*, **4**, 29—43.
Mohri, K., 1953: On the fields of wind and temperature over Japan and adjacent waters during winter of 1950—1951. *Tellus*, **5**, 340—358.
Namias, J., 1950: The index cycle and its role in the general circulation. *J. Meteor.*, **7**, 130—139.
Pogosian, Ch. P., 1947: *Seasonal variation of general circulation* (in Russian), Leningrad, 88 pp.
Sawyer, J. S., 1954: The structure of the intertropical front over NW India during the SW monsoon. *Q. J. Roy. Met. Soc.*, **73**, 346—370.
Scherhag, R., 1949: *Wetteranalyse und Wetterprognose*. Berlin, Springer-Verlag, 424 pp.
Sutcliffe, R. C., and Bannon, J. K., 1956: Seasonal changes in upper air conditions in the Mediterranean-Middle East area. *Scientific proc. of the International Association of Meteorology*. (Rome Sept. 1954) 317—334.
U.S. Weather Bureau, 1952: Normal weather charts for the northern hemisphere. *Tech. paper*, No. 21, Washington.
Yeh Tu-cheng, 1950: Circulation of the high-troposphere over China in winter, 1945—46. *Tellus*, **2**, 173—183.
Yin, M. T., 1949: A synoptic-aerologic study of the onset of summer monsoon over India and Burma. *J. Meteor.*, **6**, 393—400.

Some Aspects of Antarctic Geophysics*

By H. WEXLER, Chief Scientist, US-IGY Antarctic Program, National Academy of Sciences, Washington, D. C.

(Manuscript received July 5, 1957)

1. Introduction

This paper is concerned mostly with the Antarctic Ice Sheet—first, the time required for the ice to build up to its present mass; second, its present budget in terms of annual import and export; and third, its important role in the manufacture of cold air.

The discussion will be suggestive rather than conclusive and will attempt to illustrate the need for the type of data which will be collected in the Antarctic during the International Geophysical Year.

2. Time Required to Build Up the Antarctic Ice

The transfer of water from the oceanic reservoir through the narrow bottle-neck of the atmosphere to the polar ice sheets must be a very slow process, since at any one time the atmosphere contains only 10^{-5} of the water found in the ocean, while the present land ice sheets have locked up as much as 2% of the water contained in the oceans. To estimate the time required for the Antarctic Ice to build up to its present mass we must first estimate this mass.

The area covered by the thick (non-annual) inland and shelf ice attached to Antarctica has been estimated by KLEBELSBERG (1948) to be $13.5 \cdot 10^6$ km^2. An earlier figure of 1,600 meters for the average thickness is thought to be too small, SHARP (1956), GOULD (1957). Recent observations of ice: 2,800 meters thick 400 km inland from Maudheim (71° S, 11°W), (ROBIN, 1953), figure 1; 3,000 meters thick in the vicinity of the Byrd IGY Station, 80° S, 120° W, (1,515 meters m.s.l.), (BENTLEY and CRARY, 1957); and 3,000 to 3,500 meters thick in the vicinity of the Pioneerskaya IGY Station, 69° 44′ S, 95°30′ E (2,700 meters m.s.l.), 375 km inland from Mirny (AVSIUK, 1957) all point to thicker ice than formerly believed. An average thickness of ice of 2,000 meters over the $13.5 \cdot 10^6$ km^2 area is assumed which, taking an average density of 0.9 for the ice, amounts to a mass of $2.43 \cdot 10^{22}$ gm.

If we now visualize an idealized Antarctic continent bounded by the 70° S latitude circle let us estimate the transport of water vapor across this boundary. If we use the value of

* Paper presented at Fourth CSAGI Conference on the Antarctic, Paris, France, 13 June 1957.

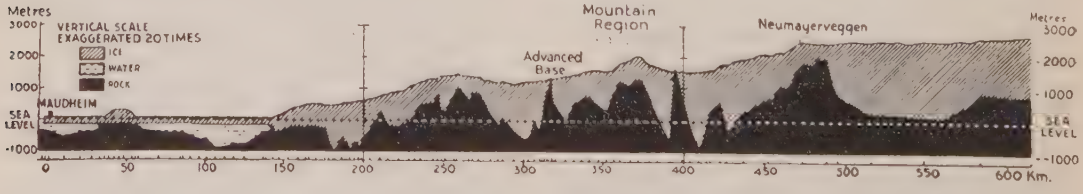

Fig. 1. The main seismic profile showing the ice and rock profiles inland from Maudheim, Antarctica. The vertical strokes above the distance scale indicate points at which seismic soundings were made [after Robin (1952)].

$0.8 \cdot 10^{11}$ grams per second crossing the 70° *North* latitude circle computed from Northern Hemisphere observations during 1950 by STARR and WHITE (1954) and assume that all the water is deposited as snow, this transfer process would take 9,650 years. Another estimate made by LOEWE (1956) for transport across the 70° *South* latitude circle is two-thirds as large, or $0.52 \cdot 10^{11}$ gm/sec, giving 14,800 years as the time required for the ice to build up to its present size. Since both these figures assume no loss during the period of ice deposition, these times must be regarded as *minimum* values provided the transport of water vapor across latitude 70° South remains the same throughout the whole period.

3. Present Antarctic Ice Budget

If we use the Starr and White Northern Hemisphere water vapor transport figure the import across 70° S is $2.52 \cdot 10^{18}$ gm/yr and, if we use Loewe's figure, it is $1.62 \cdot 10^{18}$ gm/yr; the latter figure is equivalent to an average liquid precipitation of 12 cm/yr over Antarctica.

According to LOEWE, the export by blowing snow, extrapolated from the values measured at the notoriously windy Adélie Land coast and therefore probably too high as a mean for the entire coastline, is $0.28 \cdot 10^{18}$ gm/yr and that due to calving of ice bergs is $0.04 \cdot 10^{18}$ gm/yr.

This later figure is based on an estimate by Loewe of the annual movement northward of 20 meters per year of a 150 meter thick shelf ice whose northern boundary is at 70° S. Other estimates, SHARP (1956), GOULD (1957), for the Ross Ice Shelf (in the vicinity of the Bay of Whales) are more than ten times larger.

Loss by run-off from melting snow or evaporation is nil. But the melting of the shelf ice by the sea may be appreciable and to estimate this we use Sverdrup's figure of the heat transport by that component of the wind-driven ocean current directed into the ice shelf near Maudheim (SVERDRUP, 1953). The annual average temperature of the surface layer of the ocean is 0.3°C above the freezing point of sea-water and if all the heat thus transported into the ice barrier were used to melt ice it would melt $1.30 \cdot 10^{18}$ gm/yr. The budget is summarized in Table 1.

Table 1. Antarctic Ice Budget (in 10^{18} gm/yr)

Import	
By water vapor transport across 70° S (Loewe)	1.62
Export	
By blowing snow (Loewe)	.28
By calving of ice bergs (Mawson & Loewe)	.04
By melting of ice (Sverdrup)	1.30
	1.62

Using these figures, a balanced budget is achieved but the agreement of the two numbers is probably fortuitous because of the many uncertain factors. For example, not all of the energy transported into the barrier may melt ice—some of it after sinking may not push under the ice shelf but may turn northward as illustrated in Sverdrup's figure (figure 2). Sverdrup estimates that only 10 % of the southerly transport of oceanic heat into the barrier would be required to off-set the annual accumulation of 40 cm of water equivalent along a 30 km wide strip of the shelf ice at Maudheim. But if the entire Antarctic Ice is to be in balance on the basis of the above budget, then the amount of ice to be melted each year would have to be the equivalent of a *strip of ice one meter thick, 100 kilometers wide of an ice shelf whose northern terminus is the 70° South latitude circle.*

Referring to Robin's Queen Maud Land Ice Profile in figure 1, there is evident a slight increase of the ice thickness near the 100 km mark which perhaps may be interpreted as evidence of such melting to the north.

If, however, future observations show melting of the bottom of the ice shelf to be negligible or even negative (i.e., accretion by freezing of sea water) then the above budget can be balanced only by a much larger "calving" of ice from the ice barrier than observed by Mawson and Loewe in the Adélie Land coastal area. To achieve a balanced budget by the calving process and not by melting, each year a 500 meter wide strip of shelf ice 200 meters thick would have to break away all around the 70° S latitude circle as compared to 30 meters estimated by Mawson, and 20 meters by Loewe. There is additional evidence, (CRARY, radio message, 30 May 1957 and HAWKES, private communication, June 1957, based on

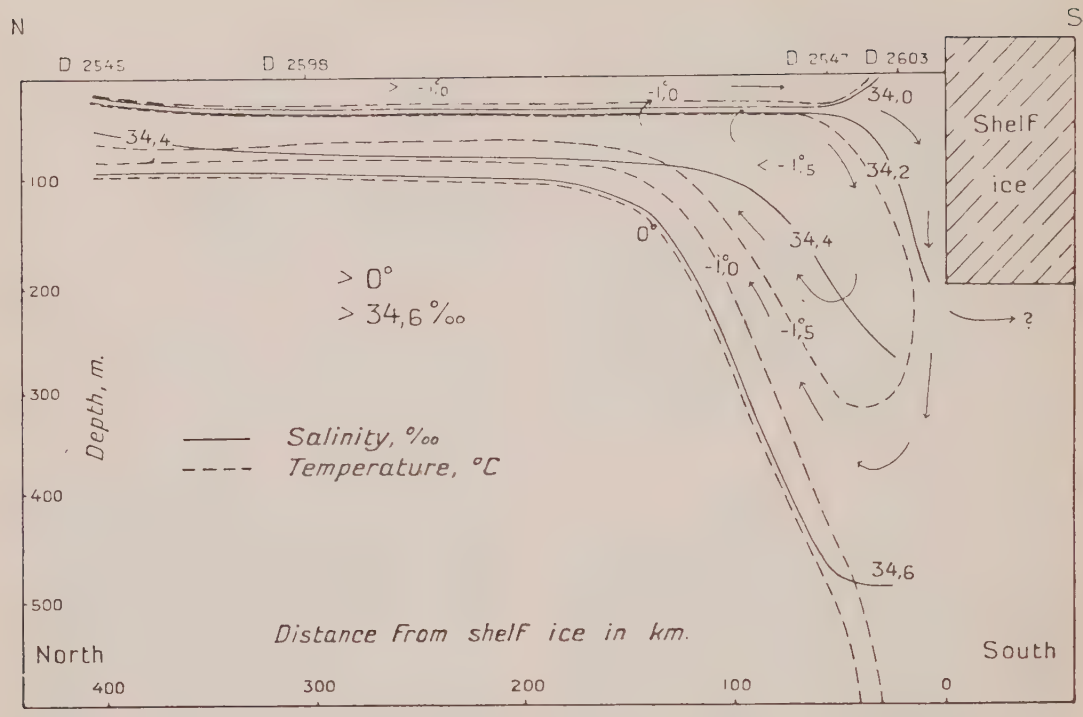

Fig. 2. Vertical section at right angles to the coast line in about longitude 2°E (Queen Maud Land), showing distribution of temperature, salinity, and probable vertical circulation [after Sverdrup (1953)].

observations made in 1947 and 1955) which supports Gould's measurement of 1929—30 that near the former Bay of Whales at Little America the ice edge is moving northward and presumably breaking off at nearly the 500 meter/year rate required but because of the influence of Roosevelt Island it is questionable whether this value is representative of the remainder of the Ross Ice Shelf and other ice shelves.

Observations taken in the International Geophysical Year should throw considerable light on the annual import of water vapor and whether the principal loss of the Antarctic ice is from melting by the sea or by the calving process.

4. The Ice as a Source Region for Polar Air

Antarctica as a whole averaged over a year is a radiative cold source. For example, Liljequist (1956) showed that at Maudheim the average net radiative loss (taking into account the effective incoming solar radiation and outgoing infra-red radiation) is 25 ly day^{-1}. (1 langley (ly) equals 1 cal/cm^2). At Port Martin (3° farther north) Loewe (1956) found a net loss 20 ly day^{-1} and for the inland ice as a whole he computed a net radiative loss of 100 ly day^{-1}.

Liljequist showed the net radiative loss at Maudheim is off-set by the turbulent transport of heat downward from atmosphere to the surface and the upward conduction of heat from the interior of the snow, but still leaves a deficit of 4.5 ly day^{-1}, which must be balanced by hoarfrost deposit of 2.4 grams per year.

What happens to mild maritime air as it moves over such an enormous cold source as Antarctica? This problem was studied under the assumption that only infra-red radiative exchanges between snow surface, atmosphere and space are involved (Wexler, 1936). The computation therefore neglected (i) solar radiation (the cooling occurred during the polar night); (ii) turbulent transport of heat downward (calm conditions were assumed); and (iii) no heat conducted upward from the snow (considered to be a perfect insulator).

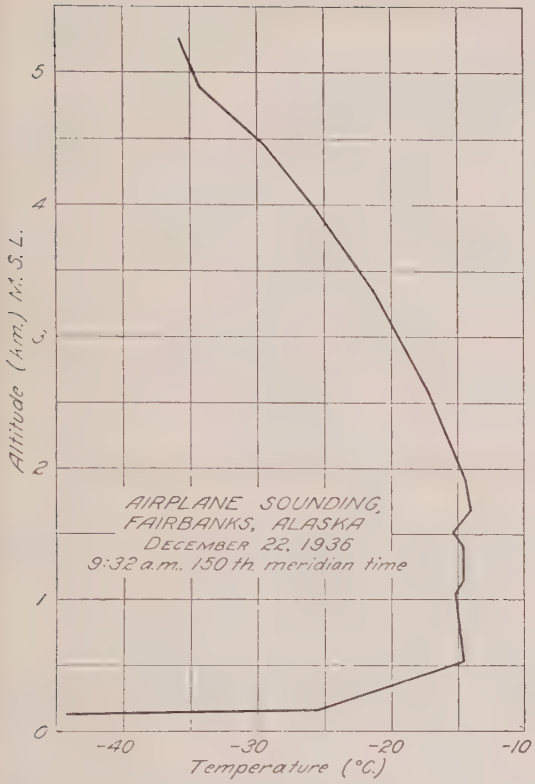

Fig. 3. Airplane sounding, Fairbanks, Alaska, December 22, 1936.

5. Rate of Cooling of the Air

Under these conditions the atmosphere cools mainly from below, undergoing a succession of quasi-radiative equilibrium states characterized by a strong increase of temperature with height above the surface (surface inversion) and isothermal conditions above to the top of the cooled layer as illustrated in figure 3 (WEXLER, 1937). Since as time proceeds, thicker and thicker layers of air are cooled accompanied by a smaller and smaller energy loss, the rate of cooling decreases asshown in figure 4 (WEXLER, 1936). Considering only the full lines (which apply to an atmosphere of normal infra-red radiative properties), the cooling initially (shown in the inset diagram) is very rapid until a "critical" temperature of —33°C is reached and progressively thicker layers of air join in the cooling. The cooling rate then slows down appreciably as shown in the larger diagram. Plotted in this diagram are large black dots showing the downward progression of surface air temperatures at the Amundsen-Scott IGY (South Pole) Station. During the past Antarctic summer (December and January) the temperatures were between —18°C and —30°C and first reached the critical value of —33°C on February 12, 1957, and successively lower temperatures at later dates as indicated by the black dots. It is interesting to note that none of the dots fell below the computed curve although this was constructed for an atmosphere resting on sea-level and not for one resting on the 2,800 meter high South Polar Plateau; the latter atmosphere should have much less water vapor and therefore be capable of cooling more rapidly than a sea-level based atmosphere.

6. Upper Air Conditions over the South Pole

On May 11, at 1445 GMT, 88 days after the "zero" day of February 12, 1957, the South Pole surface temperature dropped to —73.6°C to establish a new world's record low temperature. On September 17, 1957 the temperature fell to — 102.1° F to establish a new record. A radiosonde ascent made at 0000 GMT on May 10, thirty-nine hours before the record low temperature was measured, is shown in figure 5. The strong surface temperature inversion called for in theory is clearly present to a degree never before observed—an increase of 31°C in 850 meters. Above this height the normal temperature decline with height is found terminating in a well-marked tropopause inversion of 3°C at 8,500 meters above sea level or 5,700 meters above the station. After maintaining near-isothermalcy at approximately —62°C for the next 4 kilometers, the temperature drops to —77°C at 20 km above which another inversion, suggestive of a second tropopause, is found. (The same phenomenon was also observed 1 kilometer lower in the sounding taken 24 hours later.)

The maximum temperature of —60°C at the bottom of the stratosphere represents a drop from the —40° characteristic of polar stratospheres—both Antarctic and Arctic—in the summer. The cooling rate of the 11 to 15 km layer of air which averages 0.35°C per day from late March to April 1957, is very close to the value of 0.30°C per day computed by GOWAN (1947) by night-time radiative cooling from the ozone, water vapor and carbon dioxide present in the lower stratosphere.

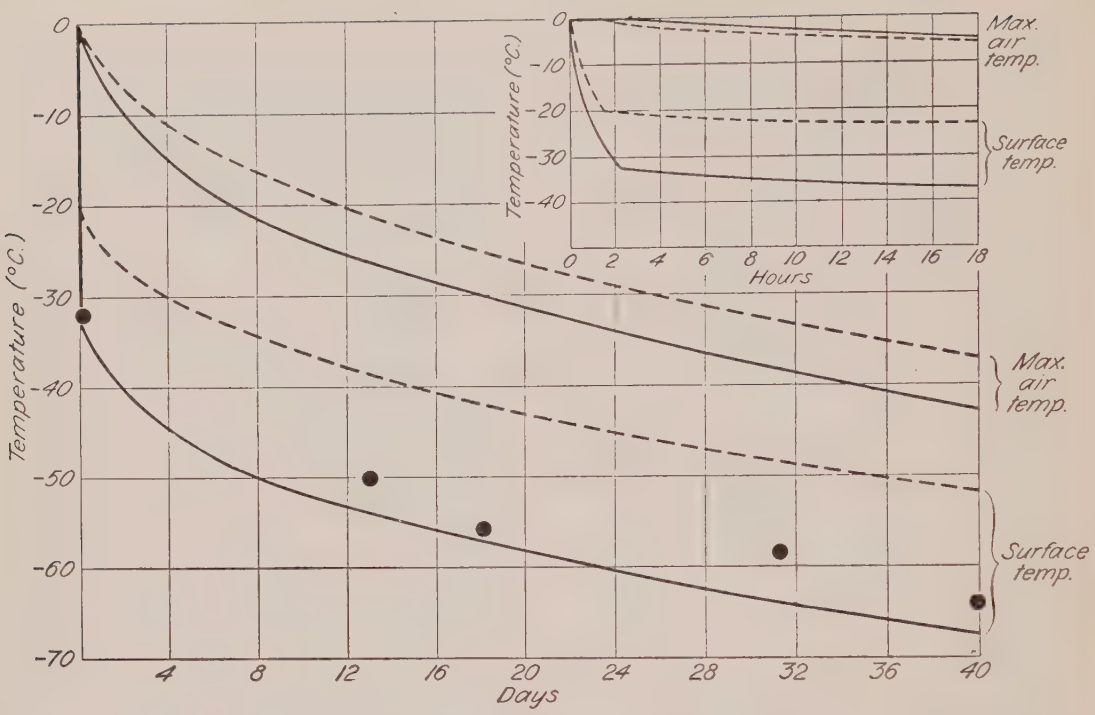

Computed thermograms based on (*a*) Hettner's data in atmosphere of abnormal CO_2 content (shown by broken lines; (*b*) Weber and Randall's data in atmosphere of normal CO_2 content (shown by solid lines).

Fig. 4. Air temperatures versus time - computed (1936) (solid lines) and observed (black dots) at IGY South Pole Station (1957).

7. Stratospheric Versus Tropospheric Cooling

Another radiosonde report from the South Pole taken on June 17 at 1200 GMT was sent to Washington and is plotted on figure 5. The lower half of this sounding is almost identical with that on May 10th but is considerably cooler in the stratosphere. If the June sounding is taken as representative of June conditions at the Pole it would indicate that unequal cooling has occurred—namely, the troposphere temperatures are virtually the same but the stratosphere has cooled by 8° to 10°C. This unequal cooling decreases greatly the intensity of the tropopause inversion and would account for the absence of the winter tropopause observed in Antarctica by COURT (1942), and more recently by SCHUMACHER (1955). The cooling rate in the lower stratosphere from May 10 to June 17 is 0.25°C per day, again very close to Gowan's computed value.

The lack of a corresponding temperature drop in the troposphere may perhaps be indicative of a very strong advection of warm air in this layer but not in the stratosphere. The very rapid fall of surface air temperature at the South Pole from February to May and recovery to higher values thereafter is believed to be indicative of a strongly overcompensating horizontal heat advection arising from the increasing winds caused by unequal radiative cooling of Antarctica and the surrounding oceans. For example, at the South Pole, the average surface air temperature for May 1957 was —55.7°C, or 0.8° higher than the —56.5°C value observed in April. At the Byrd IGY Station at 80° S, 120° W, the average surface air temperatures for April and May were exactly the same, —35.8°C, but both the minimum and maximum air temperatures for May were higher than those for April. These values, indicating a reversal of what one would expect to be a strong seasonal trend downward, has

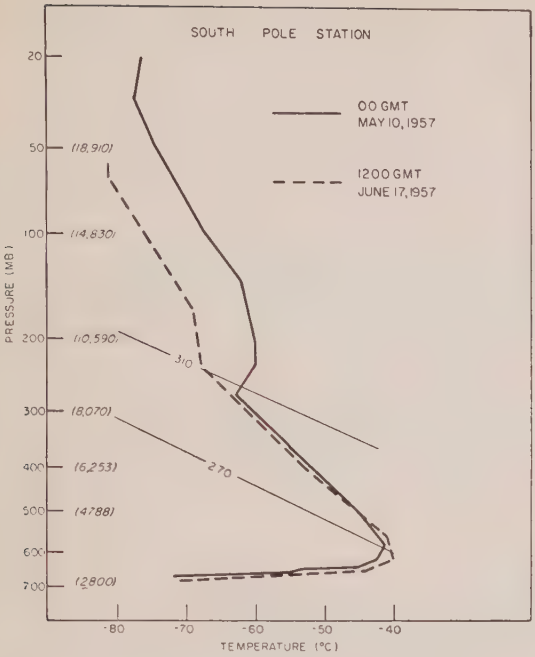

Fig. 5. Radiosondes at the IGY South Pole Station 0000 GMT, 10 May 1957 and 1200 GMT, 17 June 1957. Figures on the right hand side of the ordinate refer to the height above sea level in geopotential meters.

its counterpart in Little America where, on the basis of six years of observations, the June temperature averages 5°C higher than the May temperature (COURT, 1949 and unpublished data for 1956 and 1957). If, after a few years more of observations, this reversal of the "normal" seasonal decline of temperature in the autumn and early winter is found to be characteristic of much of Antarctica, it may reveal that horizontal advection of heat from lower latitudes more than makes up for the loss by outgoing radiation, thus requiring far stronger northerly winds aloft than formerly believed. It is of interest to note that at the same time that the South Pole IGY Station had its —73.6°C temperature, Little America, 1,200 km to the north, was enjoying a temperature of —1°C with a 60-knot gale from the ocean.

8. Micrometeorology of the Record Low Temperature

The time-sequence of the vertical air temperature profile 10 meters above the snow, wind and cloud amount is shown in figure 6. The temperatures at the snow surface, 2 meters (shelter level), 5 meters, and 10 meters are plotted in a series of vertical profiles starting at 0000 GMT on May 9th and ending at 1800 GMT on May 11th.

The wind speed is given in meters per second, the wind direction is the meridian along which the air blows to the south and the extent of cloud cover is shown by the partial filling of the circle. Initially, starting with a wind speed of 5.7 m/sec from 110° East and the skies clear, there are some unexplained variations of the temperature profile culminating in a large surface inversion of 6°C in 10 meters. However, when the wind speed dropped to the low value of 2.1 m/sec the air temperature at the shelter height of 2 meters achieved its record low of —73.6°C while the snow surface temperature fell to —74.2°C ($T_c \sim -84$°C refers to the snow surface temperature which would have been observed if there had been no eddy flux of heat downward from the atmosphere or conduction upward from within the snow).

However, in the next few hours strong advection of air from the Ross Sea, which was clearly indicated on the 500 mb and 300 mb weather charts drawn at the IGY Antarctic Weather Central at Little America, brought in clouds which covered half the sky. The black-body radiation from this cloud, which can be no colder than the tropopause temperature of —62°C, warms the snow surface temperature from its minimum of —74.2°C to —65.3°C in less than 4 hours. Compared to the effect of clouds the slight increase in wind speed makes a negligible contribution to the observed increase of the surface temperature from 1445 to 1800 GMT. The increased radiation from clouds to the snow surface is the actual mechanism by which heat, brought in by the compensating advection mentioned earlier, warms the snow surface and adjacent air.

In closing this brief account of some aspects of Antarctic geophysics I wish to pay particular tribute to the observers, both those at the present IGY Stations and those who manned the earlier stations, who, under most difficult conditions, took the observations which formed the basis of this paper. I wish also to thank my colleagues Mr. R. A. McCormick and Mr. M. J. Rubin for their assistance in the preparation of this paper.

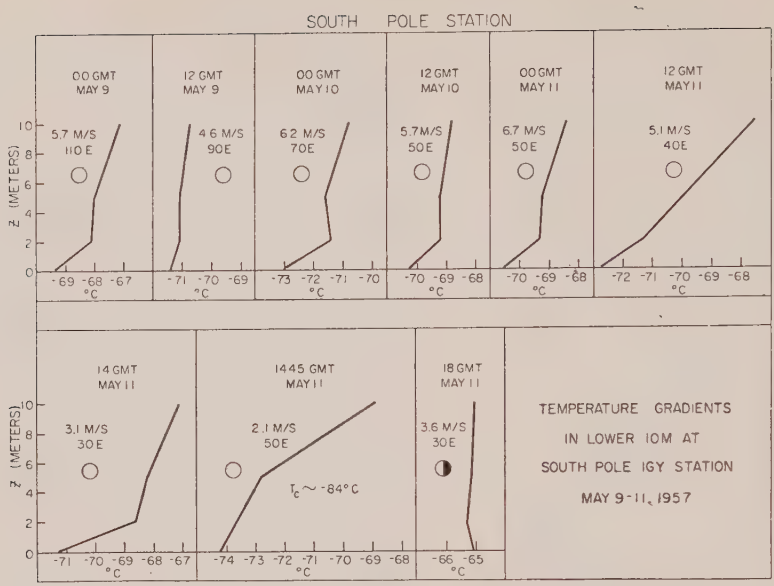

Fig. 6. Time sequence, lower 10 meters temperature profile, winds and sky cover at IGY South Pole Station.

REFERENCES

Avsiuk, G. A., 1957: Études Glaciologiques Faites par L'Éxpedition Antarctique Soviétique, paper presented at IV CSAGI Antarctic Conference, Paris, 13 June 1957.

Bentley, C. R., and Crary, A. P.: radio message, 31 March 1957.

Court, A., 1942: Tropopause Disappearance during the Antarctic Winter, *Bull. Amer. Met. Soc.*, **23**, pp. 220—238.

— 1949: Meteorological Data for Little America III, *Mo. Wea. Rev.* Suppl. 48.

Gould, L. M., 1957: Antarctic Prospect, *Geogr. Rev.*, XLVII, No. 1, pp. 1—28.

Gowan, E. H., 1947: Night Cooling of the Ozonosphere, *Proc. Roy. Soc., A.* **190**, pp. 227—231.

Klebelsberg, R. V. 1948—49: *Handbuch der Gletscherkunde und Glazialgeologie*, Wien.

Liljequist, G. H., 1956: Energy Exchange of Antarctic Snow Field, Long-Wave Radiation and Radiation Balance, Norwegian-British-Swedish Antarctic Expedition, 1949—52, *Scientific Results*, II.

Loewe, F. 1956: Études de Glaciologie en Terre Adélie, 1951—52, Act. Scient. et Industr. 1247, Exp. Pol. Fran., Hermann & Cie, Paris.

Robin, G. de Q., 1953: The Norwegian-British-Swedish Antarctic Expedition, 1949—52. Part II: Summary of Seismic Shooting Investigations in Dronning Maud Land, *Jour. Glaciol.*, **2**, n. 13, pp. 204—211.

Schumacher, N. J., 1955: Upper Air Temperatures over an Antarctic Station, *Tellus*, **7**, pp. 87—95.

Sharp, R. P., 1956: Objectives of Antarctic Glaciological Research, Chapter in *Antarctica in the Geophysical Year*, Geophys. Monogr. No. 1, American Geophysical Union, Wash., D. C., pp. 27—35.

Starr, V. P., and White, R. M., 1954: Balance Requirements of the General Circulation, in *Studies of the Atmospheric General Circulation*, Mass. Inst. Technol., Final Report, Par i, Gen'l Circ. Proj. pp. 186—242.

Sverdrup, H. U., 1953: The Currents off the Coast of Queen Maud Land, *Norsk Geogr. Tidsskrift*, Bd XIV, nr. 1—4.

Wexler, H., 1936: Cooling in the Lower Atmosphere and the Formation of Polar Continental Air, *Mo. Wea. Rev.*, **64**, pp. 122—136.

— 1937: Absorption of Radiation by Water Vapor as Determined by Hettner and by Weber and Randall, *Mo. Wea. Rev.*, **65**, pp. 102—104.

Comparison of Aerological Soundings made Simultaneously by Radio-Sonde and Aircraft

By F. H. LUDLAM and P. M. SAUNDERS, Imperial College, London*

(Manuscript received April 26, 1957)

Abstract

On five separate occasions soundings were made at the same time by Väisälä radio-sonde and by an aircraft equipped with electrical resistance thermometers. Display of the results leads to the conclusion that the temperature indicated by the radio-sonde was too high by an amount which usually was between 1 and 1½° C, but occasionally reached 2½ to 3½° C. The usual difference can be accounted for by the known effects of lag and radiation error, and it is recommended that even in the lower troposphere appropriate corrections should be made as a routine in conditions of sunny weather and steep lapse rate. Because of the excessive lag often shown by the radio-sonde hygrometer unit (of hair), shallow layers of very dry air are not indicated at all in the radio-sonde soundings.

1. Introduction

It is well known that radio-sonde observations of temperature and humidity are subject to noticeable errors arising from the lag of the thermometer and hygrometer, and from the warming of the thermometer element which occurs when it, or its housing, is exposed to strong sunshine.

It is increasingly common practice to make corrections for these errors, but it is still widely believed that in the lower troposphere, where the sensing elements are fairly efficiently ventilated, the errors are unimportant. Certainly in routine synoptic analysis the significant errors are only those of one instrument with respect to the others used in the synoptic network, but in the analysis of individual soundings it may be necessary to consider the variation of the errors with height, or even the absolute values of the errors in the measurements made at particular levels. Such considerations are necessary, for example, for studies of cumulus growth and abnormal radio propagation, in which vertical gradients of temperature and humidity are important.

It is sometimes held that the existence of local variations of temperature and humidity render unnecessary the precise reporting of the sounding as recorded at the observing station, and even make corrections for lag and radiation of doubtful value. It is certainly true that the synoptic meteorologist involved in forecasting practice can hardly benefit from a study of the detail of soundings, nor can he afford to have his communication channels and plotting assistants overburdened with reports of such detail. Nevertheless the routine soundings contain a remarkable wealth of information for the meteorologist who studies meso-scale processes in the atmosphere and in our view it is unfortunate that often only

* The observations described were made during field work carried out while the writers were attached to the International Institute of Meteorology, Stockholm.

smoothed and partially corrected versions appear in published aerological records.

During our field work in Sweden, which was concerned mainly with the structure and growth of shower clouds, we were fortunate to have our ground observations supplemented by soundings made at the nearby radio-sonde station of Frösön, and by reconnnaissance flights of an aircraft of the Swedish Air Force, equipped with electrical resistance thermometers. It became apparent that their observations were not always in perfect agreement, and by the kind co-operation of both establishments we arranged for the aircraft to make some soundings in the vicinity of the radio-sonde station at the time of release of radio-sondes. We then compared the respective soundings and confirmed that the radio-sonde indicated temperatures which differed by amounts which are significant in our studies. Similar comparisons have been made by other investigators, but their results have not, to our knowledge, been given unrestricted publication, and so we believe that an account of our own work will be interesting.

2. The aircraft instrumentation

The aircraft was equipped with British Meteorological Office balanced bridge resistance thermometers, with knife-type wet- and dry-bulbs mounted in anti-radiation housings on the under-surfaces of the main wings. The thermometers are brought separately into the bridge circuit, and readings are made against a scale marked in Fahrenheit degrees upon a rheostat which is used to bring a galvanometer needle to a zero-point. A practised observer under normal flight conditions can read the scale with an accuracy of 0.2° F.

When a sounding was made the thermometers were read during level flight when two or three successive measurements at intervals of about 20 seconds had shown steady values to have been attained (the lag coefficient of these thermometers is known to be only a few seconds). It is necessary to apply corrections to the height indicated by the altimeter, and to the temperatures indicated by the thermometers.

Atmospheric pressure was determined from the reading of an ordinary aircraft altimeter, whose millibar sub-scale was set at 1,013.2 mb, so that the height-pressure relation was that of the I.C.A.N. atmosphere. From observations during flights made at a height of 25 m above the airfield barometer it was established that the position-error amounted to less than 1 mb. The altimeter was carefully calibrated against a mercury barometer; the departures of the indicated from the true I.C.A.N. height were less than 12 m (about 1 mb) at all heights up to 2 km, and increased from 20 m at 2,500 m to 35 m at 3,500 m: the appropriate corrections to the indicated heights were made during the evaluation of the soundings.

The indicated temperatures during flight exceed the true air temperatures by an amount $\Delta T°$ F which is related to the true air speed v km/hr by the equation

$$\Delta T = \alpha_D (v/100)^2 \ldots\ldots\ldots \quad (1).$$

There is some evidence that the coefficient α_D is not constant, but a function of Reynolds Number at the thermometer bulb; however, during horizontal flights on two separate occasions at eight indicated air speeds ranging from 140 to 275 km/hr we found α_D practically constant and deduced values of α_D as 0.40 and 0.42. From calibration flights made the previous summer with a similar thermometer we had deduced a value of 0.40. We used a mean value of 0.41 for the new thermometer, and by a similar procedure derived another coefficient for correcting the temperatures indicated by the wet bulb. At the usual flight speed of 220 km/hr the corrections applied to the dry- and wet-bulb readings amounted to about 2° F. We believe that the deduced values of true air temperature and dew point are unlikely to have errors exceeding 0.5° F and 2° F, or about 0.3° C and 1° C, respectively.

3. Comparison of temperatures measured at the ground and during flight just above

At 0815 on 1 September 1955 the aircraft was flown over the airfield at an estimated height of 35—40 m above the ground. The indicated temperature was 53.9° F and the corrected value 51.1° F, or 10.6° C. At the same time an observer on the ground measured a temperature of 11.0° C with an Assmann pyschrometer. The surface wind

was NW, 5—7 m/sec, and the sky was overcast with stratus layers; the lowest clouds were 2/8 stratus fractus with base 300 m above the airfield. The convective condensation level was deduced from the Assmann readings to be at 320 m. It is therefore reasonable to suppose a dry adiabatic lapse-rate near the ground and to deduce a temperature of about 10.6° C at the flight-level, in agreement with the value obtained from the aircraft thermometer. The exact correspondence is perhaps fortuitous and we had no opportunity to make other tests, but believe this result justifies our confidence in the temperatures deduced on the aircraft soundings.

4. Comparison of aircraft and radio-sonde soundings

Aircraft soundings were made for comparison with 3 routine and 2 special soundings by Väisälä radio-sonde. The results are represented on T-Φ diagrams in Figs 1 to 5. All the soundings were made in fair weather, when there was little or no cloud.

It will be observed in Figs. 2 and 5 that on occasions of the special radio-sonde ascents there is a quite remarkable similarity in the trend of the temperature curves obtained by the two methods. The same feature is less strikingly displayed on the remaining occasions, and strongly indicates that the soundings are equally representative of the atmosphere in the neighbourhood of the radio-sonde station, and that the differences between the simultaneous soundings cannot be attributed to purely local temperature variations.

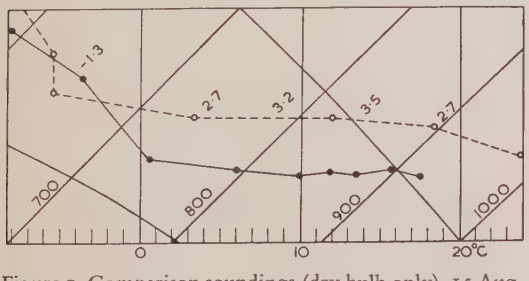

Figure 1. Comparison soundings (dry bulb only), 15 Aug. 1955. The pecked curve shows the record of the radio-sonde, the full line that of the aircraft sounding. The figures beside the pecked curve indicate the differences between the temperatures at particular levels. The radiosonde was released at 1530 local time and the aircraft sounding was made between 1455 (highest level) and 1515 (lowest level). There were scattered Cumulus with base 760 mb and tops to 550 mb.

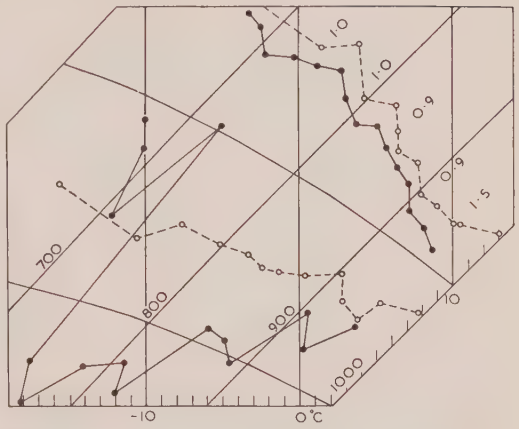

Figure 2. Comparison soundings (including dew points), 22 August 1955. The radiosonde was released at 1040 and the aircraft sounding was made between 1020 (lowest level) and 1114 (highest level). There was less than $^1/_8$ Cumulus with base 910 mb and tops to 880 mb.

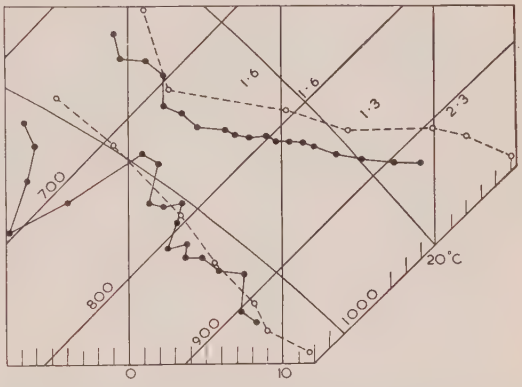

Figure 3. Comparison soundings, 25 August 1955. The radiosonde was released at 1530, and the aircraft sounding was made between 1508 (lowest level) and 1605 (highest level). There was less than $^1/_8$ Cumulus with base 800 mb and tops to 770 mb.

The diagrams also show that the radio-sonde consistently records higher temperatures, the difference amounting to between about 1.0 and 3.5° C and tending to be greater when the lapse-rate has a high value. The largest differences occur on two afternoons when the radio-sonde indicates a lapse-rate near the ground (Figs. 1, 3) which is *less* than the dry adiabatic, whereas under these conditions a superadiabatic lapse rate would be expected, and is indeed found by joining the points representing surface conditions to those corresponding to the measurements made in the aircraft at its lowest flight level.

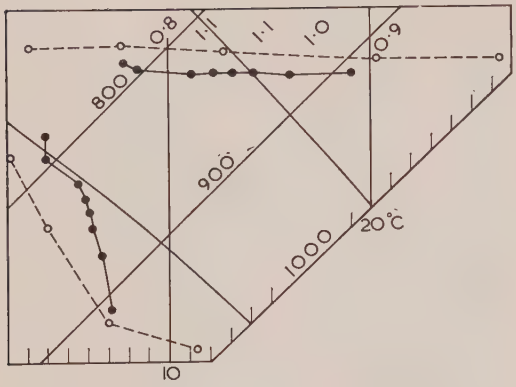

Figure 4. Comparison soundings, 26 August 1955. The radiosonde was released at 1530, and the aircraft sounding was made between 1515 (lowest level) and 1535 (highest level). There was less than 1/8 Cumulus with base 776 mb and tops to 690 mb.

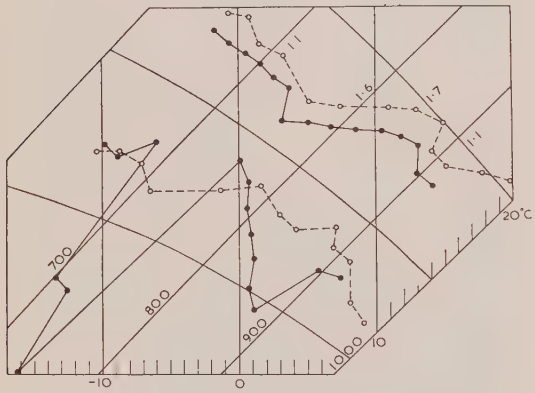

Figure 5. Comparison soundings, 27 August 1955. The radiosonde was released at 1111 and the aircraft sounding was made between 1059 (lowed level) and 1135 (highest level) in a cloud-free sky.

Consequently there is good reason to believe that in these conditions the radio-sonde temperatures are too great, by 1.0 to 3.5° C.

On the four occasions when comparisons of dew-points can be made the respective soundings are in reasonable agreement near the ground. The general agreement up to 3 km on 25 August 1955 (Fig. 3) is striking, but on other occasions the aircraft sounding tends to indicate dew points which are lower than those on the radio-sonde record. In particular the radio-sonde fails to portray rather shallow layers of very dry air, which are a feature of 3 of the aircraft soundings (Figs 2, 3 and 5).

5. Discussion

On all occasions there was strong sunshine, and it is reasonable to attribute the errors in the records of the radio-sondes to the combined effects of radiation and lag.

Nyberg (1940) has measured the lag coefficient α of the Väisälä radio-sonde at different ventilation speeds under room pressure and has found a mean value of 15 sec. for its usual speed of ascent through the atmosphere. If the rate of change of temperature is β and is constant, the radio-sonde thermometer records a steady-state temperature which is too high by an amount $\alpha\beta$. If therefore v is the speed of ascent (relative to the ground) of a radio-sonde through air with a lapse-rate γ, the steady-state temperature error is $\alpha v \gamma$. The speed v in still air is usually about 6 m/sec, so that the error due to lag during rise through air having a dry-adiabatic lapse rate can be expected to be about $6 \times 10 \times 10^{-2}$ ° C, that is, about 0.9° C. On occasions when the lapse rate is a fraction of the dry adiabatic, the error is correspondingly reduced, and becomes zero in an isothermal layer.

On the other hand the maximum computed error due to lag may be considerably increased on occasions owing to the use of a thermometer element having a lag coefficient greater than the average, and possibly it can be further increased when the balloon enters a thermal. The speed of ascent may then be increased by up to 100 %, with a corresponding increase of the lag error; moreover the balloon may then be in air which has a temperature a few tenths of a degree Centigrade higher than the mean temperature over distances of more than a kilometre, which is that determined by the aircraft. Consequently the total discrepancy due to these two effects could then conceivably attain 2.0° C.

The error due to sunshine falling upon the radiation shield of the thermometer is known to amount to about 1° C at a height of 10 km when the sun has an elevation of 25—30° (as during the comparison soundings), but is usually regarded as negligible in the lower troposphere. In the evaluation of the Väisälä radio-sonde records it is assumed to be zero below the 500 mb level, for there clouds frequently and effectively shield the thermometer from sunshine. However, at the

solar elevations mentioned and at the 800 mb level the formulae for radiation error in clear skies given by VÄISÄLÄ (1941) and by RAUNIO (1951) give a value of about 0.5° C, and for similar conditions SCRASE (1954) calculates a radiation error of about 0.5° C for the British radio-sonde, on which the thermometer element is protected by a shield of the same kind as that used on the Väisälä radio-sonde.

It therefore appears that the discrepancies found during the comparison soundings can on the whole be accounted for by the combined errors known to be due to the effects of lag and radiation. It is possible that on the occasion of the excessive differences shown in Fig. 1 some contribution was also made by two sources of error mentioned by NYBERG (1952): inaccurate corrections made when measuring temperatures at the ground just before the release of the radio-sonde, and minor shocks during the release.

Since sunny weather and strong lapse rates are not altogether uncommon, and result in radio-sonde temperatures which are too high by more than 1° C, we recommend that appropriate corrections should be made in these circumstances for the effects of lag and radiation even in the lower troposphere.

The lag of most hygrometer elements is so great that the record of relative humidity provided by the radio-sonde cannot be expected to represent such sudden changes as may actually be encountered. In particular the remarkable shallow layers of very dry air which are recorded during some aircraft soundings are not revealed at all. HOOPER (1957) has recently commented upon the variable qualities of radio-sondes in their capacity to detect strong gradients of vapour pressure, which are important in the study of radio wave propagation. As water vapour plays such an important part in atmospheric behaviour, and as changes in its concentration are a sensitive indicator of atmospheric processes, we hope that a solution will soon be found to the old problem of devising a hygrometer element with a rapid response, or some means of correcting its indications for the errors due to excessive lag.

Acknowledgements

We are glad to express our appreciation of the cordial co-operation of the Swedish Air Force and the staff of the S.M.H.I radio-sonde station, not only in the work described here but also in our principal field studies with staff of the International Institute of Meteorology, Stockholm. We are grateful to Lt. L. Larsson for his painstaking flight observations. These studies were supported by Statens Tekniska Forskningsråd, Sweden and the Munitalp Foundation, U.S.A.

REFERENCES

HOOPER, A. H., 1957: Heterogeneity in the measurements of humidity made by the radio-sonde network of Europe, *Met. Mag.*, **86**, p. 13.

NYBERG, A., 1940: The lag coefficient of aerological instruments and the function of hair hygrometers at low temperatures, *Medd.*, Ser. Upps. No. 32, S.M.H.I., Stockholm.

— 1952: On the comparison of radio-sonde data in Payerne, May 1950, *ibid.* Ser. B., No. 9.

RAUNIO, N., 1951: Amendments to the computation of the radiation error of the Finnish (Väisälä) radio-sonde, *Geophysica* **4**, p. 14.

SCRASE, F. J., 1954: Radiation and lag errors of the M. O. radio-sonde and the diurnal variation of upper-air temperature, *Quart. J. R. Met. Soc.*, **80**, p. 565.

VÄISÄLÄ, V., 1941: Der Strahlungsfehler der finnischen Radiosonde, Univ. of Helsinki, Inst. of Met., *Mitt.* No. 47.

An Experiment in Numerical Prediction with two Non-Geostrophic Barotropic Models

By A. BRING and E. CHARASCH*, International Meteorological Institute in Stockholm

(Manuscript received March 1, 1957)

Abstract

The result of a test with two simple non-geostrophic barotropic models are discussed. One of these models is based on ideas presented in a previous article (CHARASH 1957).

The forecasts obtained are found to differ significantly from forecasts obtained with the quasi-geostrophic model. Both non-geostrophic models appear to be free from one major weakness of the non-geostrophic model, i.e. the hypertrophy of anticyclones.

It is suggested that the disappointing forecasting performance of baroclinic models hitherto to a considerable degree springs from a similar weakness as exposed here in the quasi-geostrophic barotropic model.

Introduction

In practically all atmospheric models constructed for the purpose of numerical prediction the height field of an isobaric surface is treated as a pseudo-streamfield. That procedure implies the neglect—partially at least—of the variation of the Coriolis parameter. Justification for doing so has been found in the fact that that variation is comparatively small, and it has been concluded that the so-called geostrophic vorticity constituted a very good first approximation.

One of the authors in a previous paper (CHARASCH 1957) argues that failure to take into account fully the variation of the Coriolis parameter in evaluating the geostrophic vorticity is responsible for a systematic aberration in the exchange of kinetic energy between the basic current and the disturbances. That energy conversion constitutes an effective mechanism for the growth of disturbances and it is the only mechanism of wave growth available in the barotropic model.

Systematic appreciable differences may be expected therefore, in numerical predictions with a barotropic model which—in contrast to the quasi-geostrophic model—does account for the full variation of the Coriolis parameter.

The results of an experiment along those lines are presented in this paper.

1. The equations

The prognostic equation for the barotropic model is

$$\frac{\partial \zeta}{\partial t} = -\mathbf{v} \cdot \nabla (\zeta + f) \qquad (1)$$

where ζ denotes the relative vorticity, $\mathbf{v}$ the wind-velocity, and f the Coriolis parameter. If we introduce the *quasi*-geostrophic vorticity

* Whilst on leave from Israel Meteorological Service.

$$\zeta_g = \frac{1}{f} \nabla^2 \varphi \tag{2}$$

eq. (1) becomes

$$\frac{1}{f} \frac{\partial}{\partial t} \nabla^2 \varphi = - \mathbf{v} \cdot \nabla \left(\frac{1}{f} \nabla^2 \varphi + f \right) \tag{3}$$

If we use the geostrophic wind we get

$$\frac{1}{f} \frac{\partial}{\partial t} \nabla^2 \varphi = \left(\frac{1}{f} \nabla \varphi \times \mathbf{k} \right) \cdot \nabla \left(\frac{1}{f} \nabla^2 \varphi + f \right) \tag{4}$$

or

$$\nabla^2 \frac{\partial \varphi}{\partial t} = J \left(\frac{1}{f} \nabla^2 \varphi + f, \varphi \right) \tag{4a}$$

If we instead introduce the complete geostrophic vorticity

$$\zeta_g = \frac{1}{f} \nabla^2 \varphi - \frac{\nabla f}{f^2} \nabla \varphi \tag{5}$$

in eq. (1), we obtain

$$\frac{\partial}{\partial t} \left(\frac{1}{f} \nabla^2 \varphi - \frac{\nabla f}{f^2} \nabla \varphi \right)$$

$$= - \mathbf{v} \cdot \nabla \left(\frac{1}{f} \nabla^2 \varphi - \frac{\nabla f}{f^2} \nabla \varphi + f \right) \tag{6}$$

It is convenient to introduce here a streamfunction ψ_a defined by

$$\nabla^2 \psi_a = \zeta_g = \frac{1}{f} \nabla^2 \varphi - \frac{\nabla f}{f^2} \nabla \varphi \tag{7}$$

The wind field in which the advection of the vorticity takes place—to be consistent—is then defined by

$$\mathbf{v} = \mathbf{k} \times \nabla \psi_a \tag{8}$$

i.e. the streamfunction which is defined by the geostrophic vorticity in turn defines a (divergence-free) wind field (Bolin 1955).

With these definitions in mind, it is now possible to substitute in equation (6) and to reformulate the barotropic prognostic equation

$$\frac{\partial}{\partial t} \nabla^2 \psi_a = J \left(\nabla^2 \psi_a + f, \psi_a \right) \tag{9}$$

In equation (9) the vorticity is derived initially from the geostrophic equation, however, (9) is the prognostic equation for a non-geostrophic barotropic model.

Equations (4a) and (9) are both derived from Eq. (1), but differ from each other in two respects, namely

1. The neglect of the β-term in computing the geostrophic vorticity in (4a).
2. The introduction of the geostrophic divergence in (4a).

In order to investigate the importance of these differences it was decided to compare a number of forecasts using (4a) and (9) respectively. This does not make it possible to separate the two effects, but in the light of the theory presented by Charasch (1957) it is felt that the β-term is more important than the geostrophic divergence.

The significance of the streamfunction ψ_a is illuminated by the following consideration.

The balance equation may be written

$$\nabla^2 \psi = \frac{1}{f} \nabla^2 \varphi - \frac{\nabla f}{f} \nabla \psi - \frac{2}{f} J \left(\frac{\partial \psi}{\partial x}, \frac{\partial \psi}{\partial y} \right) \tag{10}$$

If the geostrophic approximation is made in the second term on the right hand side, we obtain

$$\nabla^2 \psi_b = \frac{1}{f} \nabla^2 \varphi - \frac{\nabla f}{f^2} \nabla \varphi - \frac{2}{f} J \left(\frac{\partial \psi_b}{\partial x}, \frac{\partial \psi_b}{\partial y} \right) \tag{11}$$

It should be stressed that (11) is a very good approximation to (10) as:

the approximated term is small compared to $\frac{1}{f} \nabla^2 \varphi$ and the error in the approximated term is a fraction of its true value.

If the non-linear term is neglected we get back to equation (7). ψ_a may thus be regarded as a first approximation to the streamfunction ψ_b, which in turn is an approximation to the exact streamfunction ψ defined by (10). ψ_a and ψ_b differ only with respect to the non-linear term and it was decided to investigate the importance of this term by making parallel forecasts with ψ_a and ψ_b. The prognostic equation using ψ_b is exactly similar to the one using ψ_a.

$$\frac{\partial}{\partial t} \nabla^2 \psi_b = J \left(\nabla^2 \psi_b + f, \psi_b \right) \tag{12}$$

II. Set-up of the experiment

A. The forecasts were computed with finite difference formulae corresponding to eqs. (4a), (9) and (12). The timestep was in all cases one hour and the meshwidth was 300 km at 50° N in a polar stereographic projection. The boundary conditions were

$$\frac{\partial \varphi}{\partial t} = \frac{\partial \zeta}{\partial t} = 0 \tag{13}$$

and analogous for ψ_a and ψ_b. Smoothing was applied at 0^h, 24^h and 48^h using the formulae (Best, 1956)

$$\varphi^{(1)} = \varphi^{(0)} + k \nabla^2 \varphi^{(0)} \tag{14}$$

and

$$(\nabla^2 \varphi)^{(1)} = (\nabla^2 \varphi)^{(0)} + k \nabla^2 (\nabla^2 \varphi)^{(0)} \tag{15}$$

and the corresponding formulae for ψ_a and ψ_b (∇ denotes the finite Laplace operator).

B. The ψ_a-field was obtained from the φ-field by solving the Laplace-equation (7). To obtain suitable boundary values the geostrophic approximation was made use of in the following way:

$$\frac{\partial \psi}{\partial s} = \frac{\dfrac{\partial \varphi}{\partial s}}{f} - \gamma \tag{16}$$

where

$$\gamma = \frac{1}{L} \oint \frac{\dfrac{\partial \varphi}{\partial s}}{f} ds \tag{17}$$

L is the length of the boundary and $\dfrac{\partial}{\partial s}$ denotes differentiation along the boundary.

In order to obtain a good first approximation to the solution in the interior the geostrophic approximation was integrated in a similar way from one side of the rectangular area across the region to the opposite boundary.

The φ-fields corresponding to the 24^h and 48^h ψ_a-forecasts were obtained in an exactly analogous way with equation (11).

C. The ψ_b-field was computed from the ψ_a-field by a second relaxation procedure.

If equation (7) is used equation (11) can be written

$$f \nabla^2 \psi_b = f \nabla^2 \psi_a - 2J\left(\frac{\partial \psi_b}{\partial x}, \frac{\partial \psi_b}{\partial y}\right) \tag{18}$$

It was decided to solve ψ_b from this equation utilizing the boundary values already computed for ψ_a.

Some problems occurred in connection with the transformation of (18) to difference form and regarding the relaxation scheme. Schuman (1955) describes a method for solving the balance equation that has several advantages. However, in his presentation the non-linear term $(\psi_{xx}\,\psi_{yy} - \psi_{xy}^2)$ is approximated by

$$\frac{m^4}{(\triangle s)^4}\Big\{(\psi_{i+1,j} + \psi_{i-1,j} - 2\psi_{i,j})\,(\psi_{i,j+1} + \psi_{i,j-1} - 2\psi_{i,j}) - \frac{1}{16}(\psi_{i+1,j+1} - \psi_{i+1,j-1} - \psi_{i-1,j+1} + \psi_{i-1,j-1})^2\Big\} \tag{19}$$

where m is a mapping factor.

As pointed out by Bolin (1956) this introduces a systematic error as the two terms are evaluated with different gridsizes. A proper approximation is instead

$$\frac{m^4}{4(\triangle s)^4}\Big\{(\psi_{i+1,j+1} + \psi_{i-i,j-1} - 2\psi_{i,j})(\psi_{i+1,j-1} + \psi_{i-1,j+1} - 2\psi_{i,j}) - (\psi_{i+1,j} - \psi_{i,j+1} - \psi_{i,j-1} + \psi_{i-1,j})^2\Big\} \tag{20}$$

If this approximation is introduced in Schuman's method the latter loses its advantages unless the term $\nabla^2 \psi_b$ is evaluated in a similar way, i.e.

$$\frac{m^2}{2(\triangle s)^2}(\psi_{i+1,\,i+1} + \psi_{i+1,\,j-1} + \psi_{i-1,\,j+1} + \psi_{i-1,\,j-1} - 4\psi_{i,\,j}) \tag{21}$$

However, a ψ-field determined in this way consists of two almost independent sets only coupled to each other by the non-linear term. A field computed in this way showed, as could be expected, short wave deviations from the true field, the deviations being distributed in the following way

$$\begin{array}{cccc} + & - & + & - \\ - & + & - & + \\ + & - & + & - \end{array}$$

The possibility to remedy this defect by further manipulations with the difference

formulae was not investigated, but instead a line of attack somewhat different from Schuman's was taken.

In (18) we approximate $\nabla^2\psi$ in the usual way by

$$\frac{m^2}{(\triangle s)^2}\{\psi_{i+1,j}+\psi_{i,j+1}+\psi_{i,j-1}+\psi_{i-1,j}-4\psi_{i,j}) \tag{23}$$

and the non-linear term by (20). Let us denote the difference equation obtained in this way

$$L(\psi_{i,j})=0 \tag{24}$$

Suppose now that we have an approximate solution

$$L(\psi'_{i,j})=\varepsilon_{i,j} \tag{25}$$

Next we want to change the value of ψ' in the point (i, j) by an amount $\delta\psi'_{i,j}$ so that $\varepsilon_{i,j}$ is diminished. Due to the non-linear character of L we get a second order equation

$$a_{i,j}(\delta\psi'_{i,j})^2+b_{i,j}\ \delta\psi'_{i,j}=\delta\varepsilon_{i,j} \tag{26}$$

We neglect the quadratic term and put $\delta\varepsilon_{i,j}=-\varepsilon_{i,j}$ and obtain

$$\delta\psi'_{i,j}=\varepsilon_{i,j}\Big/\left(4f+\frac{m^2}{(\triangle s)^2}(\psi_{i+1,j+1}+\psi_{i+1,j-1}+\right.$$
$$\left.+\psi_{i-1,j+1}+\psi_{i-1,j-1}-4\psi_{i,j})\right) \tag{27}$$

In this way we determine a new value

$$\psi''_{i,j}=\psi'_{i,j}+\delta\psi'_{i,j} \tag{28}$$

Then we proceed to the next point and make now use of the new value ψ'' in the points already treated.

Using this method the residuals in a field of 1,200 points were found to decrease by a factor ten in on the average slightly less than twenty iterations. The total time needed to compute ψ_b from ψ_a using the Swedish computer BESK was around fifteen minutes when the residuals were decreased to about one per cent of their initial value.

The method described above is very similar to a method used by Bolin (1955 and 1956). The only difference lies in fact in the denominator in the quotient determining $\delta\psi'$. Bolin had here

$$f+\frac{m^2}{\triangle s^2}(\psi_{i+1,j}+\psi_{i,j+1}+\psi_{i,j-1}+\psi_{i-1,j}-$$
$$-4\psi_{i,j}) \tag{29}$$

In this context we will touch shortly on the ellipticity criterion.

For the differential equation (18) it can easily be shown that the ellipticity criterion

$$f\nabla\psi_a+\frac{f^2}{2}>0 \tag{30}$$

implies

$$\nabla^2\psi_b+f>0 \tag{31}$$

When we transform the differential equation to a difference equation we would expect to find analogous conditions. That is we would expect to find a condition corresponding to (31) to be an immediate consequence of a condition corresponding to (30). If in the difference equation we combine either expressions (19) and (23) or expressions (20) and (21) this can easily be shown to be true. Combining (20) and (23) as we have done here, makes things more difficult and so far we have not been able to find any difference relations for this case that correspond to (30) and (31) and are coupled in the same way as these.

In the relaxation scheme used by Bolin where the same expressions (20) and (23) were utilized, it is necessary that expression (29) is always larger than zero. Bolin accordingly made certain that a condition corresponding to (30) was fulfilled and this proved to be sufficient in the cases ha ran. The denominator in (27) corresponds to

$$\nabla^2\psi+2f \tag{32}$$

and could for a 500-mb surface be expected to be positive everywhere even if (30) is not fulfilled everywhere. Experiments showed also that a ψ_b-field could be determined by the method described above even when condition (30) was not fulfilled. However, the ψ_b-fields used for the forecasts presented here were computed from ψ_a-fields where (30) was fulfilled. (The ψ_a-forecasts were computed from the unchanged ψ_a-fields.)

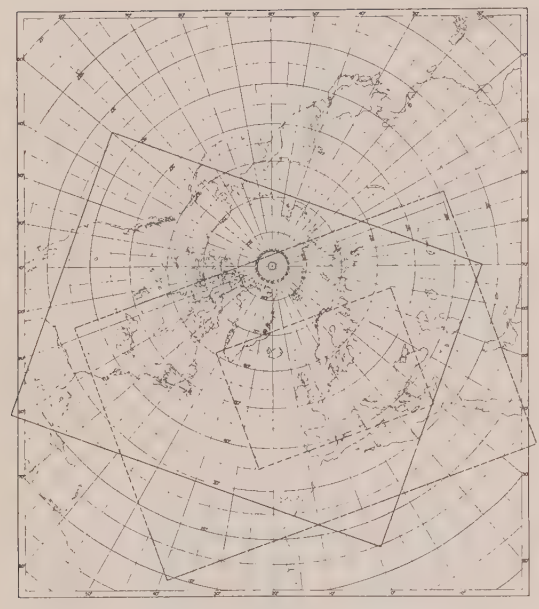

Fig. 1.

Altogether five synoptic cases have been chosen for the experiment. They have been picked arbitrarily from five different months. The analyses of two of the cases have been done by the conventional subjective method and of the remaining three cases the analyses have been obtained by the numerical procedure developed by Bergthorsson and Döös. The arbitrariness of choice of the latter three cases has been restricted merely by the requirement that their analyses should agree generally with a reasonable subjective analysis of the respective situations. Only analyses obtained by the subjective method were used for the purpose of verification of forecasts. The forecast area is shown by the solid line in fig. 1. In one case, the 13.12.51, the forecast area was oriented differently. The area for this case is shown by the dashed line.

For each of the cases 24^h- and 48^h-forecasts have been computed using the prognostic equations (4 a), (9) and (12).

The time required to obtain a 48^h-forecast with the geostrophic prognostic equation is about 50 minutes using BESK. The ψ_a-forecasts require about 65 minutes and the ψ_b-forecasts about 80 minutes.

III. Results

The results of the forecasts are summarized in table 1. Here r denotes the correlation coefficient between observed and computed height changes, ε denotes the mean error, and σ the observed mean change. $\bar{y}$ is the average computed change and $\bar{x}$ the average observed change. The subscripts g, a and b refer to the geostrophic forecast, the ψ_a-forecast and the ψ_b-forecast respectively.

Table I.

24^h	r_g	r_a	r_b	ε_g	ε_a	ε_b	σ	$\bar{y}_g$	$\bar{y}_a$	$\bar{y}_b$	$\bar{x}$
30.1.56	0.72	0.71	0.75	86	96	93	95	18	— 43	— 53	— 2
20.2.56	0.65	0.66	0.67	89	107	90	79	47	69	50	0
19.3.56	0.49	0.57	0.59	98	77	76	80	53	25	24	— 12
13.4.56	0.65	0.69	0.74	56	48	43	65	32	11	11	11
13.12.51	0.81	0.81	0.74	77	61	75	101	60	17	— 5	31
mean	0.66	0.69	0.70	81	78	75	84	42	16	5	6

48^h	r_g	r_a	r_g	ε_g	ε_a	ε_b	σ	$\bar{y}_g$	$\bar{y}_a$	$\bar{y}_b$	$\bar{x}$
30.1.56	0.58	0.51	0.60	154	167	188	121	— 18	— 92	—126	7
20.2.56	0.64	0.63	0.64	163	194	168	105	92	120	96	— 18
19.3.56	0.49	0.52	0.60	136	113	105	93	102	73	66	8
13.4.56	0.68	0.75	0.80	88	70	59	91	46	35	30	23
13.12.51	0.61	0.81	0.77	173	91	114	137	76	14	— 23	42
mean	0.60	0.64	0.68	143	127	127	109	60	30	9	12

Fig. 2 Height changes in cyclone centers

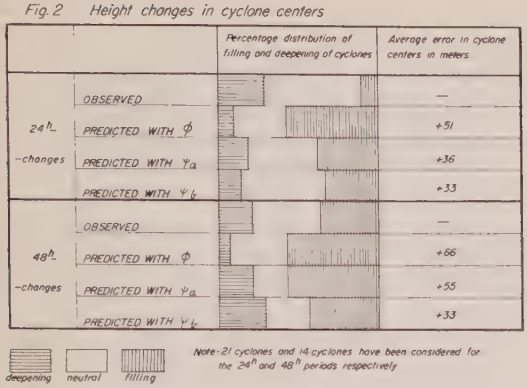

Fig. 2.

The verification was made over the area indicated by the dotted line in fig. 1. The verification area for the 13.12.51 is shown by the dash-dotted line.

1. The table shows a noticeable improvement from the quasi-geostrophic model to the non-geostrophic ones and also a slight improvement due to the non-linear term. The average changes in the non-geostrophic forecasts are not predominantly too high as in the quasi-geostrophic forecasts, but show on the other hand a much larger dispersion.

2. A subjective inspection of the maps reveals that systematic and in some cases great differences result from the inclusion of the β-term. These changes are generally of a rather large scale and the most striking feature is that the exaggeration of anticyclones, which is a rather common phenomenon in quasi-geostrophic forecasts, is substantially suppressed by including the β-term. In one case, however, namely the one based on the 20.2.56 an anticyclone intensifies inordinately in the non-geostrophic models rather than in the quasi-geostrophic model; but in this case the dimension of the anticyclone does not even approach that of a "super-anticyclone", the central height being predicted at 48^h about 120 m and 100 m too high using ψ_a and ψ_b respectively.

3. Another fact revealed by the test is that the tendency to fill out cyclones, which is strongly present in the quasi-geostrophic model, is much weakened in the non-geostrophic models. This is illustrated by figure 2 which shows the percentage distribution of filling and deepening of cyclones in the different forecasts. The average error in the cyclone centers is also shown.

4. The observed differences with respect to prediction of the intensity of disturbances are in agreement with the theory formulated by Charasch (1957).

5. As regards prediction of positions of cyclones and anticyclones no systematic differences have been observed in this very small material.

IV. Summary

Significant differences have been observed between predictions with the quasi-geostrophic and the non-geostrophic models in all of the cases tested. These differences appear to be due mainly to the neglect of the β-term in computing the "geostrophic" vorticity of the quasi-geostrophic model; an investigation is required to establish clearly the effect of the geostrophic divergence. The above differences are great enough to be comparable with the neglect of baroclinic factors and divergence; there is also evidence that the non-geostrophic models are devoid of a certain bias with regard to the average height changes that is present in the quasi-geostrophic model.

The non-linear term appears also to have a significant influence; the differences observed due to this term are on a much smaller scale than those due to the β-term.

Although the sample of forecasts investigated is statistically inadequate it is felt, in the light of the simple theory underlying the investigation, that the β-term must not be neglected in any numerical prediction model, barotropic or baroclinic, and that non-linear term should be included whenever it is possible for practical reasons.

Acknowledgement

Prof. C.-G. Rossby's generous support of this work is gratefully acknowledged. Dr. B. Bolin has given many valuable suggestions and Mr. Wiin-Nielssen and Mr. B. Döös as well as many other members of the International Institute of Meteorology, Stockholm, have contributed to the general discussion in this paper. All these contributions are gratefully acknowledged.

REFERENCES

Bergthorsson, P., Döös, B., 1955: Numerical Weather Map Analysis, *Tellus*, **7**, pp. 329—340.

Best, W., 1956: Differences in Numerical Forecasts arising from Differences in Analyses. *Tellus*, **8**, pp. 351—356.

Bolin, B., 1955: Numerical Forecasting with the Barotropic Model. *Tellus*, **7**, pp. 27—49.

Bolin, B., 1956: An Improved Barotropic Model and some Aspects of Using the Balance Equation for Three Dimensional Flow. *Tellus* **8**, pp. 1—15.

Charasch, E., 1957: Note on numerical prediction of intensity changes of disturbances with the aid of the quasi-geostrophic barotropic model. *Tellus* **10**, pp. 95—98.

Schuman, F., 1955: A method for solving the balance equation. *Technical Memorandum 6*, Joint Numerical Weather Prediction Unit.

Note on Numerical Prediction of Intensity Changes of Disturbances with the Aid of the Quasi-Geostrophic Barotropic Model

By ELIAHU CHARASCH*, International Meteorological Institute in Stockholm

(Manuscript received October 4, 1956)

Abstract

It is shown by a simple analysis that the introduction of a small but systematic error in the evaluation of vorticity causes a significant aberration in the conversion process between disturbance and basic flow kinetic energy in barotropic motion. The neglect of the variation of the coriolis parameter in the geostrophic vorticity is shown to be responsible for large errors in the prediction of the intensity changes taking place in a barotropic model.

Introduction

Reliable indication of intensity changes of disturbances, such as the deepening or filling of a cyclone, constitutes a principal aspect of forecasting.

The evolution of a disturbance is associated with complex energy transfer and transformation processes. Baroclinic as well as barotropic factors are involved in those processes. That a pure barotropic model cannot simulate the evolution of disturbances in an adequate manner is evident. Multi-parameter models developed and tested during recent years attempt to account in one way or another for the baroclinic nature of the atmosphere. It is gradually being recognized, though, that the performance of the so-called baroclinic models is not markedly superior to that of the barotropic model (of course that is as far as the prediction of the 500 mb contour field is concerned) (GATES, 1955).

In the light of that experience it is pertinent to enquire whether the entire hierarchy of atmospheric models developed and tested up to the present does not suffer from one certain defect which all models have in common. The defect may reside in a fundamental postulate, such as the geostrophic approximation, which is incorporated in all those prognostic equations.

It is the aim of this analysis to show that the application of the geostrophic approximation in the representation of the vorticity field introduces a serious error in the evaluation of the intensity changes of disturbances taking place in barotropic motion.

The Equation

A barotropic, homogeneous and incompressible fluid sheet in non-divergent motion and quasi-hydrostatic and quasi-geostrophic equilibrium contains no effective source of kinetic energy (K.E.). The total amount of K.E. of such an atmosphere is invariant if it is a closed system (or provided the net inflow through the boundaries is accounted for). The change of the K.E. of the disturbances is accounted for by the change of the K.E. of the basic current.

In applying that consideration to a practical

* Whilst on leave from Israel Meteorological Service.

case it is convenient to consider the two-dimensional wind field to be composed of a mean value along the X-axis and a deviation from the mean. The X-axis is considered to be directed eastwards and the Y-axis northward.

The mean value of the velocity and the deviation from the mean will represent the basic current and the disturbance respectively.

$$U = \bar{u} = \frac{1}{L}\int_0^L u\,dx$$

$$\bar{v} = \frac{1}{L}\int_0^L v\,dx$$

or generally

$$\overline{F} = \frac{1}{L}\int_0^L F\,dx$$

and

$$u = U + u',\ v = \bar{v} + v' \cong v'$$

The continuity equations:

$$\frac{\partial u}{\partial x} + \frac{\partial v}{\partial y} = 0$$

$$\frac{\partial u'}{\partial x} + \frac{\partial v'}{\partial y} = 0$$

$$\frac{\partial \bar{v}}{\partial y} = 0$$

and the following substitutions are valid:

$$\overline{uu} = \bar{u}\,\bar{u} + \overline{u'u'}$$

$$\overline{vv} = \bar{v}\,\bar{v} + \overline{v'v'} \cong \overline{v'v'}$$

$$\overline{uv} = \bar{u}\,\bar{v} + \overline{u'v'}$$

The equations of motion may then be written in the form:

$$\frac{\partial u}{\partial t} + \frac{\partial}{\partial x}(uu) + \frac{\partial}{\partial y}(uv) = fv - \frac{\partial \phi}{\partial x} \quad (1\,a)$$

$$\frac{\partial v}{\partial t} + \frac{\partial}{\partial x}(uv) + \frac{\partial}{\partial y}(vv) = -fu - \frac{\partial \phi}{\partial y} \quad (1\,b)$$

Multiplying (1 a) and (1 b) with u and v respectively and taking the mean along the X-axis one obtains, after suitable transformations and rearrangements:

$$\frac{1}{2}\frac{\partial}{\partial t}(\bar{u})^2 = f\bar{u}\,\bar{v} - \bar{u}\,\bar{v}\frac{\partial \bar{u}}{\partial y} - u\frac{\partial}{\partial y}\overline{u'v'} \quad (2\,a)$$

$$\frac{1}{2}\frac{\partial}{\partial t}(\bar{v})^2 = -f\bar{u}\,\bar{v} - \bar{v}\frac{\partial}{\partial y}\left(\bar{\phi} + \overline{v'v'}\right) \quad (2\,b)$$

Adding (2 a) and (2 b)

$$\frac{1}{2}\frac{\partial}{\partial t}\left[(\bar{u})^2 + (\bar{v})^2\right] \approx \frac{1}{2}\frac{\partial U^2}{\partial t} = -U\bar{v}\frac{\partial U}{\partial y} - U\frac{\partial}{\partial y}\overline{u'v'} - \bar{v}\frac{\partial}{\partial y}\left(\bar{\phi} + \overline{v'v'}\right) \quad (3)$$

and after some rearrangements

$$-\frac{1}{2}\frac{\partial}{\partial t}U^2 = -\overline{u'v'}\frac{\partial U}{\partial y} + \frac{\partial}{\partial y}\left[U\overline{u'v'} + \bar{v}\left(\frac{1}{2}U^2 + \bar{\phi} + \overline{v'v'}\right)\right] \quad (4)$$

Integrating over the entire volume of the fluid sheet, and recalling that we are considering a closed system:

$$\frac{\partial}{\partial t}\int_0^H\int_0^D\int_0^L \frac{1}{2}U^2\,dx\,dy\,dz = \int_0^H\int_0^D\int_0^L \overline{u'v'}\frac{\partial U}{\partial y}\,dx\,dy\,dz \quad (5)$$

If the depth H of the fluid is taken to be unity (5) may be written

$$\frac{\partial}{\partial t}\int_0^D\int_0^L \frac{1}{2}U^2\,dx\,dy = \int_0^D\int_0^L \overline{u'v'}\frac{\partial U}{\partial y}\,dx\,dy \quad (5)$$

The expression on the left of (5) represents the K.E. of the basic current, K_U. In consequence of the invariance of the total K.E. of the fluid system:

$$\frac{\partial K_U}{\partial t} = -\frac{\partial K_D}{\partial t}$$

where K_U and K_D are the K.E. of the basic zonal current and of the disturbance respectively. It follows

$$\frac{\partial K_D}{\partial t} = -\int_0^D L\overline{u'v'}\frac{\partial U}{\partial y}\,dy \qquad (6)$$

A similar expression has been derived in a more general form by KUO (1949, 1951). Equation (6) gives the intensity change of the disturbance in terms of the eddy momentum transfer $\overline{u'v'}$ and the vorticity of the basic current $-\bar{\zeta} = \frac{\partial U}{\partial y}$.

It follows from (6) that a disturbance superimposed on a uniform basic current is neutral, i.e. the K.E. of the disturbance does not change.—The eddy momentum transfer is proportional to the tilt and its sign according to the angle of tilt of the trough resp. ridge line in the case of sinusoidal waves (MACHTA). It follows that a sinusoidal wave with positive i.e. SW—NE tilt superimposed on a basic zonal current with cyclonic shear will amplify, —a sinusoidal wave with negative i.e. SE—NW tilt superimposed on a basic zonal current with anticyclonic shear will amplify and vice versa (KUO, HASSANEIN). A simple sinusoidal wave, i.e. a Rossby wave, is neutral unconditionally. Theoretically there are a number of possible combinations.

If the geostrophic approximation is made in (6) for $\frac{\partial U}{\partial y}$ one obtains:

$$\frac{\partial K_D}{\partial t} = \int_0^D L\overline{u'v'}\frac{1}{f}\frac{\partial^2\bar{\phi}}{\partial y^2}\,dy \qquad (7)$$

The variation of the coriolis parameter is neglected here, as is the case generally in the geostrophic vorticity. The complete expression should be:

$$\frac{\partial K_D}{\partial t} = \int_0^D L\overline{u'v'}\frac{1}{f}\frac{\partial^2\bar{\phi}}{\partial y^2}\,dy - \int_0^D L\overline{u'v'}\frac{\beta}{f^2}\frac{\partial\bar{\phi}}{\partial y}\,dy \qquad (8)$$

It can be seen that the neglected β-term assumes here the same order of magnitude as the term comprising the geostrophic vorticity.

It follows from (8) that the error incurred by the neglect of the β-term becomes great when the basic zonal current is intense, and when the meridional extent of the disturbance is great. It is readily seen that disturbances superimposed on a basic zonal current which has a vorticity proportional to the variation of the coriolis parameter will behave spuriously as neutral waves ; on the other hand disturbances superimposed on a uniform basic current will be seen to have lost their neutral character. It may be concluded that the geostrophic approximation, implying the neglect of the full variation of the coriolis parameter, may distort fundamentally the development of disturbances in a barotropic model. It is proposed to examine a practical case in the light of the aforementoined conclusions.

From the period December 7—18, 1951 a series of four numerical forecasts with the quasi-geostrophic model has been analysed with a view to expose the character of the energy changes taking place in such a model.

The forecasts have been made using a rectangular grid on a Mercator projection as it appeared convenient to be able to define the boundaries of the forecast region by latitude and longitude. The forecast area extends over 180 degrees longitude and 65 degrees latitude from 120° W to 60° E and from 15° N to 80° N respectively. The mesh width varies from about 100 km near lat. 80° N to about 500 km near lat. 15° N; it corresponds to the conventional width of 300 km around lat. 55°.

A time step of 1 hour has been used with the described grid; there has been no indication of computational instability during any of the forecasts executed.

A smoothing factor varying with lat., has been used in order to eliminate the small-scale motions which otherwise might obtain undue weight in higher latitudes.

During the above mentioned period a rather sudden amplification of the disturbances takes place. This amplification is missed by the forecasts. In order to throw some light on the role of the geostrophic approximation in causing this failure instantaneous tendencies of K_D have been evaluated using the equations (7) and (8). The tendencies evaluated using the geostrophic approximations show a bias similar to that of the forecast 24^h-changes whereas the tendencies including the β-term generally deviate much less from the observed changes.

Although these results are in accordance with the theory outlined in the discussion one should be careful to draw far-reaching conclusions. Instead of tendency computations parallel forecasts with and without the β-term should be run preferably on hemispherical basis (cf. Bring Charasch, 1957).

The ultimate value of the hypothesis concerning the effect of the β-term will become evident when it is applied to a baroclinic model.

REFERENCES

Bring, A., Charasch, E., 1957: An experiment in numerical prediction with two non-geostrophic barotropic models. *Tellus*, **9**, pp. 88—94.

Gates, W. Lawrence, Pocinki, L. S., Jenkins, C. F., 1955: Results of numerical forecasting with the barotropic and thermotropic atmospheric models. *Geophys. Research Papers*, **46**.

Hassanein, S. A. M., 1949: A wave pattern changing with time as a solution of the vorticity equation for non-divergent motion. *Tellus*, **1**, **4**, pp. 58—60.

Kuo, H. L., 1951: A note on the kinetic energy balance of the zonal wind systems. *Tellus*, **3** pp. 205—207.

— 1949: Dynamic instability of two-dimensional nondivergent flow in a barotropic atmosphere. *Journal of Meteorology*, **6**, pp. 356—358.

Machta, L., 1949: Dynamic characteristics of a tilted trough model. *Journal of Meteorology*, **6**, pp. 261—265.

Annual Deposition of Cosmic Ray Produced Be^7 at Equatorial Latitudes

By RAMA THOR and P. K. ZUTSHI, Tata Institute of Fundamental Research. Bombay

(Manuscript received May 13, 1957)

Abstract

The concentration of cosmic ray produced Be^7 in rain water has been measured at two stations in the equatorial latitudes. Its rate of deposition at the earth's surface has been estimated to be about 5×10^5 atoms cm^{-2} yr^{-1} and the deposited quantity seems to be independent of latitude.

Introduction

The cosmic ray produced radio-isotope Be^7 has been detected in rain water (Arnold and Al-Salih, 1955; Goel et al, 1956) and aerosol (Cruikshank et al, 1956). Its half life is 53 days and its production varies strongly with latitude and altitude (Benioff, 1956; Lal, Malhotra and Peters, 1958). It, therefore, provides a useful tool for studying some meteorological phenomena.

In this paper, we present the analysis of Be^7 concentrations in rains collected at Kodai-Kanal (geog. lat. 10° N) and at Bombay (geog. lat. 19° N) between January and December 1956. Some qualitative checks indicate that the Be^7 observed in rain water is mainly cosmic ray produced and the contribution due to thermonuclear explosions, if any, is not substantial. The long term observations permit us to obtain its average yearly deposition in equatorial regions. Some very qualitative conclusions regarding general features of large scale air circulations and mean removal time for Be^7 from the troposphere can be derived.

Experimental:

These days, a major part of the radio-activity in the atmosphere comes from nuclear explosions. The cosmic ray produced activities are much smaller in comparison. Consequently, in the study of any cosmic ray produced isotope, one is faced with the following two problems.

(1) One must find a chemical procedure which removes all the interfering fission activities.
(2) One must assess the contribution of nuclear explosions, if any, to the isotope under investigation.

These problems had to be faced in the present work with the isotope Be^7. A chemical procedure for its extraction from rain water was worked out. It was found to remove all the interfering activities. The details of the method have been described earlier (Goel et al., 1956).

The solution to the second problem is not straight-forward. The possibility of producing Be^7 in thermo-nuclear explosions can not be ruled out. However, we believe that its contribution to the Be^7 observed in rain water is not substantial in our experiment. The basis

★ On leave from Victoria College, Gwalior, Madhya Pradesh (India).

for this belief are the following three qualitative arguments.

(1) If substantial amounts of Be^7 originate from thermo-nuclear explosions, then its occasional high concentration in rain water should always be accompanied by high fission activity. No such correlation was observed.[1]

(2) The Be^7 deposition actually observed in the course of a year is of magnitude which one would expect on the assumption that it is produced by cosmic rays only.

(3) Some fraction of the activity produced in nuclear explosion must be expected to form a part of dust or metal grains. Some of this activity, therefore, may not be soluble in water at pH3. On the other hand the cosmic ray produced Be^7 must be in solution because there is no likelihood of its entering into the crystal structure of dust. The presence of dust carrying insoluble Be^7 would be difficult to understand if the isotope were produced by the cosmic ray induced disintegrations in the atmosphere. In order to check this we proceeded in the following way.

The dust was removed from the rain water by filtering it. The filtered water was passed through the resin (Dowex: 50). The resin extracts only the soluble part of the activity by cation exchange.

Beryllium was extracted from the resin using the method described earlier (GOEL et al., 1956). The same method was used for extracting Beryllium from the dust after it was fused with $K_2S_2O_7$ and digested with HCl.

The Be^7 activity recovered from the resin was 47.2 ± 2.0 cpm and that from the dust was 1.3 ± 1.2 cpm. This indicates that either Be^7 is already in solution in water or can be dissolved off the surface of dust grains at pH 3.

These considerations lead us to the conclusion that we are dealing primarily with cosmic ray produced Beryllium.

We have analysed 47 rain samples from Kodai-Kanal and 29 rain samples from Bombay. In some of our later samples, Beryllium was precipitated from rain water with Ferric Hydroxide carrier. The purification procedure was the same as described earlier (GOEL et al., 1956).

[1] We are grateful to Dr K. G. Vohra of Atomic Energy Establishment, Bombay, for making the fallout data available.

The geographic location and the annual rainfall at the two stations are summarised in table I.

Table I

Station	Kodai-Kanal	Bombay
Geographic latitude	10° N	19° N
Height above sea level	7,600 feet	0
Average annual rainfall	169 cms	180 cms
Rainfall during the year 1956	150 cms	256 cms
Rains from	Summer & Winter monsoons.	Summer monsoons only

The Be^7 concentrations at Kodai-Kanal and Bombay are given in tables II and III respectively.

Discussion:

As seen from tables II and III, the Be^7 concentration varies widely in individual rains. It will not only depend on the history of air mass, i.e. the time spent in the stratosphere and troposphere where the production rates of Be^7 are known to be widely different, it will also depend on local effects:

(1) Meteorological factors, in particular height and moisture content of the cloud.

(2) Topography of the station.

Measurements involving a single cosmic ray produced isotope do not give sufficient information for correlating concentrations in individual rains with such local phenomena. However, when one considers the average Be^7 deposition from a large number of rains over an extended period, one must expect that it will be roughly proportional to the amount of isotope produced in the air mass circulating in that particular latitude belt. It is known that circulation within zonal belts is fairly rapid and, therefore, we tentatively take the average Be^7 concentration observed at Kodai-Kanal and Bombay to be representative of their respective zones. On multiplying these concentrations by the mean annual rainfall (BROOKS and HUNT, 1932) in the respective belts, we obtain the yearly deposition of Be^7 at 10° N and 19° N geographic latitudes. These are listed in table IV, the results derived from the Be^7 observations made by ARNOLD and AL-SALIH (1955) at Chicago are given in same table.

Table II (Kodai-Kanal)

	Date of rainfall	Amount of rainfall (cms)	Number of Be^7 atoms per ml.	Number of Be^7 atoms deposited per cm^2 area
1	30-1-56	1.17	1,750 ± 170	2,000
2	25-2-56	0.48	6,200 ± 1,500	3,000
3	10-3-56	2.87	5,100 ± 300	14,500
4	4-4-56 & 5-4-56	3.98	6,400 ± 300	25,500
5	7-4-56	0.13	10,000 ± 800	1,300
6	18-4-56	0.71	2,800 ± 200	1,990
7	20-4-56	0.91	4,800 ± 350	4,400
8	22-4-56	3.71	5,350 ± 300	19,900
9	24-4-56	0.69	4,400 ± 300	3,000
10	25-4-56	1.78	7,900 ± 250	14,100
11	26-4-56	1.19	9,900 ± 300	11,800
12	28-4-56 & 29-4-56	1.60	7,200 ± 200	11,500
13	18-5-56	2.34	2,800 ± 150	6,600
14	23-5-56	3.15	2,400 ± 200	7,600
15	13-6-56	1.27	2,700 ± 120	3,400
16	14-6-56	0.97	2,100 ± 300	2,000
17	19-6-56	0.36	2,000 ± 350	700
18	21-6-56	0.81	1,600 ± 200	1,300
19	22-6-56 & 23-6-56	1.01	550 ± 350	600
20	25-6-56	0.71	4,900 ± 300	3,500
21	26-6-56 to 28-6-56	2.29	3,500 ± 200	8,100
22	30-6-56	0.53	2,800 ± 200	1,500
23	8-8-56 to 10-8-56	2.10	1,600 ± 150	3,400
24	15-8-56 to 18-8-56	3.13	1,700 ± 200	5,300
25	19-8-56	3.40	1,200 ± 200	4,100
26	21-8-56	1.88	5,500 ± 400	10,300
27	25-8-56	1.17	2,990 ± 550	3,500
28	28-8-56	2.59	11,000 ± 2,800	28,500
29	12-9-56	0.74	1,600 ± 1,400	1,200
30	15-9-56	1.37	2,400 ± 600	3,300
31	16-9-56	2.24	1,160 ± 1,500	2,600
32	29-9-56	0.97	1,840 ± 800	1,800
33	13-10-56	2.74	2,300 ± 350	6,300
34	15-10-56	1.85	600 ± 500	1,100
35	17-10-56	0.94	1,400 ± 650	1,300
36	19-10-56	0.99	3,200 ± 650	3,100
37	25-10-56	1.55	4,700 ± 500	7,200
38	26-10-56	3.81	1,000 ± 400	3,700
39	31-10-56	5.61	1,300 ± 1,000	7,500
40	1-11-56	2.72	900 ± 300	2,400
41	6-11-56	1.52	500 ± 250	700
42	8-11-56	1.12	1,100 ± 350	1,200
43	11-11-56	3.45	200 ± 180	600
44	16-11-56	0.13	1,200 ± 300	200
45	19-11-56	2.41	300 ± 160	600
46	21-11-56	1.37	400 ± 400	500
47	26-12-56 to 28-12-56	3.10	600 ± 600	1,900
		85.3 cms		

	Mean concentration	Weighted mean concentration
	$\frac{147,700}{47}$ = 3,100 atoms/ml.	$\frac{250,600}{85.3}$ = 2,900 atoms/ml.

Total Be^7 precipitated per cm^2 area at Kodai-Kanal during the year $1956 = 2,900 \times 150 = 4.3 \times 10^5$ atoms.

Table III Bombay

	Date of rainfall	Amount of rainfall (cms)	Number of Be^7 atoms per ml.	Number of Be^7 atoms deposited per cm^2 area
1	24-5-56 & 25-5-56	1.65	9,300 ± 250	15,400
2	27-5-56 & 28-5-56	0.61	9,250 ± 700	5,600
3	12-6-56	2.67	5,500 ± 320	14,600
4	14-6-56	2.03	8,000 ± 600	16,300
5	16-6-56	1.73	8,150 ± 350	14,100
6	17-6-56	4.83	7,900 ± 370	38,000
7	24-6-56	2.87	4,500 ± 550	13,000
8	26-6-56	9.07	4,100 ± 325	36,900
9	30-6-56	4.34	1,400 ± 300	6,000
10	12-7-56	1.65	4,400 ± 400	7,300
11	26-7-56	8.05	6,500 ± 300	52,100
12	13-8-56	0.56	4,100 ± 1,100	2,300
13	14-8-56 & 15-8-56	0.65	2,100 ± 500	1,300
14	18-8-56 & 19-8-56	2.00	2,500 ± 800	5,000
15	25-8-56 & 26-8-56	1.55	6,900 ± 430	10,600
16	30-8-56	2.98	6,600 ± 500	19,600
17	1-9-56	2.00	1,500 ± 1,000	3,000
18	3-9-56	0.43	7,200 ± 450	3,100
19	12-9-56 to 14-9-56	2.49	6,350 ± 800	15,800
20	23-9-56	1.52	4,250 ± 400	6,500
21	24-9-56	3.86	1,550 ± 500	6,000
22	26-9-56	1.32	2,250 ± 700	3,000
23	27-9-56	0.76	4,400 ± 700	3,400
24	30-9-56	1.22	3,300 ± 500	4,000
25	1-10-56	2.97	1,200 ± 500	3,600
26	3-10-56	0.48	1,650 ± 1,300	800
27	6-10-56	0.63	800 ± 650	500
28	8-10-56	1.30	4,750 ± 1,200	6,200
29	9-10-56	0.51	1,800 ± 600	900

66.7 cms

Mean concentration	Weighted mean concentration
$\frac{132,100}{29}$ = 4,600 atoms/ml.	$\frac{314,900}{66.7}$ = 4,700 atoms/ml.

Total Be^7 precipitated per cm^2 area at Bombay during the summer Monsoon, 1956 = 4,700 × 256 = 1.2 × 10^6 atoms.

Table IV

Station	Kodai-Kanal	Bombay	Chicago
Geographic latitude	10° N	19° N	42° N
Mean concentration of Be^7 in rain water (atoms ml^{-1})	2,900	4,700	6,000
Annual rainfall in the latitude belts (cms)	175	98	89
Deposition of Be^7 (atoms cm^{-2} yr^{-1})	5.1 × 10^5	4.5 × 10^5	5.3 × 10^5

The depositions calculated, on the basis of these assumptions, for three latitudes are nearly the same inspite of the very considerable variation of cosmic ray intensity with latitude. It has been pointed out by PETERS (1957) that this fact can be explained if one assumes that most of the Be^7 observed in rainwater originated in the troposphere.

Recent calculations of LAL, MALHOTRA and PETERS show that the average global production of Be^7 amounts to 7.5 × 10^5 atoms cm^{-2} yr^{-1} in the troposphere. A deposition rate of

5×10^5 atoms cm^{-2} yr^{-1} on the earth's surface, if all of tropospheric origin, indicates that about 34% of Be^7 decays in the troposphere before being brought down to earth by rainfall. This leads to an average tropospheric removal time of the order of forty days. However, a small fraction of Be^7 may be settling on earth directly from the air. In that case the tropospheric removal time would be correspondingly shorter.

Recently, other cosmic ray produced short-lived isotopes have been discovered in rain water. They are P^{32} (14d, 1.7 Mev β^-) (Marquez & Costa, 1955), P^{33} (25d, 0.25 Mev β^-) (Lal, Narsappaya & Zutshi, 1956) and S^{35} 87d, 0.167 Mev β^-) (Goel, 1956). A study of the ratios of Be^7 to these isotopes is likely to provide detailed information on the amount of radiation received by a particular air mass in the interval between two successive precipitations.

Acknowledgements

We are greatly indebted to Prof. B. Peters for his guidance throughout the work and to Prof. K. R. Ramanathan for useful discussions. We are also grateful to Mr T. S. G. Sastry and Mr S. R. Kane of Physical Research Laboratory, Ahmedabad for their co-operation in collecting rain samples at Kodai-Kanal.

REFERENCES

Arnold, J. R. and Al-Salih, H., 1955: Beryllium-7 produced by cosmic rays. *Science*, **121**, 451 – 453.

Benioff, P. A., 1956: Cosmic-Ray production rate and mean removal time of Beryllium-7 from the atmosphere. *Phys. Rev.*, **104**, 1122 – 1130.

Brooks, C. F. P. and Hunt, Theresa M., 1932: The zonal distribution of rainfall over the earth. *Mem. of Roy. Met. Soc.*, **3**, No. 28, 195 – 199.

Cruikshank, A. J., Cowper, G. and Grummitt, W. E., 1956: Production of Be^7 in the atmosphere. *Canad. J. Chem.*, **34**, 214 – 219.

Goel, P. S., Jha, S., Lal, D., Radhakrishna, P. and Rama, 1956: Cosmic ray produced Beryllium isotopes in rain water. *Nuclear Physics*, **1**, 196 – 201.

Goel, P. S., 1956: Radio-active sulphur produced by cosmic rays in rainwater. *Nature*, **178**, 1458 – 1459.

Lal, D., Malhotra, P. K. and Peters, B., 1958: J. Atmosph. Terr. Phys. (To be published).

–, Narasappaya, N. and Zutshi, P. K., 1957: Phosphorus isotopes P^{32} and P^{33} in rainwater. *Nuclear Physics*, **3**, 69 – 75.

Marquez, L. and Costa, N. L., 1955: The formation of P^{32} from atmospheric argon by cosmic rays. *Nuovo Cimento*, **2**, 1038 – 1041.

Peters, B., 1957: The Be^{10} method for studying long term changes in cosmic radiation and the chronology of the ocean floor. *Zeitschrift für Physik*, **148**, 93 – 111 (In German).

On the Theory of Magnetic Storms and Aurorae

By H. ALFVÉN, Royal Institute of Technology, Stockholm

(Manuscript received April 6, 1957)

Abstract

A. Chapman-Ferraro's theory of magnetic storms is discussed. It is pointed out that the fundamental assumption about a non-magnetized beam is in conflict with cosmic ray evidence. It is further shown that there is a fundamental objection against any theory of the main phase based on a non-magnetized beam.

B. The objections, which Cowling and Chapman have raised against the electric field theory, are discussed, and the discharge mechanism during a magnetic storm is analysed. When a magnetized beam enters the earth's magnetic field, it is heated due to the compression. In the hot plasma the earth will act as a "probe" so that it gets a negative charge in relation to the plasma. As a result of ambipolar diffusion to the earth, the ionosphere in the auroral zones will be bombarded by high energy protons and electrons.

It is shown that a mechanism of this type is not subject to the objections which have been raised.

A. Discussion of Chapman-Ferraro's theory

Chapman and Ferraro have made a very careful study of what happens when a beam of ionized non-magnetized gas approaches the earth. There is little reason to doubt that their calculations—as far as it has been possible to carry them out—really tell us what would happen under the assumed circumstances. On the other hand the following arguments indicate that the beam probably has other properties than they have assumed and, as a consequence, phenomena fundamentally different from those which they treat are likely to be responsible for magnetic storms and aurorae.

§ 1. Beam properties from cosmic ray observations

Cosmic ray evidence indicates that the storm-producing beam must be associated with a magnetic field or an electric field or both. It has been shown by JOHNSON (1938), TREIMAN (1953) and HAYAKAWA (1955) that the Forbush decrease in connection with magnetic storms cannot be due to changes in the magnetic cut-off of the earth. This is further confirmed by the fact that the cosmic radiation decreases even at stations close to the geomagnetic pole, as shown by SINGER (1954). It seems inevitable to conclude that the cosmic ray change is produced directly by the beam.

There are only two ways known in which a change in cosmic ray intensity can be produced by the beam *viz.*, 1) by a magnetic field which is strong enough to produce forbidden cones or 2) by an electric field.

Measurements show that the cosmic rays of a rigidity of $H\varrho = 10^8$ gauss cm exhibit a storm variation. The breadth of the beam near the earth could not exceed 10^{13} cm. Hence the magnetic field which is necessary in order to produce variations is $H \geq 10^{8-13} = 10^{-5}$ gauss. A smaller field can deflect the particles but —according to Liouville's theorem—not change the intensity, unless an electric field is present.

An electric field may change the cosmic ray intensity by acceleration or retardation of the particles. In order to explain a decrease of 1 % in the cosmic radiation, an electric voltage difference of about 10^8 volt is necessary (ALFVÉN 1954, LUNDQUIST 1954). If the breadth of the beam is $\leq 10^{13}$ cm, the field is $E \geq 10^{-5}$ volt/cm. With a beam velocity $v = 10^8$ cm/sec, this field reveals the existence of a magnetic field $H \geq 10^{-5}$ gauss.

The conclusion of this discussion, which has been carried out more in details elsewhere (loc. cit.), is that as soon as a cosmic ray storm variation of 1 % or more is observed, the beam must contain a frozen-in magnetic field of at least the order of 10^{-5} gauss. (If the beam has an irregular turbulent structure the value becomes larger.) In the rather rare cases when a decrease of 10 % is observed the field should be at least of the order 10^{-4} gauss. Certainly there are many storms, in connection with which no decrease as large as 1 % is observed. This may indicate that the breadth of the beam is smaller than 10^{13} cm, that the field H is smaller than 10^{-5} gauss, or that the field is irregular.

In a critical review of the electric field theory Chapman (1952) writes that the field in the beam cannot be more than 10^{-6} gauss. This value is obtained under the assumption that the field in the beam is the same as the solar dipole field at the distance of the earth (an assumption which I have also made in my earlier publications). However, as the magneto-hydrodynamic coupling in interplanetary space is certainly very good, it seems impossible to reconcile the existence of beams with an undisturbed solar dipole field. Instead we are led to assume that the field falls off much more slowly than a dipole field. A possible model of the interplanetary magnetic field has been given elsewhere (ALFVÉN 1956). As we do not know with certainty according to which law the field falls off, the magnetic field near the earth's orbit cannot be derived directly from the value of the magnetic field at the sun. The cosmic ray value of the field seems not to be in conflict with any other observations.

As the earth's field at the distance of the ring current is of the order 10^{-3} gauss, a beam field which is much smaller than this may appear to be negligible. This is not necessarily correct because when approaching the earth the beam is braked with the result that the gas of the beam is compressed. This process causes an increase in magnetic field at the same time.

CHAPMAN (1952) considers a beam field of 10^{-6} gauss to be negligible. As we have seen, this conclusion is doubtful. Moreover, cosmic ray evidence indicate that the beam field often is 10^{-5} gauss or even more.

§ 2. *Beam properties and the conservation of magnetic flux*

During an auroral display the ionosphere is hit by clouds of particles which obviously arrive from above, at least in part. The energy of these particles may be of the order of 10^5 eV, which means a rigidity of $H\varrho = 10^3$ gauss cm for electrons and $H\varrho = 4 \cdot 10^4$ gauss cm for protons. In the earth's field they spiral along the lines of force. Even near the equatorial plane, where the magnetic field reaches a minimum of about 10^{-3} gauss for a line through the auroral zone, the radius of curvature does not exceed 10^6 cm for the electrons and $4 \cdot 10^7$ cm for the protons.

All theories of magnetic storms agree in postulating a ring current in the equatorial plane during the main phase. Although the pictures about the formation and the structure of it differ, the theories also seem to agree that the current is due to the differential motion of electrons and ions in a cloud of ionized gas. The thickness of the ring is estimated by Chapman and Ferraro to about $3 \cdot 10^8$ cm. The gas temperature may be rather low so that the rigidity of the particles does not exceed the values mentioned above. In the electric field theory the ring is asymmetric, consisting of electrons with energies of up to 10^5 eV and protons with probably lower energies.

Thus auroral observations indicate, and a reasonable interpretation of magnetic disturbances confirm, that during a storm there are extended clouds of ionized gas in the earth's magnetic field. One of the fundamental problems in magnetic storm theory is how these clouds have been brought into the earth's magnetic field, and a still more fundamental question is how a magnetic field has been brought into the gas clouds, in other words, how the clouds have been magnetized.

In order to realize the importance of this question, let us consider a closed line limiting

a region which is much larger than the radius of curvature of the particles. If the line follows the motion of the cloud, the magnetic flux inside it must remain constant under very general conditions (high conductivity, etc.), which are likely to be satisfied in most problems in cosmical physics. If a cloud expands isotropically by a linear factor α, the density decreases as α^{-3}. At the same time the magnetic field decreases as α^{-2}. Hence the particle density n is proportional to $H^{3/2}$;

$$n \sim H^{3/2} \qquad (1)$$

This holds only for an isotropic expansion or contraction. An expansion along the field lines may change n without affecting H.

Tracing backwards the history of the magnetized clouds in the terrestrial magnetic field, we should expect that they have initially been part of the beam. If we accept this, it seems natural that the clouds were magnetized already when they were parts of the beam. In other words, the beam should have a frozen-in magnetic field.

The invariance of the flux offers no difficulty to the electric field theory. In fact, the theory is based on the flux invariance in a volume of magnetized gas, which can be followed from the solar corona the whole way to the border of the forbidden region near the earth. In the solar atmosphere the beam is formed of ionized gas, which is already magnetized by the general magnetic field (or by a sunspot field).

When the beam is emitted, the density as well as the magnetic field decreases very much. When the gas enters the terrestrial field a compression occurs, which is connected with the increase in field strength.

In Chapman-Ferraro's theory the demand for the flux invariance seems to constitute a difficulty, which may be superable in the case of the solar phenomena but is much more serious for the terrestrial phenomena. Chapman considers the beam to be formed of solar gas (an idea which—as mentioned above—has been taken up by the electric field theory) and he gives a value $\alpha^3 = 10^5$—10^8 for the volume expansion (loc. cit.). If the expansion is isotropic the magnetic field should decrease by a factor $\alpha^2 = 10^{10/3}$—$10^{16/3}$. Thus in order to come down to a beam field of 10^{-6}, which Chapman considers to be negligible, the beam must originate in a region where the field is much lower than 1 gauss, or the expansion must be strongly anisotropic. Both alternatives are not very probable but by no means unreasonable. However, as the gas in the beam becomes compressed when it is braked by the earth's magnetic field, the beam field increases, and there is no reason to assume that a primary field of 10^{-6} gauss is negligible.

§ 3. *The main phase*

The flux invariance introduces a much more serious difficulty in the treatment of the phenomena in the earth's magnetic field. As far as the strict calculations by Chapman and Ferraro go, the ionized matter of the beam cannot penetrate into the earth's magnetic field. What happens according to their analysis, which no doubt is correct, is that the gas of the beam pushes the field before it, but remains non-magnetized itself. Ferraro (1952) has made a calculation where he divides the approaching stream into a series of sheets and shows that the front can advance in a magnetic field. It seems that this process rather indicates that the field is pushed away than that the gas becomes magnetized. In any case he has not shown clearly how the flux invariance can be avoided.

Chapman and Ferraro suggest that electrons and ions start from the front of the beam and produce the ring current, but they do not claim to have shown how this process occurs, not even that the process is possible in principle. The ring current flows in a gaseous ring which is *permeated by the earth's magnetic field*. This is essential, because a non-magnetized gas ring will no doubt be strongly diamagnetic with the result that it breaks into pieces and is expelled from the dipole field very rapidly. At this point the theory encounters the fundamental difficulty that the non-magnetized gas of the beam must be transformed into the magnetized gas of the ring. How serious this objection is, can be shown by calculating the time constant T of the magnetization of a gas cloud. We have

$$T = \sigma\left(\frac{l}{c}\right)^2$$

where σ is the conductivity and l the linear dimension of the cloud and c the velocity of light. The conductivity is

$$\sigma = 1.4 \cdot 10^7 \; T^{3/2}$$

where T is the temperature. Chapman has not given any value for the temperature of the beam, but he has estimated the temperature of the interplanetary gas to $2 \cdot 10^5$ degrees. This may give the order of magnitude for the temperature of his beam and ring. With $l = 3 \cdot 10^8$ cm we find

$$T = 10^{11} \text{ sec.} = 3{,}000 \text{ years.}$$

This is the time in which the field in a cloud decays, but it is also a measure of the time required to magnetize a non-magnetic cloud by putting it into a magnetic field.

This does not mean with certainty that a magnetized cloud could not be produced in a shorter time—experience teaches us that theorems of the impossibility of a certain process are dangerous in astrophysics. In fact a magnetized cloud in the earth's magnetic field could be produced by ionization of a non-ionized gas which is situated in the earth's field. This is the process which Hulbert's ultraviolet light theory of magnetic storms makes use of, so this theory does not violate the theorem of flux constancy. Another possibility is that the cloud is divided into very small units, which are magnetized, or that the temperature or degree of ionization is very low in the ring-cloud. None of these possibilities seem to be attractive, because we have to change T by eight powers of ten in order to make it comparable to the real time of formation of the ring current. Until the contrary has been shown, it seems legitimate to conclude, that the theorem of flux invariance prevents the main phase of a storm to develop from the initial conditions assumed by Chapman and Ferraro.

The difficulties of Chapman-Ferraro's theory are increased still more by the fact that their postulated ring current is unstable, as shown by Herlofson (1957). Even if some mechanism could be found, by which the ring current could be produced, this would not be of much help because the ring current will break up in less than 30 seconds, according to Herlofson.

The instability demonstrated by Herlofson does not occur for a ring current of the type of the electric field theory because of the trochoidal motion, which is stable.

The following point of view may also be of interest. In Störmer's theory of the aurora one of the difficulties was that particles with a reasonable energy (10^5 eV) could reach the earth only in very small regions around the geomagnetic poles. By assuming that the beam is non-magnetized Chapman and Ferraro meet the same difficulty, only in a slightly different form. The non-magnetized gas can reach singular points at the axis and very small region around them. Certainly the pressure which the beam exerts on the field may change the shape of this field so that the singular points are displaced (the "horns"), but in principle the theory does not allow the occurrence of magnetized clouds in the earth's magnetic field far away from the field lines through singular points.

Our conclusion is that *if* the earth is approached by a cloud which has the properties which Chapman and Ferraro assume, there is no doubt that those phenomena will occur which they have found by their admirably stringent analysis: A hollow will be formed and the earth's magnetic field will be disturbed in a certain way. On the other hand, there is no support for their suggestion that a ring current will be formed and the main phase of a storm will develop. On the contrary, there are strong arguments for the view that a state resembling the main phase would *not* be produced by a beam of the assumed type.

It should further be observed that no convincing arguments have been given that beams with the assumed properties exist. Certainly at the time when Chapman and Ferraro made their theory it was natural to assume that the beam was non-magnetized, but our increased knowledge of magneto-hydrodynamic phenomena in astrophysics makes this assumption look improbable today. As shown above it is much more likely that the beam is magnetized.

§ 4. *The initial phase*

If independent arguments had been given for the existence of beams of Chapman-Ferraro's type, and if there had been a reasonable probability of making a theory of the main phase along their lines, their theory of the initial phase would have been attractive. As these premises are not satisfied, there are good reasons to doubt that the phenomena they treat has anything to do with a magnetic storm and it is legitimate to scrutinize what support there is for their claim that their

theory does describe the initial phase of a storm.

According to the theory the arrival of a beam should disturb the magnetic field and currents should be produced at the front surface of the beam, which should result in an increase in the horizontal component.

This is all which the theory has given so far.

§ 5. *Summary of the criticism of Chapman and Ferraro's theory*

No one can study Chapman-Ferraro's theory without the deepest admiration for the stringent analysis they have given and no one can avoid to conclude that they really describe what would happen, if the conditions they assume were realized. Yet at the same time at least the present author cannot avoid the feeling that their theory has nothing to do with a magnetic storm. To summarize what is said above, the reasons for this view are:

1. Cosmic ray observations indicate that the beam has other properties than supposed by Chapman and Ferraro.
2. The initial phase is not adequately described by the theory.
3. A development of the theory into a theory of the main phase will probably be impossible without violating the theorem of flux invariance.
4. As Herlofson has shown Chapman-Ferraro's ring current is unstable so that even if it had been possible to create it, it would break up in less than 30 seconds.

B. The electric field theory

§ 6. The electric field theory of magnetic storms was presented in a paper 1939 (Part I) and developed in two papers 1940 (Part II and III). These three papers give a brief sketch of a theory of the emission of a beam from the sun and a more detailed outline of the phenomena near the earth during the main phase of a magnetic storm.

The theory of the emission of the beam cannot be upheld today. The development in magneto-hydrodynamics has shown that magnetic fields may be frozen-in, and this changes essentially the picture of the properties of the beam when it is emitted from the sun.

On the other hand, the theory of the phenomena near the earth seems to be essentially correct. The new knowledge accumulated since the first presentation of the theory has given good support to it, and only some details call at present for a revision. Even the numerical values given in the cited papers seem acceptable today. However, a more careful treatment of some of the phenomena is urgently needed especially as parts of the theory seem to have caused some misunderstanding. It is the purpose of the following paragraphs to elucidate some obscure points.

The scale-model experiment by MALMFORS (1946) gave a good support to the general lines of the theory. Some of his results (about the self-sustained discharge) seemed to call for a modification of the theory. This was the state when a new review of the theory was written (ALFVÉN 1950). However, the subsequent experiments by BLOCK (1955) supported the original theory.

In 1953 the theory was developed so that it also gives at least an outline of the initial phase. In this connection the existence of an inner auroral zone was predicted, and independent investigations by NIKOLSKIJ (1955) seem to give some confirmation of this.

§ 7. *Objections by Cowling and Chapman*

COWLING (1942) has made several objections against the electric field theory. The most important of these are:

1. If the particles move with $\mu = eV/H = \text{const.}$ as is supposed in the theory, they cannot reach the ionosphere unless their energy is extremely large.

This objection will be discussed in detail in § 8. The result is that the objection is correct under the condition that the particles really move exactly according to the idealized mathematical model, but that already very small disturbances are enough to allow the particles to reach the ionosphere. In other words, the objection hits the earlier formulation of the theory but not its physical content.

2. If positive charges entering the forbidden zone build up space charges strong enough to drive charges to the auroral zones, they must be strong enough to modify the electric field near the forbidden region seriously.

This objection can be met with a reference to Block's experiment, which shows that even when space charge is of great importance, as it is in the light discharge, the basic pattern

of the motion is not changed. However, COWLING (1957) does not accept such a reference to an experiment. I think that this attitude is partly justified, because in a final theory we want to express all phenomena in clear mathematical formulae and not by a reference to an experiment. On the other hand, as we are still far from a definite theory, a reference to an experiment is allowed. The experiment demonstrates that an assumed process is physically possible, and this shows that even if the objection hits the present formulation of the theory, it does not hit the essential physical picture. In other words, the experiment makes probable that we may find another formulation, which is free from the objection. An attempt to satisfy Cowling's justified request for a more clear picture is made in § 10. The discussion leads to a more detailed theory of the aurorae.

3. Cowling has objected against the mechanism of ejection of the beam according to the paper of 1939. This objection is fully justified. As pointed out in § 6, this part of the theory cannot be upheld today.

4. Cowling has also objected against the shape of the forbidden region on the night side. This criticism of a detail in the theory will be discussed further in a following paper.

Against the electric field theory Chapman (1952) has made a generally formulated objection which he considers so fatal that he does not consider it worth to take up any particular part of the theory to a serious discussion. This objection is that "the theory goes astray at the outset" because "Alfvén ignored the powerful electrostatic forces existing between the positive and negative charges" (loc. cit. p. 207). If Chapman's objection is only a summary of some of Cowling's objections, I hope that the present paper will clarify the matter. If not I must invite Chapman to specify his criticism so that it is possible to discuss it.

§ 8. *Isotropy of electron velocities*

Electrons invading the earth's magnetic field under the influence of an electric field will gain energy from the electric field, so that their velocity perpendicular to the magnetic field increases. (This is only another way of describing that when the cloud enters the magnetic field it is compressed and that the increase in the magnetic field accelerates the electrons by betatron action.) During this motion their velocity parallel to the field remains constant. Consequently, when they arrive to the neighbourhood of the forbidden region, their velocity vector is almost parallel to the equatorial plane. This means that the amplitude of oscillation perpendicular to the equatorial plane is small. Hence an electron cannot go from the equatorial plane along the lines of force to the upper atmosphere of the earth.

From this COWLING (1942) concludes that a discharge from the equatorial plane to the ionosphere is impossible, and this is one of his most important objections against the theory.

This objection would no doubt be valid if no other effects were of importance. However, already a very small disturbing effect is enough to make the electron velocity distribution more or less isotropic or even Maxwellian with the result that electrons will move along the field lines and reach the earth.

As the electrons need a few hours in order to reach the neighbourhood of the forbidden region and as their velocity is of the order of 10^{10} cm/sec, the path is of the order 10^{14} cm. Hence the question is whether the electrons could move 10^{14} cm without changing the angle between their velocity and the magnetic field.

Taking account of the high energy of the electrons (10^5 evolt) and the low density in space, we could say with certainty that the ordinary mean free path is much larger than 10^{14} cm, so that no change in velocity is accomplished by collisions with other particles. In spite of this it seems reasonable to assume (as was done already in the earlier presentations of the theory) that there exist magnetic field irregularities strong enough to accomplish a change in velocity. An electron will complete 10^7 turns with a radius of curvature of 10^6 cm. If the angle between H and the velocity vector changes statistically by only 0.1 degrees for each turn, e.g. due to irregularities in the electric or magnetic field, the changes will add up as random contributions and produce an almost completely isotropic velocity distribution. The fact that the aurora often has an irregular and rapidly changing structure, and the fact that magnetograms often show very large oscillations favour the view that the path of the electrons is likely to be disturbed.

In fact, a numerical calculation shows that only if extreme assumptions are made concerning the regularity of the fields, this conclusion can be avoided.

Recent results by GABOR, ASH and DRACOTT (1955) give additional evidence of scattering processes. In their classical investigations on plasmas, Langmuir and Mott-Smith have shown that in a discharge tube the plasma sets up a thin boundary sheath which separates the plasma from the wall or from a probe. In the boundary sheath there is an electric field which accelerates the ions towards the wall but retards the electrons, so that in case the wall is an insulator, the same number of electrons and of ions reach it. Inside the plasma the electric field is small. The electron temperature is usually much higher than the ion temperature.

The plasma theory of Langmuir is founded on the assumption that the velocity distribution of the electrons is Maxwellian. Experimental investigations show that this assumption is usually rather well satisfied. In a plasma at so high pressure that the mean free path is small compared to the linear dimensions, this is a natural result of the collisions between the particles in the plasma. However, it is observed experimentally that even at so low pressures that theoretically the collisions are too rare to give any considerable energy exchange, the velocity distribution is Maxwellian to a high degree of approximation. This is what Gabor, Ash and Dracott call Langmuir's paradox.

Gabor, Ash and Dracott have made a series of experimental investigations in order to make this paradox understandable. Their result is that the energy exchange takes place in an oscillating boundary layer, the existence of which they have demonstrated with an electron beam used as a probe. They conclude that "plasma-boundary oscillations are likely to arise at almost any boundary, not necessarily abrupt or permanent, which is in contact with a plasma however slightly off equilibrium. These oscillations constitute a powerful mixing, entropy-increasing mechanism."

It seems reasonable that their results are applicable also to the boundary between our ionized gas and the forbidden region. Hence we should expect that an oscillating sheath is produced which makes the electron distribution Maxwellian at least near the forbidden region. Whether even far outside the forbidden region a similar phenomenon takes place is more difficult to decide. It is a possibility worth considering that during the whole time when the cloud invades the magnetic field the electron distribution is isotropic. Under this assumption BLOCK (1955) has calculated the motion of the ionized cloud in the terrestrial magnetic field. This motion is rather similar to the motion with $\mu \doteq$ const. For the present discussion it is, therefore, not very important whether we assume approximate isotropy in the whole space or only close to the forbidden region.

We may summarize the arguments for a redistribution at least near the forbidden region in the following way:

1. If an electron when it completes a circle with a radius of curvature of 10 km, changes its velocity vector in an irregular way by as little as 0.1 degrees, a good isotropy will be produced.

2. Observed fluctuations in the aurora and magnetic records make it likely that the path of the electrons will be disturbed in an irregular way.

3. Oscillations of Gabor's type near the forbidden region will easily produce a Maxwellian distribution.

It should be stated clearly that none of these arguments is absolutely convincing. Our present knowledge of a plasma is not sufficient to rule out Cowling's objection. However, the arguments seem to be so plausible that it is worth while to continue our analysis under the assumption that at least near the forbidden region the velocity distribution is Maxwellian. If the distribution is isotropic but not Maxwellian, essentially the same results will be obtained.

§ 9. The voltage of the earth in relation to the plasma

We shall now study what happens in a flux tube through an element F, if the velocity distribution of the electrons is Maxwellian near the equatorial plane.

The pressure of the ionized gas, which essentially is due to the electrons, will tend to make the gas expand along the field lines, so that the whole tube will be filled by the ionized gas. The time scale of this process is

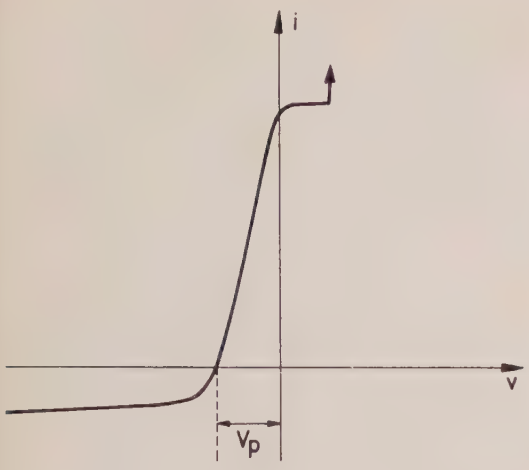

Fig. 1.

difficult to estimate. Near the forbidden region the length of a field line from the equatorial plane to the ionosphere is of the order 10^{10} cm. A velocity of the front of 10^6, 10^7 or 10^8 cm/sec would give 10^4, 10^3 or 10^2 seconds.

The electron temperature T_e is

$$T_e = \frac{2}{3}\frac{eV_e}{k}$$

where k is Boltzmann's constant. eV_e is of the order 10^4—10^5 eV. The mean free path of the electrons is very long (10^{14} cm) compared to the dimensions of the flux tube (cf. § 8). It is difficult to determine the velocity of the ions. As earlier we assume that the kinetic energy of the spiralling motion of the ions is much smaller than the electron energy. The number of neutral atoms is probably so small that it is negligible.

Suppose that in the ionized gas we put a plane conducting electrode perpendicular to the magnetic field. This "probe" will be hit by electrons and ions moving parallel to the magnetic field, and the current to it may be determined according to Langmuir's theory of a probe in a plasma (Fig. 1). If the probe is insulated so that the electron current must be equal to the ion current (ambipolar diffusion) the probe is negative in relation to the plasma, and the voltage difference V_p is a few times the voltage $V_e = \frac{3}{2}\frac{kT}{e}$ which corresponds to the electron temperature T. The voltage drop is confined to a thin sheath with thickness of the order

$$\Delta \equiv \sqrt{\frac{V_e}{en}}$$

and the electric field is small in the rest of the plasma.

The probe will be hit by the Maxwell tail of the electrons (energies above eV_p) and by positive ions. The ions will impinge on the probe with the kinetic energy eV_p (to which should be added their thermal energy which we have assumed to be small).

In nature we have no solid probe. Instead the invading plasma will at first be limited by a free surface or perhaps a shock front. Later it will reach the ionosphere, and the ionosphere will to some extent replace a solid probe. There is a considerable difference, however, because the ionosphere will emit electrons if acted upon directly by the plasma sheath. The analysis of the details of these complicated phenomena must be reserved for a future investigation. The only certain conclusion which can be drawn now is, that even if the solid probe is replaced by an element of the ionosphere, there must still be a voltage drop of the order V_p, because if this were not present the plasma electrons would leave the flux tube in a very short time and an unreasonable high positive space charge would be produced. The voltage drop will accelerate positive ions. Hence the ionosphere will be hit by electrons and positive ions with energies of the order of 10^4—10^5 eV in a typical case. It is reasonable to identify these particles with the protons observed by GARTLEIN and MEINEL (1952) in some types of aurorae.

Let us now consider the case when we have two flux tubes containing exactly similar plasmata and being both in contact with the ionosphere, which is supposed to be an infinitely good conductor. In both flux tubes there will be an ambipolar diffusion to the ionosphere. The plasmata in both flux tubes will be charged to the voltage $+ V_p$ in relation to the ionosphere.

Let the two flux tubes be situated at the border of the forbidden region, one on the day side and the other symmetrically at the night side (Fig. 2). Let us further suppose, in accordance with the theory, that there is a net flow of positive ions into the flux tube at

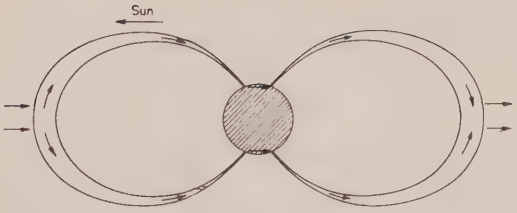

Fig. 2.

the dayside and a net outflow of positive ions from the flux tube at the night side. Both flows take place especially near the equatorial plane. The drift of the electrons does not produce any net flow into the tubes.

The increase of positive charge in the flux tube on the dayside will increase its voltage to $V_p + \Delta V_p$ in relation to the ionosphere. In a similar way the flux tube at the night side will attain a lower voltage $V_p - \Delta' V_p$. This causes a current from the day side to the ionosphere and further on to the night side. This is the current over the auroral zone in the electric field theory.

An ordinary probe is hit by both electrons and positive ions not only in the case of ambipolar diffusion but also when a net current (below a certain limit) flows to the probe. It is reasonable that a similar phenomenon occurs in our case. This means that we may expect the auroral zone to be hit by both electrons and ions on the dayside as well as the night side. On the day side the number of ions is larger than the number of electrons and on the night side the reverse is the case, so that a current over the auroral zone is produced. As mentioned above it is beyond the scope of this paper to analyze the very interesting details of the interaction between the plasma and the ionosphere, but some important features may be pointed out. It is possible that a plasma sheath may be situated very high up in the ionosphere, or perhaps in space far above the ionosphere, and that from this sheath the ionosphere will be bombarded by positive ions and electrons. This state would produce a quiet auroral arc, excited by ions and electrons impinging on a "passive" ionosphere. It is also possible that under certain conditions (e.g. when a large current is drawn) the plasma sheath is broken up so that the voltage drop occurs in an irregular way in the ionosphere itself. This would perhaps give the vivid auroral forms in which the ionosphere plays an active role in the discharge. The different auroral forms may be accounted for as due to the direct action of the electric field. This would be in accordance with some of the views expressed by CHAMBERLAIN (1956) and by LEBEDINSKY (1956).

§ 10. *Influence of space charge*

One of Cowling's most important objections against the electric field theory is that in order to produce a discharge over the auroral zones a large space charge is necessary and this space charge will seriously disturb the drift motion in and near the equatorial plane. This objection is quite plausible from a qualitative point of view, but a quantitative analysis, which we shall make here, will show that it is not serious. This is due to two circumstances:

a) The drift motion is very insensitive to field disturbances.

b) Only a small space charge is necessary in order to produce a discharge over the auroral zones.

In order to find how much the drift motion is disturbed by a space charge, let us put the voltage V in the equatorial plane

$$V = V^1 - Ex \tag{1}$$

in the undisturbed case (see Fig. 3). Here V^1 is the voltage at the y-axis. Electrons entering the earth's magnetic field along the asymptote $x = x_0$ will pass the line $x = x_1$ at a point $(x_1 y)$ given by

$$\frac{H}{H_0} = \frac{V_0 + E(x_0 - x_1)}{V_0} \tag{2}$$

$$\left(\frac{\lambda}{R}\right)^3 = \frac{E(x_0 - x_1)}{V_0} \tag{3}$$

where H_0 is the magnetic field at infinity (in the beam), V_0 the energy of the spiralling motion of the electrons in the beam, $\lambda = \sqrt[3]{\frac{a}{H_0}}$ and a the dipole moment of the earth. Further,

$$H = H_0\left[1 + \left(\frac{\lambda}{R}\right)^3\right] \tag{4}$$

is the field at the point $(x_1 y_1)$.

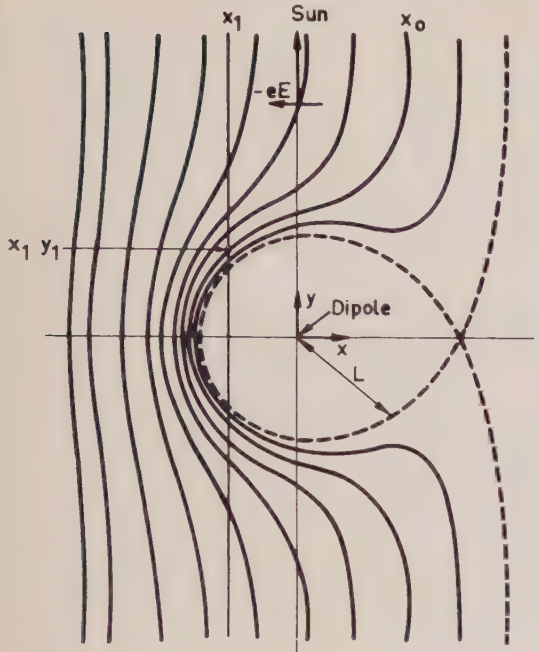

Fig. 3.

Suppose that an accumulation of ions or electrons in the environment of $(x_1 y_1)$ changes the voltage of this region by ΔV. The result is that the electrons will cut the line $x = x_1$ at another point $(x_1 y^1)$ given by

$$\left(\frac{\lambda}{R}\right)^3 = \frac{E(x_0 - x_1) + \Delta V}{V_0} \qquad (5)$$

As this formula shows, the value of R is insensitive to changes in V. In fact, if ΔV is as much as 50 % of $E(x_0 - x_1)$, this produces a change in R by only about 15 %. If we project R along the field lines to the auroral zone, we find that the change in the polar distance is only 7 %, i.e. about 1.5°, in latitude, or 160 km.

If space charge is accumulated in a systematic way so that all along the border of the forbidden region a similar charge is accumulated, a systematic displacement of the auroral zone is produced, which is so small that with the present accuracy of the theory it will be impossible to detect it. If on the other hand the space charge is only local, so that the voltage is changed only in the environment of the point $(x_1 y_1)$ a local displacement of the aurorae by 160 km will be produced. A displacement of this size is a normal occurrence at most displays, especially in connection with the formation of draperies.

Hence we have found that a change in voltage by a factor of 1.5 produced by space charge, will give no remarkable change in the drift motion. This means that we could allow space charge to produce a voltage of 5—50 kV in the equatorial plane in a typical case ($eV = 10^4$—10^5 e volt), and still consider the theory to be valid as a first approximation.

We shall next see whether an electromotive force of 5—50 kV is enough to produce a discharge over the auroral zones.

According to the theory the drift of the ions is confined to a plane $x = \text{const.}$, which is the plane of fig. 2. The ions arrive from the left in the figure with the drift velocity

$$v_L = cE/H_L \approx v_0 \left(\frac{L}{\lambda}\right)^3 \qquad (6)$$

where $H_L = H_0\left[1 + \left(\frac{\lambda^3}{L}\right)\right] \approx H_0 \frac{\lambda^3}{L^3}$ is the field at the border of the forbidden region, which is situated at about the distance L from the dipole, and v_0 is the velocity of the beam. With $v_0 = 2 \cdot 10^8$ cm, $L/\lambda = 4$ (compare ALFVÉN 1955, p. 55) we obtain

$$v_L = 3 \cdot 10^6 \text{ cm/sec.} \qquad (7)$$

For protons this translational velocity corresponds to a kinetic energy of only 4 eV.

According to the theory the ions cannot continue their motion towards the night side (in fig. 2) because when they reach the border of the forbidden region, their space charge is no longer compensated by electrons. Instead they must go parallel to the field lines to the ionosphere in the auroral zone. The velocity v_A of this motion must be at least of the same order as v_L. In order to confine the motion towards the auroral zones to a resonably thin layer we should require that v_A is at least a few times v_L, say

$$v_A \geq 5\, v_L \qquad (8)$$

or, with the numerical value from (7)

$$v_A \geq 1.5 \cdot 10^7 \text{ cm/sec.}$$

The kinetic energy of protons with this velocity is 100 eV. This means that the space charge need only produce a potential of 100

volt near the equatorial plane in order to send away the ions towards the auroral zones with a sufficient energy.

Thus we see that only a very small fraction of the voltage (5—50 kV) from a reasonable space charge is enough to send the ions away from the equatorial plane towards the auroral zones. As the mean free path of the ions in the plasma is long compared to the distance from the equatorial plane along a field line to the auroral zone, the motion will not be impeded by collisions. On the other hand, the increase in magnetic field when we approach the ionosphere will brake the motion and reflect the ions in case their spiralling motion is large enough. Suppose for a moment that the ion temperature is zero and the space charge field acts only in the direction of the magnetic field. Then the effect of the magnetic inhomogeneity is negligible. The ions move along the magnetic field lines to the plasma sheath, and when passing this they become accelerated before they impinge on the ionosphere. Thus in this case only a very small fraction of a reasonable space charge voltage is enough to produce a discharge to the auroral zone.

If the ion temperature differs from zero and the space charge also accelerates the ions in the plane perpendicular to the magnetic field, the discharge will probably require a larger electromotive force. Only a detailed analysis, which it is beyond the scope of this paper to give, can show how high ion temperature is permissible without impeding the discharge. As at present the ion temperature is unknown, it would not be possible to check an obtained value of this quantity.

A similar discussion shows that also the electrons in the plasma are easily set into motion even by small fields.

Our ignorance of the ion temperature and the fact that the theory of a hot plasma in contact with the ionosphere is still undeveloped makes it impossible to state that the conditions during a storm necessarily are such as to make a discharge possible. However, as in that case which we have treated only 100 volt out of available 5—50 kV are necessary for the discharge, we may be confident that the conditions often are such as to allow a discharge of positive charge to the ionosphere.

An accumulation of negative charge in or near the equatorial plane at the night side may give rise to a slightly different phenomenon. As the electrons are easily movable a very small field is enough to send them away towards the auroral zones. When they reach the plasma sheath, most of them are turned back by the opposing voltage, but they transfer the voltage from the equatorial plane to the sheath. Hence an accumulation of negative space charge in the equatorial plane will diminish the voltage V_p over the sheath (compare Fig. 1), with the result that a current of electrons flows to the ionosphere.

What has been said makes it reasonable that a space charge, which is small enough not to disturb seriously the drift in the equatorial plane may suffice to produce a discharge over the auroral zones. To this should be added the support we get from the similarity with Block's experiment, and the fact that the mechanism we are considering gives a fairly good picture of the basic phenomena observed during auroral displays and magnetic storms.

§ 11. *Remarks on frozen-in field lines of force*

In a fluid with infinite electric conductivity the magnetic field lines can often be considered as "materialized" or "frozen-in". A discussion of the behaviour of the field lines (the "spaghetti" method) gives a good survey of many problems, such as magneto-hydrodynamic waves travelling along the field lines, changes in the field geometry when the fluid moves, etc. It is of interest to note that in the present problem the limitations of this spaghetti method are obvious. In the two-dimensional case (motion in the equatorial plane) which is treated in the electric field theory, the motion of the field lines of the initial beam can be followed. When the ionized gas passes the λ-region or approaches the L region, the electrons move in a way which is different from the ions. Especially in the L region, this difference is large: the electrons move along almost circular arcs around the dipole whereas the ions move in straight lines up to the forbidden region. At least in a stationary state it is not very important whether we consider the field lines to follow the motion of the electrons or of the ions. In the former case we could follow the motion of the field lines from the initial beam all way round the earth and further on in the continuation of the beam.

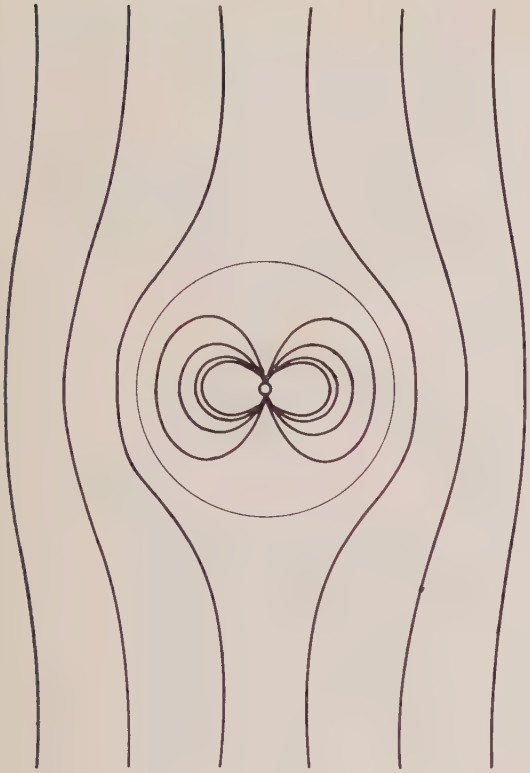

Fig. 4.

geneous magnetic field H (Fig. 5). Suppose that A moves downwards perpendicular to the plane of the paper and B upwards. The polarisation $v \times H$ produces electric fields E with opposite directions in A and B.

If space between A and B is a good electrical conductor, currents will be produced which tend to brake the motion. In case of infinite conductivity we could regard the lines of force to be frozen in both in A, in B and in the medium between, and a well-known type of discussion will show that the breaking could be envisaged to be produced by elastic field lines.

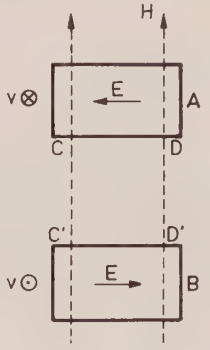

Fig. 5.

In the latter case the field lines move up to the dayside of the forbidden region, but as the matter frozen on them is discharged there, we lose track of them. On the nightside of the forbidden region new field lines are materialized and move on outwards.

Hence there is an ambiguity but no real difficulty in the two-dimensional case. If from this we turn to the three-dimensional case an apparent difficulty occurs (Fig. 4). As long as the ionized matter is outside the sphere $R = \lambda \sqrt[3]{2}$, the field lines go from the equatorial plane to infinity (or in reality in some way to the sun), whereas inside the sphere they go to the earth. When the beam has passed the distance $\lambda \sqrt[3]{2}$, field lines from the earth should go to the cloud, and if the same field line is frozen into the ionosphere at the same time as in the cloud, the advance of the cloud would be impossible.

In order to solve this paradox, let us consider two conducting bodies A and B in a homo-

On the other hand, if space between A and B is electrically insulating, no current will result from the polarizations, and the motions will not be braked. The voltage difference V_C between C and C', and the difference V_D between D and D', will not be equal: $V_C \neq V_D$. We could say that as space between A and B is insulating, the lines of force could not be identified, and it is of no use to speak of a continuation of a certain line of force from A to B.

The same holds also in the case that the medium between A and B is conducting under the condition that there is a double layer, which takes up the voltage difference produced by the polarisation. This is what occurs in the case of a plasma invading the earth's magnetic field. Between the plasma and the ionosphere there is a plasma sheath which is able to take up a voltage difference of the order of 10^5 volt. This makes possible a relative motion between the plasma and the ionosphere. This means that the lines of force are "cut" by this plasma

sheath so that a "slip" in the motion is allowed. In the mathematical treatment it is important to introduce the temperature of the ionized gas and the voltage difference which is produced by the inhomogeneous temperature.

I wish to thank Professor Cowling for discussions and correspondence. His criticism has helped me to clarify the ideas and develop the theory. (This does by no means imply that Professor Cowling accepts the theory even in its present form.)

Like most of my papers the last years, this paper has been written in close contact with Dr. Herlofson. I have also profited from numerous discussions with Dr. Lehnert and Dr. Åström.

REFERENCES

Alfvén, H., 1939: A theory of magnetic storms and aurorae, I, *Kungl. Sv. Vetenskapsakad. Handl.* (3). **18**, No. 3.

— 1940: A theory of magnetic storms and aurorae, II, III. *Ibid.* **18**, No. 9.

— 1950: Cosmical electrodynamics, Oxford.

— 1954: On the origin of cosmic radiation. *Tellus*, **6**, p. 232.

— 1955: On the electric field theory of magnetic storms and aurorae. *Ibid.*, **7**, p. 50.

— 1956: The sun's general magnetic field. *Ibid.*, **8**, p. 1.

Block, L., 1955: Model experiments on aurorae and magnetic storms. *Ibid.*, **7**, p. 65.

Chamberlain, J. W., 1956: Discharge theory of auroral rays, *Airglow and aurorae* (Symp. Belfast), p. 206.

Chapman, S., 1952: Theories of the aurora polaris. *Ann. Géophys.*, p. 205.

Cowling, T. G., 1942: On Alfvén's theory of magnetic storms and of the aurora. *Terr. Mag.*, **47**, p. 209.

— 1957: Priv. comm.

Ferraro, V. C. A., 1952: On the theory of the first phase of a geomagnetic storm. *Journ. Geophys. Res.*, **57**, p. 15.

Gartlein, C. W., 1952: The appearance of H in auroral spectra, 1942—51. *Mem. Soc. Roy. Sci. Liège*, **12**, p. 195.

Gabor, D., Ash, E. A., and Dracott, D., 1955: Langmuir's paradox. *Nature*, **176**, p. 916.

Hayakawa, S., 1955: *IUPAP Cosm. Ray Congress* Mexico.

Herlofson, N., 1957: In course of publication.

Hulburt, E. O., 1937: Terrestrial magnetic variations and aurorae. *Rev. Mod. Phys.* **9**, p. 44.

Johnson, T. H., 1938: Cosmic-ray intensity and geomagnetic effects. *Ibid.*, **10**, p. 193.

Lebedinsky, A. I., 1956: Electrical discharges and the interpretation of auroral types. *Airglow and aurorae* (Symp. Belfast), p. 222.

Lundquist, S., 1954: A note on the variation of cosmic ray intensity produced by an electric field. *Tellus*, **6**, p. 260.

Malmfors, K. G., 1946: Experiments on the aurorae. *Ark. f. mat., astr. o. fysik*, **34** B, No. 1.

Meinel, A. B., 1952: Excitation mechanisms in the aurora. *Mem. Soc. Roy. Sci. Liège*, **12**, p. 203.

Nikolskij, 1955.

Singer, S. F., 1954: Storm decrease of the cosmic radiation at the pole. *Phys. Rev.*, **95**, p. 647.

Treiman, S. B., 1953: Effect of equatorial ring current on cosmic-ray intensity. *Ibid.*, **89**, p. 130.

Changes in Amplitude of the 27-day Variation in Cosmic Ray Intensity during the Solar Cycle of Activity

By D. VENKATESAN, Royal Institute of Technology, Stockholm

(Manuscript received April 6, 1957)

Abstract

The 27-day recurrence tendency in the cosmic ray intensity has been studied by the Chree method of analysis for the period 1937—55, using the ionisation chamber records at Huancayo. The amplitude of the 27-day variation changes from year to year. The variation in the amplitude is in general agreement with the changes in solar activity as revealed by the sun-spot number only for the years 1937—46 and 1952—55. This is in agreement with the results of Meyer and Simpson for the same periods, obtained from a slightly different method of analysis. The correlation breaks down for the period 1946—52 and this is discussed in terms of possible changes in the electromagnetic conditions in the interplanetary space during the solar cycle.

1. Introduction

The quasi-periodic variation in the intensity of cosmic rays with a recurring tendency of about 27 days has been studied by MONK and COMPTON (1939), BROXON (1949), LANGE and FORBUSH (1949), SIMPSON (1954) and others.

Since the synodic period of rotation of the sun is about 27 days and since SIMPSON et al. (1952) had observed in 1951 that individual solar regions could be associated with the 27-day variation in cosmic rays, they have searched for an association between the amplitude of the 27-day variation and the changes in solar activity as revealed by the sunspot number. They have studied the ionisation chamber data for the period 1937—46, and neutron data for the period 1951—53. It would be worth-while comparing the results of their analysis with the present analysis.

The 27-day variation in cosmic ray intensity could be interpreted as modulation effects in the interplanetary space produced by the deceleration in the electric field associated with the beams of rarified ionised gas emitted from the sun, as pointed out by BRUNBERG and DATTNER (1954), ALFVÉN (1956), and VENKATESAN (1957). The beams with the frozen magnetic field and the electric field arising from polarisation effects were invoked by ALFVÉN (1950, 54, 55) to explain the essential features of magnetic storms and aurorae.

It is reasonable to suppose that the beams which are expected to govern and regulate the electromagnetic conditions in the interplanetary space to a large extent, would be affected by the changes in solar activity occurring during its eleven year cycle. In view of the general dependence of the beams on solar activity, it would be of interest to study one of the effects attributed to the electric field, namely the cosmic ray intensity decreases, to see whether there is any association between them.

Since the recurrence phenomena are attributed to the beams, it would therefore not be surprising if a relation, for example between the amplitude of the 27-day variation and

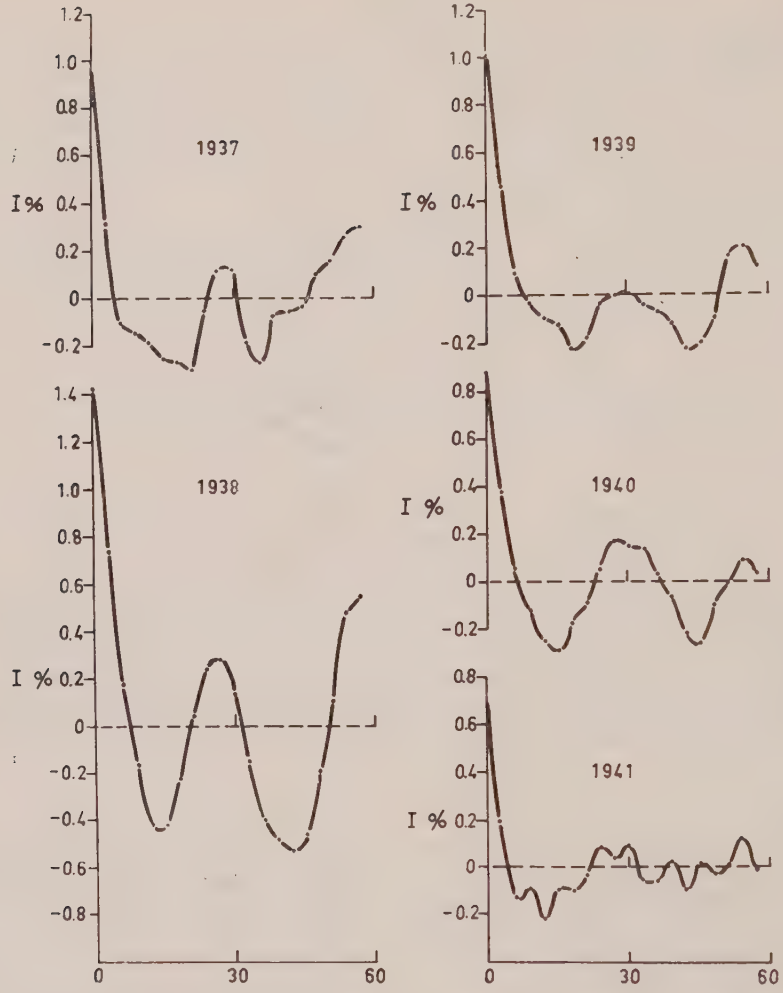

Fig. 1. The Chree analysis of the daily mean cosmic ray intensities at Huancayo for the years 1937—41. The ordinate gives the intensity and the abscissa, the days.

solar activity were observed. MEYER and SIMPSON (1954) from a study of the neutron intensity data over the years 1951, 52 and 53 find a progressive decline in the amplitude, which is consistant with the decreasing solar activity.

2. Data and Method of Analysis

The data chosen for study are the daily mean intensities of the ionisation chamber at Huancayo for the years 1937 to 1955. This covers a period corresponding to more than one complete cycle. The years 1937 and 1947 were ones of high solar activity and 1944 and 1954 were ones of low activity.

The method of analysis is the one originally devised by CHREE (1913) in connection with the study of recurrence phenomena in geomagnetic character figures. It should be pointed out that the method is free from any preconceived notions about the length and significance of the recurrence tendency. The method consists in summing up the intensity values on all days exhibiting a minimum (or a maximum) tendency by choosing, say, five days per month. This is designated as the zero day. Similarly the same procedure is carried out for, say, 60 days preceding and following the selected zero days. It is possible that the recurrence tendency is obscured to some extent either by seasonal effects or by

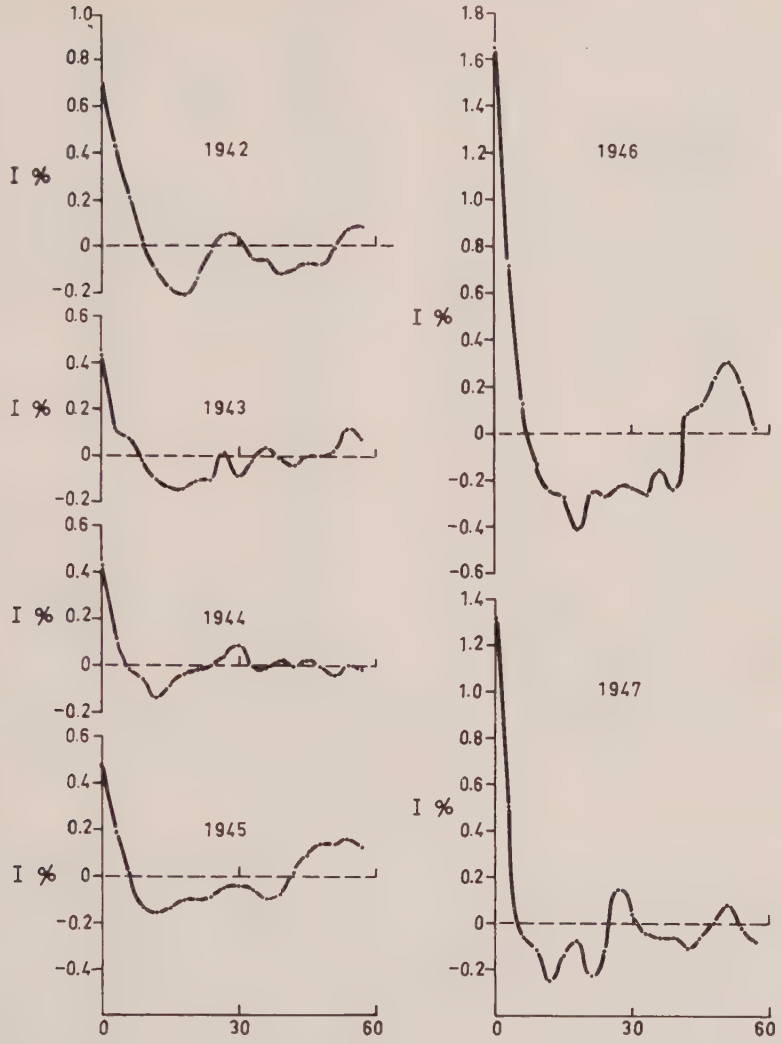

Fig. 2. The Chree analysis of the daily mean cosmic ray intensities at Huancayo for the years 1942—47. The ordinate gives the intensity and the abscissa, the days.

systematic drifts in the measuring instrument. As these effects would be nearly the same for both the analyses corresponding to minimum and maximum intensity days, it could be removed by subtracting the sums of the former from the sums of the corresponding day in the latter. The difference curve is plotted with each point representing the average intensity over three days as is usually done in such analyses. The final results are obtained by folding the difference curve about the zero day so that values corresponding to the preceding and following days are combined.

3. Results and Discussions

Figures 1—4 give the final results for Huancayo for the years 1937—55. It can be seen from the figures that the recurrence tendency undergoes changes during the solar cycle. The recurrence tendency near the 27th day is most pronounced in the years 1938, 1948, 1951 and 1952. While the years 1938 and 1948 correspond to periods when the solar activity was high, the other two years correspond to epochs when the solar activity was near the end of the cycle. It should be pointed out that 1954 was the year of minimum solar activity.

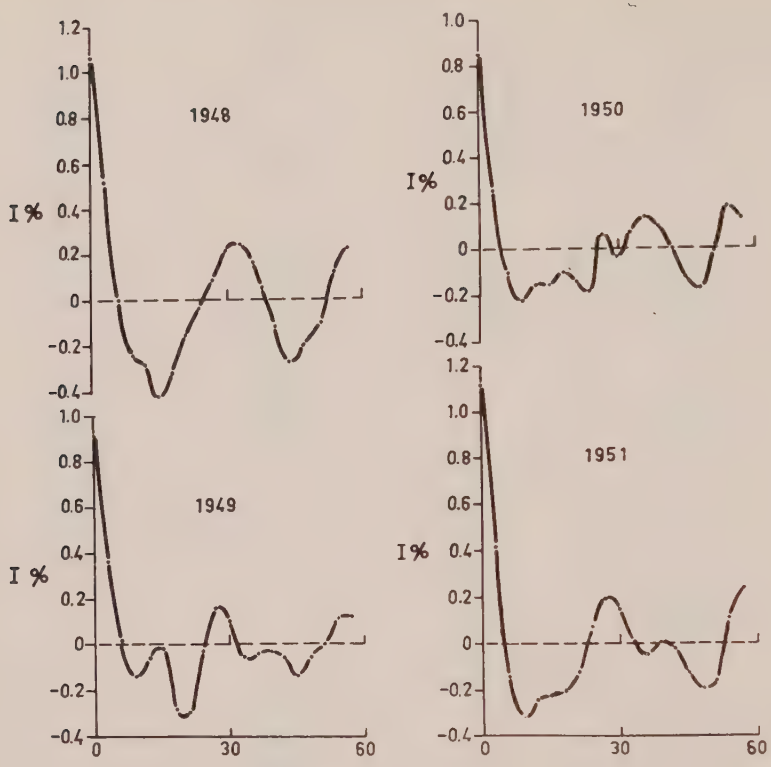

Fig. 3. The Chree analysis of the daily mean cosmic ray intensities at Huancayo for the years 1948—51. The ordinate gives the intensity and the abscissa, the days.

In fig. 5, a comparison is made between the changes in solar activity as revealed by the sunspot numbers and the amplitude of the 27-day variation. R is the mean annual sunspot number for the year, while 'a' refers to the value of the intensity corresponding to the zero day measured from the mean level for each year. 'a' could be considered as a measure of the amplitude. On the same fig. are also given the values of σ for each year, which is defined by MEYER and SIMPSON (1954) as a quantitative measure of the 27-day amplitude. σ_H refers to Huancayo while σ_{Cl} refers to Climax. σ_{Cl} is plotted for the station Climax using neutron intensity instead of ionisation chamber data. The scale ratio for neutron/ionisation chamber is taken to be approximately 5.

$\sigma = <\delta>^{\frac{1}{2}}$ is the standard deviation of a set of δ^2, where $\delta = [I(t) - I(t+\tau)]/<I>$. $<I>$ refers to the average intensity, $I(t)$ and $I(t+\tau)$ refer to the intensities at Huancayo on day t and $t+\tau$, where $\tau = 14$. This is a consequence of the existence of recurrence tendency of 27—28 days in the intensity variations. They have pointed out that this selection preferentially chooses those variations which have a quasi-periodicity of 27 days.

In fig. 6 also a comparison is made between the changes in solar activity as revealed by the sunspot numbers and the amplitude of the 27-day variation defined in a slightly different way. R as before is the mean annual sunspot number, while 'A' is half the difference between the values on day 0 and day 14, and which could be taken as a measure of the amplitude. It should be pointed out that there could be a certain measure of uncertainty in 'A' since another sequence of 27-day variations which is often found showing up after 14 days, would reduce it. This has to be borne in mind, as it could very well happen that these secondary series are more prominent in one year than in others. On the same fig. are also given σ (tracking), defined by MEYER and SIMPSON (1954) as a measure of the ampli-

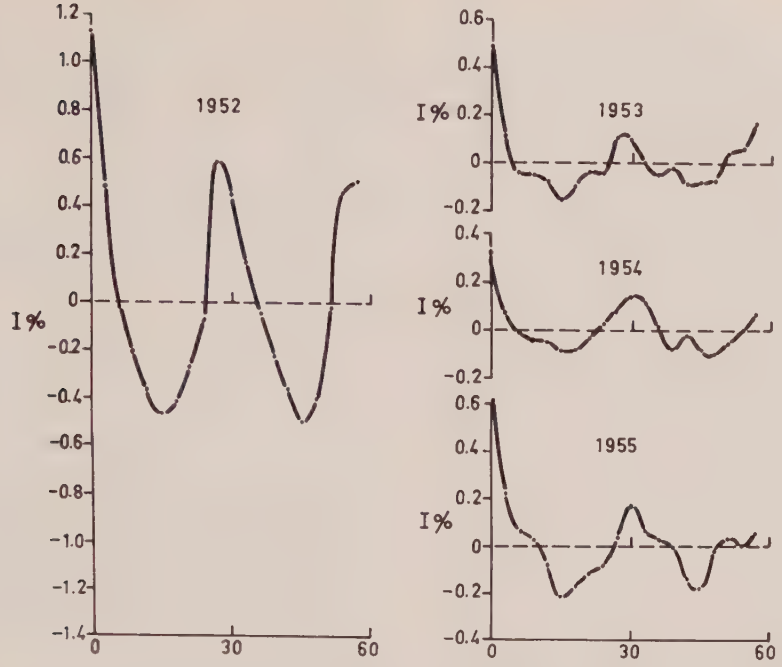

Fig. 4. The Chree analysis of the daily mean cosmic ray intensities at Huancayo for the years 1952—55. The ordinate gives the intensity and the abscissa, the days.

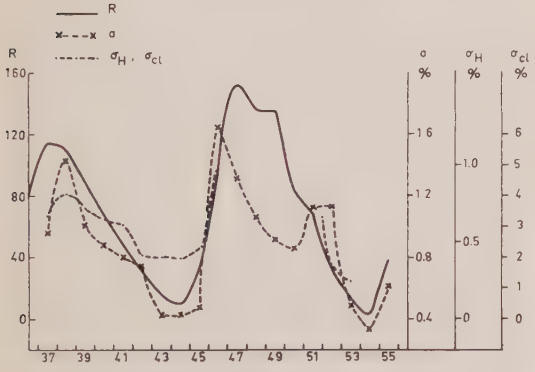

Fig. 5. The variation of the amplitude of the 27-day variation in cosmic ray intensity during the years 1937—55. R refers to the mean annual sunspot number, 'a' to the amplitude of the 27-day variation at Huancayo as measured in the present investigation, from the mean level of intensity, σ_H, σ_{Cl} to the amplitude of the 27-day variation as defined by Meyer and Simpson, at Huancayo and Climax.

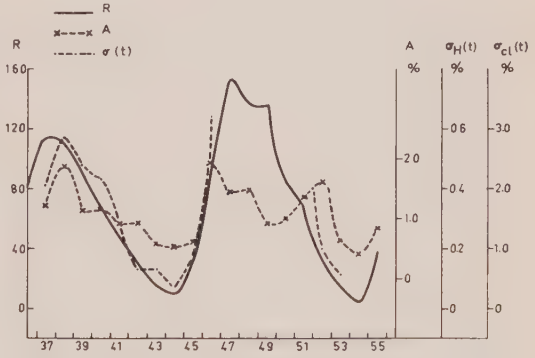

Fig. 6. The variation of the amplitude of the 27-day variation in cosmic ray intensity during the years 1937—55. R refers to the mean annual sunspot number, 'A' to the amplitude of the 27-day variation at Huancayo as measured in the present investigation and equal to half the difference between the values on zero day and 14th day, $\sigma(t)$ to the worldwide amplitude of the 27-day variation as defined by Meyer and Simpson, at Huancayo and Climax.

tude of the worldwide 27-day variation. It is the product of σ_H and γ, the correlation between the δ^s for Huancayo and some other station.

In their analysis Meyer and Simpson remove some periods from the data, namely those containing temporary increases due to solar flare and Forbush decreases which they consider to be different from the 27-day variations.

We have not deleted the flare period data

corresponding to 28th Feb., 1942 and 26th July, 1946 since we do not find any increase at Huancayo and since we do not use the data of any other station. Since we consider the so-called non-recurring Forbush decreases differ only in the matter of degree, we have not deleted these periods. We attribute both the 27-day variation as well as Forbush decreases to be the effect of deceleration in the beams from the sun. In this connection, it should be pointed out that SINGER (1946) holds a similar view about the two effects. He has further referred to a case of recurrence in Forbush decreases. GALLI and GALLI (1956) have pointed out the 27-day recurrence in Forbush decreases.

MEYER and SIMPSON (1954) have determined a measure of the amplitude of the 27-day variation in cosmic ray intensity for the periods 1937—46 and 1951—53. As their result for 1951 is only for six months we have not considered that for the comparison with our results. It can be seen from figs. 5 and 6 that the measure of amplitude as defined by them and as given here reveal a good agreement for the period for which their data is available in spite of certain differences in the mode of selection of the data and the method for analysis. This close agreement for 1937—46 and 1952—53 leads one to expect that the same agreement is likely to be there for the intervening period also.

The close agreement between the amplitude of the 27-day variation in cosmic ray intensity and the solar activity as revealed by the sunspot number, is clearly seen from figs. 5 and 6 for the periods 1937—46 and 1952—55. The departure from this behavior during 1946—52 stresses the importance of a careful study needed for this period before one can draw any general conclusions about the whole solar cycle.

The correlation between sunspot number and the amplitude of the 27-day variation does not mean that the sunspots are the underlying cause of the cosmic ray changes. It is only an index of solar activity with which one can reasonably associate the emission of beams. For example, one could say that with increased activity of the sun, the number of beams emitted would be greater and perhaps that the beams extend to a larger extent. The departure from the expected correlation during 1946—52 could be reasonably accounted for by an interpretation in terms of possible changes in the characteristics of the beams. Since the solar activity has increased even after 1946, the number of beams could not have decreased. In this connection it is worth-while pointing out that the years 1947—49 had the highest sunspot numbers since the last seventy years, and moreover the year 1947 had the highest value since 1778, indicating an unusually heavy activity.

The amplitude of the 27-day variation is governed by the voltage across the beams, which in turn depends on a number of factors. It is not possible to say at this juncture, from the cosmic ray evidence alone, whether there is any systematic variation in the characteristics of the beam like the value of the magnetic field frozen in the beam, the velocity of the particles in the beam, the width of the beam etc., with the changes in solar activity. It is necessary to look into geomagnetic and auroral data also before one can arrive at unambiguous conclusions.

It can be seen from fig. 6 that the amplitude of the 27-day variation in 1946 does not reach a value much higher than in 1938 although solar activity is very much higher. It is worth-while to point out that in 1946, there were a series of heavy Forbush decreases starting from Feb. and lasting for nearly six months. If it is reasonable to assume that the beams, to which could be attributed this unusually heavy activity, had transported a major quantity of the flux available, there would be a relatively weaker magnetic field for new beams to freeze. Hence it would be reasonable to expect these beams not to produce heavy geomagnetic disturbances or heavy cosmic ray decreases. This would reduce the amplitude of the 27-day variation. It can be seen from fig. 6 that the amplitude of the 27-day variation decreases from 1946 although the solar activity goes up and remains high. In other words some sort of saturation of the electromagnetic state of the interplanetary space is reached.

It is of importance to find out whether the breakdown in the relationship between the amplitude of the 27-day variation in cosmic ray intensity and solar activity during 1946—52 is reflected in any other effects attributed to the electric field of the beams emitted from

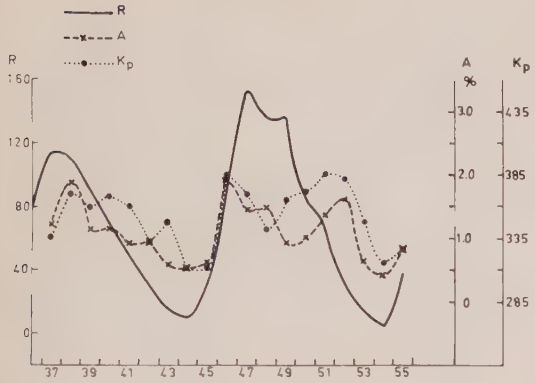

Fig. 7. The variation of the amplitude of the 27-day variation in cosmic ray intensity and a measure of the geomagnetic disturbance during the years 1937—55. R refers to the mean annual sunspot number, 'A' to the amplitude of the 27-day variation at Huancayo as measured in the present investigation and equal to half the difference between the values on zero day and 14th day, and K_p to the sum of K_p maximum values for the 60 most disturbed days in each year.

the sun. For example, we could consider the geomagnetic disturbances. The planetary index, K_p, is a reliable though arbitrary measure of geomagnetic disturbance. One could choose either the maximum value of K_p or the sum of the eight K_p values available for each day. We use the former. Instead of using the elaborate method adopted above for cosmic rays, one could obtain an idea of the behavior of geomagnetic disturbances during a solar cycle by the following method. The 60 most disturbed days in each year are selected and the sum of the K_p maximum values for these 60 days is determined and plotted against time as in fig. 7. It can be seen from that fig. that the geomagnetic disturbances as revealed by K_p also show changes from year to year in fair agreement with the changes in sunspot number for 1937—46 and 1952—55, just as the cosmic rays behaved. But, for the period 1946—52, they show the same departure from sunspot number as is observed in the case of cosmic rays. This supports the earlier observation pointing out the necessity of looking into this period carefully.

If it is reasonable to assume some sort of saturation of the electromagnetic conditions in the interplanetary state is reached in 1946, then the absence of the occurrence of heavy geomagnetic disturbances immediately after 1946 is understandable although the solar activity goes up and remains high. The gradual resetting of the pre-saturation conditions takes place by about 1948. Further emission of beams thereafter would result in the occurrence of comparatively heavier geomagnetic activity as can be observed from fig. 7.

Fig. 8 shows 'A' the amplitude of the 27-day variation in the intensity of cosmic rays and the sum of the K_p maximum values for the 60 most disturbed days in each year against R the sunspot number. It can be observed from this figure that they both appear to reach a maximum value corresponding to the value of sunspot number in about the range 80 to 100. The figure also seems to indicate a decline

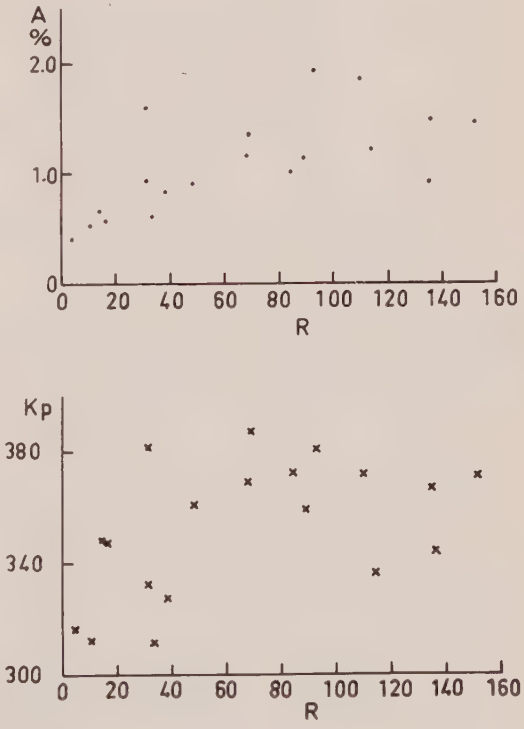

Fig. 8. The relation between the amplitude of the 27-day variation in cosmic ray intensity and sunspot number; and the relation between the geomagnetic disturbances and the sunspot number. R refers to the mean annual sunspot number, 'A' to the amplitude of the 27-day variation at Huancayo as measured in the present investigation and equal to half the difference between the values on zero day and 14th day, and K_p to the sum of K_p maximum values for the 60 most disturbed days in each year.

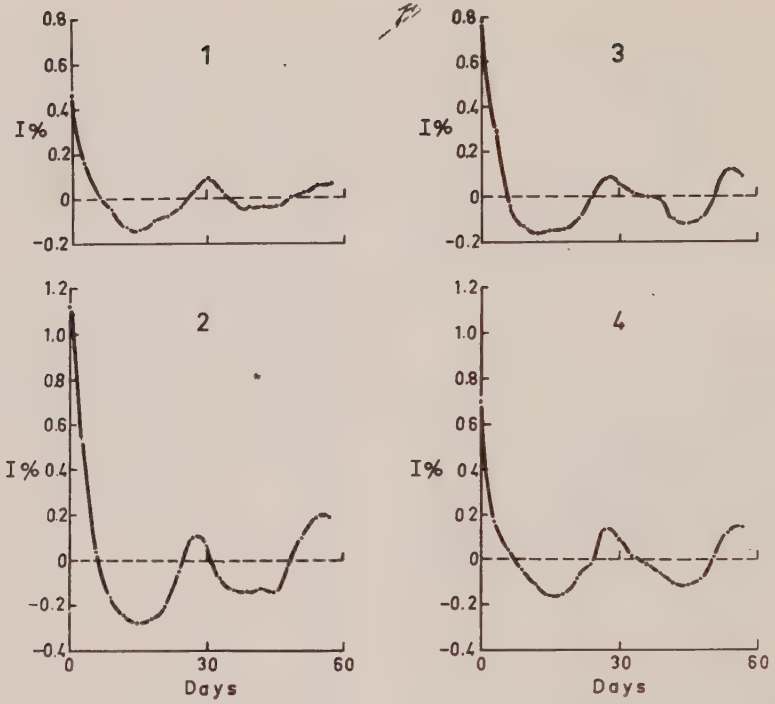

Fig. 9. Changes in the periodicity of the recurrence tendency in the variation of the cosmic ray intensity. The four curves correspond to recurrence during various stages in the solar cycle of activity.

with further increase of sunspot number. This indicates that some sort of saturation of the electromagnetic state is reached at a particular level of solar activity.

If changes in the electric field of the beams during the solar cycle do take place, then it could very well be due to changes in any of the three parameters governing the same, namely the frozen magnetic field, the velocities of the particles in the beam and the width of the beam. This would also raise the question whether it is the general dipole field of the sun that is frozen in the beam or whether at least at times the local high regional magnetic field could be frozen in the beam. The latter possibility would easily allow for a wide range in the variation of the frozen field from year to year. The shrinking of the auroral zone during the minimum solar activity years would support the view that the electric field gets weaker.

The recurrence period also seems to vary during the solar cycle. It is of course not definite whether on the evidence available one could point out a definite systematic variation with solar activity. It would therefore be worth-while to look at other data in addition to cosmic rays to arrive at an unambiguous conclusion. It appears from table 1 that the period of recurrence is larger for the years when the new cycle starts. A combination

Table 1. Recurrence period for years grouped according to solar activity.

No.	Group corresponding to	Years combined	Recurrence interval days
1	beginning of new cycle	1944, 1945 1954, 1955	30
2	maximum of activity	1937, 1938 1946, 1947 1948, 1949	Between 27 and 30
3	fall of activity	1939, 1940 1941, 1950, 1951	Between 27 and 30
4	end of cycle	1942, 1943 1952, 1953	27

of the data for the whole period into 4 groups, (a) rising part of solar cycle, (b) period of maximum activity, (c) fall of activity, and (d) end of cycle, reveals that at least for group (a) the recurrence period is greater than for the other groups. This is seen from figure 9. Such a behavior, if it is definite, would be understandable. The 'butterfly pattern' of the distribution of the sunspots is wellknown. If the region of origin of the beams changes during the solar cycle in a systematic way such a behavior could be expected. The problem needs further study.

The author is extremely grateful to Dr. S. E. Forbush for providing unpublished data for analysis. The statistical part of the analysis has been done on the I.B.M. computor (Type 650). The author is thankful to Dr. D. Eckhartt for programming and to Mrs. Bharathi Venkatesan for help for the I.B.M. analysis. Thanks are due to Prof. H. Alfvén and Dr. N. Herlofson for useful discussions and to the Statens Tekniska Forskningsråd for financial assistance which has enabled the analysis to be completed.

BIBLIOGRAPHY

1. Alfvén, H., 1950: *Cosmical Electrodynamics*, ch. VI.
— 1954: On the Electric Field Theory of Magnetic Storms and Aurorae. *Tellus*, **6**, p. 232.
— 1955: On the origin of Cosmic Radiation. *Tellus*, **7**, p. 50.
— 1956: Interplanetary Magnetic Field. International Astronomical Union Symposium on Electromagnetic Phenomena in Cosmical Physics.
2. Broxon, J. W., 1941: Recurrence Phenomena in Cosmic Ray Intensity. *Phys. Rev.*, **59**, p. 773.
3. Brunberg, E. Å., and Dattner, A., 1954: Variations of the Cosmic Ray Intensity during Magnetic Storms. *Tellus*, **6**, p. 254.
4. Chree, C., 1913: *Phil. Trans.*, A **212**, p. 76.
5. Galli, M., and Galli, A. M., 1956: On the 27-day Recurrence trains of Forbush type minima in the Cosmic Ray Intensity. Private Communication.
6. Hogg, A. R., 1949: *Memoirs of the Commonwealth Observatory*, Canberra, No. 10.
7. Lange, I., and Forbush, S. E., 1949: Search for Systematic Variations in Cosmic Ray Intensity. *Phys. Rev.*, **76**, p. 164.
8. Meyer, P., and Simpson, J. A., 1954: Changes in Amplitude of the Cosmic Ray 27-day Intensity Variation with solar activity. *Phys. Rev.*, **96**, p. 1085.
9. Monk, A. T., and Compton, A. H., 1939: *Rev. of Mod. Phys.*, **11**, p. 175.
10. Simpson, J. A., 1954: Cosmic Radiation Intensity Time Variations and their origin III. *Phys. Rev.*, **94**, p. 426.
11. Simpson, J. A., Fonger, W., and Wilcox, L., 1952: A Solar component of the Primary Cosmic Radiation. *Phys. Rev.*, **85**, p. 366.
12. Singer, S. F., 1956: The Primary Cosmic Radiation and its Time Variations. *Maryland University Physics Department Technical Report* 40.
13. Venkatesan, D., 1957: Magnetic Storm Effects and the Interplanetary Electromagnetic State. *Tellus*, **9**, p. 209.

On the Increase in Cosmic Ray Intensity and the Electromagnetic State in Interplanetary Space during the Solar Flare of Feb. 23, 1956

By DIETER ECKHARTT, The Royal Institute of Technology, Stockholm

(Manuscript received March 3, 1957)

Abstract

The solar flare increase of cosmic ray intensity observed at various ionization chamber stations has been studied. The orbits of the flare cosmic ray particles have been corrected for their deflection in the geomagnetic field. A detailed discussion of the different onset times of the solar flare increase registered at these stations is given. These differences in onset times serve as a means to study the electromagnetic state in interplanetary space during the cosmic ray outburst.

Special attention is paid to those stations which observed the earliest onset times. For one of these, Hobart, it can definitely be shown that cosmic ray particles of momenta up to around 40 GeV/c did not arrive from the direction of the sun. The station did not lie inside one of FIROR's impact zones at the beginning of the solar flare. This shows the existence of deflecting magnetic fields between the sun and the earth.

It appears from this investigation that the cosmic ray particles which caused the earliest onset times had come from directions towards a solar beam which—according to ALFVÉN's beam model—would be expected to produce the large magnetic storm observed two days after the flare. A probable mechanism of trapping and guiding the flare low energy cosmic ray particles by such a beam is also discussed.

Introduction

The sudden increase in cosmic ray intensity in connection with the solar flare of Feb. 23, 1956, was observed to have commenced at different times at various places around the earth. Cosmic ray particles having started at the same time from the vicinity of the sun, must have travelled along orbits of different lengths before they entered the geomagnetic field from various directions. Thus, the differences in onset times are of great importance when studying the electromagnetic properties of the interplanetary space.

On Feb. 25, two days after the flare, the largest magnetic storm since four years ago, with sudden commencement at 0307 UT, was observed. A series of relatively sharp decreases in the daily mean cosmic ray intensity occurred around Feb. 23. Even these phenomena may be understood in terms of the electromagnetic state around the earth.

In the following paper the implications of the different onset times of the cosmic ray intensity increase are discussed in detail. Further, an attempt is made to connect the earliest onset times observed with an interpretation of the magnetic storm which occurred two days later.

The stations for which the onset times are accurately known are given in Table 1. The orbits in the geomagnetic field for cosmic ray particles which arrive at the ionization chamber stations, listed in the first group of Table 1, have been investigated to determine their directions outside the geomagnetic field. Thus we are able to connect these different direc-

Table 1. List of stations where well-defined onset times of the cosmic ray intensity increase on Feb. 23, 1956 were registered.

IO: ionization chamber. NM: neutron monitor. GM: GM-counter telescope. SH: shower apparatus. SC: scintillation counter.

Station	Geomagnetic		Geographic		Type of App.	Onset time UT	References
	lat.	long.	lat.	long.			
Godhavn	79.8°	33°	69° N	53° W	IO	3^{53}	Forbush, 1956
Cape Schmidt	63.0°	227°	69° N	180° E	IO	3^{42}	Dorman et al., 1956
Amsterdam	54.0°	89°	53° N	5° E	IO	3^{43}—3^{45}	Assies & Jongen, 1956
Moscow	52.0°	121°	56° N	37° E	IO	3^{38}, 3^{40}	Dorman et al., 1956
Hobart	52.0°	225°	43° S	147° E	IO	3^{39}—3^{43}	Fenton et al., 1956 A
Halle	51.8°	96°	52° N	12° E	IO	3^{45}	Messerschmidt, 1956
Yakutsk	51.0°	194°	62° N	129° E	IO	3^{42}	Dorman et al., 1956
Derwood (Cheltenham)	50.5°	350°	39° N	77° W	IO	3^{48}	Forbush, 1956
Freiburg	49.3°	90°	48° N	8° E	IO	3^{42}	Sittkus et al., 1956
Christchurch	— 48.1°	253°	44° S	173° E	IO	3^{48}—3^{51}	Elliot & Gold, 1956
Sverdlovsk	48.1°	141°	56° N	61° E	IO	3^{40}	Dorman et al., 1956
Mexico	29.4°	327°	20° N	99° W	IO	3^{45}	Forbush, 1956
					NM	3^{45}—3^{50}	Simpson et al., 1956 A
Mt. Norikura	25.6°	204°	36° N	138° E	IO	3^{43}—3^{45}	Sekido et al., 1956
					NM	3^{43}—3^{45}	
Huancayo	— 0.6°	354°	12° S	75° W	IO	3^{44}—3^{46}	Forbush, 1956
							Simpson et al., 1956 A
Resolute	82.9°	289°	75° N	95° W	GM	3^{53}—4^{00}	Rose & Katzmann, 1956
Ottawa	56.8°	351°	46° N	76° W	GM	3^{57}—3^{59}	Dito
					NM	3^{49}—3^{51}	Dito
Harwell	54.7°	83°	52° N	1° W	SH	3^{45}	Marsden et al., 1956
MIT	53.9°	357°	43° N	71° W	SC	3^{45}—3^{47}	Elliot & Gold, 1956
Chicago	52.6°	337°	42° N	88° W	NM	3^{49}—$3^{50.5}$	Simpson et al., 1956 A
Climax	48.1°	316°	40° N	106° W	NM	3^{48}	" " " 1956 A
Wellington	— 45.5°	254°	41° S	175° E	NM	3^{47}—3^{49}	" " " 1956 A
Sacramento Peak	41.6°	318°	33° N	106° W	NM	3^{48}	" " " 1956 A
Tbilisi	36.3°	122°	42° N	45° E	IO	3^{40}	Dorman et al., 1956 A

tions outside the geomagnetic field and far away from the earth, with the observed onset times.

The direction of a cosmic ray particle orbit outside the earth's magnetic field is called the asymptotic direction of the particle. An asymptotic direction is determined by two angles, a longitude angle and a latitude angle.

The Measurement of Onset Times

Some details concerning the measurement of onset times will be discussed first. We refer to protons as primary particles in the following. They are thought to account for the major part of the observed flare intensity increase at higher geomagnetic latitudes (Simpson et al., 1956 A).

1) An increase in intensity $\Delta n(E, h)$, measured by a device at atmospheric depth h, is —quite generally—related to an increase $\Delta j(E)$ of primary protons of kinetic energy E according to:

$$\Delta n(E, h) = \Delta j(E) \cdot S(E, h)$$

where $S(E, h)$ stands for the yield function of the measuring device. Analytical expressions for $S(E, h)$ have been given by Fonger (1953) for a neutron monitor and for a sea-level ionization chamber, and by Neher (1952) for an unshielded GM-telescope. The yield functions approach small values for low primary energies. In the expressions given by Fonger they are put equal to zero at a certain value E_0 of the kinetic energy of the primaries. This

means that, because of the atmospheric attenuation, no primary particles of kinetic energy smaller than E_0 can be detected by the corresponding apparatus. The value E_0 may, therefore, be denoted as the atmospheric cut-off energy.

Consider now a station lying at a high geomagnetic latitude. Assume for the moment that only low energy primary protons arrive at this station during the first instants of the increase. For small primary energies the yield function of the neutron monitor has a considerably higher value than that of the ionizing particle detector. Consequently, a certain increase in the intensity of the primary protons is more easily detected by a neutron monitor than by an ionizing particle detector. Thus, allowing for a finite rate of increase in intensity of the incoming flare primaries, a neutron monitor will measure an earlier onset time. This might be an explanation for the results reported by the Ottawa station, where the neutron monitor indicated the increase to start at 0350 ± 1 UT, whereas the counter telescope indicated 0358 ± 1 UT.

On the other hand, for a station at a low latitude the magnetic cut-off energy, i.e. the lowest permissible energy of the primary protons, is so high that the yield functions for a neutron monitor and, say, for an ionization chamber have nearly the same values. We consequently expect the same onset time for the two apparatus. This was the case at the Japanese stations and in Mexico. See Table 1.

2) The difference in onset times between a neutron monitor and a GM-telescope observed at Ottawa could also be attributed to the different angular openings of the two instruments. We mention this possibility even if it appears to be less probable because of the large angular spread of the secondary radiation in the atmosphere. But it should be borne in mind that several observers have reported that the secondary radiation, originating from the extra flare cosmic ray particles and measured by GM-directional telescopes, did not show a symmetrical distribution with respect to azimuth angle at the measuring station. GM-directional telescopes which were inclined at the same zenith angle and pointing to the north and to the south did not record the same relative increases even one hour after the onset of the increase (Brunberg & Eckhartt, 1956). A GM-directional telescope inclined at a zenith angle of 45° to the west measured a higher relative increase than that pointing towards zenith, though atmospheric attenuation is larger for the inclined directions, and there was practically no difference in the geomagnetic cut-off energies for the two telescopes. (Fenton et al., 1956 A).

These results indicate a non-uniform distribution over the directions of incidence in either the energy or the intensity of the extra flare particles or in both during the first instants of the increase. The deviations from the isotropic distribution over all directions of incidence were definitely more pronounced for the primary particles than for the secondary radiation measured at sea-level. This may be understood since scattering in the atmosphere, especially for the low energy primaries involved, tends to smooth out these deviations.

3) In the vicinity of the geomagnetic cut-off energy the asymptotic directions show a rather complicated behaviour. (See, for example, Firor (1954.) The longitude angle of the asymptotic direction increases very rapidly and can assume any value, whereas at the same time the latitude angle oscillates around the value zero, i.e. the geomagnetic equatorial plane. This means that a low latitude station, having a geomagnetic cut-off energy much higher than the atmospheric cut-off value, can measure primary particles which come from nearly all asymptotic directions in the equatorial plane. For these low latitude stations, therefore, we do not expect the onset times to depend very critically upon the longitude position of the measuring station. The stations in the second group of Table 1 show nearly the same onset time.

From the arguments mentioned above it is clear that one should only compare onset times which have been measured by omnidirectional detectors. Further, the geomagnetic cut-off energy should be smaller than the atmospheric cut-off. In this case, the main contribution of the measured increase originates from primary particles which come from a limited range of asymptotic directions, as described above.

Following this reasoning, the ionization chamber stations listed in the first group of Table 1 have been chosen. They lie at geomagnetic latitudes greater than about 50°. We

assume that protons of momentum range 3.5 to 15 GeV/c are responsible for the onset of the increase at the chosen high latitude stations. The lower limit of the chosen momentum range is somewhat smaller than the value 4.5 GeV/c, equivalent to an energy per nucleon of 3.7 GeV, which has been given by FONGER (1953) for the cut-off energy of a sea-level ionization chamber.

The Asymptotic Directions for Particles of the Chosen Momentum Range Arriving at the Different Stations

The asymptotic direction is a function of the geomagnetic position of the measuring station, of the angles of incidence at this station, and of the primary particle momentum. The asymptotic direction may be represented by a vector the foot point of which rests at the centre of the earth. The arrow point of the vector is defined by a longitude angle and a latitude angle in a spherical coordinate system which coincides with the geographic system of the earth. Then, for a particular station and for each direction of incidence, the locus of arrow points for different momenta forms a curve which may be plotted on a globe (BRUNBERG, 1956). The two-dimensional representation which we are going to use here is the polar projection of such a globe seen from a point above the geographic north pole. The latitude angle appears as the length of a radius, the longitude angle as an azimuthal angle. For each of the chosen stations the curves of asymptotic directions for arrival from zenith angles 0°, 32° E, 32° W, 32° N, and 32° S have been drawn for the range of momenta 3.5 to 15 GeV/c. For each station the envelope of these curves is given in Figs. 1 and 2.

The values of JORY (1956) have been used for the angular coordinates of the asymptotic directions. Some intermediate values have been taken from MALMFORS' model-experiment (1945), the results of which are in excellent agreement with the computations of JORY.

It follows that each envelope curve in Figs. 1 and 2 encloses an area which is filled by arrow points for asymptotic directions of particles having momenta from 3.5 to 15 GeV/c and arriving at the chosen stations within a cone with a half apex angle around the zenith direction of 32°. Thus, the solid angle at the chosen stations which corresponds to a half apex angle of 32° is transformed by the geomagnetic field into a solid angle $\Delta\Omega$ outside the earth's magnetic field. It is this solid angle $\Delta\Omega$, relevant far away from the earth and for the mentioned range of momenta, which appears as an area in the two-dimensional representation of our figures. The solid angle $\Delta\Omega$ could also be considered as being composed of the individual solid angles which belong to the various momentum values. Turning clockwise—with respect to the geomagnetic north pole—one proceeds from lower to higher momenta on each area in our figures. The asymptotic directions for 5.5 GeV/c particles are shown in each area. They are marked by dots and crosses to distinguish between different stations.

Consider the relatively small area corresponding to Godhavn. The asymptotic directions form a narrow bundle for the chosen range of momenta and angles of incidence at that high latitude station. This is a consequence of the focusing effect of the geomagnetic field upon low energy cosmic ray particles which move near the axis of the geomagnetic dipole. This focusing effect has been studied by ÅSTRÖM (1956).

The plotted areas of asymptotic directions refer only to zenith angles of incidence between 0° and 32° at the measuring station. We have to discuss to what extent these areas are representative for angles of incidence greater than 32°. This question is not important as long as primary particles arrive simultaneously from nearly all zenith angles. In this case the measured increase is mainly caused by primaries incident with small zenith angles which are the most efficient ones for detection at sea-level. But it is possible that at some stations the earliest onset was caused by primary particles which arrived from zenith angles larger than 32°. Atmospheric attenuation puts an upper limit upon the angles of incidence. Particles arriving from still larger zenith angles are hardly detected. We have assumed an upper limit of 60° for the following reasons. From a production level at about 100 mb the secondary intensity decreases exponentially with increasing atmospheric depth. Let us assume that this is valid down to sea-level. The atmospheric mass to be penetrated by the secondary particles would increase by a

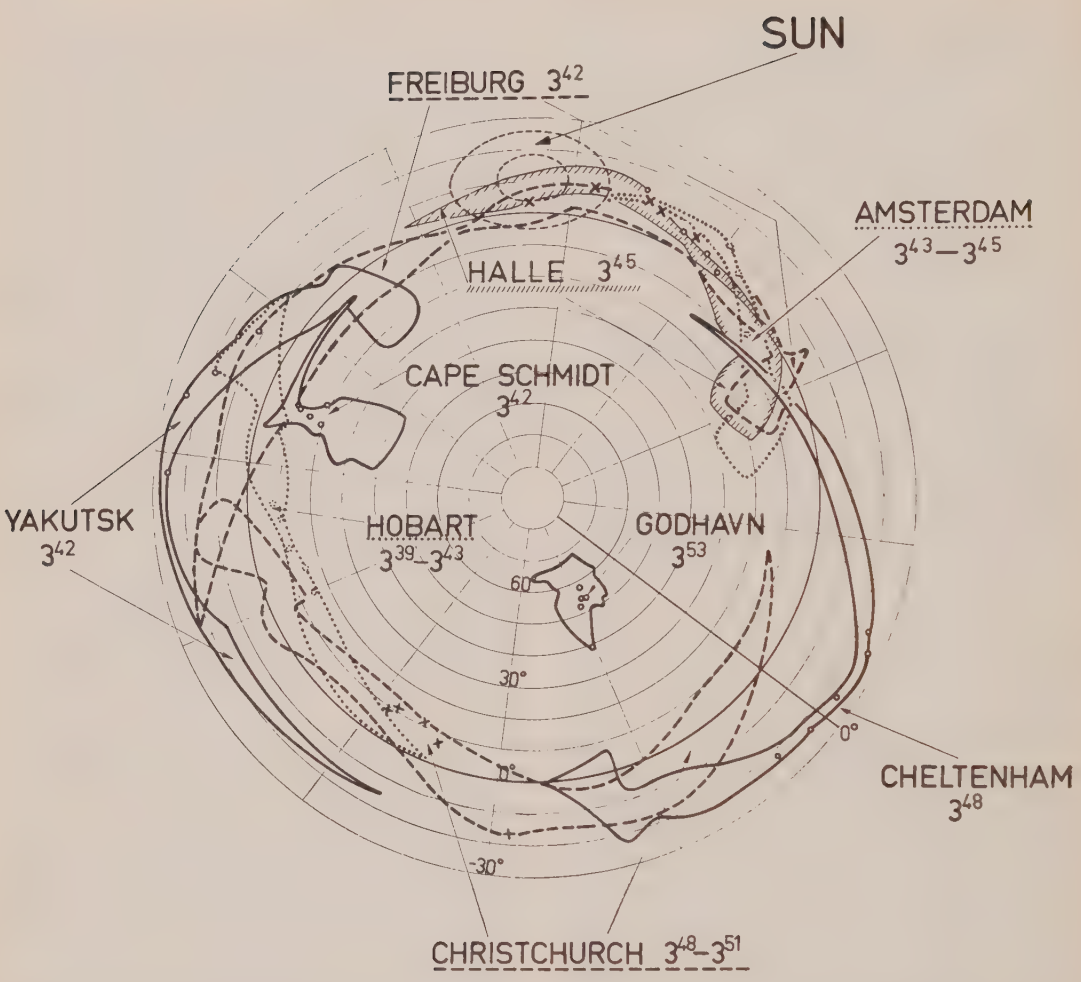

Fig. 1. The asymptotic directions for stations where the increase was observed to have started after 0341 UT. The directions towards the sun at the beginning of the solar flare are indicated by the dashed line figure at the top. A station lies inside one of FIROR's impact zones on the earth when the corresponding area of asymptotic directions covers this dashed line figure.

factor $1/\cos\Theta$ for primaries inclined at an angle Θ with respect to zenith.

For 13 GeV-protons an absorption mean free path of 150 g/cm² has been given (NEHER, 1952). If the secondary radiation at sea-level that originates from a vertically incident beam of primary particles is taken as 100 %, it drops down to 34 % (26 %) for the same beam arriving from zenith angle 32° and to 0.25 % (0.06 %) for zenith angle 60°. The values within brackets refer to a mean free path of 120 g/cm² as found by SIMPSON et al. (1956 A) for the absorption of the flare-produced nucleonic component.

Thus, restricting the maximum zenith angle of arrival to 60°, we have to find out how much the asymptotic directions for arrival from zenith angles between 32° and 60° deviate from those for angles between 0° and 32° in the chosen momentum range. This question is obviously related to the focusing properties of the geomagnetic field upon cosmic ray particles. ÅSTRÖM (1956) has shown that for a station near the geomagnetic pole

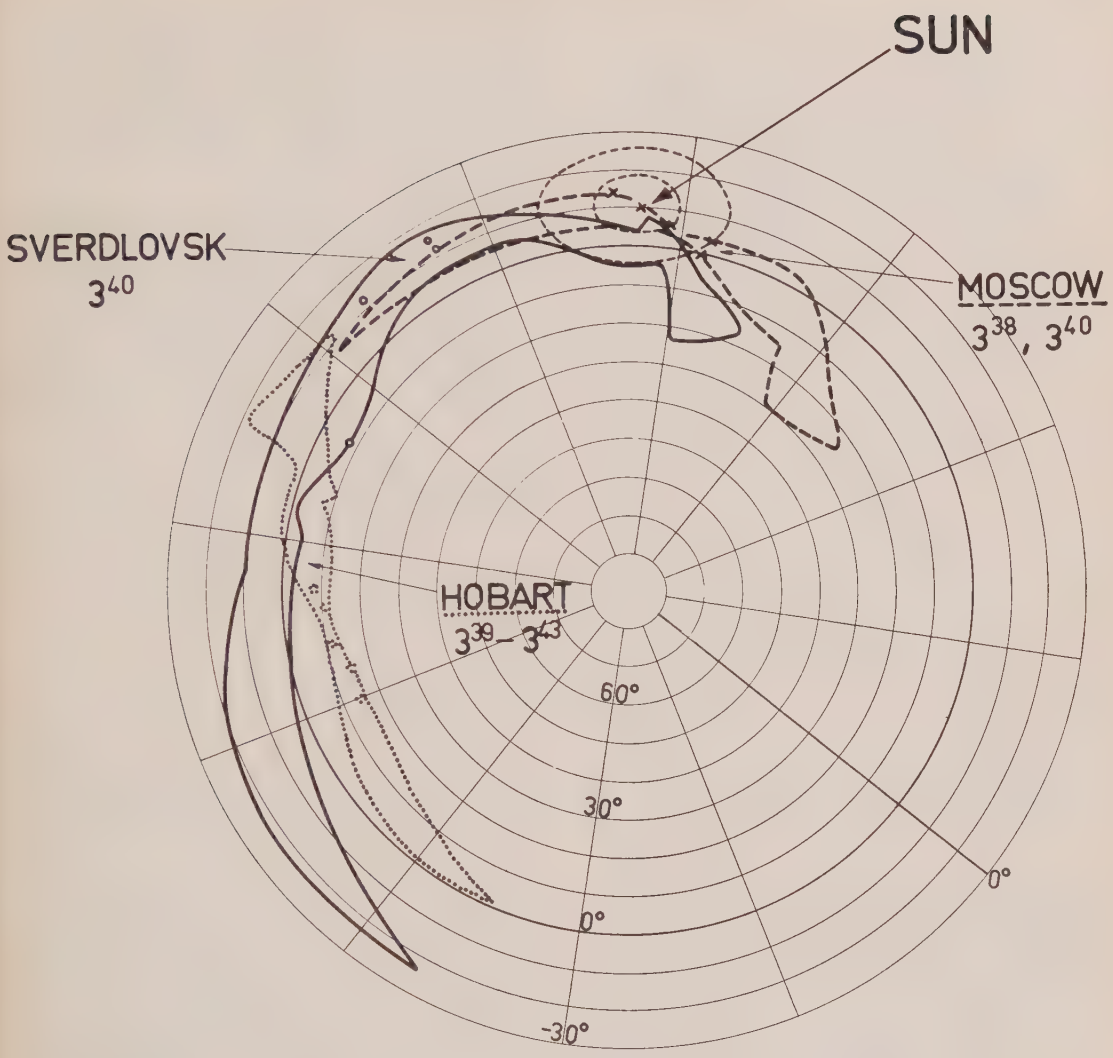

Fig. 2. The asymptotic directions for stations where the increase was observed to have started before 0341 UT.

and for proton energies up to about 15 GeV the solid angle $\Delta\Omega$ outside the geomagnetic field is not larger than one tenth of the solid angle at the measuring station. This holds qualitatively up to a 60° angle of incidence at the measuring station.[1] Increasing the cone of incidence from a half angle of 32° to a half angle of 60° at a station near the pole is, therefore, equivalent to increasing the half apex angle of the cone of asymptotic directions by about 10°. When this is applied to Godhavn, the area of asymptotic directions for this station in Fig. 1 should be enlarged on all sides by an amount which corresponds to an asymptotic angle of 10°.

The focusing properties of the geomagnetic field upon the bundle of directions of incidence as a whole become less pronounced for a station which lies at a lower geomagnetic latitude. The measurements by Malmfors (1945) and by Brunberg & Dattner (1953) for arrival at Stockholm (magn. latitude 58°) allow a direct comparison between the asymptotic directions for arrival from 32° zenith

[1] Private communication from Dr. Åström.

angle and those for arrival from 60°. From these data it is found that the deviations are still small for the lower momenta in our chosen momentum range. The highest deviations are about 15° for both asymptotic longitude and asymptotic latitude angles.

Regarding the chosen stations which lie at still lower geomagnetic latitudes, the situation at the high momentum limit of our chosen momentum range is probably not different from that at Stockholm. But at the low momentum end focusing breaks down, since we approach geomagnetic cut-off for those 3.5 GeV/c particles which arrive from large zenith angles from the eastern and northern horizon of the measuring station (Malmfors, 1945). It has already been mentioned in the previous section that near geomagnetic cut-off the asymptotic directions oscillate around the geomagnetic equatorial plane, whilst their longitude angles increase beyond all limits. From the general appearance of the curves which represent Jory's results of asymptotic angles vs. latitude of incidence for 3.5 GeV/c particles, and from the dependence of geomagnetic cut-off energies upon different directions of incidence, several conclusions can be drawn concerning the deviations from the areas of asymptotic directions given in Figs. 1 and 2. These areas of asymptotic directions should still be looked upon as the central regions around which the following corrections should be applied when the angular opening of the measuring station is increased from 32° to 60° half apex angle.

For stations lying above 52° geomagnetic latitude the corrections are probably not greater than for Stockholm, i.e. about 15° for each asymptotic angle.

For Yakutsk and Cheltenham the deviations in asymptotic longitude angles are about 40°, caused by the approach towards cut-off for arrival from 60° E.

As regards arrival at the lowest latitude stations Freiburg, Christchurch and Sverdlovsk, the geomagnetic cut-off for 3.5 GeV/c particles is reached for certain directions of incidence from the eastern and northern horizon. The Christchurch and Sverdlovsk areas in Figs. 1 and 2 have been interpolated. No definite corrections for the asymptotic longitude angles can be given when increasing the angular openings at these stations.

The above-mentioned corrections refer to particles of momentum 3.5 GeV/c. Shifting the lower limit of the chosen momentum range to 4.5 GeV/c removes the uncertainties as regards arrival from the eastern and northern horizon.

The difference between the position of the dipole geomagnetic equator and that derived from cosmic ray observations has been studied recently (Simpson et. al., 1956 B). If these deviations are constant with time and if, as is supposed, they can be extrapolated to higher geomagnetic latitudes, the above statements concerning the low momentum particles and their cut-off relations should be substantially affected when considering the European stations. But for the higher momentum particles the changes in asymptotic directions which are induced by the effective geomagnetic coordinates, are probably not greater than the uncertainties discussed above.

The Connection Between Asymptotic Directions and Onset Times

Consider the areas enclosed by the dashed lines at the tops of Figs. 1 and 2. These areas indicate directions towards the sun at the beginning of the solar outburst. Following Firor (1954) it is assumed that the solar cosmic ray source had an angular diameter of 15° and 30° resp. When the corresponding area of asymptotic directions covers the area enclosed by the dashed line, a station lies inside one of Firor's impact zones on the earth.

The times of onset are written next to the name of each station. Fig. 1 represents those stations where the increase was observed to have started after 0341 UT. It is surprising that Hobart and Christchurch registered the earliest and latest onset respectively in spite of the fact that their asymptotic directions lie quite near to each other. Generally, asymptotic directions close to the directions towards the sun are connected with earlier onset times than asymptotic directions pointing in the opposite direction. Asymptotic directions lying close to the equatorial plane are connected with earlier onset times than those pointing in the direction of the polar axis. The latter argument can be applied to Cape Schmidt. The relatively early onset at this station would then be caused by primaries of low momenta, the asymptotic

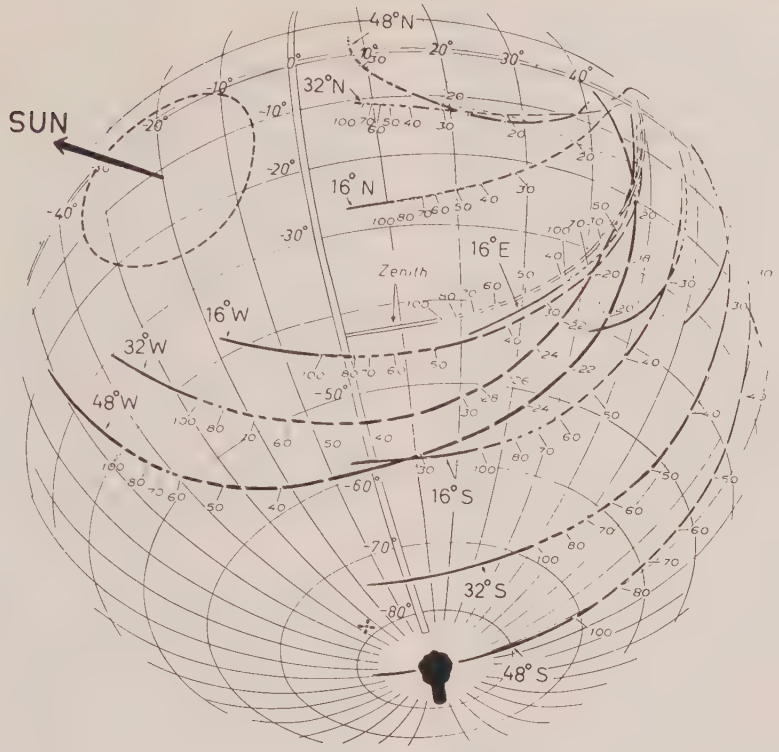

Fig. 3. The angular coordinates of the asymptotic direc-tions for arrival from different zenith angles at Hobart, Tasmania. The directions towards the sun at the beginning of the flare are indicated by the dashed line figure.

directions of which lie almost in the equatorial plane.

It is seen from Fig. 1 that the areas filled by arrow points of asymptotic directions overlap each other for stations which registered different onset times. Several conclusions could be drawn from this, concerning those cosmic ray flare particles which arrived first. A check on these conclusions might be possible if the apparent spectra of the extra flare particles which arrived at the different stations during the first instants of the increase were known more exactly.

When considering the connection between the azimuth angles of asymptotic directions and onset times in Fig. 1, it is seen that there is no symmetry with respect to the direction towards the sun. The earliest onset times seem rather to be connected with asymptotic directions which point somewhat to the left with respect to the direction towards the sun in our figure.

In Fig. 2 are shown the stations where the onset was observed to have commenced before 0341 UT. From this figure it is again evident that the asymptotic directions for earliest arrival are concentrated in the upper left sector, i.e. around directions which point more to the east than towards the sun.

Special attention should be paid to the Hobart station (0339—0343 UT) as it lies outside the impact zones for the given range of momenta. Communicated short-interval records indicate that the increase started rather at the earlier limit of the time interval cited above, i.e. around 0340 UT (Fenton et al., 1956 B). Even for greater momenta, the asymptotic directions do not point towards the sun, as is seen from Fig. 3 (Brunberg, 1956). Only particles of momenta greater than about 40 GeV/c and arriving from zenith angles greater than 48° from the north-western horizon could possibly have come directly from the sun. But under such extreme condi-

tions, particles of the same momenta should have arrived simultaneously at the Japanese stations from the low south-eastern horizon. The onset at the latter stations was observed at 0343—0345 UT. The above-mentioned observations concerning the effective geomagnetic coordinates for cosmic rays are certainly of minor importance for these high momentum values.

Thus, in the case of Hobart, it is shown that the first cosmic ray flare particles to arrive at the earth, did not come from directions pointing towards the sun in our figures. This conclusion is supported by the results reported from the ionization chamber at Halle (0345 UT). As is seen from Fig. 1, this station lay inside one of FIROR's impact zones for particles of about 4 GeV/c momentum but, nevertheless, it registered a relatively late onset time.

These experimental facts prove the existence of magnetic fields between the sun and the earth which deflected the solar flare cosmic ray particles before they entered the geomagnetic field.

The Electromagnetic State in the Interplanetary Space and its Influence upon the Onset Times

It has been suggested that magnetic storms are caused by the electric field which arises inside a beam of ionized gas sent out by the sun (ALFVÉN, 1950). Decreases in cosmic ray intensity, frequently observed in connection with the magnetic storms, should be an effect of the same electric field set up in the interplanetary space (ALFVÉN, 1949; BRUNBERG & DATTNER, 1954; VENKATESAN, 1957). Applying this model to the violent magnetic storm of Feb. 25, the relative positions of the earth and the beam at the time of the solar flare would be as shown in Fig. 4. In this figure it is assumed that the beam particles need about one day to travel from the sun to the earth. The breadth of the beam was tentatively put equal to a one day's arc on the orbit of the earth. The beam is supposed to have no connection with the solar flare itself for the following reasons. The flare was situated on the western part of the solar disc, as indicated in Fig. 4. A beam of ionized gas sent out in connection with this flare and travelling radially outwards from the sun could not hit

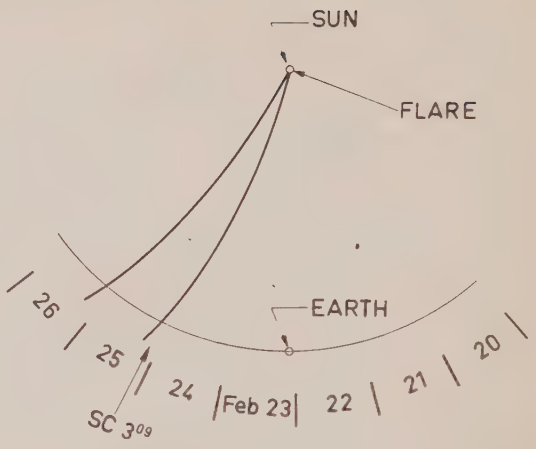

Fig. 4. The earth and the solar beam of ionized gas which is supposed to be responsible for the magnetic storm on Feb. 25, 1956. The position of the flare on the sun is indicated by the arrow.

the earth two days later. The time interval of two days between the flare and the magnetic storm was too long compared to former events (Magnetic Data in the Collection of ELLIOT & GOLD, 1956). On the other hand, the 27-day recurrences of high values of the daily Kp-sums following the storm event and lasting for several solar rotations, give strong support to the assumption that the beam was already present when the solar flare occurred on Feb. 23.

It is seen from Fig. 4 that the asymptotic directions, which we have found above to be connected with the earliest onset times, point towards this beam.

When the sun emits such a beam of ionized gas, the solar magnetic field in the region of the origin of the beam should be dragged outwards (ALFVÉN, 1956). Cosmic ray particles in the vicinity of the sun may escape more easily into the regions inside the beam, which have been swept free from magnetic fields by the ionized matter. In this way, cosmic ray particles are guided by the beam, and they may leave the beam sooner or later. At the earth, the beam appears as a source of solar cosmic ray particles. Thus, the earlier onset for asymptotic directions pointing towards the beam rather than towards the sun might be understood.

The curves of daily averages of the cosmic ray nucleonic component show a number of

decreases occurring before Feb. 23 (SIMPSON et al., 1956 A, ROSE & KATZMANN, 1956). The K_p-sums rose to small peaks on Feb. 16, 19, 22, but the individual values for K_p never exceeded 4+ on these days, compared to 8+ reported for Feb. 25 (BARTELS et al., 1956). One could ascribe these fluctuations to the presence of another beam which, in terms of Fig. 4, was on the right hand side of the earth. But, as is evident from the preferred directions towards the first beam, the latter beam did not appear to have the requisite conditions for trapping and guiding low energy cosmic ray particles to the same extent as the first beam had. The weaker effect of the latter beam on the geomagnetic field might support this assumption.

Comparison with Results of Other Authors

Two models have been presented up to now which attempt to explain the differences in onset times and other features of the cosmic ray increase. SIMPSON et al. (1956 A) assume a field-free spherical region around the sun extending beyond the orbit of the earth and surrounded by a barrier of turbulent magnetic fields which reflect cosmic ray particles. The solar cosmic ray particles should travel along straight paths from the sun to the earth and thus cause the earliest onset at stations lying inside FIROR's impact zones (1954). Particles which have passed the earth and have been scattered back by the magnetic field barrier should reach the stations on the night side, i.e. the American stations, a few minutes later.

It has been mentioned above that at a station which lies completely outside FIROR's impact zones, an earlier onset time was observed than at stations lying inside FIROR's impact zones. The connection between asymptotic directions and onset times does not display any symmetry with respect to the direction towards the sun. This means that particles, which should have the same effective distance from the sun in SIMPSON's model, nevertheless caused different onset times. Furthermore, the results from GM-directional telescopes mentioned in a previous section are in contradiction to the high degree of isotropy in the primary flare radiation which should be a consequence of SIMPSON's model.

The model presented by EHMERT (1956) is able to make a more detailed description of the different onset times. It implies a constant magnetic field in the interplanetary space which guides the solar cosmic ray particles to the earth. The assumed magnetic field comes out to be in close agreement with a general interstellar magnetic field derived from other observations. Such a magnetic field, however, must be heavily distorted in the vicinity of the active sun. Moreover, the calculated field strength puts a cut-off on the low energy solar primaries, as EHMERT himself has pointed out.

The author wishes to thank Prof. Hannes Alfvén for many valuable discussions.

REFERENCES:

ALFVÉN, 1949: On the Solar Origin of Cosmic Radiation. *Phys. Rev.*, **75**, p. 1732.

— 1950: *Cosmical Electrodynamics*, Chapter VI. Oxford. 1956: The Sun's General Magnetic Field. *Tellus*, **8**, p. 1.

ASSIES & JONGEN, 1956: Cosmic Ray Intensity During Solar Flare of February 23, 1956. *Physica*, **XXII**, p. 355. (Letter to the Editor.)

BARTELS ET AL., 1956: International Data on Magnetic Disturbances, First Quarter, 1956. *J. Geophys. Res.*, **61**, p. 559.

BRUNBERG & DATTNER, 1953: Experimental Determination of Electron Orbits in the Field of a Magnetic Dipole. *Tellus*, **5**, p. 135, p. 269.

BRUNBERG & DATTNER, 1954: Variations of the Cosmic Ray Intensity During Magnetic Storms. *Tellus*, **6**, p. 254.

BRUNBERG, 1956: Cosmic Rays in the Terrestrial Magnetic Field. *Tellus*, **8**, p. 215.

BRUNBERG & ECKHARTT, 1956: Some Remarks on the Sudden Cosmic Ray Increase on February 23, 1956. *Tellus*, **8**, p. 508.

DORMAN ET AL., 1956: Observations of the Large Cosmic Ray Increase of Feb. 23, 1956, in the *USSR*. *Nuclear Physics*, **1**, p. 585.

EHMERT, 1956: Solar Cosmic Radiation and the Interstellar Magnetic Field. (Contribution to the *Symposium on Electromagnetic Phenomena in Cosmical Physics, Stockholm*, 1956.)

ELLIOT & GOLD, 1956: The Solar Cosmic Ray Ourburst 1956 February 23. Collection of Cosmic Ray, Solar, Ionospheric and Magnetic Data Relating to the Event. (Private communication.)

Fenton et al., 1956 A: Cosmic Ray Increase Observed at High Southern Latitudes on February 23, 1956. *Nature*, **177**, p. 1173.

Fenton et al., 1956 B: Cosmic Ray Flare Effect—23. 2. 56. (Private Communication.)

Firor, 1954: Cosmic Ray Intensity-Time Variations and Their Origin. IV. Increases Associated with Solar Flares. *Phys. Rev.*, **94**, p. 1017.

Fonger, 1953: Cosmic Ray Intensity-Time Variations and Their Origin. II. Energy Dependance of the 27-Day Variations. *Phys. Rev.*, **91**, p. 351.

Forbush, 1956: Large Increase of Cosmic-Ray Intensity Following Solar Flare on February 23, 1956. *J. Geophys. Res.*, **61**, p. 155. (Letter to the Editor.)

Jory, 1956: Tables of Selected Cosmic-Ray Orbits in the Earth's Magnetic Field. *Phys. Rev.*, **103**, p. 1068.

Malmfors, 1945: Determination of Orbits in the Field of a Magnetic Dipole with Applications to the Theory of the Diurnal Variation of Cosmic Radiation. *Ark. f. mat., astr. och fys.*, **32 A**, p. 1.

Marsden et al., 1956: Variation of Cosmic Ray Nucleon Intensity During the Disturbance of 23 February 1956. *J. Atm. Terr. Phys.*, **8**, p. 278.

Messerschmidt, 1956: Ultrastrahlung von der Sonne. *Naturwissenschaften*, **43**, p. 174.

Neher, 1952: Recent Data on Geomagnetic Effects. Chapt. V in *Progress in Cosmic Ray Physics*, **1**, p. 243.

Rose & Katzmann, 1956: The Sudden Increase in Cosmic Ray Intensity of February 23, 1956. NRC. Ottawa. *Can. J. Phys.*, **34**, p. 884.

Sekido et al., 1956: The Universal Increase of Cosmic Ray-Intensity on Feb. 23, 1956, Observed by Japanese Observatories. (Private communication.)

Simpson et al., 1956 A: Solar Cosmic Rays of February, 1956 and Their Propagation Through Interplanetary Space. *Phys. Rev.*, **104**, p. 768.

Simpson et al., 1956 B: Effective Geomagnetic Equator for Cosmic Radiation. *Phys. Rev.*, **102**, p. 1648.

Sittkus et al., 1956: Die Beobachtung der Ultrastrahlungseruption vom 23. Februar 1956 in Freiburg i. Brg. *Zeits. f. Naturfrschg.*, **11 a**, p. 325.

Venkatesan, 1957: The Magnetic Storm Effects and the Interplanetary Electromagnetic State. *Tellus*, **10**, p. 117.)

Åström, 1956: Focusing of Paraxial Rays in a Magnetic Dipole Field. *Tellus*, **8**, p. 254.

On the Nature of the 20°—Discontinuity in the Earth's Mantle

By EIICHI NISHIMURA, YOSHIMICHI KISHIMOTO, and AKIRA KAMITSUKI

Geophysical Institute, Kyoto University, Kyoto

(Manuscript received March 18, 1957)

Abstract

The structure of the earth's mantle, mainly its upper part, having been investigated by the analysis of seismic waves of five Kamchatka-Kurile Islands earthquakes of shallow focus and some others, the problems on the existence and property of the 20°-discontinuity and the low-velocity layer in the mantle are discussed in some detail. The time-distance graphs obtained in Japan are in fair agreement with JEFFREYS-BULLEN's Table (1939), and also the 20°-discontinuity is considered to exist certainly at nearly the same depth as given by Jeffreys. The amplitude relation observed at the epicentral distance near 20° between the direct wave propagating through the medium entirely above the 20°-discontinuity and the refracted wave penetrating down into that discontinuity is just the reverse of that commonly expected, that is, the former being small and the latter large, both for the P- and S-waves. Concerning this phenomenon some arguments are given. Moreover, the existence of a new discontinuity was ascertained at some depth below the 20°-discontinuity, as deduced from the appearance of a prominent later phase. As to the existence of a low-velocity layer in the mantle, it is somewhat questionable at least in the form after Gutenberg from the analysis of seismic waves observed at the stations in Japan of the earthquakes of Kamchatka-Kurile Islands. But its existence is still probable in some forms, which is uncertain at present, at some depths below the Mohorovičić discontinuity. This problem will be postponed to a succeeding paper.

1. Introduction

Concerning the nature and structure of the earth's mantle there exist two essentially different opinions. One is that the seismic wave velocities in the earth's mantle increase with depth and at the so-called 20°-discontinuity the rate of velocity increase begins to rise abruptly (JEFFREYS, 1939). The other is GUTENBERG's maintenance (1953) that a low-velocity layer exists at the ranges between 60 km and 150 km for P-wave and between 60 km and 250 km for S-wave, and the 20°-discontinuity does not exist at any depth.

Which structure is more applicable to the earth should not simply and hastily be judged only by the analysis of arrival time of P- and S-waves of earthquakes observed at any limited area in the world, because the local character to a certain degree of the mantle's structure is possibly supposed from the various standpoints of seismometric and geodetic investigation. From these reasons the investigation of the earth's mantle should desirably be made by the seismometric and other methods at as widely divergent areas as possible in the world to advance our knowledge on the nature of the earth's interior. And moreover, in this case, not only the analysis of P- and S-waves, but also those of other phases observed should necessarily be investigated, with regard to their travel-times, amplitudes, periods and others. In the present article a synthetic investigation was made of some large earthquakes which occurred at an area near Japan, especially taking into consideration the change of wave-mode with distance observed at many stations with

the successively increasing distance as seen from their epicenters.

Namely, several earthquakes, whose observations extended over a territory of from about 6° to 26° of epicentral distance, were analysed by means of the preceding principle for the purpose of examining two different opinions, and of the further investigation of the local character, if existing, of the mantle's structure.

2. Data and Treatments

The earthquakes examined were five Kamchatka-Kurile Islands earthquakes in the main and two Formosa ones for reference. The data of these earthquakes are given in Table 1. These earthquakes were recorded at 23 observatories attached to the Japan Meteorological Agency, and with Wiechert seismographs. Instrumental constants of the Wiechert seismograph are as follows:

Component	Mass kg	Magnification	Period sec	Damping ratio
H	200	70—100	about 5	5—10
V	80	50— 80	»	»

i) Time-distance graph

A typical example is the earthquake of Jan. 5, 1953 (No. 3 in Table 1), its seismograms being shown in Fig. 1. Its time-distance graphs of both P and S are shown in Fig. 2, in which the time-distance graphs of the earthquake of March 18, 1955 (No. 5 in Table 1) are together plotted. In Fig. 2, it is to be noted that both P- and S-graphs are divided into two branches, which are represented by dots and crosses, intersecting at about 18°, and that the later branches are extended back down to 13° in both the P- and S-graphs. As the focal depth of the former earthquake is approximately estimated as 0.01 R according to Jeffreys' notation after pP – P duration at each observatory, the epicentral distance of 18° above-mentioned will correspond to the so-called 20°-discontinuity referring to the Jeffreys-Bullen Table (JEFFREYS, 1939), and moreover, two branches represented by dots and crosses in Fig. 2, may be expected to correspond to the waves annexed by the letters d and r after Jeffreys' notation respectively. Accordingly, the fitness of respective branches to the J.-B. curves will next be examined. The earlier P-branch (represented by dots) fits best to Pd curve of the J.-B. 0.01 curve, as shown in Fig. 2. The later P-branch (represented by crosses beyond 18°) fits approximately to the Pr curve of the above-mentioned curve referring to its gradient, although there are systematically positive residuals of a few seconds. As to two S-branches, the same results as P-branches are deduced as seen in Fig. 2. The time-distance graphs of other earthquakes in Table 1 are approximately the same as that of the present earthquake. In the present case, since the positions of observatories are all nearly on a straight line seen from the epicenter of each earthquake, a small shift of epicenter will change their epicentral dis-

Table I.

List of the earthquakes used in the present investigation. Latitude and longitude of epicenter, magnitude, focal depth and some origin times (*) are after the U.S.C.G.S. The Greenwich Mean Time is adopted for the origin time.

No.	Date	Origin time	Epicentral region	Epicenter	Focal depth	Magnitude (Pasa.)	Observational range
		h m s		N E	km		
1	1952 June 22	21 43 02	SE off Shinshiru Is., Kurile Is.	46°, 153½°,	—	7	6°—17°
2	1952 Nov. 4	16 58 33	Near east coast of Kamchatka	59½, 159	—	8¼	13°—25°
3	1953 Jan. 5	10 06 30	N part of Kurile Is.	4'6 156	—	6¾	9°—22°
4	1953 Oct. 11	13 08 34*	»	50, 155½	60	6¾	10°—23°
5	1955 Mar. 18	00 06 46	Near east coast of Kamchatka	54½, 161	—	—	19°—26°
6	1936 Aug. 22	06 51 37	Near SE coast of Formosa	22.1, 121.2	—	—	17°—24°
7	1955 Apr. 4	11 11 21*	»	22, 121	—	6	17°—24°

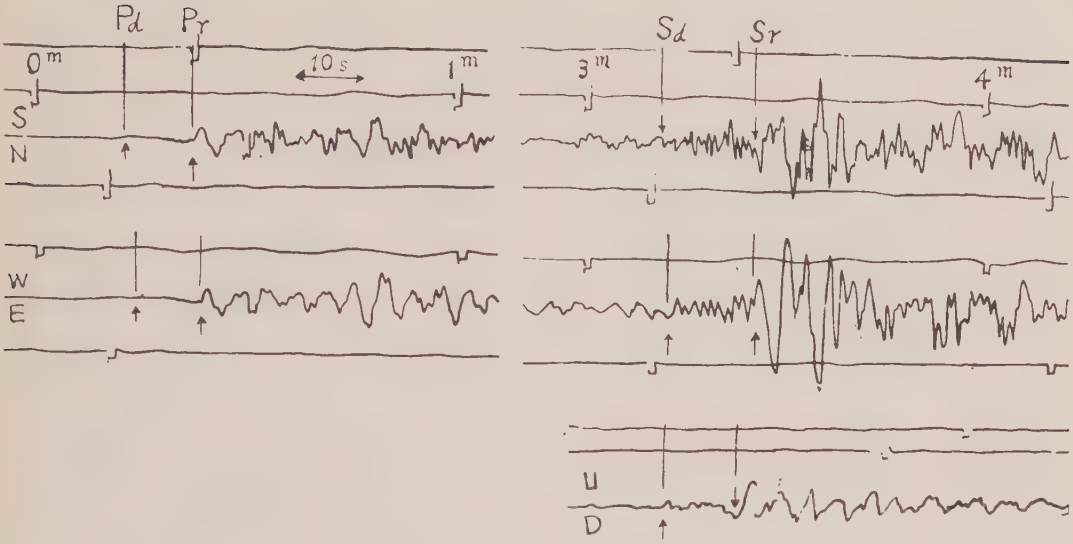

Fig. 1. Wiechert-seismograms, Jan. 5th 10h 06m, 1953, N Part of Kurile Islands, observed at Fukushima ($\triangle = 16°.03$).

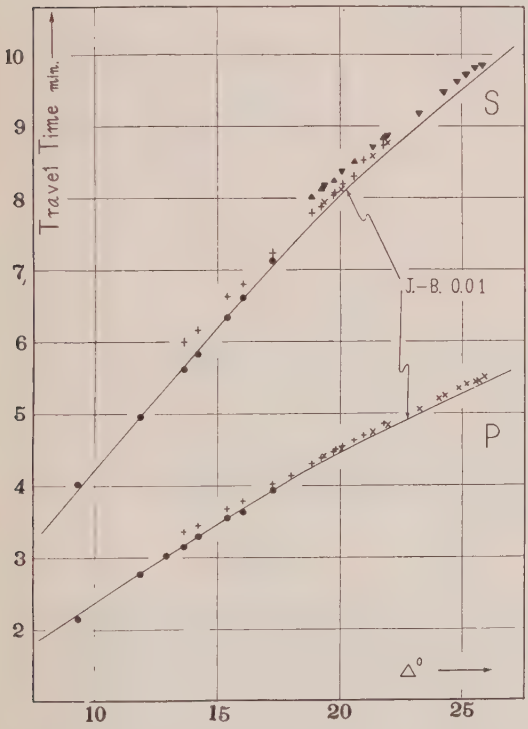

Fig. 2. Travel-time graphs superposed of two earthquakes of Jan. 5, 1953 and March 18, 1955. ●, + and ▲ belong to the former and × and ▼ to the latter. ● representing the Pd and Sd, + and × the Pr and Sr, and ▲ and ▲ represent the Sr_2.

tances and azimuths slightly. Consequently, the gradient of the time-distance graph may be considered to be nearly unchangeable; the fitness of the time-distance graph to the J.-B. 0.01 curve is kept also unchangeable by the small shift of epicenter.

It may, consequently, be concluded that two branches represented by dots and crosses in Fig. 2, correspond to two branches annexed with d and r in the J.-B. Table respectively, and, therefore, that the existence of the 20°-discontinuity was ascertained, at least, by the present analysis of the time-distance graph of earthquake which occurred in the northern area near Japan. Moreover, the extensions backward down to about 13° of both Pr- and Sr-branches coincide with what was given as an extreme case by Jeffreys in his paper of 1939 (1939). But, in the present step, the problem is not immediately solved as to whether the 20°-discontinuity is of the first order or the second order.

ii) Amplitude and period of each phase

Amplitude-distance relations of respective phases are given in Fig. 3, in the instances of some earthquakes in Table 1. In Fig. 3, a clearly discernible and remarkable fact is that the amplitudes of Pd and Sd become smaller and smaller with increasing distance and are much

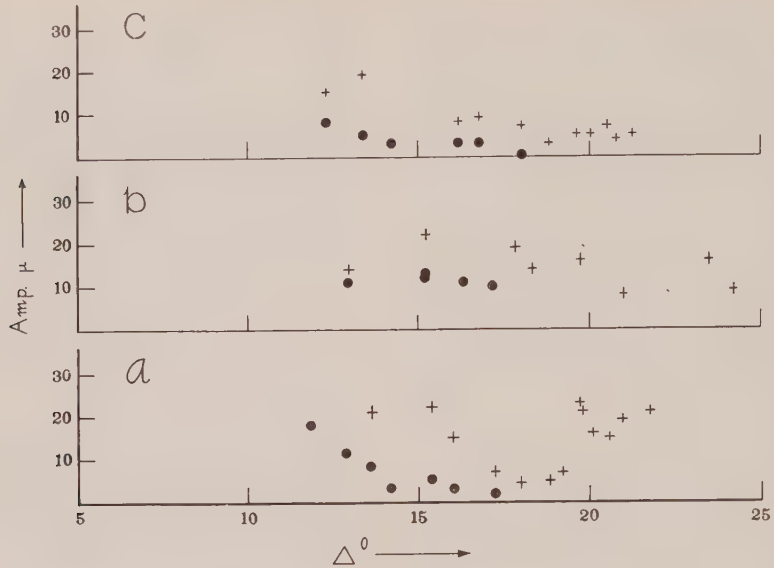

Fig. 3 (a). Amplitude-distance graphs for P-wave. Notations have the same meanings as in Fig. 2.

a) The earthquake of Jan. 5, 1953
b) The earthquake of Nov. 4, 1952
c) The earthquake of Oct. 11, 1953

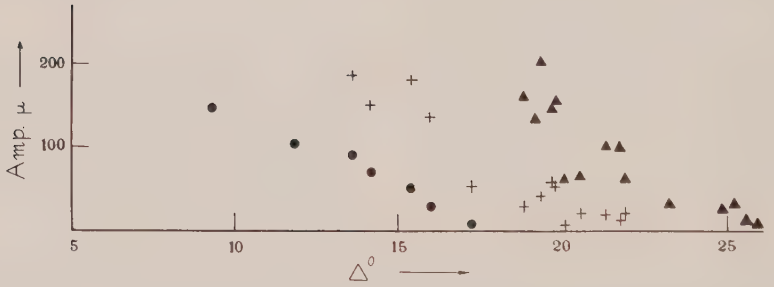

Fig. 3 (b). Amplitude-distance graph for S-wave superposed of two earthquakes of Jan. 5, 1953 and March 18, 1955, in which the corrections are made for some observatories allowing for the local structural character. Notations have the same meanings as in Fig. 2.

smaller than those of Pr and Sr near 18°. Beyond 18°, Pr and Sr of large amplitude first arrive, and the concomitant small Pd and Sd cannot usually be identified, because they may be disturbed by the wave train of the large Pr and Sr.

This behaviour with regard to the amplitude can clearly be recognized in Fig. 3, but the schematical representation of this relation, as shown in Fig. 4, will afford a reliable guide for discussing the nature of this sort of phenomena.

The periods of four phases, Pd, Pr, Sd and Sr of the five Kamchatka earthquakes in Table 1, are plotted together in Fig. 5, with the period and epicentral distance as ordinate and abscissa respectively. The periods of both Pr and Sr are concentrated in a range of about 4 sec. to 6 sec., independent of epicentral distance, ob-

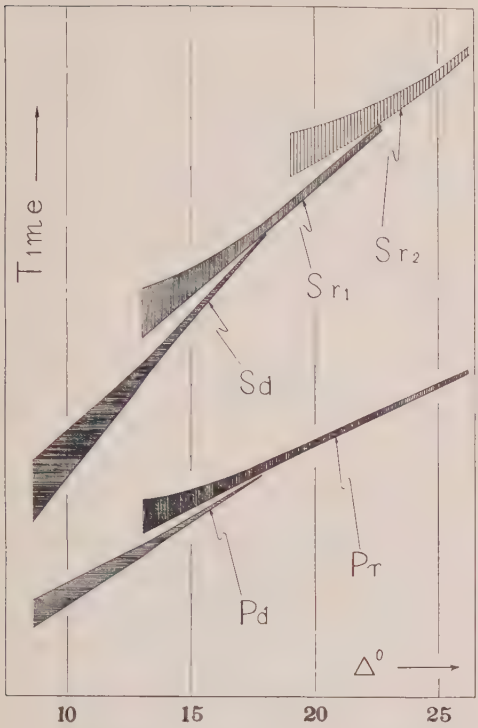

Fig. 4. Schematical representation of the amplitude-distance relation. The breadth of each branch corresponds to the amplitude at the respective distances.

servatory, and earthquake. On the other hand, the periods of Pd and Sd differ considerably. They consist, roughly speaking, of periods shorter than 2 sec. and of ones longer than 8 sec.

Therefore it can safely be said that two phases whose branches intersect at about 18° are clearly distinguished from each other by the difference in their amplitudes and periods, and so that the danger of confusing both phases does not occur. From these, it is supposed that both phases have considerably different characters in their generation and transmission.

iii) Sr_2-wave

As shown in Fig. 2, a phase of large amplitude (represented by the triangle) is observed after Sr beyond about 19°, and the duration between Sr and this phase becoming shorter and shorter with increasing distance, and two branches intersect at about 24°. And, this new phase in S-wave beyond 24° fits well to the J.-B. curve as shown in Fig. 2. An example of this phase is presented in Fig. 6, and the amplitude-distance relation is given in the previous Figs. 3 and 4.

From these data, it may be concluded that there is a discontinuous surface at some depth below the 20°-discontinuity, namely, that

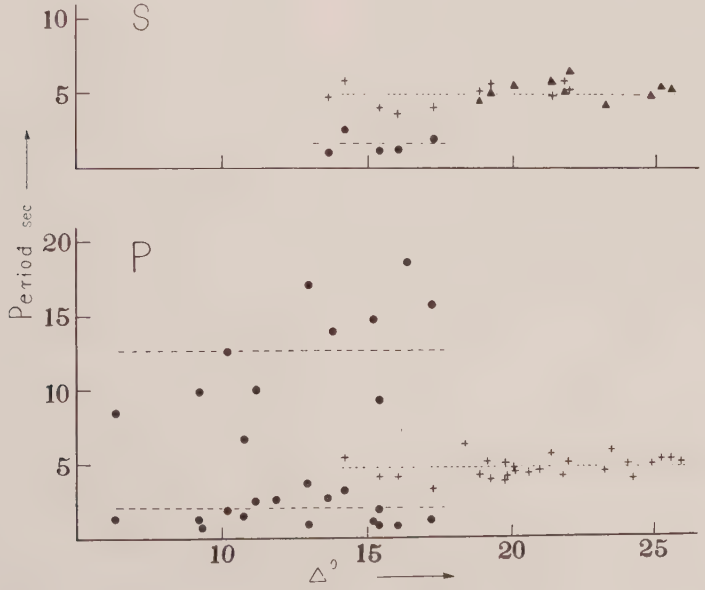

Fip. 5. Period-distance relation of each phase. Notations have the same meanings as in Fig. 2.

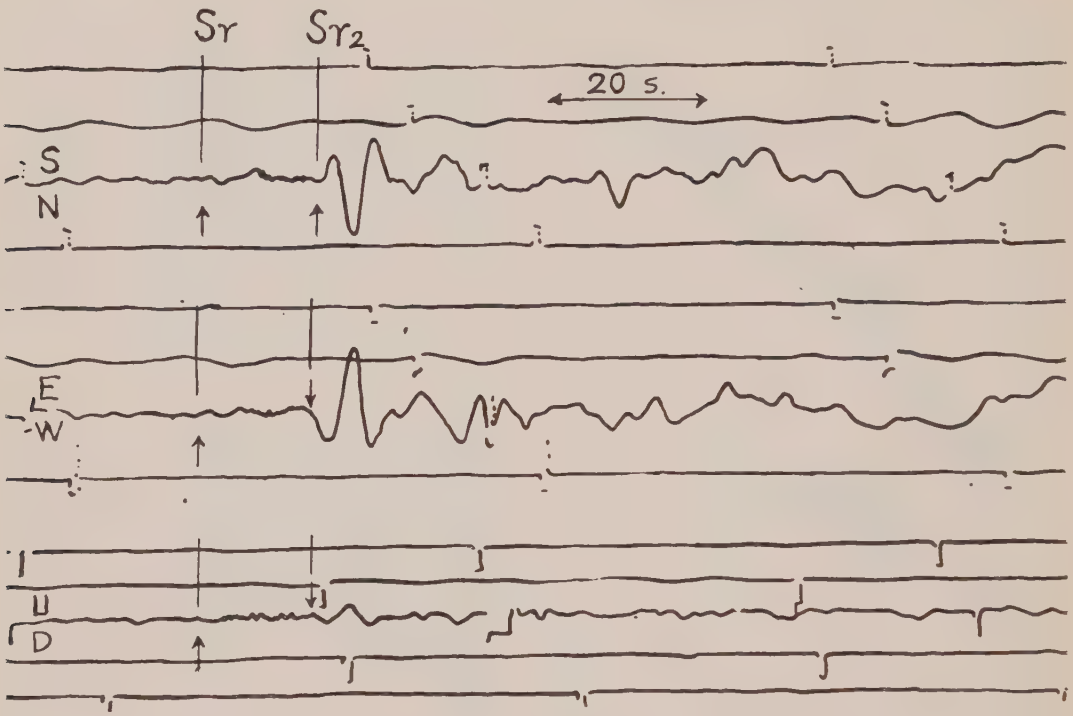

Fig. 6. Wiechert-seismograms, March 18th 00h 06m, 1955. Near east coast of Kamchatka, observed at Morioka ($\Delta = 20°.05$).

this new phase which will tentatively be called Sr_2 is the refracted wave at that discontinuity. It is, however, to be noted that this result was deduced only from the analysis of the S-wave, and regarding P-wave, the reliable identification of the later phase corresponding to the Sr_2 at distances concerned was not obtained. Consequently, it is said that the new discontinuity, if existing, is effective especially for S-wave and not for P-wave.

This new discontinuity probably relates to the behaviour of k/μ in the so-called "C-layer" calculated from the Jeffreys-Bullen's velocity distribution, as worked out by NISHITAKE (1956).

3. Discussion

Gutenberg's opinion concerning the low-velocity layer is referred to the following three phenomena, namely; 1) the abrupt diminution of amplitude of the first arrival at about 5° and its continuation up to about 15° both for P- and S-waves; 2) its gradual increasing from about 15° up to beyond 20° especially for P-wave; and, 3) the considerable difference of the time-distance curve from the J.-B. curve, especially in the range of from 5° to 20° both for P- and S-waves (GUTENBERG, 1948, 1954).

With regard to 2) and 3), as described in the preceding section number 2, the time-distance curves of the Kamchatka earthquakes fit fairly well to the J.-B. curve without the gap at any distance, and an intersection of two branches at 18°, which corresponds to 20° in normal earthquakes, are certainly observed for both P- and S-graphs. Moreover, as shown in Figs. 3 and 4, the increase of amplitude between 15° and 20° is not observed.

Next, in order to examine the phenomenon 1) mentioned above, three near earthquakes were treated, that is, May 1, 1939 (shallower than 10 km), July 28, 1951 (about 10 km deep) and July 17, 1952 (about 70 km deep). In Fig. 7, the natural logarithm of amplitude of the first P-motion is plotted against epicentral distance as abscissa for each earthquake. In any case, the sudden diminution and its continuation of the amplitude as stated by Gutenberg was not observed.

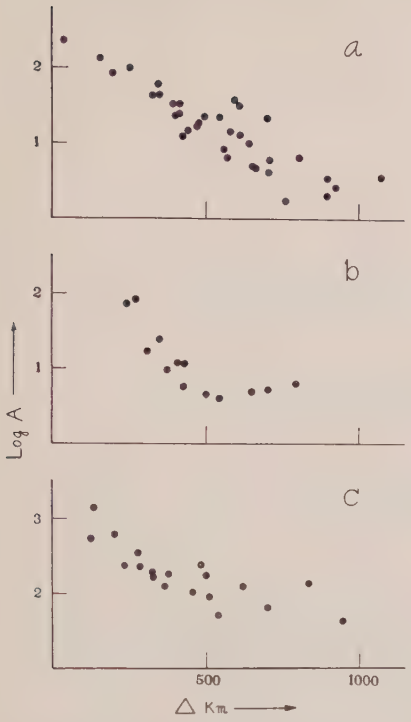

Fig. 7. Amplitude-distance graphs for the first P-motion at short distances.

a) The Oga Eartquake of May 1, 1939
b) The earthquake of July 28, 1951
c) The Yoshino Earthquake of July 18, 1952

Considering these results, it is reasonably concluded that the existence of the 20°-discontinuity is ascertained mainly by the analysis of time-distance graphs, and that the existence of a low-velocity layer, in the arrangement as mentioned not only by Gutenberg but also by Lehmann (1953), is considered questionable, at least in the case of the Japanese earthquakes. With reference to these criteria the local character of the earth's mantle is reasonably presumed referring to the areas in Europe, America and Japan.

At any rate the phenomena concerning the amplitude of two phases annexed by d and r will be interpreted as being caused by an abnormally strong attenuation of Pd and Sd observed near 18° or an abnormal enlargement of Pr and Sr. In order to examine this reverse relation between the amplitudes of Pd (or Sd) and Pr (or Sr) near 18° a deep earthquake was investigated for reference. The focus of this earthquake was seated at 350 km-depth, which is considered to be shallower than the 20°-discontinuity but deeper than the supposed low-velocity layer. In Fig. 8, the amplitude-distance graph of the first P-motion is given. This figure visibilizes the amplitudes as small in some ranges before 12°, and shows abrupt increase at 12° which corresponds to 20° in the normal earthquake. Thus, in spite of the deeper orientation of the focus than the supposed low-velocity layer, the same anomalous diminution of amplitude is observable at the distance corresponding to 20°.

But to return to the main subject, the reasonable interpretation of the anomalous amplitude relation between the direct and refracted waves is, at present, fairly difficult. One probable interpretation is the diminution of Pd and Sd due to the existence of a transient layer just above the 20°-discontinuity. On the other hand, the enlargement of the Pr and Sr by the channel-effect between the 20°-discontinuity, and the supposed new discontinuity just below the 20°-discontinuity, may possibly be assumed, when considering the constancy of the period of Pr and Sr, and allowing for the existence of the supposed new discontinuity. The detailed argument will conveniently be referred to KISHIMOTO's paper (1956, a).

Hence, several interesting behaviours of seismic waves were favourably interpreted by the effect of the 20°-discontinuity and its neighbouring region. But a problem still remains unsolved. Namely, in our previous article (1956, b), 8.1 km/sec. was obtained as the P-wave velocity at the top of the mantle, while the travel-times of seismic waves at the considerably larges distances fit fairly well to the Jeffreys-Bullen's Table, as mentioned above. This result needs inevitably the existence of a low-velocity layer at some depths below the Mohorovičić discontinuity. But this low-velocity layer is not in the form after Gutenberg but some different form will be expected. This problem will be postponed in a succeeding article.

4. Summary

Seismograms observed at observatories in Japan of five prominent earthquakes of the Kamchatka-Kurile Islands were analysed to investigate the existence and nature of the 20°-discontinuity and the low-velocity layer in the

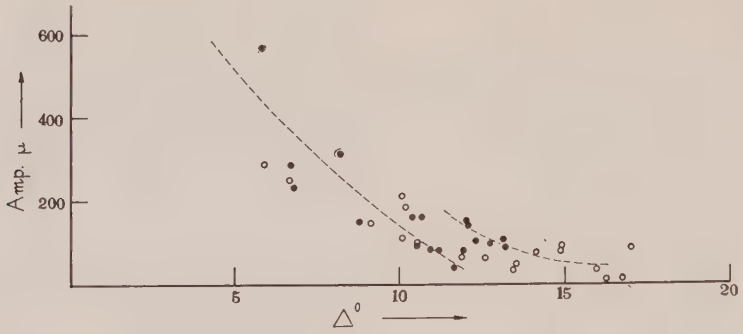

Fig. 8. Amplitude-distance graph for the first P-motion of the deep earthquake (h = 350 km) of Feb. 28, 1950. Dots and circles represent the readings by the authors and by the Japan Meteorological Agency respectively.

earth's mantle. Some results obtained in the present treatment are as follows:

i) The existence of the 20°-discontinuity was ascertained in Japan.

ii) The existence of the low-velocity layer was somewhat questionable in the form as characterized by Gutenberg at least in Japan, but it is probable in some different forms.

iii) The abnormal diminution of amplitude of the direct seismic wave, and, reversely, the large and clear appearance of the refracted wave through the 20°-discontinuity were definitely observed for both P- and S-phases near the epicentral distance of 20°. For these remarkable facts two explanations of the large attenuation of direct wave at the transition layer close above the 20°-discontinuity, or any enlargement-effect for the refracted wave by the layer-channel between the 20°-discontinuity, and the 25°-discontinuity newly found, were tentatively postulated.

iv) From the present treatment, it is reasonable to conclude that the nature and structure of the earth's mantle may have a somewhat regional character when it is compared with the regions in Europe, America, Japan and others.

REFERENCES

Gutenberg, B., 1948: On the layer of relatively low wave velocity at a depth of about 80 kilometers. *Bull. Seism. Soc. Amer.*, **38**, pp. 121 – 148.

–, 1953: Wave velocities at depths between 50 and 600 kilometers. *Ditto*, **43**, pp. 223 – 232.

–, 1954: Low-velocity layers in the earth's mantle. *Bull. Geol. Soc. Amer.*, **65**, pp. 337 – 348.

Jeffreys, H., 1939: The times of P, S and SKS, and the velocities of P and S. *Mon. Not. Roy. Astr. Soc., Geophys. Suppl.*, **4**, pp. 498 – 533.

Kishimoto, Y., 1956, a: Seismometric investigation of the earth's interior, Part III. On the structure of the earth's mantle. *Mem. Coll. Science, Kyoto Univ.*, Ser. A, **28**, pp. 117 – 142.

Lehmann, I., 1953: P and S at distances smaller than 25°. *Trans. Amer. Geophys. Union*, **34**, pp. 477 – 483.

Nishimura, E. and Kishimoto, Y., 1956, b: On the Local Structural Character of the Earth's Crust, *Tellus*, **8**, pp. 329 – 334.

Nishitake, T., 1956: Elastic properties of rocks with relation to the earth's interior. *Mem. Coll. Science, Kyoto Univ.*, Ser. A, **28**, pp. 73 – 98.

On Anomalous Time-Distance Curves Observed in Local Earthquakes

By EIICHI NISHIMURA, TAKESHI MIKUMO, and MICHIO OTSUKA

Geophysical Institute, Kyoto University, Kyoto

(Manuscript received March 18, 1957)

Abstract

The precise observations of local earthquakes were carried out in Wakayama District, Japan, for the purpose of studying the crustal structure and the nature of local shocks.

The travel-time anomalies were detected, and the anomalous time-distance curves were separable into two groups which seemed to be related with the directions of the initial motion of shocks recorded at their respective stations. The causes of the travel-time anomalies may reasonably be attributed to the condition of the hypocentre and mechanism of earthquake occurrence.

1. Introduction

Seismometrical studies on minor earthquakes, as the local shocks and the aftershocks, have heretofore been made by many researchers. Contrary to the case of utilizing artificial explosions, however, the determination of local fine structure of the crust from these shocks of small magnitude seems to be difficult in spite of the various attempts to do so. The artificial explosion method is certainly powerful for ascertaining the underground structure, owing to previous knowledge of the shot point and origin time, but the mechanism of occurrence and the nature of the emitted waves in this case are regarded as being certainly and widely different from the natural earthquake. From such a standpoint, the precise observation of minor shocks frequently occurring in their epicentral region is expected, with great interest, to offer an effective clue to such problems.

2. Observation

The present seismometric observations of local earthquakes were carried out in Wakayama District, western part of the Kii-Peninsula, Honshû, with many sets of high magnification seismometers, for the purpose of studying the unsolved above-mentioned problems of minor shocks and the crustal structure in the district concerned. These observations were pursued in close co-operation with the Earthquake Research Institute of Tokyo University (abbr. E.R.I.), from Nov. 24th to Dec. 2nd in 1954, and from April 10th to 22nd in 1956. Observation stations were installed in a limited region with a 10 km radius having Kainan City as its centre, where local earthquake-swarms have frequently occurred since 1920. Really the number of humanly felt shocks amounted to 250 and those non-felt 865 during one year of maximum seismic activity in this region. The superficial layer in this area consists of metamorphic rocks, termed crystalline shist and phyllite. The locations of all stations and the epicentres of earthquakes mentioned in this paper are shown in Fig. 1. (The co-ordinates of these stations determined from triangula-

Fig. 1. Positions of the observation stations and the epicentres of the earthquakes concerned.

□ observation station of the E.R.I. with the electromagnetic seismometers
△ observation station of the E.R.I. with the acceleration seismomegraphs
○ observation station of the Kyoto Univ. with the electromagnetic seismometers
● epicentre

tions and aerial photographs by the E.R.I. were used in our analysis by the courtesy of the Institute.)

The instruments used in the present observations were both the vertical and horizontal electromagnetic seismometers of the variable reluctance type. Their natural period and voltage sensitivity are 0.45 sec. and 1.79 volt/kine, respectively. Maximum magnification of these seismometers in direct connection with the galvanometer of 0.35 sec. in free period and 3.11×10^{-8} amp/mm in direct current sensitivity is approximately 80,000 at the optical distance of 1 metre. The three of our stations were fully equipped with three components of these seismometers, and the others with only vertical component. The JJY standard short wave (4 or 8 Mc) was used as the time marker. The paper speed of the oscillogram was nearly 5.0 mm/sec. Most stations of the E.R.I. made an observation with electromagnetic seismometers using a line carrier telerecording or radio telerecording, and the remainder of them with acceleration seismographs.

3. Observed Results and Discussion

The well-recorded 27 earthquakes which seem to have occurred inside or near our observation network were selected from those observed at more than five stations and were used in the present analysis. In the ensuing discussions the data obtained at the stations of the E.R.I. will concomitantly be used with our own.

For the first step usual methods were adopted to determine the focal positions of the previously mentioned shocks, applying the P-S duration times (i.e. S-P time) or the arrival times of the first P-wave at all stations, and assuming the crust in the observed area to be of a uniform medium. And, as a result, their foci were approximately determined by utilizing the S-P times, but those for the major part of the shocks could hardly be determined by the application of arrival times of the P-waves. With respect to this anomalous result some detailed discussion will follow.

(a) Firstly, when a graphical method or a least square method from *the S-P times* clearly

recorded at more than four stations was used in determining the hypocentre of each of 17 shocks, the focus could be determined with errors of less than several hundred metres, and the Omori's constants[1] were calculated as values from 5 to 8. However, the plotted points on a time-distance graph taking the hypocentral distance as the abscissa, obtained by the present method excessively diverged in a wide range. The propagation velocities estimated from a mean straight line, provisionally represented as the time-distance curve, have a great diversity in every shock, even in several shocks which occurred at approximately the same position. The deviation of travel times at each station from its line is considered to be beyond the limit of observational errors.

Considering, however, the time-distance curve to consist of minor groups, from another point of view, it can advantageously be divided into two groups accommodating most of the shocks analysed here. The respective groups of the time-distance curve can plausibly be represented as straight lines approximately paralleling each other with the travel-time difference of about ¼ sec., having small deviation of observed values at each station from either line. This fact can be verified for the S-waves as well as for the P-waves. The velocity differences estimated from two straight lines are within 0.1 km/sec., and the propagation velocities themselves obtained from 15 shocks are 4.3∼5.3 km/sec. for the P-waves and 2.3∼2.8 km/sec. for the S-waves, respectively. These values are not so diverse in every earthquake as they are in the cases of non-separation, and are considered to be reasonable ones for the velocities in the crustal upper layers.

Furthermore, the correlations between the travel times at the stations in each group of time-distance curves and various subjects were examined in all the shocks above treated. It seems, then, in every shock that the arrival times at the respective stations in two groups of the time-distance curves are closely related with the recorded directions of the initial motion at each observatory, but not with the geographical locations of stations, the position of hypocentre, the focal distance etc., as easily seen in Table 1. Namely, the travel times at the stations in the anaseismic region have a tendency to belong to either group on the time-distance graph, and the other group consists of the stations in the kataseismic area. But at the stations near the nodal lines some exceptional cases were found. Two examples of the travel time-distance curves are shown in Fig. 2. In two of 17 shocks the time-distance curve could be represented as a straight line, but the recorded directions of the first movement are anaseismic at all stations.

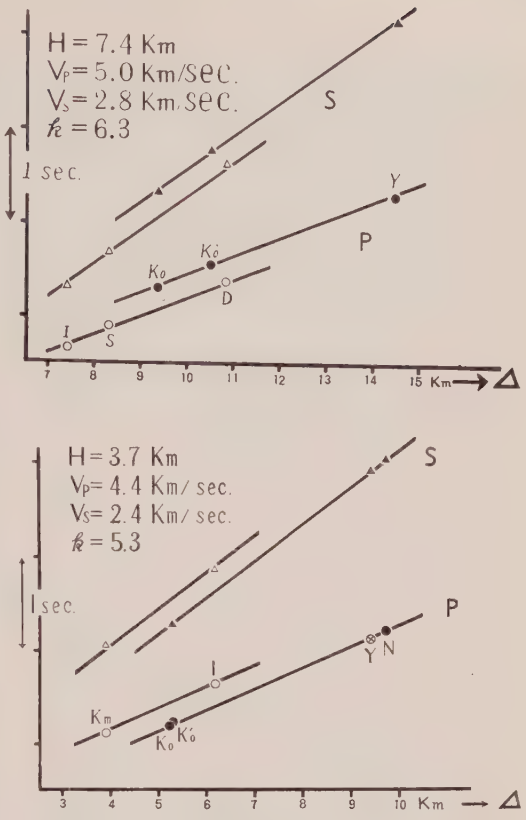

Fig. 2. (a) Time-distance curves (No. 140).
(b) Time-distance curves (No. 122).

(b) Secondly, the arrival times of *the initial wave* at more than five stations were used applying a least square method for estimating the positions of hypocentres. In this case, however, the focus, for most of the shocks, could not analytically be determined with some ex-

[1] The Omori's constant (k) shows the constant combining the S-P time (t) and the hypocentral distance (△) under the assumption of a homogeneous medium. This relation is expressed as △ = kt and k = VpVs/(Vp − Vs), where Vp and Vs are the velocities of the P- and S-waves, respectively.

ceptions. That is, their focal depths resulted in imaginary values, the velocities were calculated as unreasonable values, or the probable errors in travel-time curves were found to be exceedingly large. In the analysis by this method, the cases in which the focus was determinable were only as follows:

i) When the directions of initial motion recorded at all stations were the same, in other words, only in the anaseismic or kataseismic sense, the hypocentre could be determined with good accuracy, and the time-distance curves could be represented as straight lines with small probable errors and reasonable velocities. Fig. 3 shows an example of the time-distance curves in these 6 cases.

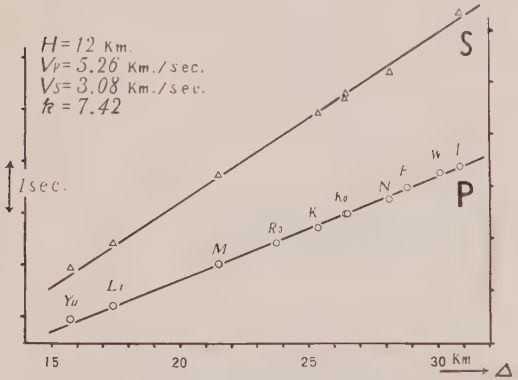

Fig. 3. Time-distance curves (No. 247).

ii) When both the anaseismic and kataseismic first movements were recorded at various stations, the focus was well determined, only when the arrival times at the stations with the same initial direction were used in calculation. On a time-distance graph, the travel times at these stations successfully lie on a straight line with reasonable velocities. But the travel times at other stations with another initial direction, which were excluded from this calculation, deviate from the above-mentioned line, and the straight line suitably connecting these plotted points runs parallel approximately with the former with a time difference of 0.2~0.4 sec. An example of these 7 cases is shown in Fig. 4.

(c) As described in this paragraph, the time-distance curve has an indication both for the P- and S-waves that the travel times are separable into two groups relating to the direction

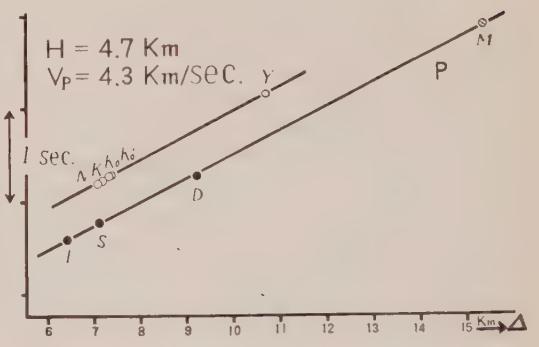

Fig. 4. Time-distance curves (No. 137).

of initial movement of shock at each station, when the arrival times as well as the S-P times were made use of in the hypocentre's determination.

Synthesizing all of 27 shocks analysed here, the time-distance curve could be represented as a straight line in 6 shocks and could be separated into two groups in 21 shocks. In the former instances the recorded directions of initial motion at respective stations are all the same, and in the latter, with regard to 12 shocks among 21, the stations with the initial anaseismic direction belong to a group of the shorter travel time, and the initial kataseismic stations form that of the longer one in 12 shocks, and contrary cases to these were found in 9 shocks. The travel-time difference is in the range from 0.2 to 0.4 sec.

The locations of epicentres, focal depths, velocities of the P- and S-waves, Omori's constants, the travel-time differences between two groups and abbreviations of stations constructing the time-distance curves, in every shock, are tabulated in Table 1. The velocity—focal depth graph in many shocks obtained from calculations under the uniform medium assumption is shown in Fig. 5. The examples of seismograms are shown in Fig. 6.

(d) The various problems in the present analysis will be mentioned and discussed as follows.

First, the time error accompanied by a precise reading of time-marks of every second on the seismograms is considered to be about $^1/_{50}$ sec. in good records and less than $^1/_{20}$ sec. in other ones, judging from the clearness of the initial P- and S-waves in most of the shocks treated here. Consequently, the travel-time

Table 1. Analyzed results.

X, Y; location of epicentre, Z; focal depth, Analytical method: P-S; using the P-S times, P; using the arrival times of the P-waves, Vp; velocity of the longitudinal waves, Vs; velocity of the transversal waves, k; Omori's constant, (1), (2); groups of travel time, U; initial 'Upward'-motion, D; initial 'Downward'-motion, δT; difference of the travel times between two groups.

The shoulder mark * indicates that the direction of initial motion at the marked station recorded the opposite one or it was not clearly recorded.

The observed data (the arrival times of the initial wave, the P-S times and the directions of initial motion) at the stations of the E.R.I.; R_2, R_3, L_1, L_2, Kó, Ko^1, Kh, Ka, T, T′, D, S, Ni, M, Yu, were used in our analysis by the courtesy of the institute. Positions of all stations are graphically referred to Fig. 1, and the station W is adopted as the origin point in the present treatment. The positive X, Y and Z indicate the southward, eastward and downward directions, respectively, seen from the origin point.

Shock No.	X (km)	Y (km)	Z (km)	Anal. Method	Vp (km/sec)	Vs (km/sec)	Vp/Vs	k	Time-Distance Curves	δT sec.
121	12.17	5.20	11.20	P-S	4.83	2.58	1.87	5.54	(1) Y, N (D); (2) Km, D, I (U)	0.20
122	0.47	3.15	3.70	P-S	4.36	2.40	1.82	5.34	(1) Ko, Ko′, Y*, N (D); (2) Km, I (U)	0.20
123	2.77	6.20	3.30	P-S	4.25	2.43	1.75	5.68	(1) I, Km*, Y (U); (2) Ko, N (D)	0.35
124	—0.28	6.20	4.40	P-S	5.04	2.52	2.00	4.78	(1) Y (U); (2) I, Ko, N (D)	0.25
135	3.57	0.60	4.60	P-S	4.64	2.47	1.87	5.30	(1) D, Y, S (U); (2) Ko, I, N (D)	0.20
136	7.37	1.50	4.70	P-S	4.62	2.54	1.82	5.65	(1) Y, D*, I (U); (2) Ko, Km, N (D)	0.25
137	2.77	6.95	4.75	P	4.40	—	—	—	(1) I, S, D, M* (D); (2) Km, N, Ko, Ko′, Y (U)	0.40
140	—1.23	7.35	7.40	P-S	5.07	2.81	1.81	6.31	(1) I, S, D (U); (2) Ko, Ko′, Y (D)	0.25
151	1.72	5.40	5.80	P-S	4.73	2.70	1.85	5.88	(1) Km, I, S, D (U); (2) Ko, N, Y* (D)	0.20
201	25.65	5.67	10.30	P	5.11	2.92	1.75	6.84	(1) L_1, Y, R_3, K, Kh, Ko, N, I (U)	—
202	2.45	—3.85	6.20	P	5.10	—	—	—	(1) F, K*, I, N* (U); (2) Ni, Ko, Ko′, R_3*, Kh, L_1 (D)	0.20
206	11.97	—5.98	9.25	P	5.43	3.13	1.74	7.35	(1) M, R_3, Y, Ko, Ko′, Kh, K, W, Ka, L_1, L_2, T′ (D); (2) Yu (U)	0.15
207	2.30	3.05	3.60	P-S	4.31	2.67	1.62	(7.01)	(1) Y, N (D); (2) Ko, Ko′, K, W, I (U)	0.40
217	—0.98	—0.36	7.90	P	5.35	(3.56)	(1.58)	7.64	(1) Ni, W, F, Ko, Ko′, L_2, Y, N, T′ (U); (2) K, Ka, L_1 (D)	0.20
220	—1.20	7.25	5.10	P	4.66	2.85	1.64	7.35	(1) W (D); (2) I, F, N, K, Ko′, L_1 (U)	0.35
222	8.35	—1.25	4.40	P	4.72	2.96	1.60	5.94	(1) Y, Ko, K, W, F*, I, N (U)	—
223	3.35	1.59	5.15	P-S	4.72	2.72	1.73	6.41	(1) Ko, W, Y, I, N (U); (2) F (D)	0.20
224	—0.70	0.65	8.90	P-S	5.38	2.91	1.85	6.35	(1) F, Ko (D); (2) W, I, N (U)	0.25
228	—2.05	—2.30	7.25	P	5.65	3.54	1.60	—	(1) W, Ko, F, I, Y, K, N (U)	—
230	0.45	0.65	8.40	P	5.65	—	—	—	(1) F, I (D); (2) W, Ko, K, N, Y (U)	0.20
236	10.50	—1.75	6.30	P	4.83	2.93	1.65	7.45	(1) L_1, N, R_2 (D); Y, Ko, Ko′, K*, Ka, W, F, I (U)	0.25
247	27.30	4.15	12.00	P	5.26	3.08	1.71	7.42	(1) Yu, L_1, M, R_3, K, Ko, Ko′, N, F, W, I (U)	—
248	—0.17	2.00	4.55	P-S	4.93	2.66	1.87	5.63	(1) W, Y (U); (2) F, Ko, K, I (D)	0.40
249	—1.87	2.30	8.80	P-S	5.33	3.20	1.68	(8.00)	(1) W, F, Ko, N (U); (2) I (D)	0.20
250	3.20	2.80	3.70	P-S	4.26	2.54	1.73	5.97	(1) Ko, Ko′, W, N, R_2* (U); (2) F*, K, Ka, I (D)	0.30
251	8.96	0.46	5.30	P	4.86	—	—	—	(1) Ko, Ko′, F, W, I, N (U)	—
253	—4.10	3.60	6.60	P-S	5.00	2.88	1.80	6.78	(1) I, W, Ko, Ko′, K, N, R_2, Y (U)	—

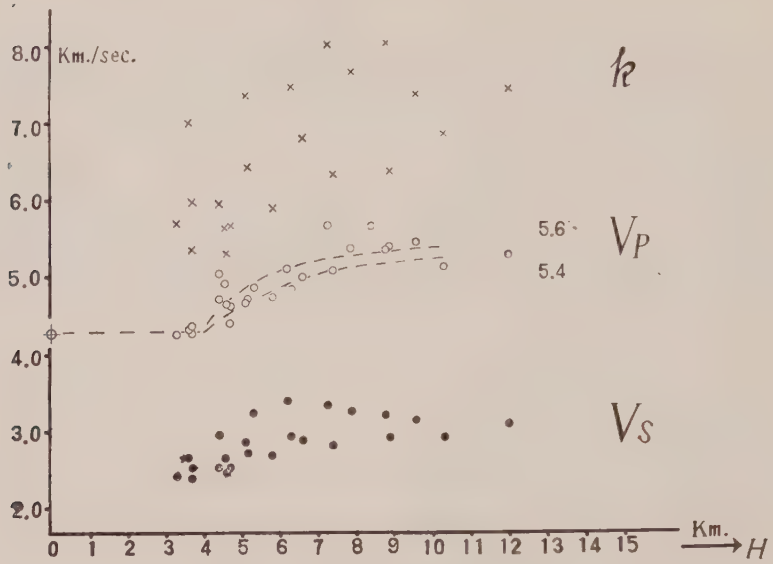

Fig. 5. Velocity — focal depth graph.

anomalies as already stated are not regarded as time errors.

Second, a possibility of mis-discrimination of the initial wave in 1/2 or 1 cycle was examined. But the time error resulted from such a mis-discrimination is insufficient to produce the travel-time difference previously mentioned, considering the wave frequency in the initial part of seismic motions. Taking, also, into consideration the distribution of the recorded initial movements, the clearly recorded first waves at most of the stations used in the analysis and so forth, the cause of separation of the travel-time curves cannot be attributed to the mis-discrimination of the initial wave.

Third, the errors of focal position caused by the observational time errors were estimated under a uniform medium assumption. The uncertainties in the present case are presumed to be less than 1 kilometre, but the general appearance of the time-distance curve is not altered within this range.

Fourth, the effect on travel-time curves was studied, by assuming a horizontally layered structure instead of the homogeneous medium. Such an effect was ascertained to be slight, namely, the large deviations in travel times cannot be explained from the influence resulted by the simple model of crustal structure.

From the various reasons above stated, it may safely be said that the cause of the anomalies in travel times is attributable to the effects of focal conditions, such as the mechanism of earthquake occurrence or the shape of the hypocentral region. The detailed description and discussion of this problem will appropriately be referred to MIKUMO's paper (1956).

4. Crustal Structure in Wakayama District

The structure of the crust in the district concerned was presumed to be composed of horizontal parallel layers.

The propagation velocities of the P- and S-waves in the surface layer consisting of metamorphic rocks and its layer thickness were estimated to be approximately 4.3, 2.5 km/sec. and 4 km, respectively, from the relationship indicated in Fig. 5, and the results of seismic prospecting already carried out.

The longitudinal velocity in the second layer was calculated so as to be adapted to the distribution of the uniformly assumed velocity against the depth shown in Fig. 5, on the basis of the already known thickness and velocities in the surface layer. The velocity of the P-waves was determined to be 5.4～5.6 km/sec., and the corresponding velocity of the S-waves was calculated to be about 3.2 km/sec.

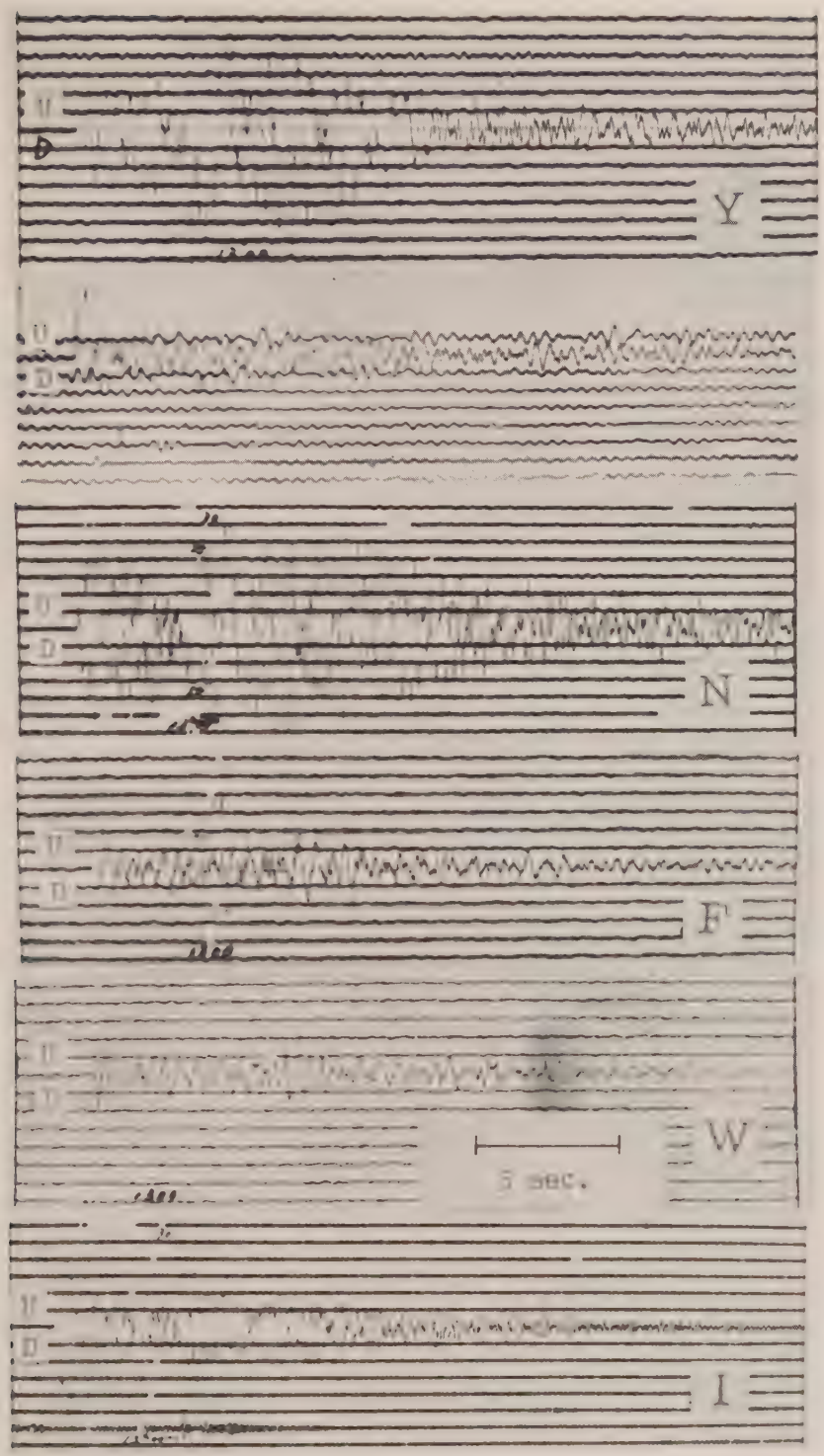

Fig. 6. Examples of seismograms recorded at six station; No. 247, April 22, 1956, 12 h 45 m.

The apparent velocities in the third layer were determined by the data obtained at five temporary stations in Wakayama District in an earthquake which occurred near Kyoto, being 100 km distant and with focal depth of about 11 km. Supposing the thickness of the second layer to be nearly 6 km (NISHIMURA and KISHIMOTO, 1956), the velocities in the third layer were considered to be approximately 6.0 and 3.4 km/sec. respectively for the P- and S-waves.

5. Conclusion

An anomalous nature in the time-distance graph was found by precise seismometric observation of the local earthquakes which frequently occurred in a swarm in a certain limited area within Wakayama District. Namely, the time-distance curve in each shock is necessarily separated into two groups for the P- and S-waves in order to obtain the definite hypocentre and normal velocities. And it was learned that the separation of the stations is intimately related to the distribution of the so-called push- (anaseismic) and pull- (kataseismic) zones of the first motion of the ground in earthquakes at each station. Consequently the obtained values of 0.2∼0.4 sec. in a time-gap between two groups are interpreted to suggest numerically the azimuthal difference in mechanism of earthquake occurrence or the deviation of focal region from a sphere. As the earthquakes treated in the present investigation are all local shocks and have a shallow foci of several kilometres, the above obtained value of time-gap may probably be increased in case of large destructive earthquakes with hypocentral region of some ten times that of these local shocks. The time difference stated above may be regarded as affording a powerful clue for detecting the behaviour of focus. From this standpoint, a precise observation with a dense net of stations in the epicentral area of large earthquakes is highly recommended, in future, in the study of the nature and mechanism of occurrence regarding these earthquakes. It should be suggested that precise seismometric observations with the high-sensitive strain seismometers are at present being operated by our institute in the area concerned, and the synthetic treatment of the present problem by the analysis of ground-motion and ground-strain should be expected to advance our knowledge about the nature of earthquakes.

The writers wish to express their heartfelt thanks to Assist. Prof. S. Miyamura of the Earthquake Research Institute, Tokyo University, for his generous permission in analysing the data obtained at the stations of the E.R.I.

REFERENCES

MIKUMO, T., 1956: Precise Seismometric Observations in the Epicentral Region of Local Shocks. *Mem. Coll. Science, Univ. of Kyoto*, Ser. A, **28**, No. 2, pp. 161 – 186.

NISHIMURA, E. and KISHIMOTO Y., 1956: On the Local Structural Character of the Earth's Crust. *Tellus*, **8**, No. 3, pp. 329 – 334.

Quartz Contents of Pelagic Sediments of the Pacific Ocean[1]

ROBERT W. REX and EDWARD D. GOLDBERG
Scripps Institution of Oceanography, University of California, La Jolla, California

(Manuscript received July 30, 1957)

Abstract

The quartz contents of pelagic clays from the Eastern Pacific Ocean show a marked latitudinal dependence with a maximum around 30° N. Present evidence indicates that the quartz is mainly transported to the deposits through the atmosphere and that the observed distribution is probably related to the latitudinal values of the atmospheric wind fluxes and exposed arid land areas. A number of sediments display a distinct change in quartz content with depth. In all cases there is a marked decrease going from the recent to the older strata. It is suggested that the changes indicate a major climatic change that occured sometime during the Late Tertiary.

Quartz is one of the major minerals in igneous rocks (12 – 20 % on the average) and is one of the most resistant substances to chemical and mechanical weathering (PETTIJOHN, 1957), yet its role in the major sedimentary cycle is poorly understood. Few determinations of its concentration in recent marine sediments have been made. CORRENS (1937), REVELLE (1944), KUENEN and NEEB (1943), and GRIM ET AL. (1949) give semi-quantitative estimates in their studies, while REVELLE ET AL. (1955) present figures of 2 – 5 % in Pacific buff clays. Inasmuch as the total amounts of quartz in sediments may serve as an indicator both of the lithogenous contribution as well as of the mechanics of deposition, it appeared worthwhile to make an intensive quantitative study of its space and time distribution in the Pacific Ocean deposits.

The determinations were made by x-ray diffractometry and the results are reproducible to ±3 % of the absolute values obtained with a minimum sensitivity of 0.3 % quartz. The details of the method will be published elsewhere.

The quartz particles in the sediments are found as chips and shards and are well sorted with maximum concentrations between 1 and 20 microns (Figure 1). There is no microscopic evidence for crystal overgrowth. Quartz bipyramids, characteristic of volcanic beta quartz, have not been observed in any of the samples. There is no evidence for the authigenic formation of quartz in the marine environment. INGERSON (1955) points out that there is no known example of the crystallization of quartz from aqueous solutions below 100° C. and no conversion of biogenous silica to quartz has been observed in unmetamorphosed sediments dating back to the Miocene (BRAMLETTE, 1946). Inspection of biogenous silica in sediments as old as Paleocene showed no significant conversion of opal to quartz. In this presentation almost all of the samples are apparently of Miocene age or younger.

[1] This paper represents in part results of research carried out by the University of California under contract with the Office of Naval Research.

Contribution from the Scripps Institution of Oceanography, New Series No. 971.

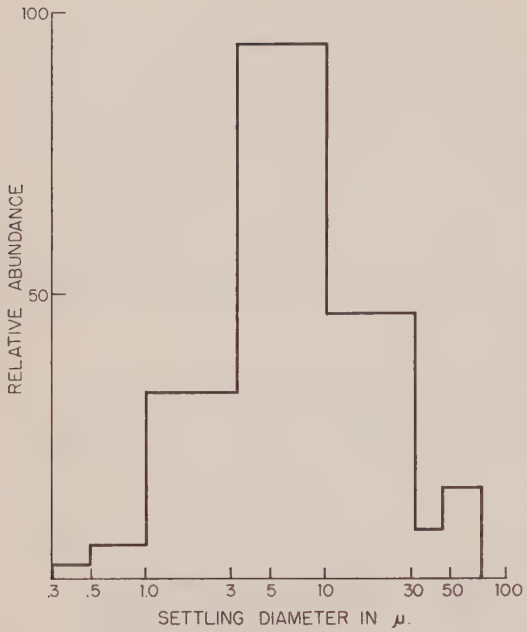

Fig. 1. The size distribution of quartz in pelagic clay sample PAS 19121 (Lat. 19°49«N; Long. 121°43.5«W; and depth 4,350 meters).

Space and Time Distribution of Quartz

The two principle results of the study are the space and the time distribution of quartz in the pelagic sediments. The major feature of the surface distribution in the Eastern Pacific is a marked latitudinal dependence of the quartz concentration with a maximum at around 30° North and decreasing in both the north and south directions (Figure 2). The values are for the calcium carbonate free fraction of the sample. Perturbations of this general pattern can be effected in the following ways. The introduction to the deposits of biogenous silica or carbonates reduces the observed quartz values. This is evident in the highly diatomaceous samples from the Bering Sea and from the area to the immediate south of the Aleutian trench and in the siliceous and carbonaceous deposits of the equatorial belt.

A second type of dilution is found in the quartz distribution in the sediments surrounding the Hawaiian Islands (Figure 3). These islands belong to a basaltic province and the magmas are strikingly deficient in quartz compared to the average abundance in igneous rocks. The deposits are diluted to a distance of 150 miles north by the weathering products from the erosion of the islands. The Hawaiian Arch appears to form the outer margin of transport of materials. Again, volcanic ash layers in cores from the Gulf of Alaska show smaller values of quartz than adjacent strata.

The latitudinal pattern can also be disturbed by turbidity current deposits which occur on abyssal plains, walls and bottom of deep trenches and archipelagic aprons. For example, on the shoreward side of the Acapulco trench area, where turbidity flows are thought to occur, the quartz ranges between 12 and 24%, while in the seaward deposits of the trench, free of such flow from the coastal area, the values are of the order of 8%. Further evidence of the influence of turbidity currents upon the quartz contents of sediments will be discussed below.

A number of red clay cores display a distinct change in the characteristics of the sediment type with depth. Such variations exist either as discrete discontinuities or gradual changes. In all such cases, there is a marked decrease in the quartz concentration in the lower levels of the cores (Table 1). The quartz values above and below the zones of change are remarkably uniform (Figure 4). In most cases the upper sediment contained a Quarternary radiolarian fauna. Three of the cores contained Middle Tertiary radiolarian fauna in the lower quartz poor strata (Riedel, W., personal communication). The remaining cores contained no age-indicating fossils below the discontinuity.

Sources of the Quartz

Two significant problems relative to these results are the sources and modes of transport of the quartz. Since we have ruled out an authigenic origin, there remains the consideration of the relative contributions of continental detritus and marine volcanic ejecta. The quartz contents of sediments containing large amounts of pyroclastics are notably low. The presence of quartz as chips and shards and the absence in the sediments of quartz phenocrysts, typical of volcanic lava, support the argument of a continental source.

The consistent appearance of the same broad band (3.18 – 3.24Å°) in the x-ray diffraction spectra of pelagic clays in the Pacific represents a composite of feldspar peaks. This indicates contributions from many sources with sub-

TABLE 1

Depth Distribution of Quartz in North Pacific Sediments

Core	Zonation (cm.)		Contact	Quartz Content		Samples Run	Notes
	Upper	Lower		Upper	Lower		
Chubasco 10 10° 21.4′ N 124° 26.3′ W 4,645 meters	0—86	86—120	Discontinuous	8%	3%	Upper: 0—4; Lower: 116—120	Upper zone contains Quaternary radiolaria with admixed Tertiary. No age-indicating fossils in lower zone.
Chubasco 9 10° 18.5′ N 125° 27.2′ W 4,545 meters	0—32	32—100	»	8%	3%	Upper: 0—4, 16—20; Lower: 44—48, 96—100	Upper zone contains Quat. rads. with admixed Tertiary. Lower zone contains Middle Tert. rads.
Mid-Pac 14 9° 57.7′ N 145° 12.7′ W 5,232 meters	0—4½	4½—79	»	8%	2%	Upper: 3—4; Lower: 74—76	Upper zone contains Quat. rads. with much admixed Tert. Lower zone contains Middle and Early Tert.
Capricorn 49 BP 9° 17′ N 124° 09′ W 4,410 meters	0—124	228—832	Gradational from 124 to 228 cm.	8%	3%	Upper: 0—4; Lower: 300—304	Upper zone to at least 40 cm. probably Quat. with Tert. admixture. Lower zone Middle Tert.
Capricorn 50 BP 14° 55′ N 124° 12′ W 4,270 meters	0—302	302—812	Discontinuous	9.8 ± 0.9%	2.8 ± 0.5%	Upper: 0—302 (72 samples); Lower: 302—812 one sample every 20 cm. (18 samples)	Upper zone perhaps Quat. Lower zone no age-indicating fossils.
Chinook 2 35° 09′ N 157° 17.5′ W 5,610 meters	0—21	21—54	»	16%	6%	Upper: 0—4; Lower: 51—54	No age-indicating fossils in core.
Chinook 4 42°29.9 N 162°8.2′W 5,400 meters	0—126	126—157	»	15%	12%	Upper: 0—5, 10—12, 12—16; Lower: 128—132, 140—144, 144—148, 154—157	Upper zone Quat. rads. Lower zone no age indicating fossils.

sequent mixing. The continents provide the necessary variety of feldspars to produce such a composite peak. Further, in samples from areas where pyroclastics are abundant in the deposits, the composite feldspar band is overshadowed by sharp peaks characteristic of the feldspars from local sources of volcanic activity.

Transport Mechanics

It is difficult to conceive of the water transport of quartz particles with their observed size distributions from the continental boundaries to pelagic areas, which are inaccessible to turbidity flow or ice rafting. For example, the area of abundant quartz, north of Hawaii, is approximately 2,000 miles from the nearest continental area. The Stoke's settling times for quartz particles of 10 micra diameter, which are near the mean of those in the sediments, is approximately 2 years for 4,000 meters. (In suggesting these Stoke's Law settling times we have not included any enhancements attributable to the aggregation of particles by filter feeding organisms and a subsequent excretion in larger, more rapidly settling masses). These data demand an *average horizontal westerly* com-

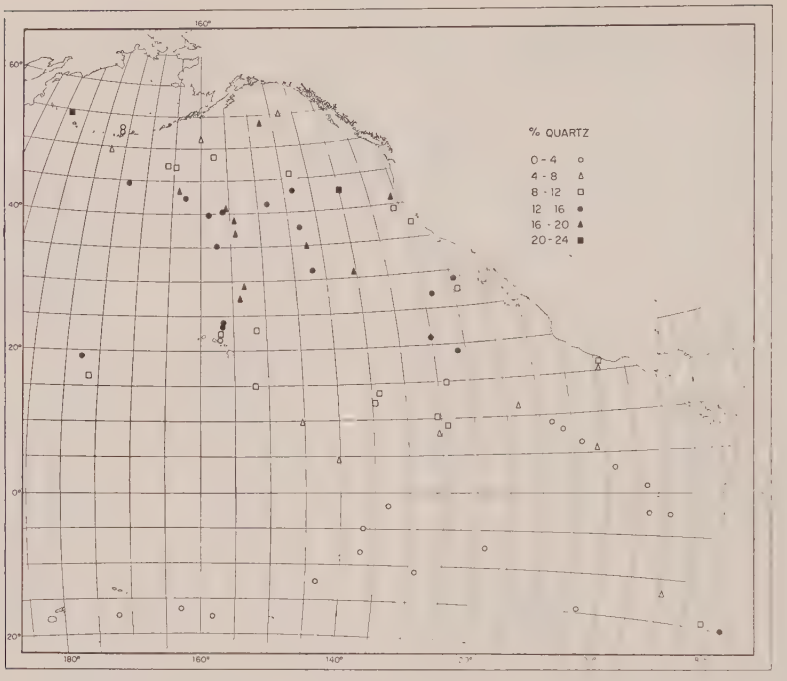

Fig. 2. The concentration of quartz in surface sediment samples from the Eastern Pacific Ocean.

ponent of ocean currents from the North American coast to the deposition site of 0.1 to 0.2 knots for that part of the water column containing the quartz. Such currents have not yet been observed in the descriptive oceanographic studies of this region. Further, the latitudinal variation in the quartz contents is inconsistent with the observed circulation of the North Pacific. Finally, it is difficult to explain the maximum in the quartz concentration in pelagic sediments that are furthest from land by a water transport mechanism. Any water fractionation mechanism that will sort quartz from the more slowly settling, small clay particles would result in a distribution in which quartz would be present in decreasing concentrations with increasing distance from land.

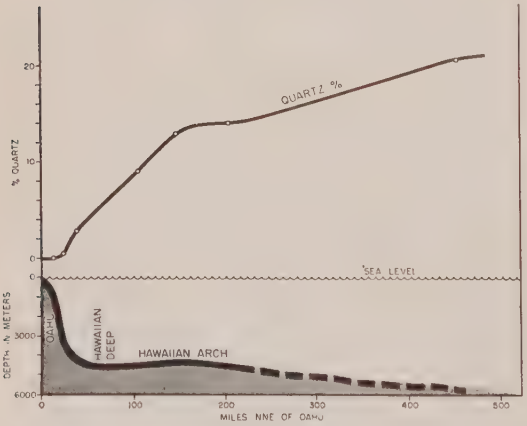

Fig. 3. The dilution of quartz contents in pelagic sediments by weathering products from Oahu Island.

The abyssal plain deposits of the Gulf of Alaska, provide examples of two possible mechanisms for the water transport of quartz: turbidity flow and ice rafting. Two samples, Cusp 5P (Lat. 43°00′N; Long. 134°27′W) and Cusp 11G (Lat. 45°34′N; Long. 143°11′W) situated at approximately 500 and 1,000 miles respectively from the continents, have high quartz contents in the sand and silt sizes and are accompanied by abundant mica which is low or absent from the nearby red clay deposits on topographic highs. The nearshore sample Cusp 5P, contained 22% quartz whereas the more distant deposits contained 10%. The values can most satisfactorily be explained by the sorting action of turbidity currents as described by KUENEN (1950) where the coarser particles are dropped out near the source of flow. The neighboring pelagic clays have values of 15% quartz

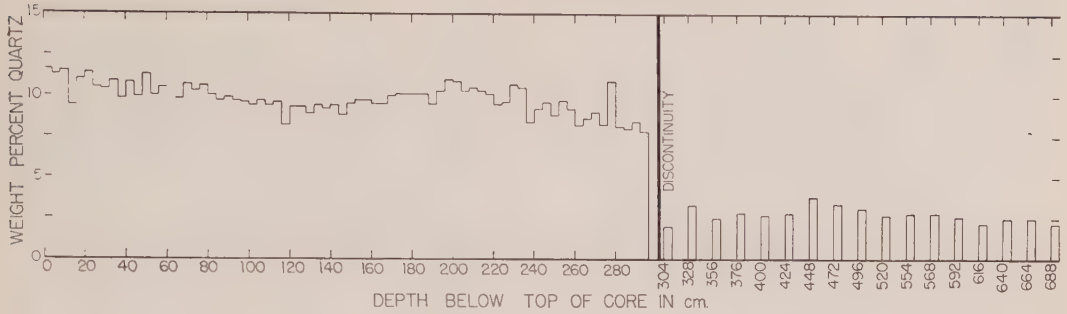

Fig. 4. The quartz concentrations as a function of depth in Capricorn 50 BP (Lat. 14°55«N; Long. 124°12«W). The depth scale is discontinuous after the discontinuity.

and this suggests that the turbidity flow at its extremeties is low in quartz and serves to dilute the quartz contents of the normal pelagic clays. Ice rafting in the Northern Gulf of Alaska, as described by MENARD (1953), introduces a wide variety of poorly sorted materials which give erratic values to the quartz contents in the sediments. For example, Northern Holiday 3, (Lat. 53°22.6′N; Long. 147°13.6′W) contains 17% quartz while nearby NH2 (Lat. 51°34′N; Long. 149°58′W) and NH5 (Lat. 55°7.8′N; Long. 142°55′W) contain 7 and 3% respectively. All of these cores show miscellaneous assemblages of continental pebbles and grit.

Transport of particles by marine organisms appears to be relatively unimportant. The ingestion and subsequent excretion of inorganic particles probably takes place over relatively short periods of time and hence of space. Further, algal transport of significant amounts of sedimentary components appears to be negligible.

In the past not much more than general statements could be made concerning the importance of atmospheric transport of particles to the marine environment, yet there has been a general recognition of the importance of eolian particles in sediments (TWENHOFEL, 1939; CORRENS, 1953). Quantitative estimates of the contribution of such transported particles are lacking, however, a number of lines of evidence from this work converge upon the significance of eolian components in some marine deposits:

(1) The latitudinal variation of quartz corresponds to (a) the intensity of atmospheric fluxes in the troposphere and (b) the amounts of exposed arid regions of the northern hemisphere (Figure 5). The wind movements in the troposphere are dominantly zonal. Both of these parameters would directly influence the amount of dust transported, yet the relative importance of each has not yet been ascertained. As yet there is a paucity of samples from the Southern Hemisphere to complement these observations, and possibly to suggest which of these two parameters is the more significant.

(2) Quartz and other detrital minerals, including feldspars, amphiboles and pyroxenes

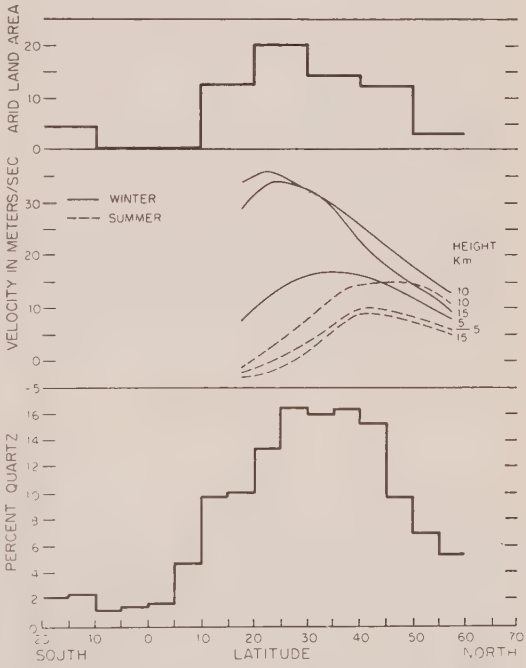

Fig. 5. Lower: The quartz distribution as a function of latitude in sediments from the Eastern Pacific; middle: Mean zonal component of the geostrophic wind. Taken from BYERS (1954); upper: the area of steppe and desert regions in arbitrary units (KÖPPEN and GEIGER, 1936).

have been observed in the guts of filter-feeding pelagic organisms living in the surface waters of the mid-Pacific ocean.

(3) The size distribution of quartz (Figure 1) is similar to observed atmospheric fallout distant from its point of origin. GLAWION (1938) reports a grain size maximum between 3 and 5 micra for Sahara dust collected high in the Swiss Alps. CORRENS (1953) has emphasized the similarity of grain size distribution of marine sediments with atmospheric deposits by matching curves from both sources. His maxima ranged between approximately 10 and 50 micra.

(4) Quartz is consistently reported as a constituent of atmospheric dusts whose mineral compositions are ascertained. KAMPE, WEICKMANN and KEDESDY (1952) detected quartz in addition to clays, lampblack and organic substances in snowcrystal nuclei in New Jersey. LEROUX and TRILLAT (1954) find as common constituents of atmospheric dusts quartz, gypsum, anhydrite, calcite, feldspar, magnetite and hematite. Further, in our laboratories, quartz has been observed in snows from the high coastal mountains of Southern California, and from the Arctic ocean area, in Anarctica and in radioactive rain water from Japan.

Certain deductions can be made from the above evidences that the quartz in most pelagic sediments is atmospherically transported from the continental areas.

Pelagic sediments, deposited below the area of the jet stream in the Northern Hemisphere, are composed to a significant extent of materials that were atmospherically transported. Quartz is not the only mineral found in atmospheric dusts that is refractory to marine weathering processes. Such weathering resistant minerals as feldspar, magnetite and certain clays are *in toto* quantitatively as important as the quartz, in the atmospheric dust, according to the work previously cited. Hence, in pelagic sediments containing 20 % quartz, it is reasonable to assume that around one half of the solid phases are of eolian origin.

Studies of quartz concentrations in areas of turbidity flow can be used to describe the hydraulic flow pattern. For example, the turbidity flows on the Hawaiian archipelagic apron (MENARD, 1956) are apparently limited by the Hawaiian arch with a relief of 600 meters. This not only establishes an upper limit to the extent of the flow, but also establishes that such flows are confined to near bottom waters.

The decrease in quartz content with depth in the North Pacific sediments provides clear evidence for a major climatic change that occurred sometime during the Late Tertiary. These changes are accompanied by changes in the gross chemical composition (REVELLE ET AL, 1955) which have been interpreted by Goldberg and Arrhenius (Geochim. Cosmochim. Acta, in press), as reflecting differences in rates of accumulation of solid phases. Thus, quartz concentrations, coupled with chemical compositions, may provide useful stratigraphic indicators for fossilfree clays.

Finally, this pattern of *natural fallout* may be of some use in studies of *radioactive fallout*. The particles in the normal atmospheric dusts may act as scavangers for the radioactive atoms and molecules and hence the distribution of such guest materials will be influenced both by paths of the host dust particles and subsequent chemical interactions with the environment.

LITERATURE

BRAMLETTE, M. N., 1946: The Monterey formation of California and the origin of its siliceous rocks. *U. S. Geol. Survey Prof. Paper* **212** 55 pp,

BYERS, H. R., 1954: In *The Earth as a Planet* (G. Kuiper, ed.). Chicago: University of Chicago Press, Chapter 7.

CORRENS, C. W., 1937: Die Sedimente des äquatorialen Atlantischen Ozeans. *Deutsche Atlantische Exped. Meteor* **1925—27 3**, 298 pp.

—, 1953: Der Anteil des Staubes an der Bildung der Sedimentgesteine. *Z. Ver. deut. Ing.* **95**, pp. 294—6.

GLAWION, H., 1938: Staub und Staubfalle in Arosa. *Beitr. physik. freien Atmos.* **23**, pp. 1—43.

GRIM, R. E., DIETZ, R. S., and BRADLEY, W. F., 1949: Clay mineral composition of some sediments from the Pacific Ocean off the California coast and the Gulf of California. *Bull. Geol. Soc. Amer.* **60**, pp. 1785—1808.

INGERSON, E., 1955: Geologic thermometry. *Geol. Soc. Amer. Special Paper* **62** pp. 465—88.

KAMPE, H. J., WEICKMANN, H. K., and KEDESDY, H. H., 1952: Remarks on "electron microscope study" of snow-crystal nuclei. *J. Meteor.* **9**, pp. 374—5.

KÖPPEN, W. and GEIGER, R., 1936: *Handbuch der Klimatologie I* Berlin: Gebrüder Borntraeger, Chapter C.

KUENEN, PH. H., 1950: *Marine Geology* New York: John Wiley and Sons, 568 pp.

—, and NEEB, G. A. 1943: *Bottom Samples, The Snellius Expedition* **5**, 268 pp.

LEROUX, J. and JACQUES-TRILLAT, J., 1954: Etude comparativ des poussieres atmospheriques minerales des quelques villes. *Compt. rend.* **238**, 1748—50.

MENARD, H. W., 1953: Pleistocene and recent sediment from the floor of the Northeastern Pacific Ocean. *Bull. Geol. Soc. Amer.* **64**, pp. 1279—94.

—, 1956: Archipelagic aprons. *Bull. Amer. Assoc. Petrol. Geol.* **40**, pp. 2195—2210.

PETTIJOHN, F. J., 1957: *Sedimentary Rocks* New York: Harper and Brothers, 718 pp.

REVELLE, R. R., 1944: Marine bottom samples collected in the Pacific Ocean by the Carnegie on its last cruise. *Carnegie Inst. Wash. Publ.* **556** Pt. **1**, 180 pp.

—, BRAMLETTE, M., ARRHENIUS, G., and GOLDBERG, E. D., 1955: Pelagic sediments of the Pacific. *Geol. Soc. Amer. Special Paper* **62** pp. 221—36.

TWENHOFEL, W. H., 1939: *Principles of Sedimentation* New York: McGraw-Hill, 610 pp.

An Economical Net Radiometer

By V. E. SUOMI, Department of Meteorology, The University of Wisconsin, and P. M. KUHN, Office of Meteorological Research, U.S. Weather Bureau

(Manuscript received Jan. 10, 1957)

Abstract

A net radiometer of moderate accuracy but of simple construction and very low cost is described. The value of net radiation is obtained from the difference of fourth power temperatures of the upper and lower radiating surfaces. Conduction losses are held to a low value by employing a good insulating material and ventilation losses above and below are kept to a low value by two layers of thin polyethylene film. Field tests, calibration data, and applications are described.

1. Introduction

The net radiation normal to the earth's surface is the difference between the total upward radiation flux and the total downward radiation flux. Net radiation is important to many meteorological problems because it is a measure of the energy available at the earth-atmosphere interface. The energy exchange at the earth's surface represents the major input to the giant heat engine which circulates the atmosphere.

A number of instruments which measure net radiation are already available (ALBRECHT, 1933; GIER and DUNKLE, 1951; SUOMI, FRANSILLA, and ISLITZER, 1954). Most of them, however, are fairly expensive. As a result there are only a few stations over the entire earth which make net radiation observations. It is not possible to study the effects of a variable heat input on subsequent weather from these isolated measurements. There are far too few to give anything even approaching a representative sample. The purpose of this paper is to describe a net radiometer of moderate accuracy but very low cost. The low cost and simple construction will make it possible to obtain many more observations of net radiation over land and ocean. The errors due to the performance of the instrument can be more than offset by far better sampling.

2. Simplified theory of the instrument

The following symbols will be employed:

$R_s\downarrow$ vertical component of sun and sky insolation (short wave)

$R_s\uparrow$ vertical component of insolation reflected from the ground

L_s fractional loss in transmission through the polyethylene films due to absorption, scattering, and reflection for short wave radiation

$R_l\downarrow$ downward flux of long wave radiation

$R_l\uparrow$ upward flux of long wave radiation

L_l fractional loss in transmission through the polyethylene films due to absorption, scattering, and reflection for long wave radiation

ε long wave emissivity of polyethylene film

T_p Absolute temperature of polyethylene film

a absorptivity of blackened aluminium foil sensor

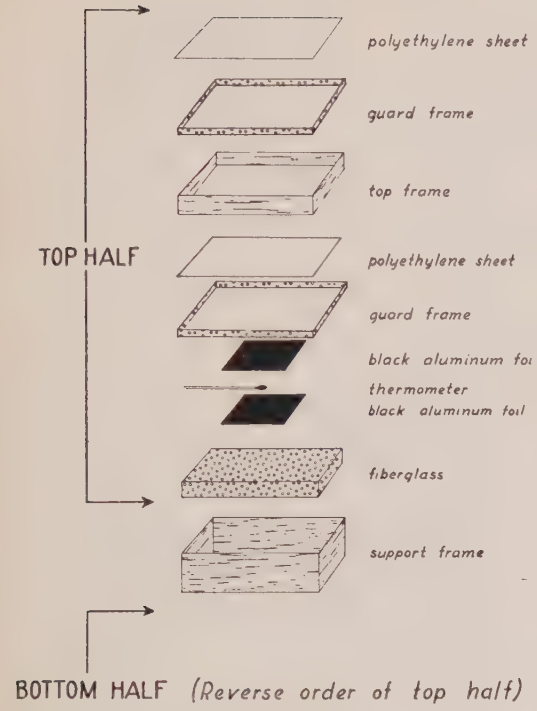

Fig. 1. Exploded view of the Net Radiometer.

K thermal conductivity of insulation
G_1, G_2 effective convective heat transfer of air films, top and bottom
T_t Absolute temperature of top blackened aluminium foil
T_b Absolute temperature of bottom blackened aluminium foil

Fig. 1 shows an "exploded" view of the instrument. The blackened aluminium foil sensing element is supported by a block of light rigid material of low heat capacity and thermal conductivity such as fiberglass insulation. Two sheets of 0.50 mil thick polyethylene film, an insulating guard, and a wooden box framework form a wind screen. The upper and lower surfaces are assembled in reverse order.

When the instrument is oriented above and horizontal to the earth's surface, and equilibrium is reached, the energy balance of the upper surface in sunlight is

$$a[R_s\downarrow(1-L_s)+R_l\downarrow(1-L_l)+\varepsilon\sigma T_p^4]=$$
$$=a\sigma T_t^4+G_1(T_t-T_p)+K(T_t-T_b) \quad (1)$$

The energy balance for the lower surface is

$$a[R_s\uparrow(1-L_s)+R_l\uparrow(1-L_l)+\varepsilon\sigma T_p^4]=$$
$$=a\sigma T_b^4+G_2(T_b-T_p)-K(T_t-T_b) \quad (2)$$

In each equation the terms on the left represent the most important heat gains by the blackened surface. The terms on the right are, in order, the losses due to radiation, convection and conduction. When four inches of insulation such as OWENS-CORNING type PF-612, two and one-half pound density, rigid fiberglass is used, the conduction terms comprise only about 10 per cent of the energy exchange. It is possible to evaluate the magnitude of the convection term using the dimensionless numbers of NUSSELT, GRASHOF, and PRANDTL. This was done following the method of DE GRAAF and VAN DER HELD, 1953. The value of this term should be greatest when the air film is heated from below as the upper blackened surface is in the presence of sunlight. The value varies between 10 and 20 per cent of the total energy exchange. Thus the remaining radiation term is the most important mode of heat loss from the sensor surface.

Fig. 2 shows the per cent transmission of 1.0 mil polyethylene film in the range of from 2 to 15 microns. The polyethylene absorption bands are located in the same region of the spectrum as the water vapor bands, but are much narrower. Polyethylene films of this thickness absorb only about 1 per cent of the incident solar radiation but the scatter due to

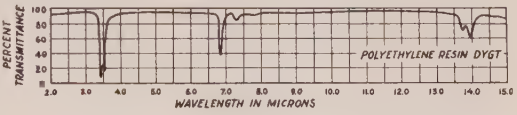

Fig. 2. Per cent transmission of 1.0 mil polyethylene after U.S. Department of Commerce Publication 111438, 1955.

the milky color of the film is several times this value. The combined effects of fractional transmission of short wave energy, absorption of long wave energy and re-radiation from the polyethylene film was determined experimentally by holding two large sheets of polyethylene film above a ventilated net radiometer (SUOMI, FRANSILLA, and ISLITZER, 1954) and noting the change in observed net radiation. This loss is about 10 per cent of the incident radiation.

The loss due to incomplete transmission is about 10 per cent of the left hand side of (1) and (2), while the convection and conduction is about 20 per cent of the right hand side of these equations. Since these terms are proportional to the incident radiation, we can rewrite equations (1) and (2), taking these approximations into account, take their difference, and obtain

$$R_{Net} = A\sigma(T_t^4 - T_b^4) + k(T_t - T_b) + \text{error} \quad (3)$$

where $A = 1.25; k = .0025$

Figs. 3 and 4 show a comparison between a ventilated radiometer (SUOMI, FRANSILLA, and ISLITZER, 1954) of good accuracy and the radiometer just described when the temperature of the upper and lower blackened surfaces, measured with mercury thermometers or thermocouples and averaged for one hour are substituted in (3). If equations (1) and (2) were used the agreement between the two sets of observations would be even better.

At low sun angles the flat, milky polyethylene film will cause the cosine response of the instrument to be poor. For example, at zenith angles of 25°, the ratio of the net radiation measured with the ventilated radiometer over that measured with the economical net radiometer is 1.1 whereas at 65° the value is 1.2 and at 80° it averages 1.37. However, at most latitudes the error in the *total daily* radiation will be small. During the night with diffuse radiation, the cosine error is not as important, and the ratio averages 1.2 for all angles.

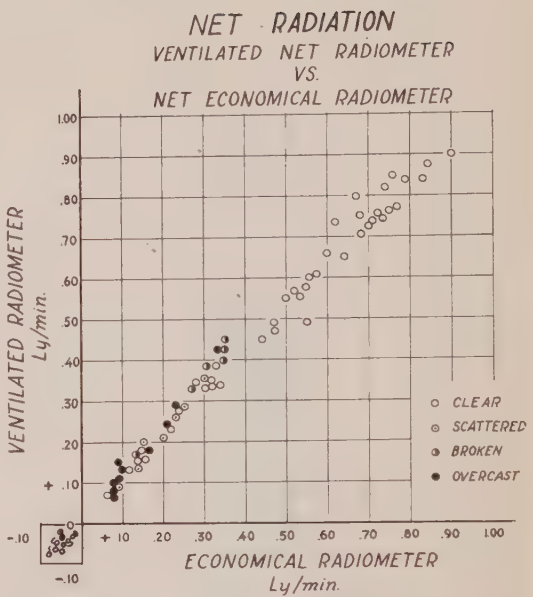

Fig. 3. Hourly net radiation comparison between Economical Net Radiometer and Ventilated Net Radiometer.

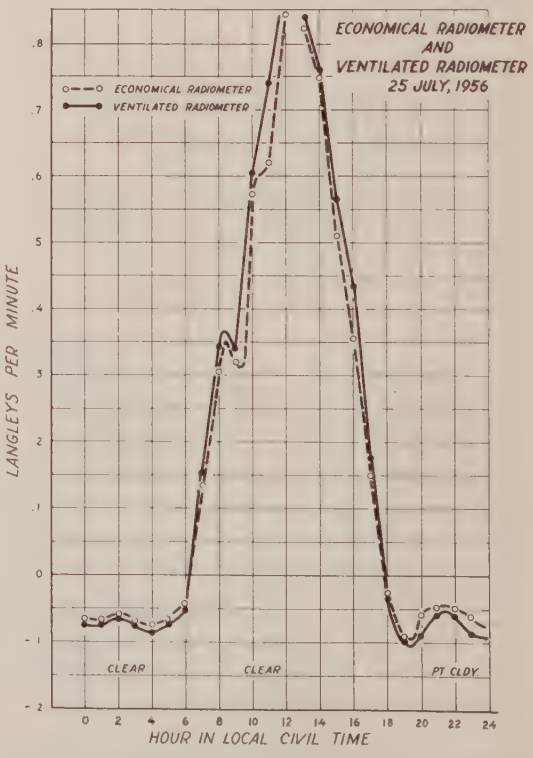

Fig. 4. Scattergram of net radiation measurements using economical net radiometer and ventilated net radiometer.

3. Discussion

Equations (1) and (2) contain *four* unknown radiation currents but the *two* equations only allow the evaluation of the total downward and total upward radiation flux, and, of course, their sum and difference. If a second radiometer whose sensors are painted *white* is used in addition to the black surfaced radiometer, and the ratio of the black and white paints' short wave absorptivities and ratio of the black and white paints' long wave absorptivities are known, two more equations with no additional unknowns can be written. This is enough additional information to separate $R_s\downarrow$, $R_l\downarrow$,

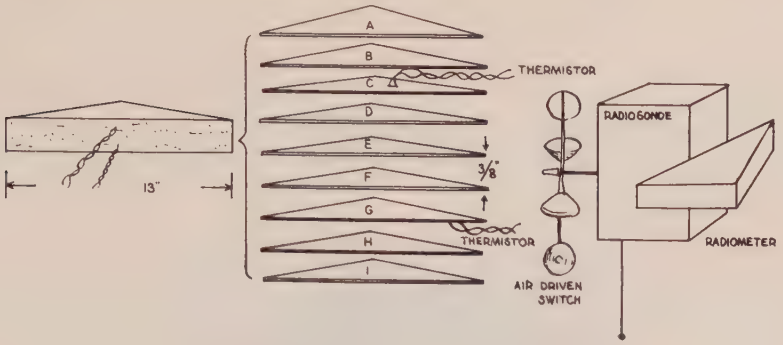

Fig. 5. Balloon-borne economical net radiometer.

$R^s\uparrow$, and $R_l\uparrow$. This application and tests of its validity will be given in another paper.

If one uses thermistors to measure the temperature of the upper and lower blackened surfaces of such a radiometer it is possible to telemeter this information in a manner similar to that used to transmit air temperature in the ordinary radiosonde. By employing very light weight material for insulation and framework, the net radiometer can be made light enough to be carried aloft by a radiosonde balloon. Fig. 5 shows such an instrument which weighs only 125 grams. In order to telemeter air temperature, humidity, and upper and lower surface temperatures it is necessary to add a sequencing switch. The figure illustrates the instrument with such a wind-driven switch. This instrument makes it possible to obtain measured values of the vertical profile of net radiation. Tests of this instrument are under way.

It is possible to compute minimum surface temperatures given the net radiation at sunset and the soil thermal properties. Therefore, the economical net radiometer can be useful in frost forecasting.

Penman, 1948, and others have shown that evaporation from a growing field crop is highly correlated to net radiation. Irrigation control from net radiation data is thus feasible.

4. Conclusion

We have described a very low cost net radiometer of moderate accuracy. This accuracy is, however, quite sufficient for many meteorological applications.

REFERENCES

Albrecht, F., 1933: Ein Strahlungsbilanzmesser zur Messung des Strahlungshaushaltes von Oberflächen. *Meteor. Z.*, **50**, pp. 62—65.

de Graaf, J. C. A., and van der Held, E. F. M., 1953: The Relation between the Heat Transfer and the Convection Phenomena in Enclosed Plane Air Layers. *App. Sci. Res.*, **3 A**, pp. 393—409.

Gier, J. T., and Dunkle, R. V., 1951: Total hemispherical radiometers. *Proc. Amer. Inst. Elect. Engrs.*, **70**, pp. 339—343.

Penman, H. L., 1948: Natural evaporation from open water, bare soil and grass. *Royal Soc. London, Proc.*, **A. 193**, pp. 120—145.

Suomi, V. E., Fransilla, M., and Islitzer, N., 1954: An Improved Net Radiometer. *J. Meteor.*, **11**, pp. 276—282.

Dr. Anders Ångström, 70 years on February 28, 1958.

The name of Anders Ångström is well-known all over the world. His contribution to the science of meteorology is outstanding. He has published a very large number of papers, especially in the fields of climatology and radiation, many of which are of a pioneering character.

As chief of the Meteorological bureau and later on as director of the Swedish Meteorological and Hydrological Institute he has had a great administrative influence on the meteorological activity in Sweden and also has played an important part in many international conferences and meetings, for instance of the World Meteorological Organization and the International Union of Geodesy and Geophysics. After his retirement in 1955 he has continued his scientific work and is now among other things working on a further development of the Ångström pyrheliometer. When the Swedish Geophysical Society was founded in 1920 Dr. Anders Ångström belonged to the first group of members and after one year he was elected secretary of the Society, which post he held for 15 years. He has also been President of the Society for two periods, namely 1936—38 and 1948—50. In the discussions he has always taken an active part and with his stimulating enthusiasm and personal charm he has contributed in an extraordinary way to the spirit of the Society and to an atmosphere of comfort. In 1956 Dr. Ångström was elected honorary member of the Society.

The Swedish Geophysical Society wants to pay homage to and to congratulate him on his 70th anniversary, wishing him still many years of success in the science of meteorology.

A. Nyberg.

The Fourth Annual Conference in Atmospheric Chemistry May 20—22, 1957

By GEORG HUGO NEUMANN, International Meteorological Institute in Stockholm

The fourth in a series of informal conferences on atmospheric chemistry was held at the International Meteorological Institute in Stockholm, May 20—22, 1957.

The first two days were devoted to lectures and discussions at the Institute in Stockholm, whereas the third day was traditionally spent at the Royal Agricultural College in Ultuna.

The conference was attended by the following representatives.

A. P. Baez, Mexico
L. D. Baver, Hawaii
W. Bleeker, Netherlands
B. Bolin, Sweden
J. Bouquiaux, Belgium
G. Brodin, Sweden
K. Buch, Finland
L. K. Coachman, Norway
W. Dansgaard, Denmark
D. Djurić, Yugoslavia
B. R. Döös, Sweden
M. Eaton, U.S.A.
H. Egnér, Sweden
T. Enns, Norway
E. Eriksson, Sweden
S. Fonselius, Sweden
E. M. Fournier d'Albe, Mexico
J. Grandjean, Belgium
K. Groth, Sweden
Edw. Hemmingsen, Norway
B. Holma, Sweden
Ed. Jess, U.S.A.
O. Johansson, Sweden
Chr. Junge, U.S.A.
F. Koroleff, Finland
O. Lang-Rasmussen, Denmark
S. K. Love, U.S.A.
J. Låg, Norway
W. Mordy, U.S.A.
G. Neumann, Sweden
B. C. V. Oddie, England
C. Rooth, Sweden
E. Schmacke, Sweden
P. Scholander, Norway
B. Torsell, Sweden
S. Williams, U.S.A.
A. Wiin-Nielsen, Denmark
G. Witt, Sweden

In some introductory remarks it was pointed out by Mr. Erik Eriksson that there had been a considerable expansion of the general field of atmospheric chemistry since the first conference, held in 1954. New topics have been included in the field and it is no longer possible to cover the whole field in a small conference of the present make up. Hence those subjects which are of greatest common interest have to be favoured in the program.

For tracing and recognizing the paths of various compounds through the atmosphere, isotope-techniques have gained increasing importance during the last few years. Consequently several lectures will be devoted to the application of isotope studies.

Another topic of major importance concerns surface films, their properties and possible geochemical significance.

The first day of the conference was devoted primarily to subjects concerning the CO_2-

content in the atmosphere. This series of lectures was begun by Dr. Bolin, who gave a general survey of the CO_2-circulation in nature.

It is possible at present to give a rather complete picture of this circulation between the different natural reservoirs of carbon dioxide. By the work of several investigators (Craig, Revelle & Suess, Arnold & Anderson, Tellus 9: 1 pp. 1—32 1957) the possibility of quantitative estimates of exchange rates using radiocarbon data has been demonstrated. Especially remarkable is the good agreement for the half-life of CO_2 in the transport between the atmosphere and the upper part of the sea (the so called mixed layer) obtained by different workers.

It would, however, be of great importance to know more about the CO_2-transport between the mixed layer and the deep sea. Dr. Bolin concluded by suggesting the following four topics to be subjected to more intensive research.

1) Determinations of C^{14} in the ocean and especially in the mixed layer.
2) Simultaneous measurements of CO_2 in the sea and in the atmosphere.
3) Carbon dioxide measurements in the free atmosphere.
4) Measurements in critical regions (Polar-regions and the Equator).

In the discussion following this general survey the interest was concentrated around questions of the general circulation of CO_2, the C^{14}-dilution process by combustion of fossil carbon (the "Suess effect") and on the representativity of the CO_2-data from the Scandinavian network.

Dr. Christian E. Junge pointed out that the average time for the transport of CO_2 from the stratosphere to the troposphere is probably of the same order as the corresponding figure for the transport from the atmosphere to the mixed layer (10 years according to Revelle & Suess).

On a question of Dr. E. M. Fournier d'Albe, Mr. S. Fonselius said that there has not been observed any systematic seasonal variations in the Scandinavian CO_2-data.

In a short lecture Mr. Erik Eriksson gave a brief account on some CO_2-measurements he had made during a cruise on board the Soviet icebreaker "Ob" in the sea between Spitzbergen and Greenland. The air samples taken in this area, partly covered with drift-ice, showed rather high CO_2-values but with considerable variations. He thought that the explanation for this is the slow exchange with sea water of descending CO_2-rich air, probably of tropical origin.

In another short paper Mr. S. Fonselius showed some CO_2-data recently obtained from air samples taken on a voyage from Montevideo to Stockholm. It was remarkable that these data fitted very well into the pattern of the CO_2 partial pressure in the ocean at 100 m depth obtained during the "Meteor"-expedition in 1927—28. This indicates that the upwelling regions are important sources for CO_2 in the atmosphere.

Mr. W. Bischof described some flights (both with propeller-plane and with glider) which he had undertaken to obtain CO_2-analyses of air sampled from air planes. Data from the Mälar-district west of Stockholm and from Åre in the north showed large variations both with time and altitude.

The possibility of obtaining information on past atmospheric compositions was demonstrated by Mr. L. K. Coachman, who presented some figures on the composition of glacier-ice gas enclosures. As both nitrogen and argon can be regarded as strictly conservative, the expected composition with respect to oxygen and carbon dioxide can be computed and compared to actual data. He showed that for Greenland glacier ice the oxygen content of the enclosed air was close to that expected, but for CO_2 the analyses were scattered around a value nearly twice as high as at present. This could be due to a different composition of air with respect to CO_2 in the past. The technique used in the determinations was illustrated by an excellent colour film.

In connection with this work Mr. Edward Hemmingsen described some measurements of CO_2- and O_2-diffusion through ice. The rate constants obtained were very low, thus excluding the possibility of gas escape from ice-enclosures. Furthermore Mr. Hemmingsen described a technique for sampling CO_2 from enclosed air in glacier ice in quantities large enough for C^{14} dating. The technique is ingenious and simple, though

necessarily time consuming. At least five cubic meters of ice have to be melted and extracted.

The next session was devoted to surface films. Mr. C. Rooth gave an orientation of theoretical questions involved under both idealized conditions and field conditions. He pointed out that surface active agents present on cloud droplets could have some influence on the rate of evaporation from these.

Mr. K. Groth gave a brief survey of the surface chemistry of long chain alcohols and acids and showed some practical results he had obtained in field experiments on evaporation control by spreading mixtures of cetyl alcohol and red iron oxide on snow surfaces.

The possible effect of surface films on the coalescence of cloud droplets was discussed by Mr. W. A. Mordy. He described some experimental arrangements for studying the process of coalescence of droplets as a function of size and relative velocity. The experiments were illustrated by an interesting film taken by means of a high speed camera at a rate of 3,000 frames per second, showing the process of collision between different droplets. It was obvious from the film that the simple Langmuir theory cannot account for the observed processes. The presence of surface films in some examples was apparently related to elastic bounces of the colliding droplets. In the discussion possible electric effects were also mentioned.

In the next paper Mr. G. H. Neumann drew attention to the fact that the content of organic matter in precipitation frequently amounts to about 50 % of the total solid content. There are great difficulties involved in the determination of the total organic carbon present but it has been possible to develop a few relative micro-methods based on the consumption of suitable oxidizing agents under standardized conditions. Even ultraviolet absorbtion spectra from precipitation samples gave some interesting results. Mr. Neumann concluded his talk by showing some results obtained from the Scandinavian network and some data from micro-elementary analysis of snow samples.

In the discussion that followed Professor J. Låg remarked that the elementary analyses indicated that humic substances were important organic constituents in precipitation. Mr. Eriksson agreed upon this and said that the ultraviolet spectra supported this conclusion.

The second day of the conference was partly devoted to a review concerning atmospheric chemical networks. Of special interest were some reported extensions of the present European network. If possible, stations in South-Eastern Europe will be incorporated. The conference even got reports about some new stations in Belgian Congo.

Dr. E. M. Fournier d'Albe mentioned that there are plans to develop a rather extended network in Mexico. The topography of the country makes it possible to make studies of the variation of the chemical climate with altitude. In spite of difficulties in organization four sampling stations are now in operation.

Dr. Fournier d'Albe also mentioned that the Mexican stations will possibly be equipped with an automatic rainwater collector which permits to collect fractions of a single shower. This will be of great interest from the cloud physics point of view. Concerning this later subject Dr. Fournier d'Albe discussed the theoretical possibilities of studying the mechanism of NaCl-cloud seeding by observing changes of the Cl/Na-ratios in artificially initiated showers.

The American network plans were discussed by Dr. S. K. Love. He emphasized that much would be gained by a critical review of many analytical methods now used by various networks. There is surely still a great risk that some of the data obtained may be unreliable, in spite of the representative sampling. He also recommended that different network organizations have their own analytical laboratories instead of depending upon analyses made by commercial companies.

Speaking of plans for a network which could succeed the US Air Force network formerly organized by Dr. Junge, Dr. Love said that there were preliminary plans for running a limited US network during the IGY. Furthermore there are plans for a world-wide investigation of dissolved matter carried by surface streams to the sea. This investigation should comprize about 65 of the most important rivers in the world, and Dr. Love mentioned that it would be enough to take four samples per year from every river.

The analyses will be carried out in the United States or, if facilities are available, also in other countries. Because of the short preparatory time available these investigations will probably just get started during the IGY, but should then be continued at least for another year.

In connection with this Dr. Bolin mentioned the possible importance of direct ground water transport of dissolved material from land to sea.

The next session was concerned with isotopes in atmospheric chemistry. Three papers were devoted to this topic.

Professor W. Bleeker gave an account on the organizational work hitherto done in order to set up a network for regional radioactivity measurements. The working group, selected at the radioactivity conference in Brussels last year, made some preliminary recommendations at the meeting in Utrecht in January this year. Air filtration samples should be taken in 24-hour periods using a uniform method described in a manual by the working group. For a world-wide network, a density of one sampling station in every 10^5 km^2 is recommended. It would be of great value to coordinate the radioactivity determinations with radiosondings. Besides measurements of the total natural radioactivity, special samples should be taken for determination of fission products such as Sr^{90} and Cs^{137}. For tracing air masses in general and determining vertical mixing ratios and particle storage times there is also need for radioactivity measurements. Finally Professor Bleeker pointed out the possibility of determining the "preatomic" tritium content in air from ice-samples.

Dr. Bolin mentioned in the discussion that there had been recommendations on total fallout networks of the same density. The latitudinal distribution of radioactivity would be most interesting from a meteorological point of view as it should give some hint on where the essential mixing between stratosphere and troposphere takes place.

A second contribution to the isotope-discussion was made by Dr. W. Dansgaard who had made mass-spectrometric studies of the O^{18} content of different natural waters. There was much evidence for a "distillation column" effect in atmospheric evaporation and condensation. This effect seems to result in a correlation between the yearly mean temperature and the O^{18} content of fresh water in a geographical region. With this relation it would be possible to study past climatic conditions by analysing O^{18} in glacier ice of known age.

Finally Mr. E. Eriksson discussed the use of tritium in the study of the hydrological cycle. With a paper by Begemann & Libby (1956) as a starting point, Mr. Eriksson showed that with a more refined model of the circulation of water than that of Begemann & Libby, quite different results are arrived at. The estimated ground water storage becomes much less than in their case and their assumption about a short residence time of tritium in the stratosphere can be questioned.—Their assumption about rapid mixing of ground water seems to be unsatisfactory and may lead to unlikely results. An empirical method based upon tritium determinations in river water for obtaining the time characteristics of ground water basins was suggested.

On the last day of the conference Dr. Christian E. Junge discussed results obtained from the US Air Force precipitation-sampling network. An impressive amount of work has been done in collecting data from 63 stations involved in the network. The character of this network was rather different from that in Scandinavia, not only with respect to the lower density of stations in the United States, but also with respect to the careful precautions taken by Dr. Junge to prevent atmospheric dust and dry fall-out to mix with the precipitation samples. Dr. Junge showed the regional distribution of various inorganic ions. The data involved the same ions as the Scandinavian current data. Dr. Junge made some interesting remarks on the Cl/Na ratio in precipitation. In all inland stations this ratio was considerably smaller than the corresponding value in sea water. The same phenomenon was much discussed in connection with the analysis of the Scandinavian data. Dr. Junge thought it rather unlikely that this effect was due to a depletion of chloride from the precipitation. The other possibility would thus be an addition of sodium. But this could not probably be effected by sodium contamination from continental sources. According to Dr. Junge there might perhaps be an addition of

extra-terrestrial sodium from the stratosphere. There was no direct evidence against such a hypothesis. Finally Dr. Junge described some laboratory experiments showing the formation of ammonium sulphate aerosols from gaseous ammonia, sulphur dioxide and water at different pH.—Such a process could be responsible for the formation of a "London fog".

In the discussion Mr. Eriksson pointed out that addition of such amounts of extra terrestrial sodium are not compatible with the geochemistry of the sea. There are already difficulties involved in explaining the great excess of sodium in river waters after subtraction of "cyclic" sodium based upon the chloride-content in river water, unless one considers a separation of Cl from sea salts in the free atmosphere. There are likely processes that can well explain this separation.

Mr. G. Brodin concluded the series of papers by reporting some preliminary results obtained by him from analyses of precipitation for iodine, phosphorus and boron. These three elements are present in lower amounts than the elements hitherto considered. It is therefore necessary to apply certain micro-methods in the determinations. In spite of great technical difficulties the work will be continued, especially because of the medical and agricultural importance of these minor elements in the atmosphere.

In the evening the participants of the conference were guests at a dinner party given by the Agricultural College in Ultuna.

Map and Coordinates of the Chemical and CO_2 Stations Western Europe

Prepared by STIG FONSELIUS, International Meteorological Institute in Stockholm.

Note: The Station Kn is analyzed by the Swedish Finnish Swiss Expedition at Murchinson Bay, Spetsbergen, the stations Ri to Hi, Rj and Za at R. Agricult. College, Uppsala, Sweden, the stations So to Tv at Inst. Marine Research, Helsinki, Finland, Vn to Ad at Statens Planteavlslaboratorium, Lyngby, Denmark, Lw to Ca at Met. Office, Air Ministery, London, England, The station Va at Met. Office, Dublin Airport, Ireland, Sc to Bl at Staatl. Landwirtschaftl. Versuchs- und Forschungsanst. Augustenberg, Germany and DH to Ae at Institu td'Hygiene et d'Epidemiologie Bruxelles, Belgium. The CO_2 samples are analyzed at Int. Met. Inst. Stockholm, Sweden, except Kn, which is analyzed at Murchinson Bay and the stations So to Tv, which are analyzed at Inst. Marine Research, Helsinki.

In order to standardize the Code systems for the two networks, the names and codes for following stations are changed in the CO_2 network:

Station	Code	New Name	New Code
Abisko.....	Ab	Abisko.....	Ao
Bodö.....	Bo	Vågönes.....	Vg
Rissala.....	Ri	Kuopio	Ku
Luonetjärvi ...	Lu	Jyväskylä.....	Jy

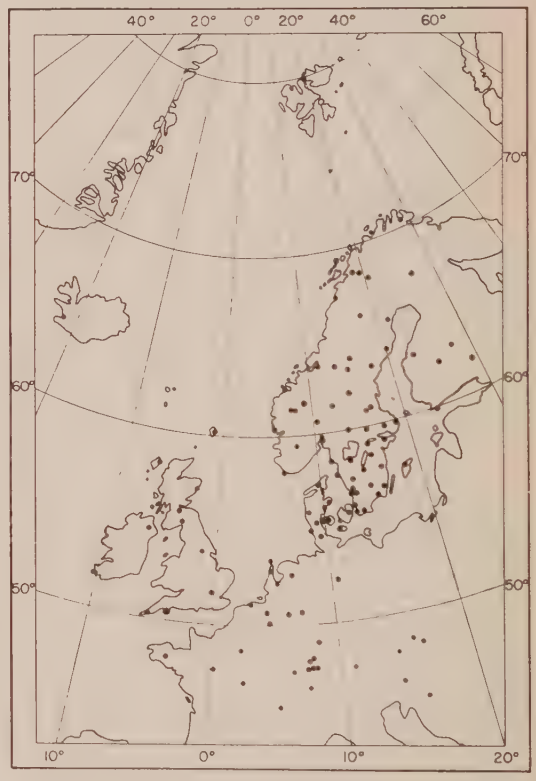

Coordinates of Stations for Precipitation, Air and CO_2

Name	Code	Altitude m	Latitude N	Longitude	Greenwich	Precip.	Air	CO_2
Kinnvika	Kn	—	80°03′	18°18′	E	×	×	×
Riksgränsen	Ri	508	68°26′	18°08′	E	×	×	
Abisko	Ao	390	68°20′	18°45′	E			×
Kiruna	Ki	412	67°52′	20°14′	E	×	×	
Arjeplog	Ar	434	66°03′	17°54′	E	×	×	
Öjebyn	Öj	—	65°24′	21°30′	E	×	×	×
Röbäcksdalen	Rö	—	63°48′	20°12′	E	×	×	
Offer	Of	—	63°12′	17°48′	E	×	×	
Bredkälen	Br	400	63°54′	15°18′	E	×	×	×
Åre	ÅF	440	63°24′	13°06′	E	×	×	
Åre Hummeln	ÅH	900	63°24′	13°06′	E	×		
Frösön	Fö	364	63°12′	14°29′	E	×		
Sveg	Sv	356	62°02′	14°22′	E	×		
Rättvik	Rä	200	60°54′	15°06′	E	×	×	
Åmot	Åm	175	60°58′	16°25′	E	×	×	
Sala	Sa	80	60°00′	16°36′	E	×	×	
Ultuna	Ul	50	59°48′	17°42′	E	×	×	
Erken	Er	12	59°54′	18°42′	E	×	×	×
Strängnäs	St	20	59°18′	17°06′	E	×	×	
Forshult	Fo	192	60°10′	13°47′	E	×	×	
Kvarntorp 7	Kv7	100	59°12′	15°30′	E	×	×	
Vreta Kloster	VK	40	58°36′	15°38′	E	×		
Lanna	La	100	58°24′	13°06′	E	×	×	
Bornö	Bo	5	58°24′	11°36′	E	×	×	
Vinga	Vi	19	57°38′	11°37′	E	×	×	
Falsterbobruk	Fa	50	57°42′	16°12′	E	×	×	
Flahult	Fl	225	57°42′	14°12′	E	×	×	×
Ambjörnarp	Am	220	57°25′	13°17′	E	×		
Fröslida	Fi	70	56°53′	13°03′	E	×		
Simlångsdalen	Si	150	56°42′	13°00′	E	×		
Plönninge	Pl	50	56°42′	12°45′	E	×	×	×
Söraby	Sö	180	57°00′	14°54′	E	×		
Smedby	Sm	20	56°42′	16°12′	E	×	×	
Sylfaste	Sy	40	57°36′	18°24′	E	×	×	
Bräkne-Hoby	BH	40	56°12′	15°06′	E	×	×	
Skurup	Sk	40	55°28′	13°30′	E	×	×	
Alnarp	Al	20	55°42′	13°06′	E	×	×	
Hilleshög	Hi	—	55°54′	12°54′	E	×		
Tana	Ta	9	70°24′	28°12′	E	×	×	×
Andenes	An	5	69°19′	16°07′	E	×		
Vågönes	Vg	19	67°16′	14°20′	E			×
Ytterøy	Yt	74	63°48′	11°13′	E	×		
Gjermundnes	Gj	51	62°37′	7°10′	E	×		
Fortun	Fn	27	61°30′	7°42′	E	×		
Fanaråken	Få	2 026	61°31′	7°54′	E	×		
Vågåmo	Vå	371	61°52′	9°06′	E	×	×	×
Trysil	Tr	362	61°20′	12°15′	E	×		
Kise	Ke	128	60°46′	10°49′	E	×		
Stend	Sd	—	60°17′	5°20′	E	×		×
Dalen	Da	77	59°27′	8°00′	E	×		
Ås	Ås	95	59°40′	10°47′	E	×	×	
Lista	Li	14	58°06′	6°34′	E	×	×	
Sodankylä	So	180	67°22′	26°39′	E	×	×	×
Kauhavia	Ka	50	63°06′	23°03′	E	×	×	×
Kuopio	Ku	95	63°00′	27°44′	E	×	×	×
Jyväskylä	Jy	145	62°24′	25°40′	E	×	×	×
Punkaharju	Pu	90	61°48′	29°20′	E	×	×	×
Tvärminne	Tv	5	59°54′	23°12′	E	×	×	×
Rjupnahæð	Rj	120	64°05′	21°51′	W	×	×	
Vildmosen	Vn	—	57°12′	9°48′	E	×		
Grenå	Gr	—	56°25′	10°53′	E	×		
Ødum	Ød	—	56°12′	10°05′	E	×	×	×
Borris	Bs	—	55°58′	8°38′	E	×		
Lyngby	Ly	—	55°47′	12°29′	E	×		
Askov	As	—	55°30′	9°08′	E	×	×	×
Væde	Vd	—	55°26′	10°10′	E	×		
Blangstedgård	Bl	—	55°23′	10°27′	E	×		
Tystofte	Ty	—	55°12′	11°10′	E	×	×	
Højer	Hö	—	54°57′	8°41′	E	×		
Abed	Ad	—	54°50′	11°20′	E	×		
Lerwick	Lw	83	60°08′	1°11′	W	×		
Stornoway	Sw	14	58°13′	6°19′	W	×		
Aberdeen	Ab	—	57°10′	2°15′	W	×	×	
Edinburgh	Ed	—	55°53′	3°15′	W	×	×	
Eskdalemuir	Es	242	55°19′	3°12′	W	×		
Aldergrove	Ag	67	54°39′	6°13′	W	×		
Leeds	Le	—	53°50′	1°20′	W	×	×	
Rothamsted	Ro	—	51°48′	0°20′	W	×	×	
Newton Abbot	NA	—	50°32′	3°23′	W	×	×	
Camborne	Ca	88	50°13′	5°19′	W	×		
Valentia	Va	14	51°56′	10°15′	W	×		
Westerland	We	12	54°55′	8°20′	E	×	×	
Schleswig	Sc	48	54°30′	9°32′	E	×	×	
Braunschweig Völkenrode	BV	83	52°17′	10°34′	E	×	×	
Bonn	Bn	62	50°45′	7°06′	E	×	×	
Augustenberg	Au	145	49°00′	8°30′	E	×	×	
Feldberg	Fe	1 493	47°52′	8°01′	E	×	×	
Baldenwegerhof	Ba	348	47°59′	7°57′	E	×	×	
Hohenpeissenberg	Ho	975	47°48′	11°01′	E	×	×	
Ringsheim	Rm	170	48°15′	7°46′	E	×	×	
Ettenheim	Et	202	48°16′	7°49′	E	×	×	
Heitersheim	He	225	47°52′	7°40′	E	×		
Retz	Rz	243	48°46′	15°58′	E	×	×	
Wien	Wi	203	48°15′	16°22′	E	×	×	
Linz	Lz	309	48°04′	14°25′	E	×	×	
Klagenfurt	Kl	448	46°39′	14°20′	E	×	×	
Bern-Liebefeld	BL	550	46°56′	7°25′	E	×	×	
Vlieland	Vl	—	53°15′	4°55′	E			×
Den Helder	DH	6	52°58′	4°45′	E	×	×	
De Bilt	DB	10	52°06′	5°11′	E	×	×	
Witteveen	W	18	52°48′	6°40′	E	×	×	
St. André	SA	14	51°10′	3°11′	E	×	×	
Uccle	U	100	50°48′	4°21′	E	×	×	
Botrange	B	694	50°30′	6°06′	E	×	×	
Dourbes	D	224	50°06′	4°36′	E	×	×	
Magny-les-Hameaux	MH	165	48°44′	2°04′	E	×		
Rostrenen	Rs	268	48°14′	3°20′	W	×		
Le Mans	LM	52	47°56′	0°12′	E	×		
Luxeuil	Lx	269	47°47′	6°21′	E	×		
Bourges	Bg	162	47°04′	2°22′	E	×		
Amberieu	Ae	254	45°59′	5°20′	E	×		
Zagreb	Za	163	45°49′	15°59′	E	×	×	

Current Data on the Chemical Composition of Air and Precipitation XII

(For further information see Egnér, H., Eriksson, E., *Tellus* **7**, pp. 134—139, **8**, p. 285 and 517)

Code	mm	mg/m²								pH	HCO_3^- — $\frac{\mu val}{l}$	$\frac{\varkappa \cdot 10^6}{\Omega \cdot cm}$	μg/m³ (= kg/km³)						
		S	Cl	NO_3–N	NH_3–N	Na	K	Mg	Ca				S	Cl	NH_3–N	Na	K	Mg	Ca
	Precipitation June 1957 (D 706)												Air June 1957 (L 706)						
BL	163	167	0	10	20	10	33	8	98	5.4	0	9	8.9	5.1	8.3	2.3	2.2	1.4	1.2
	Precipitation July 1957 (D 707)												Air July 1957 (L 707)						
BL	132	32	24	19	22	12	26	12	106	5.5	0	10	10.9	7.4	7.1	2.9	3.3	1.7	2.7
	Precipitation Aug. 1957 (D 708)												Air Aug. 1957 (L 708)						
Ri	88	37	20	0	0	8	5	8	47	5.8	23	6	1.7	2.1	1.8	0.7	0.7	1.0	5.7
Ki	106	62	11	2	1	7	3	4	20	5.5	0	7	2.2	3.1	1.2	3.2	1.6	1.1	7.0
Ar	127	48	16	2	1	10	10	5	48	5.7	11	6	1.6	*	1.2	0.5	0.4	0.6	3.0
Öj	110	84	25	4	4	9	17	6	80	5.6	10	10	2.3	2.1	3.6	1.2	0.9	1.2	6.7
Rö	75	77	22	5	7	12	6	14	32	5.0	0	13	4.4	4.5	2.6	6.3	1.1	1.5	5.9
Of	71	65	16	3	0	6	6	6	20	5.3	0	8	6.2	0.0	2.6	1.0	0.7	1.3	10.
Br	87	43	18	4	7	10	9	4	38	5.5	0	8	1.3	1.5	1.1	0.5	0.4	0.7	5.6
ÅF	75	57	12	2	1	7	7	5	21	5.1	0	9	*	*	*	*	*	*	*
ÅH	68	64	17	1	1	8	10	3	21	5.3	0	9	—	—	—	—	—	—	—
Fö	63	58	13	5	6	8	9	4	69	6.0	18	10	—	—	—	—	—	—	—
Sv	106	53	23	10	1	7	5	4	18	5.0	0	8	—	—	—	—	—	—	—
Rä	*	*	*	*	*	*	*	*	*	*	*	*	2.8	3.2	1.8	0.8	1.0	0.5	4.5
Åm	145	70	25	8	0	14	8	16	45	6.3	12	6	3.1	0.0	1.8	0.7	0.5	0.9	5.5
Sa	74	67	20	9	7	12	7	10	56	6.3	19	12	7.5	3.4	1.7	0.6	0.6	0.8	4.2
Ul	111	100	24	10	8	10	9	9	38	5.2	0	12	2.4	2.6	3.7	0.8	1.2	2.2	4.2
Er	106	89	44	4	7	18	14	10	35	5.5	0	18	2.4	0.0	1.3	0.5	0.7	2.0	5.5
St	68	71	27	6	6	19	12	7	76	6.0	23	14	2.5	3.3	2.5	0.5	0.7	1.1	2.4
Fo	146	110	54	8	7	25	8	10	49	5.1	0	13	2.5	2.8	2.1	0.7	0.7	1.2	5.0
Kv1	67	620	40	8	19	33	34	19	980	6.8	305	124	*	*	*	*	*	*	*
Kv7	47	88	25	5	3	20	8	7	61	5.9	0	18	3.3	2.9	3.7	1.1	1.0	1.3	14.
VK	77	73	35	11	14	18	12	6	71	6.2	22	13	—	—	—	—	—	—	—
La	73	61	72	11	48	38	35	9	47	6.3	28	18	2.7	2.8	2.5	1.2	0.8	0.7	3.5
Bo	132	69	420	32	26	260	20	39	73	5.5	0	25	2.5	4.7	1.2	2.0	0.5	1.0	7.6
Vi	95	190	2 010	16	16	1120	55	140	83	4.6	0	107	4.2	*	1.3	15.	1.2	3.2	3.4
Fa	44	52	32	7	8	15	11	5	43	5.3	0	17	1.8	2.4	1.6	0.8	0.5	0.8	3.3
Fl	104	84	57	17	8	33	14	8	28	4.8	0	15	3.3	3.7	3.1	1.5	1.5	3.5	39.
Am	141	61	180	20	15	94	19	17	76	5.4	0	16	—	—	—	—	—	—	—
Fi	—	—	—	—	—	—	—	—	—	—	—	—	—	—	—	—	—	—	—
Si	108	95	130	12	15	81	12	11	62	5.5	0	16	—	—	—	—	—	—	—
Pl	110	110	200	18	12	120	13	17	28	4.7	0	24	2.4	4.1	3.3	1.2	0.6	1.3	2.9
Sö	107	97	43	11	9	48	14	12	58	5.2	0	15	—	—	—	—	—	—	—
Sm	151	73	28	12	18	11	11	7	27	4.8	0	15	5.0	5.4	3.4	1.7	2.0	3.3	18.
Sy	109	57	41	8	1	19	13	6	95	5.7	7	10	1.6	5.6	5.3	1.4	2.0	1.7	11.
BH	109	99	49	18	26	22	17	10	45	4.6	0	24	2.4	3.0	8.5	0.7	0.6	1.3	3.7
Sk	74	94	77	15	28	52	13	11	53	4.7	0	27	6.2	3.2	3.6	1.7	1.2	0.9	2.2
Al	105	86	87	19	23	50	13	14	76	4.8	0	22	2.7	2.6	3.0	1.2	0.4	2.2	4.4
Hi	59	88	78	13	18	43	9	9	60	5.5	0	23	—	—	—	—	—	—	—
Ta	56	28	27	1	0	17	6	9	28	5.9	10	7	*	*	*	*	*	*	*
An	—	—	—	—	—	—	—	—	—	—	—	—	—	—	—	—	—	—	—
Yt	39	19	32	2	2	20	5	6	16	5.5	0	10	—	—	—	—	—	—	—
Gj	75	42	68	1	2	37	4	8	26	5.8	7	8	—	—	—	—	—	—	—
Fn	58	86	12	2	3	10	13	4	36	5.6	14	10	—	—	—	—	—	—	—
Få	*	*	*	*	*	*	*	*	*	*	*	*	—	—	—	—	—	—	—
Vå	59	45	11	3	0	24	17	8	58	6.0	21	12	12.	10.	27.	3.7	5.9	3.9	16.

Code	mm	mg/m²								pH	$HCO_3^- - \frac{\mu val}{l}$	$\frac{\varkappa \cdot 10^6}{\Omega \cdot cm}$	μg/m³ (= kg/km³)						
		S	Cl	NO_3–N	NH_3–N	Na	K	Mg	Ca				S	Cl	NH_3–N	Na	K	Mg	Ca
	Precipitation Aug. 1957 (D 708)												Air Aug. 1957 (L 708)						
Tr	143	43	32	3	5	12	9	5	31	5.4	0	6	—	—	—	—	—	—	—
Ke	95	20	18	8	9	13	8	5	36	5.2	0	9	—	—	—	—	—	—	—
Sd	101	35	114	2	5	70	10	14	29	5.4	0	13	—	—	—	—	—	—	—
Da	104	80	22	10	7	15	11	6	45	4.8	0	16	—	—	—	—	—	—	—
Ås	103	73	48	10	7	34	11	9	25	4.7	0	16	*	*	*	*	*	*	*
Li	127	130	1 720	17	8	940	59	130	140	4.9	0	66	3.2	8.0	1.6	44.	2.6	6.3	23.
So	56	0	0	11	7	4	0	0	15	4.9	0	9	—	—	—	—	—	—	—
Ka	85	150	358	19	12	8	39	9	60	5.0	0	9	14.5	12.5	6.8	0.9	2.3	0.0	2.3
Ku	73	820	270	13	7	12	5	0	39	5.1	0	8	35.0	29.5	6.3	3.7	8.4	0.4	71.0
Jy	134	0	540	88	13	—	0	0	153	4.5	0	9	0.0	12.4	6.1	0.5	1.1	0.0	1.3
Pu	62	326	115	10	4	3	0	0	36	5.2	0	7	23.6	39.5	89.0	1.0	9.5	0.5	7.6
Tv	42	166	610	7	4	30	20	2	27	5.3	0	11	26.0	696.	4.9	42.	12.6	13.2	450.
Vn	114	116	249	18	34	164	21	28	71	5.2	0	19	—	—	—	—	—	—	—
Gr	68	153	193	16	32	138	24	17	111	5.0	0	31	—	—	—	—	—	—	—
Öd	89	62	210	17	33	150	26	20	69	5.4	3	26	3.0	3.7	4.4	4.0	0.9	1.6	6.0
Bs	123	138	631	16	20	368	38	49	54	4.7	0	33	—	—	—	—	—	—	—
Ly	82	128	112	19	39	69	16	22	93	4.8	0	27	—	—	—	—	—	—	—
As	104	48	60	16	33	240	23	41	59	5.2	0	31	*	*	*	*	*	*	*
Vd	100	150	225	22	96	146	41	25	68	5.9	0	25	—	—	—	—	—	—	—
Bl	82	130	138	17	40	89	15	24	82	4.5	0	33	—	—	—	—	—	—	—
Ty	64	87	44	17	31	100	19	29	78	6.1	26	31	6.9	9.9	7.5	6.5	1.8	3.9	37.
Hö	134	172	1 498	19	30	848	51	118	62	4.9	0	55	—	—	—	—	—	—	—
Ad	74	62	138	18	36	83	13	16	39	5.0	0	22	—	—	—	—	—	—	—
Ab	184	230	370	40	76	240	48	56	84	4.6	0	32	12.	6.2	3.9	2.1	1.3	7.5	43.
Ed	119	98	190	16	28	140	37	33	150	5.8	17	22	6.8	2.5	2.4	1.1	0.4	1.1	3.7
Le	123	200	220	35	78	140	30	45	190	6.2	20	30	5.4	2.9	3.0	1.1	0.4	1.6	7.7
Ro	52	78	110	17	28	56	20	13	73	6.0	11	29	4.8	2.0	2.7	1.6	0.9	1.0	7.6
NA	61	110	430	15	126	280	170	36	130	6.5	238	75	12.	7.1	5.1	2.7	1.0	3.5	11.0
Va	84	101	916	23	13	—	—	—	—	5.4	0	50	—	—	—	—	—	—	—
Sc	170	248	765	58	78	283	36	61	109	4.9	0	30	10.0	14.2	5.1	5.9	1.8	0.8	1.2
BV	80	188	96	42	26	51	20	27	127	5.1	0	35	15.8	8.2	7.1	1.1	1.5	0.8	1.1
Bn	83	225	142	33	27	47	12	37	290	6.5	68	45	22.4	18.7	11.9	5.1	2.7	3.8	3.3
Au	101	116	141	40	3	26	97	27	145	5.5	0	19	16.0	19.2	8.1	4.3	1.2	5.3	2.0
Fe	81	74	32	15	9	25	3	3	28	5.4	0	12	16.8	5.2	3.3	1.2	1.0	1.0	1.8
Ba	94	129	37	17	0	14	15	6	60	5.2	0	12	7.8	8.2	3.4	0.9	0.8	0.6	0.7
Ho	135	143	40	35	4	12	16	26	144	6.5	45	17	13.7	22.7	4.3	1.5	0.5	0.7	1.3
Rm	85	82	34	16	5	16	9	3	269	6.7	135	31	8.0	4.8	6.9	7.6	0.8	0.5	1.7
Et	81	96	32	12	8	11	11	6	81	5.8	0	17	5.5	9.3	6.0	14.1	1.1	0.8	1.0
He	160	182	240	53	144	66	37	16	149	6.1	15	22	—	—	—	—	—	—	—
Rz	63	81	0	11	12	1	6	15	77	6.1	5	18	7.4	4.5	6.0	4.3	1.1	1.8	23.4
Wi	66	82	53	15	13	5	11	9	100	6.2	20	21	6.8	7.6	5.5	6.8	1.2	0.5	1.0
Lz	52	69	0	15	7	12	7	12	194	6.8	305	47	8.1	8.1	6.8	2.1	1.4	0.6	1.9
Kl	88	105	106	23	23	21	12	11	94	6.1	20	19	12.3	5.1	6.2	6.3	1.0	3.4	17.1
BL	84	218	17	17	20	20	21	0	92	5.8	4	13	10.5	4.4	7.9	2.4	4.9	1.2	3.3
DH	122	165	676	33	28	389	36	52	78	5.0	0	114	9.6	34.5	3.9	20.5	2.5	5.2	3.2
DB	135	358	734	61	75	486	35	32	124	4.2	0	70	6.1	5.8	4.1	1.7	0.5	3.2	1.5
W	110	107	308	23	32	204	18	35	38	4.5	0	34	10.5	3.3	4.3	3.5	1.3	5.5	0.9
SA	118	140	156	28	74	145	29	19	66	5.5	0	23	10.2	5.9	4.2	1.8	0.8	3.7	1.0
U	142	168	355	30	45	209	35	38	147	5.0	0	20	17.5	6.3	4.1	1.8	0.9	3.4	2.1
B	180	224	104	46	170	44	26	12	95	5.9	17	15	9.0	4.0	2.4	1.0	0.5	1.8	1.0
D	78	84	145	13	17	69	11	14	58	5.4	0	18	6.8	3.6	3.3	1.4	0.5	2.1	1.3
Za	103	34	55	19	29	42	44	52	270	6.4	94	29	—	—	—	—	—	—	—
	Precipitation Sept. 1957 (D 709)												Air Sept. 1957 (L 709)						
Ri	26	15	20	1	1	5	2	3	37	6.1	68	6	3.8	12.	2.0	3.0	2.7	1.0	14.
Ki	48	16	14	4	6	12	5	3	23	5.0	0	13	2.7	4.7	1.0	2.2	2.4	0.2	2.6
Ar	52	8	15	4	4	9	5	3	29	5.2	0	10	1.5	1.4	1.0	0.4	0.6	0.3	2.0

Code	mm	mg/m²								pH	$HCO_3 - \frac{\mu val}{l}$	$\varkappa \cdot 10^6 / \Omega \cdot cm$	$\mu g/m^3$ (= kg/km³)						
		S	Cl	NO_3–N	NH_3–N	Na	K	Mg	Ca				S	Cl	NH_3–N	Na	K	Mg	Ca
		Precipitation Sept. 1957 (D 709)											Air Sept. 1957 (L 709)						
Öj	83	7	22	13	14	13	9	4	53	4.9	0	13	2.0	0.6	3.4	1.0	0.8	0.4	2.1
Rö	97	64	37	8	10	21	9	14	45	4.9	0	12	7.0	10.	4.0	17.	2.4	3.3	13.
Of	110	87	28	10	7	17	15	8	20	4.9	0	14	1.9	5.9	1.7	1.1	1.0	1.5	7.6
Br	61	44	12	5	11	11	7	4	30	5.1	0	9	1.7	6.1	1.5	1.0	0.7	1.3	7.4
ÅF	99	22	29	3	4	23	5	6	52	6.1	14	6	*	*	*	*	*	*	*
ÅH	94	52	15	5	9	12	5	5	25	4.8	0	12	—	—	—	—	—	—	—
Fö	60	55	17	7	9	8	17	5	60	5.8	10	9	—	—	—	—	—	—	—
Sv	91	46	20	4	5	10	5	5	27	5.4	0	6	—	—	—	—	—	—	—
Rä	35	25	7	3	4	4	3	1	95	6.5	80	18	1.2	5.6	1.7	0.8	1.2	1.0	3.8
Åm	160	95	27	11	16	12	6	15	35	6.0	5	7	2.3	9.1	1.6	2.9	2.1	1.6	8.0
Sa	140	110	31	7	3	10	16	6	44	5.6	3	10	5.9	1.6	2.0	1.8	1.1	1.8	7.4
Ul	130	77	45	11	13	26	7	9	40	4.9	0	11	2.9	2.1	1.7	1.1	1.2	0.8	1.7
Er	120	58	63	6	6	35	12	9	37	5.0	0	10	3.9	5.5	1.1	0.9	0.7	3.0	4.1
St	120	55	31	12	16	32	13	9	100	5.9	20	10	3.8	5.1	2.0	0.6	0.5	1.4	2.5
Fo	100	86	37	10	9	31	10	10	160	6.5	40	13	3.5	6.4	1.2	0.9	0.6	1.1	4.1
Kv1	94	1040	62	11	80	37	47	30	1060	3.7	0	100	6.4	7.2	8.1	1.6	3.0	7.8	21.
Kv7	76	72	30	5	8	16	7	7	37	4.9	0	15	7.0	12.	4.3	2.0	1.6	3.2	24.
VK	130	130	39	8	10	7	5	4	45	5.5	0	9	—	—	—	—	—	—	—
La	92	71	84	11	27	27	13	10	54	5.8	6	12	2.2	4.6	2.9	1.4	1.4	3.5	22.
Bo	110	65	380	11	10	560	23	69	67	5.7	6	40	2.1	9.1	1.0	7.1	1.2	1.8	10.
Vi	69	230	430	17	14	1670	80	220	96	4.5	0	100	4.9	12.	1.4	9.2	0.9	3.7	3.3
Fa	73	52	28	6	5	17	10	7	43	5.2	0	10	3.0	2.8	1.1	1.0	0.8	0.4	1.9
Fl	120	29	140	11	9	68	23	13	36	4.8	0	15	2.6	2.8	1.1	0.5	0.7	1.6	3.2
Am	140	78	270	14	19	59	9	11	44	5.4	0	13	—	—	—	—	—	—	—
Fi	100	30	140	15	27	170	18	50	34	4.9	0	22	—	—	—	—	—	—	—
Si	210	150	540	31	51	160	18	20	47	5.0	0	21	—	—	—	—	—	—	—
Pl	120	62	330	23	37	270	20	36	37	4.8	0	32	1.1	9.0	3.0	2.9	1.1	1.2	3.5
Sö	88	67	13	14	14	25	9	10	57	5.3	0	14	—	—	—	—	—	—	—
Sm	38	34	27	3	0	16	9	9	43	5.8	35	13	2.7	13.	1.9	1.5	1.1	2.1	12.
Sy	71	67	41	9	17	40	13	8	50	5.5	3	13	3.0	19.	4.6	2.4	2.3	2.8	18.
BH	45	24	104	10	22	84	26	9	46	5.1	0	24	3.6	2.9	7.6	1.1	0.8	3.2	4.5
Sk	43	58	170	18	67	42	110	13	51	6.3	15	45	3.5	2.3	3.5	1.6	2.5	1.1	1.6
Al	52	71	43	14	22	62	13	13	53	4.8	0	31	3.7	2.7	3.3	1.3	0.2	1.8	1.9
Hi	39	17	42	6	11	67	5	8	39	5.8	10	21	—	—	—	—	—	—	—
Ta	47	27	28	2	5	21	5	5	43	5.9	21	10	2.9	2.7	3.2	1.8	2.1	0.8	1.8
An	—	—	—	—	—	—	—	—	—	—	—	—	—	—	—	—	—	—	—
Yt	58	13	61	4	5	33	6	6	27	6.0	14	9	—	—	—	—	—	—	—
Gj	170	110	380	4	11	96	7	14	23	5.7	0	14	—	—	—	—	—	—	—
Fn	72	42	17	3	3	12	7	6	43	5.6	0	8	—	—	—	—	—	—	—
Få	57	14	15	2	3	12	6	2	18	5.9	1	5	—	—	—	—	—	—	—
Vå	59	31	14	3	4	5	6	5	44	5.8	8	7	21.	36.	14.	3.4	5.0	10.	45.
Tr	130	66	7	7	7	6	15	5	20	5.4	0	5	—	—	—	—	—	—	—
Ke	110	58	29	7	6	8	1	4	36	5.4	0	7	—	—	—	—	—	—	—
Sd	110	61	57	4	4	200	16	27	45	5.3	0	17	—	—	—	—	—	—	—
Da	100	38	19	6	4	100	8	5	31	5.1	0	12	—	—	—	—	—	—	—
Ås	110	52	64	14	10	10	13	16	31	5.1	0	16	—	—	—	—	—	—	—
Li	160	210	2 620	14	10	900	63	170	85	5.0	0	0	6.6	26.	16.	14.	1.7	2.5	12.
So	58	*	*	6	6	11	5	0	22	4.9	0	10	57.	0.0	57.	60.	18.	0.0	60.
Ka	41	*	*	5	2	7	7	1	58	6.2	28	12	12.6	52.	10.6	12.5	2.5	2.0	12.5
Ku	88	*	*	9	7	8	8	0	23	4.9	0	12	0.0	48.0	6.6	2.9	1.5	0.0	19.
Jy	83	*	*	9	10	15	13	2	86	6.0	160	10	10.	1.2	—	2.0	0.7	0.0	1.7
Pu	103	*	*	11	10	11	0	0	81	5.1	0	10	7.9	47.	5.3	10.0	1.3	0.0	4.4
Tv	92	*	0	9	8	37	13	0	55	4.8	0	13	0.0	77.	18.	12.0	7.0	7.6	30.
Vn	95	100	574	15	23	316	26	45	68	5.7	0	30	—	—	—	—	—	—	—
Gr	64	96	264	23	46	166	30	20	73	4.9	0	37	—	—	—	—	—	—	—
Öd	64	57	230	13	30	150	17	17	53	5.3	7	28	1.9	4.3	4.0	1.7	0.9	1.2	5.9
Bs	120	159	1 004	20	29	568	41	87	208	6.1	14	42	—	—	—	—	—	—	—

Code	mm	mg/m²								pH	$HCO_3^- \frac{\mu val}{l}$	$\varkappa \cdot 10^6 \frac{}{\Omega \cdot cm}$	μg/m³ (= kg/km³)						
		S	Cl	NO_3–N	NH_3–N	Na	K	Mg	Ca				S	Cl	NH_3–N	Na	K	Mg	Ca
		Precipitation Sept. 1957 (D 709)											Air Sept. 1957 (L 709)						
Ly	74	108	221	21	31	134	21	23	51	4.6	0	37	—	—	—	—	—	—	—
As	110	34	500	21	46	470	24	46	71	5.1	0	35	2.0	0.6	3.1	1.6	1.2	0.9	5.5
Vd	109	123	388	20	37	216	82	44	155	5.9	16	27	—	—	—	—	—	—	—
Bl	81	111	173	19	28	111	15	20	59	4.8	0	30	—	—	—	—	—	—	—
Ty	58	26	150	19	42	180	17	33	68	6.1	40	38	13.	17.	6.0	8.3	4.7	3.5	5.5
Hö	125	165	1 469	26	36	846	60	110	69	4.8	0	59	—	—	—	—	—	—	—
Ad	84	113	289	32	97	171	39	25	68	6.2	18	31	—	—	—	—	—	—	—
Ab	*	*	*	*	*	*	*	*	*	*	*	*	*	*	*	*	*	*	*
Ed	37	38	80	9	21	68	21	11	45	5.6	16	29	5.8	5.3	1.4	1.5	0.4	1.5	3.6
Le	90	110	150	29	53	42	43	33	81	4.4	0	36	5.5	7.6	3.3	1.2	0.7	1.5	13.
Ro	73	100	63	17	17	63	26	18	67	4.6	0	26	8.2	8.0	2.5	2.6	1.1	2.5	13.
NA	85	52	400	9	43	330	35	50	170	6.6	40	40	3.6	3.5	4.9	2.4	0.6	2.3	6.3
Va	166	105	1013	25	32	—	—	—	—	5.6	2	31	—	—	—	—	—	—	—
Sc	154	250	899	32	82	447	34	59	154	4.9	0	33	13.7	13.6	10.0	2.7	2.1	0.9	2.2
BV	105	188	145	37	45	61	19	20	150	4.7	0	26	21.9	3.4	11.1	0.5	0.9	1.1	2.7
Bn	128	241	163	19	28	47	14	18	295	5.7	2	29	24.6	9.9	31.8	60.0	2.7	3.2	6.0
Au	114	156	72	28	52	34	5	15	122	5.2	0	17	17.7	7.3	8.5	0.6	0.4	1.0	1.0
Fe	106	119	90	12	6	40	3	9	61	5.1	0	11	22.6	6.8	3.1	0.8	0.0	0.4	2.6
Ba	95	34	60	8	6	21	6	4	54	4.9	0	12	8.9	4.6	3.7	0.5	0.3	0.6	1.3
Ho	87	105	92	12	23	10	38	7	87	5.3	2	16	17.0	6.4	10.0	0.7	0.4	0.8	1.5
Rm	67	10	35	8	11	24	7	5	288	6.4	20	33	2.4	2.5	9.1	6.4	0.6	0.5	2.3
Et	92	104	39	14	32	29	10	5	100	5.3	0	16	5.5	0.8	6.5	2.5	0.3	0.4	1.1
He	39	49	90	4	0	23	13	4	55	5.0	0	20	—	—	—	—	—	—	—
Rz	53	81	6	12	25	6	4	3	35	4.7	0	20	8.4	6.3	4.9	3.9	0.6	0.4	1.6
Wi	60	103	19	17	78	16	12	7	80	5.8	5	18	9.9	7.0	5.6	2.7	0.5	0.4	1.2
Lz	85	103	27	21	26	9	3	5	85	5.9	5	26	12.3	2.1	6.9	1.0	0.8	0.5	1.8
Kl	95	106	0	10	27	21	0	11	54	5.2	0	12	14.7	3.4	7.6	5.3	0.7	0.9	6.8
DH	135	323	3172	33	23	1674	78	167	115	4.7	0	101	10.9	20.2	3.4	10.8	1.2	5.5	1.4
DB	194	202	654	37	130	582	35	34	118	6.0	56	29	15.4	12.5	3.8	1.6	0.5	0.6	0.8
W	196	183	465	35	42	255	17	29	55	4.7	0	25	5.4	19.6	3.0	2.3	0.9	2.3	0.6
SA	125	65	408	20	32	231	19	24	48	4.7	0	28	11.0	3.2	3.6	1.7	0.8	0.1	1.7
U	118	121	139	17	29	80	12	11	63	4.8	0	22	22.8	3.0	4.1	1.7	1.3	3.1	1.9
B	182	222	170	28	15	150	18	12	43	4.4	0	24	9.3	6.2	2.3	0.9	0.5	0.1	1.2
D	122	95	125	12	9	78	11	9	50	5.1	0	13	2.6	14.7	2.7	1.1	0.4	0.2	1.1
Za	71	17	38	13	24	36	17	40	170	6.1	63	26	1.5	6.2	6.4	0.9	0.7	4.8	4.4

— No sampling. * Sample discarded.

H. Svensson, Uppsala F. Koroleff, Helsinki A. Riehm, E. Quellmalz, Grötzingen, Baden
J. Jensen, Lyngby J. Bouquiavx, A. Mertens, Bruxelles
S. L. Tierny, Dublin, B. C. V. Oddie, London

CO_2-values in Scandinavia August—October 1957

(Cf, Fonselius, Koroleff: Tellus **7**, pp. 258—265)

Station	August						September						October					
	Date	°C	Wind		Weather	CO_2 ml/10 l	Date	°C	Wind		Weather	CO_2 ml/10 l	Date	°C	Wind		Weather	CO_2 ml/10 l
Ab	12	11.0	N	2	● °	9 4.36	1	10.0	E	8	=	3 2.96	22	—4.0	SW	3		8 3.35
	25	12.0	SW	4		1 3.21	23	2.0	ESE	7		8 3.00	23	—3.5	ESE	8		4 3.03
	26	8.0	ESE	7	● °	9 3.14	24	2.0	ESE	8		5 3.14	24	—1.0	S	3		1 3.37
							30	4.4	ESE	3		5 3.21						
Öj	12	18.0	SE	2		9 3.17	1	13.5	NNE	2	●	9 3.76	22	4.5	Calm		≡	3.25
	25	15.6	SE	3		0 3.00	23	5.9	E	1		5 3.15	23	2.8	NE	1		1 3.29
	26	—	—		—	—	24	4.5	N	5	● °	9 2.99	24	6.2	W	1		1 3.17
							30	4.5	N	8		4 3.25						
Br	12	10.0	N	1	●	9 3.16	1	10.0	N	10	● °	9 3.98	22	3.0	NE	1		3 3.45
	25	10.0	NE	10		9 3.67	23	3.0	NE	2		9 3.10	23	1.0	S	5		10 3.23
	26						24	8.0	N	10		5 3.12	24	2.0	W	10	—	3.17
							30	1.0	NE	12	✳	10 3.14						
Er	12	17.0	S	2		9 3.40	1	14.9	S	4		6 3.31	22	8.9	Calm			8 3.17
	25	15.4	SW	11	● ’	8 2.99	23	7	Calm			8 3.28	23	7.6	Calm			6 3.14
	26	17.5	SE	7		2 3.45	24	8.2	NE	16	●	10 3.14	24	8.9	W	7		10 2.99
							30	7.1	NW	5		8 3.66						
Fl	12	17.4	W	3	● ’	8 2.95	1	12.2	W	1	●	10 4.51	22	8.0	SW	1		4 3.00
	25	12.2	S	3		10 3.10	23	11.2	SW	1		0 3.12	23	8.4	SW	2		0 3.24
	26	12.2	S	1		10 3.10	24	6.6	W	1		1 3.03	24	8.6	W	3		1 3.37
							30	7.0	N	2		0 3.28						
Pl	12	16.0	S	2	● °	10 3.11	1						22	10.0	SW	2		10 2.87
	25	14.0	W	14	● °	10 3.25	23	12.0	Calm			10 3.20	23	9.0	SE	6		10 3.43
	26	14.0	W	6	● °	10 3.24	24	6.0	E	8	● ’	9 3.04	24	10.0	E	12		1 3.49
							30											
Ka	12	19.1	SSW	5.5		5 2.96	1	16.2	SSW	5		7 3.07	22	7.3	SW	3.5		0 2.96
	25	14.6	SE	7	●	9 3.16	23	—	—		—	—	23	6.2	SSW	4		9 3.15
	26	16.8	S	4		9 3.15	24	6.1	NE	7.5		5 3.15	24	6.7	SSW	1	●	9 2.97
							30	4.2	NE	0		6 3.42						
Ku	12	18.0	SE	7		6 3.23	1	15.4	SW	4		9 3.08	22	7.6	SW	5		9 3.39
	25	15.0	SE	6	●	9 2.83	23	6.0	E	4		9 3.08	23	6.6	S	4	●	9 3.26
	26	14.6	S	4		5 3.14	24	6.4	ENE	10		0 3.43	24	6.0	SSE	8	●	9 3.54
							30	4.4	NNE	1.5		0 3.25						
Jy	12	18.6	S	2.5		5 3.16	1	15.9	SSW	3		9 3.11	22	7.6	SSW	1.5		9 3.30
	25	13.0	ESE	4	●	9 3.18	23	8.4	SSE	1		7 3.34	23	7.1	S	2.5	●	9 3.20
	26	15.4	S	6		9 3.17	24	6.1	NNE	6		6 3.10	24	5.8	SE	3	●	9 3.38
							30	3.8	NE	1.5		9 3.04						
Tv	12	19.0	S	5		6 3.46	1	15.0	SSE	3		0 3.03	22	8.0	S	11	●	9 3.19
	25	16.0	SW	13		0 3.11	23	11.0	E	2		7 3.05	23	9.0	SW	4	●	9 3.28
	26	14.0	S	3		5 3.13	24	9.0	ENE	12		8 3.33	24	9.5	WSW	11		0 3.17
							30	8.0	E	0		7 3.24						
So	12	14.2	S	5		5 3.35	1	—	—		—	—	22	—0.1	SE	3	—	2.98
	25	16.5	ENE	3	●	6 2.95	23	—	—		—	—	23	—	—		—	—
	26	13.0	SSE	3.5		6 2.99	24	—	—		—	—	24	3.2	S	4	—	3.27
							30	—	—		—	—						
Pu	12	18.9	SSE	2		5 3.30	1	17.7	S	4		9 3.28	22	6.6	S	5		9 2.95
	25	11.7	SE	4	●	9 3.04	23	8.2	E	7		8 3.19	23	5.8	SSE	4		9 3.04
	26	19.3	S	6		0 3.33	24	7.4	NE	8		7 3.24	24	6.0	SSE	4.5		9 2.90
							30	6.1	ENE	1		9 3.23						

Station	August					September					October				
	Date	°C	Wind	Weahter	CO_2 ml/1ol	Date	°C	Wind	Weather	CO_2 ml/1ol	Date	°C	Wind	Weather	CO_2 ml/1ol
Vg	12	11.4	NW 1	= 10	3.12	1	18.9	ENE 4	1	3.18	22	3.8	NNE 1	=° 3	3.44
	25	15.0	ESE 5	=° 7	2.99	23	8 6	SE 2	1	3.20	23	3.1	ESE 6	=° 7	3.21
	26	14.2	E 4	=° 9	3.28	24	3.8	E 1	=° 3	2.97	24	5.5	SSE 1	=° 9	3.05
						30	5.4	SSE 1	1	3.70					
Vå	12	14.5	S 2	●° 8	3.63	1	—	—	—	—	22	2.1	E 2	5	3.28
	25	13.0	NE 6	∞° 8	3.12	23	5.4	SW 6	8	3.55	23	3.6	NE 9	8	3.12
	26	10.7	NE 4	=● 8	3.03	24	7.0	NE 2	5	3.23	24	2.2	SW 2.4	5	3.49
						30	8.2	SSW 9	5	3.07					
Sd	12	19.0	NW 4	1	3.24	1	—	—	—	—	22	6.0	N 6	0	4.26
	25	—	—	—	—	23	10.0	N 4	0	3.20	23	7.0	SW 4	, 8	2.87
	26	12.0	NW 6	●° 8	2.61	24	9.2	N 6	0	3.68	24	6.0	NW 6	5	3.46
						30	9.0	N 6	0	3.07					
Ta	12	14.4	SSE 6	●° 8	3.09	1	—	—	—	—	22	—4.0	SW 5	8	3.88
	25	11.2	ESE 1	0	3.14	23	—1.4	WNW 2	7	3.30	23	—7.6	Calm	0	2.91
	26	2.2	SE 1	8	3.09	24	—1.6	Calm	1	2.72	24	1.0	S 13	8	3.50
						30	4.0	NE 9	●° 8	3.08					
Öd	12	18.7	SW 4	● 6	3.06	1	15.5	W 5	6	2.84	22	10.2	SW 3	● 6	2.85
	25	13.2	SW 7	▽ 7	3.25	23	11.4	SW 6	—	3.22	23	9.9	SW 3	▽ 10	3.10
	26	14.3	W 4	● 10	2.97	24	9.8	NNW 6	—	3.33	24	10.5	W 5	0	3.37
				▽		30	11.0	N 2	—	3.05					
As	12	18.4	SW 5	8	3.31	1	15.9	W 5	4	3.07	22	9.8	NW 2	● 4	3.15
	25	13.9	SW 5	4	3.08	23	10.6	Calm	8	3.96	23	8.8	SW 3	▽ 8	3.47
	26	—	—	—	—	24	11.6	NNW 2	4	3.01	24	11.0	NW 3	2	3.83
						30	11.3	NNW 2	4	3.39					
Vl	12	18.1	SW 5	●° 10	3.09	1	16.1	S 4	9	3.29	22	10.2	NNW 9	● ▽ 9	3.05
	25	12.3	WSW 13	● 9	2.85	23	13.6	S 9	● 9	2.89	23	—	—	—	—
	26	14.7	WNW 13	▽ 9	3.07	24	13.4	NNE 5	8	2.90	24	—	—	—	—
						30	11.7	N 5	5	3.14					
Kn	12	—	—	—	—	1	—	—	—	—	22	— 3	NW 12	9	3.02
	25	5.0	W 5	7	3.21	23	1.0	S 5	9	3.17	23	— 6	W 2	7	3.06
	26	4.0	W 5	9	3.18	24	1.0	S 7	9	3.11	24	— 3	E 5	5	2.97
						30	1.0	S 10	9	3.06					

Errata

Volume 9, Number 3, colour picture opposite page 368, figure legend, line 3: For "f = 250 mm" read "f = 25.0 mm".